PHOSPHINE AND PHOSPHONITE COMPLEXES OF Mn(III), Co(III) AND Rh(III) PORPHYRINS.

by

Greville Lionel Camp B.Sc. (Hons) (Natal)

A thesis submitted in partial fulfillment of the requirements for the degree of Master of Science in the Faculty of Science and Agriculture, University of Natal, Pietermaritzburg.

School of Chemical and Physical Sciences

University of Natal

Pietermaritzburg

January 2003

DECLARATION

I hereby certify that this research is a result of my own investigation that has not already been accepted in substance for any degree and is not being submitted in candidature for any other degree.

G. L. Camp

Date: 21 Nov 2003

I hereby certify that this statement is correct.

Dr. O. Q. Munro
Supervisor

Date: 21 NOV 2003

School of Chemical and Physical Sciences
University of Natal
Pietermaritzburg
January 2003

CONTENTS

ACKNOWLEDGEMENTS

LIST OF ABBREVIATIONS AND SYMBOLS

Å	Angstrom
bipy	4, 4′-Bipyridine
$BzNH_2$	Benzylamine
$C_3(CN)_5$	Pentacyanopropene
$C_4(CN)_5O$	Pentacyanobutadienolate
CNHPh	α-Phenylimine
CNpyr	4-Cyanopyridine
DEAPNO	p-(Diethyl) aminephenylnitrosyl
depp	Diethylphenylphosphine
deppt	Diethylphenylphosphonite
DiMeIm	1,2-Dimethylimidazole
DMAP	(N, N'-Dimethylamino) pyridine
DMF	N, N-Dimethylformamide
DMSO	Dimethyl sulfoxide
DMTCNQ	7, 7, 8, 8-Tetracyano-2, 5-dimethyl-p-quinodimethanide
DPPE	1, 2-bis (diphenylphosphino) ethane
$DPPF_{20}$	$meso$-Tetra(pentafluorophenyl)-(2, 3, 7, 8, 12, 13, 17, 18-octaphenyl)porphyrin
DPTHTMP	5, 15-Di(phenyl)-2, 8, 12, 18-tetrahexyl-3, 7, 13, 17-tetramethylporphyrin
edpp	Ethyldiphenylphosphine
edppt	Ethyldiphenylphosphonite
Et	Ethyl
etio-I	2, 7, 12, 17-Tetraethyl-3, 8, 13, 18-tetramethyl-21H, 23H-porphyrin
$F_{28}TPP$	2, 3, 7, 8, 12, 13, 17, 18-Octafluoro-$meso$-tetra(pentafluorophenyl)porphyrin
Fl_4BzS	Tetrafluorobenzenethiolate
HCBD	Hexacyanobutadiene
HCPD	1, 1, 2, 4, 5, 5-Hexacyano-1,4-pentadienyl
HS	High-spin

IR	Infrared
K	Kelvin
LS	Low-spin
Lut-*N*-Ox	2, 6-Lutidine-*N*-oxide
mcPh	*meta*-Cyanophenyl or 3-cyanophenyl
MeIm	1-Methylimidazole
4-mepip	4-Methylpiperidine
1-mePipz	1-methylpiperazine
mg	Milligram
mmol	Millimol
nm	Nanometer
NMR	Nuclear magnetic resonance
OC_2OPor	*meso*-(benzene-1, 2, 4, 5-tetra(2-phenyloxy)ethoxy)-2', 2'', 2''', 2''''-tetraylporphyrin
OEP	2, 3, 7, 8, 12, 13, 17, 18-Octaethyl porphyrin
OEPOH	3, 4, 8, 9, 13, 14, 18, 19-OctaEthyl-1-oxo-Phlorin
OETNP	2, 3, 7, 8, 12, 13, 17, 18-Octaethyl-*meso*-tetra(nitro)porphyrin
OETPP	2, 3, 7, 8, 12, 13, 17, 18-Octaethyl-*meso*-tetra(phenyl)porphyrin
OPTMP	2, 3, 7, 8, 12, 13, 17, 18-Octaphenyl-*meso*-tetramesitylporphyrin
ORTEP	Oak Ridge Thermal Ellipsoid Plot Program
P*	*meso*-Tetra(dimethoanthracen-9-yl)porphyrin
$P(OPh)_3$	Triphenylphosphite
Ph	Phenyl
3-pic	3-Picoline or 3-methylpyridine
Pip	Piperidine
pm	Picometer
PPh_3	Triphenylphosphine
ppm	Parts per million
Py	Pyridine
QCl_4	Tetrachloro-1, 4-benzoquinone
$SnPh_3$	Triphenyltin

TBP	*meso*-Tetra(benzo)porphyrin
TBpP	*meso*-Tetra(4-biphenylyl)porphyrin
TBrPP	*meso*-Tetra(4-bromophenyl)porphyrin
TCF$_3$PP	*meso*-Tetra{(4-trifluoromethyl)phenyl}porphyrin
TClPP	*meso*-Tetra(4-chlorophenyl)porphyrin
tcne	Tetracyanoethenide
TCNEO	Tricyanoethenolate
TCNQ	7, 7, 8, 8-Tetracyano-*p*-quinodimethenide
TDCPP	*meso*-Tetra(2, 6-Dichlorophenyl)Porphyrin
T(3', 5'-DHP)P	*meso*-Tetra(3', 5'-dihydroxyphenyl)porphyrin
TDPMP	*meso*-Tetra(diphenylmethyl)porphyrin
tep	Triethylphosphine
tept	Triethylphosphite
TF$_4$OmePP	*meso*-Tetra(2, 3, 5, 6-tetrafluoro-4-methoxyphenyl)porphyrin
TF$_5$PP	*meso*-Tetra(pentafluorophenyl)porphyrin
TF$_7$PropP	*meso*-Tetra(heptafluoropropyl)porphyrin
TFPP	*meso*-Tetra(2-fluorophenyl)porphyrin
TFTCNQ	2, 3, 5, 6-Tetrafluoro-7, 7, 8, 8-tetracyano-*p*-quinodimethenide
THF	Tetrahydrofuran
TIPP	*meso*-Tetra(4-iodophenyl)porphyrin
TMcP	*meso*-Tetra(1-methoxycarbonyl-2, 2-dimethyl)cyclopropyl porphyrin
TMe$_3$AP	*meso*-Tetra{4-(*N, N, N*-trimethyl)anilinyl}porphyrin
T(*p*-Me$_2$N)F$_4$PP	*meso*-Tetra{*o, o, m, m*-tetrafluoro-*p*-(dimethylamino)phenyl}porphyrin
TMeOPP	*meso*-Tetra(3, 4, 5-trimethoxyphenyl)porphyrin
TmesP	*meso*-Tetra(2, 4, 6-trimethylphenyl)porphyrin
TNB	1, 3, 5-Trinitrobenzene
T(*o*-OCH$_3$)PP	*meso*-Tetra(*ortho*-methoxyphenyl)porphyrin
T(*p*-OCH$_3$)PP	*meso*-Tetra(*para*-methoxyphenyl)porphyrin
TP'P	*meso*-Tetra(3, 5-di-*tert*-butyl-4-hydroxyphenyl)porphyrin

TpivPP	*meso*-Tetra(*o*-pivalamidophenyl)Porphyrin
TP$_{Mepyr}$P	*meso*-Tetra(4-*N*-methylpyridyl)porphyrin
TPP	*meso*-Tetra(phenyl)porphyrin
TPPBr$_4$NO$_2$	2-Nitro-7, 8, 17, 18 – tetrabromo-*meso*-tetraphenylporphyrin
{(TPP)(Ph)$_4$}	2, 3, 12, 13-Tetraphenyl-*meso*-tetraphenylporphyrin
TpyrP	*meso*-Tetra(4-pyridyl)porphyrin
T*t*BuPP	*meso*-Tetra(4'-*tert*-butylphenyl)porphyrin
TTP	*meso*-Tetra(*para*-tolyl)porphyrin
UV	Ultraviolet

ABSTRACT

This work is aimed at elucidating the structures and spectroscopic properties of phosphine and phosphonite complexes of Mn(III), Co(III) and Rh(III) porphyrins, a class of coordination compounds that has been little reported on in the literature to date. In this work, a range of novel bis(phosphine) and bis(phosphonite) complexes of the three aforementioned metals have been synthesized, crystalized and analysed by means of X-ray structure determination, ^{1}H NMR, ^{13}C NMR, ^{31}P NMR as well as electronic and IR spectroscopy.

[Mn(TPP)(PPh$_3$)$_2$](SbF$_6$) crystallizes in the monoclinic space group $P2_1/c$ and displays an extra-ordinarily long Mn–P bond length of 3.088(2) Å. Moderate ruffling of the porphyrin ligand is observed. This complex is paramagnetic with fast proton relaxation times, and thus did not yield any useful ^{1}H NMR data. In an attempt to crystallize [Mn(TPP){P(OPh)$_3$}$_2$](SbF$_6$), a complex bearing an O-donor contamination product, [Mn(TPP){(O)PH(OPh)$_2$}](SbF$_6$), was isolated and its solid state structure determined by X-ray diffraction methods. The structure of this complex has been included in this work as it displays interesting structural features and is the very first phosphonate complex of a metalloporphyrin. This compound crystallizes in the monoclinic space group $P2_1/n$ and shows a significantly saddled conformation. The axial Mn–O bond length measures 2.122(3) Å. The Mn–N$_{porph}$ bond lengths are 1.998(6) and 2.002(3) Å for the bis(phosphine) and phosphonate complexes, respectively. Since the diethyl phosphonate complex was an unintended reaction product, no further characterisation of it was undertaken.

[Co(TPP)(depp)$_2$](SbF$_6$), where depp = diethylphenylphosphine, crystallizes in the monoclinic space group $P2_1/c$. This complex displays inversion symmetry at the metal center and the porphyrin core is effectively planar. However, [Co(TPP)(edpp)$_2$](SbF$_6$), where edpp = ethyldiphenylphosphine, crystallizes in the monoclinic space group $P2_1/n$ and shows a significantly ruffled conformation of the porphyrin core and displays no inversion symmetry. [Co(TPP)(deppt)$_2$](SbF$_6$), where deppt = diethylphenylphosphonite, also crystallizes in the monoclinic space group $P2_1/n$, but displays inversion symmetry through the central cobalt ion. As a result, this complex does not display any significant conformational deviations of the porphyrin core from planarity. The axial Co–P bond lengths are significantly shorter than that of the equivalent bond in the manganese bis(triphenylphosphine) complex at 2.312(1) Å, 2.323(10) Å and 2.258(2) Å for [Co(TPP)(depp)$_2$](SbF$_6$), [Co(TPP)(edpp)$_2$](SbF$_6$) and

[Co(TPP)(deppt)$_2$](SbF$_6$), respectively. The Co–N$_{porph}$ bond lengths average to 1.980(3) Å, 1.972(7) Å and 1.980(4) Å for these three complexes, respectively.

[103]Rh NMR measurements of three rhodium bis(phosphine)/bis(phosphonite) porphyrins have been performed by the indirect probing of the rhodium metal center by means of the phosphorus nucleus of the coordinated axial ligand. The resulting [103]Rh NMR shifts for [Rh(TPP)(edpp)$_2$](SbF$_6$), [Rh(TPP)(edppt)$_2$](SbF$_6$), where edppt = ethyldiphenylphosphonite, and [Rh(TPP)(deppt)$_2$](SbF$_6$) are 2558, 2413 and 2365 ppm, respectively. [Rh(TPP)(edpp)$_2$](SbF$_6$) crystallizes in the monoclinic space group $P2_1/n$ and shows moderate ruffling of the porphyrin core. The axial Rh–P bond length is 2.401(2) Å. [Rh(TPP)(edppt)$_2$](SbF$_6$) and [Rh(TPP)(deppt)$_2$](SbF$_6$) both crystallize in the monoclinic space group $P2_1/c$. The porphyrin core of [Rh(TPP)(edppt)$_2$](SbF$_6$) displays a moderate degree of ruffling, as observed in [Rh(TPP)(edpp)$_2$](SbF$_6$), yet the axial Rh–P bond length is substantially shorter at 2.361(9) Å. [Rh(TPP)(deppt)$_2$](SbF$_6$) exhibits the shortest Rh–P bond length of the three complexes at 2.332(2) Å. The porphyrin core is mostly planar. The Rh–N$_{porph}$ distances average 2.034(1) Å for the S_4-ruffled complexes and 2.044(3) Å for the planar complex, the shorter distance in the ruffled derivatives being consistent with a distortion-induced compression of the Rh(III) ion.

CHAPTER ONE

INTRODUCTION

1.1 Preamble

A porphine is a methine-bridged macrocyclic system of four five-membered, nitrogen-containing ring-structures called pyrroles. The porphine nucleus forms the basic building block of porphyrins, which are porphines that have had substituents added to them. Figure 1.1 shows the porphine macrocycle, which is a generic term for the large cyclic ring-based family of compounds.
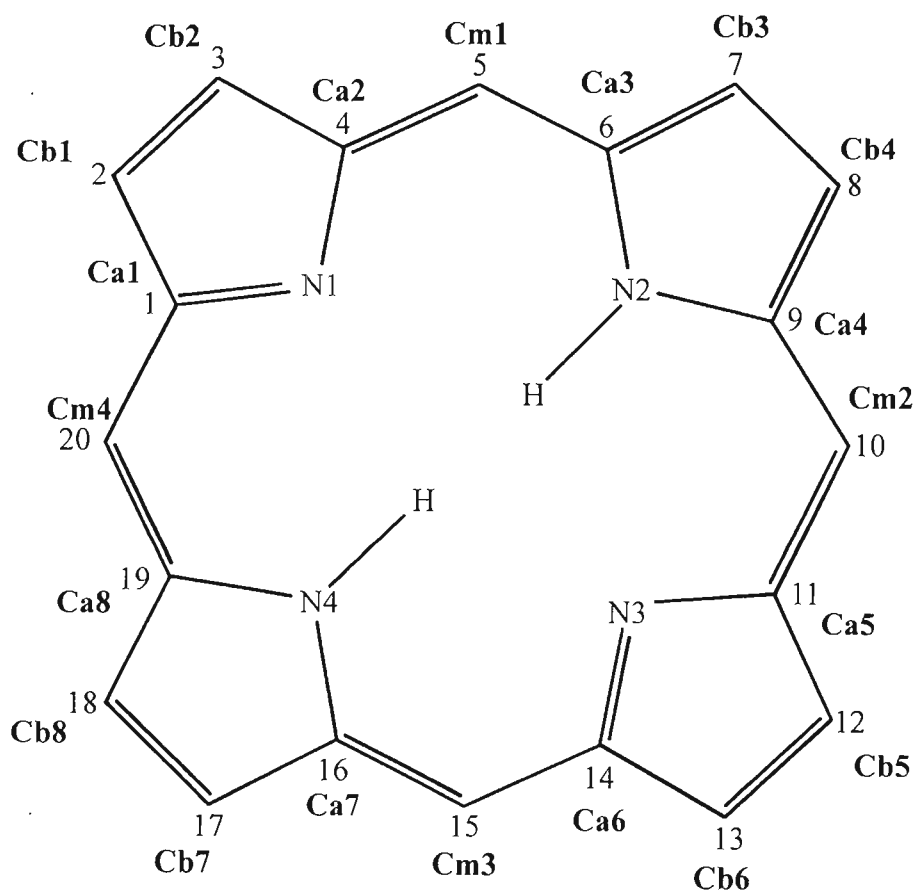
Figure 1.1: Porphine skeleton showing conventional positional numbering.

The commonly used notation and numbering pattern is shown in Figure 1.1. A pyrrole nitrogen is arbitrarily assigned as nitrogen 1 (N1). The pattern then starts at an alpha (α)-carbon (Ca1), which is the notation used for the carbon next to a pyrrole nitrogen, and proceeds in a clockwise direction onto the beta (β)-carbon (Cb1), which is the notation used for a pyrrole carbon two positions removed from the pyrrole nitrogen. The numbering then progresses to the second β-carbon and then to the second α-carbon. Accordingly, the numbering progresses onto the *meso* (bridging)-carbon (Cm1) after completing the pyrrole carbons and then on to the next pyrrole ring.

The porphine shown in Figure 1.1 shows the possibility for a central cavity to exist in the center of the macrocycle. Indeed, when the hydrogen atoms are abstracted from the pyrrole nitrogen atoms, and the porphyrin becomes negatively charged (P^{2-}), a cavity is formed where a range of metals or metal ions may be accommodated depending on whether they are of suitable dimension. It is of significance that the macrocycle is conjugated, resulting in each carbon and nitrogen in the macrocycle being sp^2 hybridised, i.e., each carbon and nitrogen has an orbital protruding from it perpendicular to the plane of the macrocycle. This creates an area of shared electron density above and below the plane of the macrocycle.

As a brief, guiding overview the following is worth pointing out with respect to research into porphyrins as a whole: When approaching the family of compounds classed together as metalloporphyrins, it soon becomes obvious that this class of compounds is so vast that it becomes necessary to define them even further. A metalloporphyrin is defined according to: **I)** The metal which has been used in the metalloporphyrin and its oxidation state. The metal in the porphyrin largely determines the reactivity of the entire complex, and paramount to this is the oxidation state of the metal. The electron configuration of the metal will determine whether the metal is high- or low-spin and thus whether it will be paramagnetic or diamagnetic in the porphyrin environment. The oxidation state of the metal is reasonably variable with most transition metals. One may, in certain circumstances, produce an array of oxidation states of a metal in a porphyrin with the employment of selected axial ligands. **II)** The porphyrin macrocycle that has been used. The basic building block of a porphyrin is a pyrrolic 5-membered ring. Four of these ring structures are fused by means of methine bridges to form the macrocycle shown in Figure1.1. The R-lettering in Figure 1.2 is to aid in pointing out the more common substitution positions on the porphine macrocycle. As mentioned previously, the R_1 position refers to the *meso*-positions and R_2 refers to the *beta*-positions commonly used in

substitution. Another position where substitution is less frequently performed is on the pyrrole nitrogens, i.e., N1 to N4. Substitution possibilities are both vast and functional. The substituents may be present to add structural or electronic character to the porphyrin and a few examples of various alternatives to porphines are provided in Section 1.3.
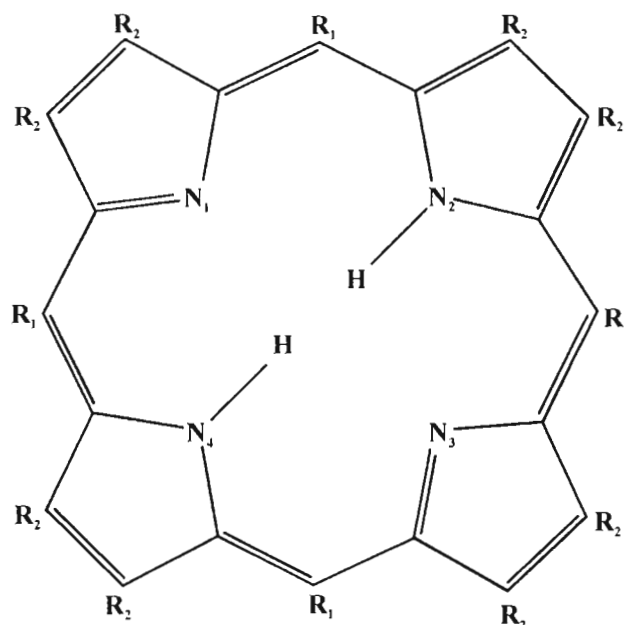
Figure 1.2: Porphine skeleton showing various substitution points.

If the research being undertaken is in the solid-state structure or solid-state properties of a family of related porphyrin complexes, then the macrocycle that crystallizes the easiest is often made use of since various porphyrins differ greatly in their crystallinity. Researchers synthesizing porphyrins for the mimicking of biological systems usually use octaethylporphyrin (OEP). This porphyrin best resembles the most common biologically occurring porphyrins. The possibility also exists for adding functional groups to a porphyrin in order to make the porphyrin itself chemically reactive, thus enabling the porphyrin to be polymerized onto a substrate. Porphyrins may be substituted at the β-position of the pyrrole framework or at the bridging *meso*-carbons. Each substitution option naturally affects the molecular orbitals of the porphyrin, depending on whether they are electron withdrawing or donating, thus changing the electronic character as a whole. The addition of certain substituents may also only allow the formation of a five-coordinate species or only allow the coordination of a certain axial ligand. These porphyrins are known as picket-fence porphyrins, variations of which may allow a lock-and-key recognition of axial ligands by the macrocycle, and have allowed the formation of many interesting complexes. **III)** The axial ligands of the metalloporphyrin. The axial ligands may impact on the electronic

character of both the metal center and the porphyrin. As mentioned previously, the choice of axial ligand may determine the spin-state and oxidation state of the metal center, depending on the crystal-field strength of the ligand and the stability of the present oxidation state. Generally, in metalloporphyrins, the stronger the crystal field splitting strength of the ligand, the lower the spin state of the metal and the more prone the metal center will be to reduction.

X-ray structural research of porphyrins and metalloporphyrins has shown that the macrocycle may in certain situations bend in a variety of manners to relieve intramolecular or intermolecular steric strain. Such distortions of the porphyrin plane are normally recognisable and have been shown in Figure 1.3.
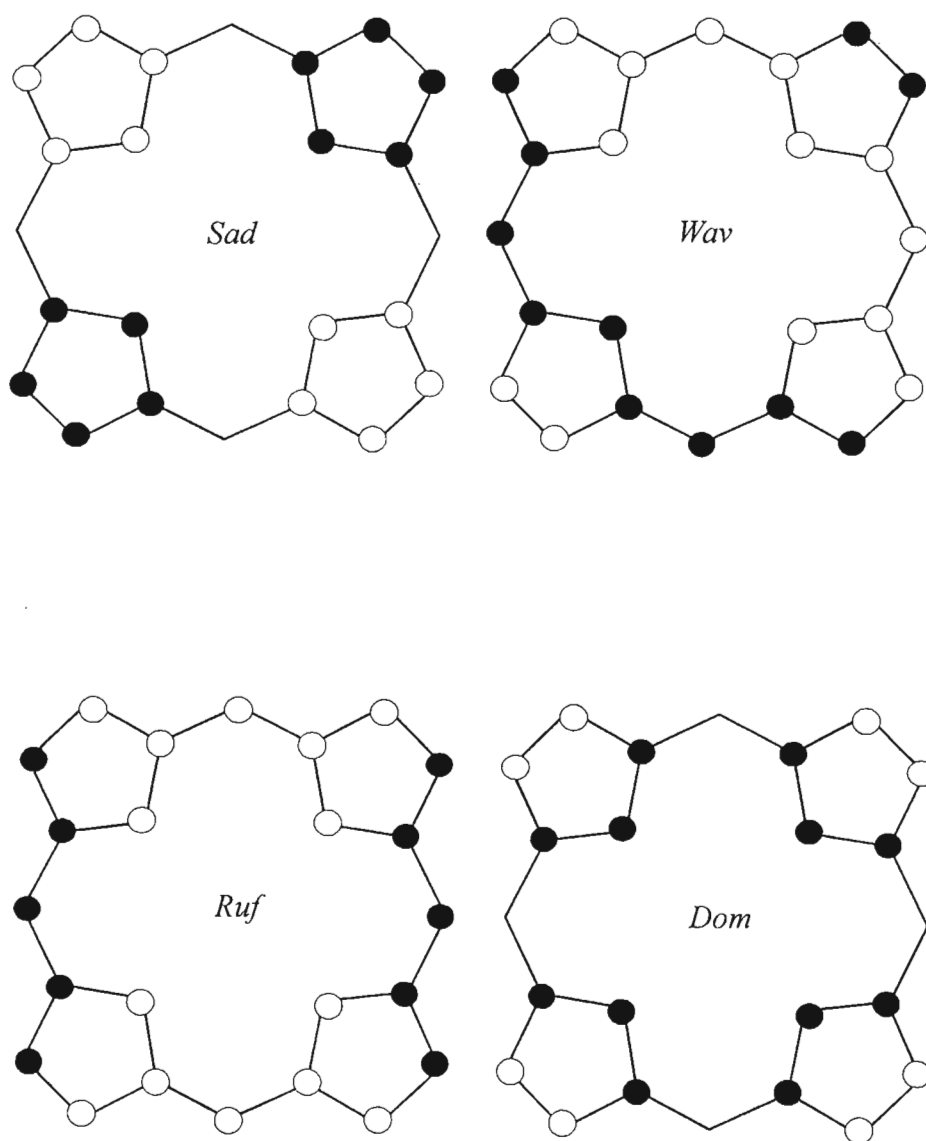
Figure 1.3: **Idealised depiction of possible out-of-plane distortions of porphyrins and metalloporphyrins.**[1] **Filled and open circles represent atoms on opposite sides of the 24 atom mean plane. Atoms with no circles are in the mean plane.**

4

The more common forms of conformational distortions within the 24 atom porphyrin core are saddling (*Sad*), wave (*Wav*), ruffling (*Ruf*) and doming (*Dom*). Some of the better examples of these conformational distortions may be found in references **58, 105, 78,** and **50,** respectively, listed in the reference list. Ruffled conformations induce a twist around the two axes lying along the *trans* N_{porph}–M–N_{porph} vectors in metalloporphyrins. More specifically, as shown in Figure 1.3, opposite pyrrole rings are counter-rotated with respect to the *trans* N_{porph}–M–N_{porph} axis. An important structural consequence of this distortion is that shorter M–N_{porph} are enabled by the twist-ruffled metalloporphyrins therefore display commensurately shorter M–N_{porph} bond lengths than planar, wave or saddled conformations.

1.2 Interesting Variations in Porphyrins

The extent to which porphyrins have been substituted is remarkable and this section is intended to aid the reader in grasping the possibilities and, in some cases, the awe-inspiring creativity that porphyrin research commands. A few examples of solid-state crystal structures of synthesized porphyrins and metalloporhyrins are shown.
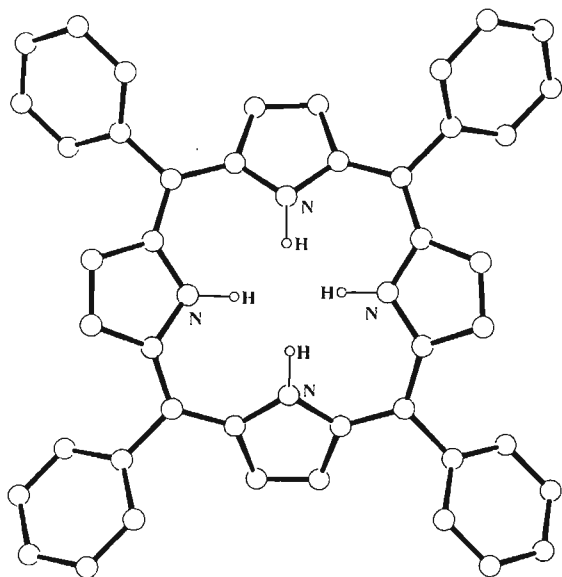
Figure 1.3: CAXHAK[2]
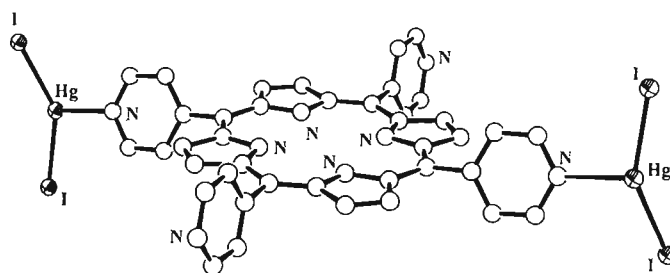
Figure 1.4: BAKJOM[3]

Note that the Cambridge Structural Database (C.S.D) codes have been used as figure captions for simplification. Figure 1.3 shows the structure of [H_4TPP^{2+}], which has the phenyl substituents at the *meso*-positions. The di-acid terminology refers to the protonation of all four pyrrole nitrogen atoms to produce an "acidic" porphyrin. This is one of the more easily synthesized and more

commonly used porphyrins. An interesting, and functional, coordination of di-iodomercury at the nitrogen atoms of a *4-pyridyl meso*-sustituted porphyrin is shown in Figure 1.4. This functionalisation allowed the synthesizers to form long chains or polymers of this porphyrin such as shown in Figure 1.5.
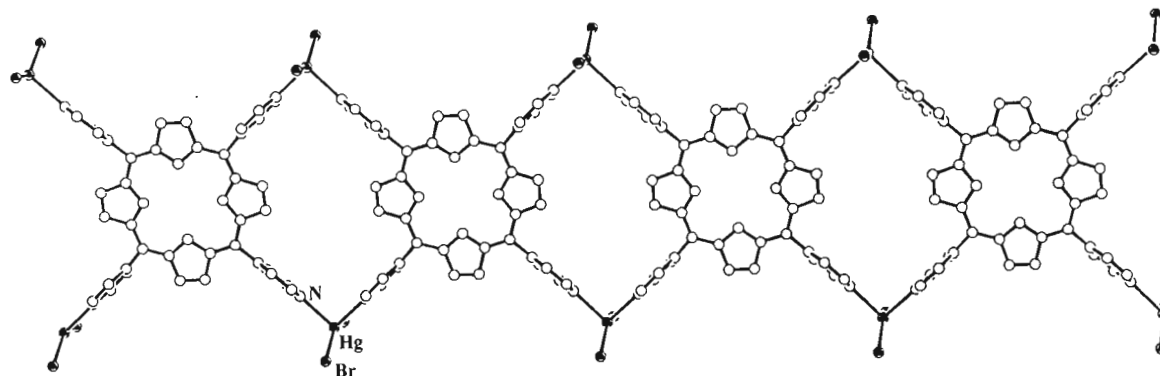
Figure 1.5: BAKPOS[3]

This type of system represents current progress towards the synthesis of light-harvesting complexes, which are being modeled on naturally existing systems.
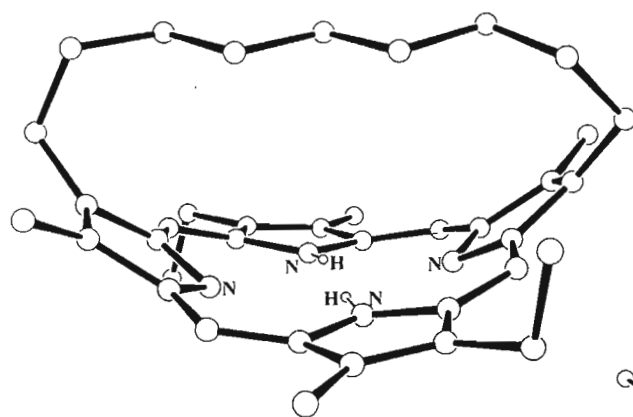
Figure 1.6: BACTEE20[4]   **Figure 1.7: COLREA[5]**
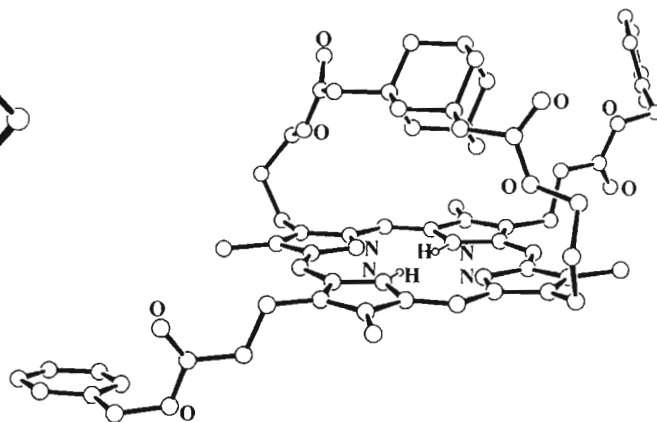
In Figure 1.6 a linkage over the macrocycle causes a forced ruffling, which allowed the researchers to establish what effect ruffling has in the chemistry of porphyrins. This has biological relevance since the haeme groups in haemoglobin and other haemoproteins show "doming" – another form of bending in porphyrins.

Figure 1.7 shows a porphyrin used for research on the coordination of carbon monoxide and dioxygen to iron (II). This research is an attempt to mimic and explain the biological action of dioxygen coordination in haeme proteins. Metal complexes of this porphyrin, with its bulky linkage, allow only small molecules such as carbon monoxide, dioxygen and nitric oxide to enter into the cavity formed between the linkage and the porphyrin plane. Such systems facilitate studies on the influence of various ligands *trans* to this linkage, on the coordination of small diatomic ligands to the face of the metal obscured by the linkage.
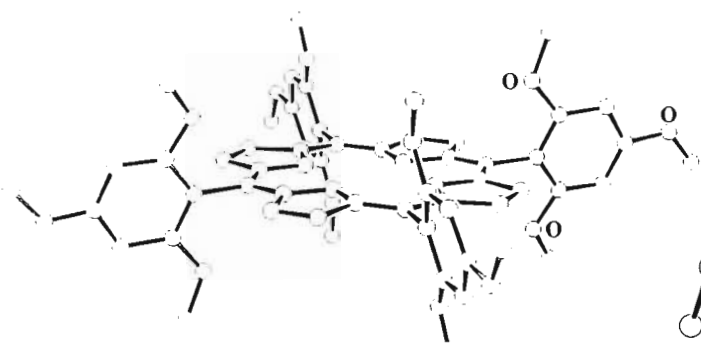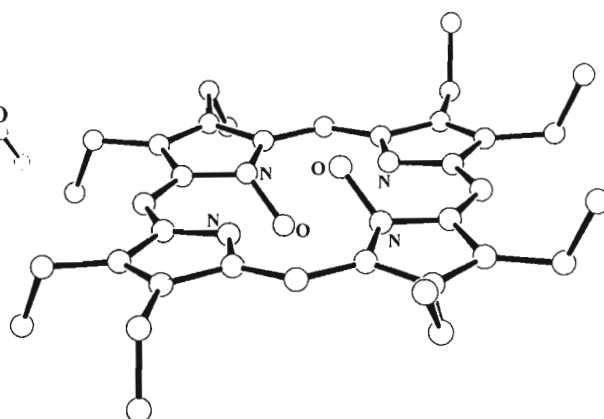
Figure 1.8: CURNOS[6]   **Figure 1.9: CUXVEW[7]**

Figure 1.8 shows a 'bis-pocket' porphyrin which makes use of the methoxy substituents on the *meso*-phenyls in forming two pockets which restrict the size af the axial reagents coordinating to the central metal ion. This porphyrin was used as a precursor to oxygen-transfer catalysis research in which the catalytic complex contained centrally coordinated iron.

Figure 1.9 shows a porphyrin that has substitution at the pyrrole nitrogen atoms. This is not a very common position for substitution. It is proposed[8-10] that a similar form of oxygen binding where the oxygen molecule exists as an *N*-oxide, and not directly over the iron atom, is present in the highly oxidized forms of haeme proteins. Examples of these highly oxidized forms are cytochrome P-450 and the peroxidases where the iron atom in the porphyrin transiently reaches an intermediate oxidation state of +5.
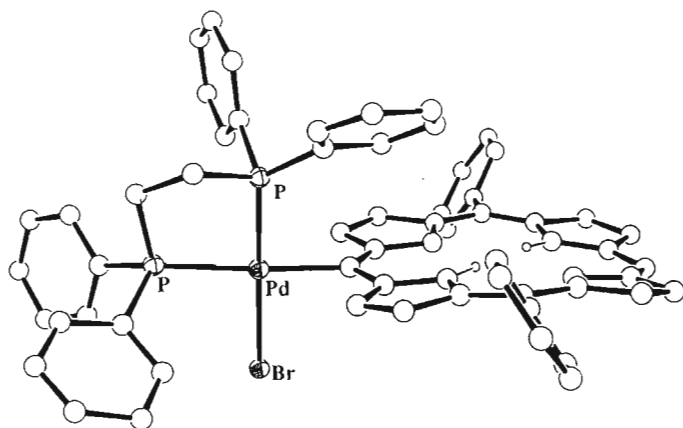
Figure 1.10: FAJKIK[11]
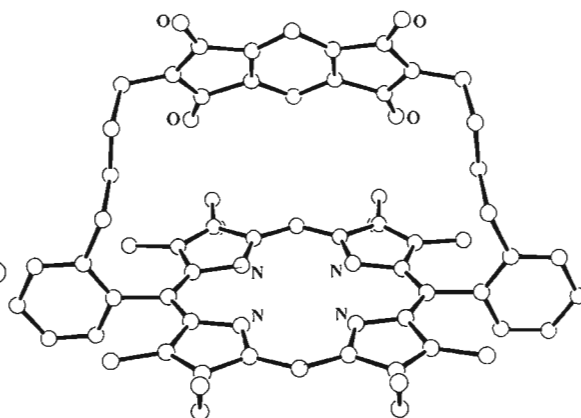
Figure 1.11: FEYJIC[12]

An uncommon form of substitution is shown in Figure 1.10, where palladium has been substituted at one of the *meso*-positions of the porphyrin (the other ligand being DPPE). This porphyrin has been synthesized in the ongoing search for more improved and specific catalysts. The porphyrin shown in Figure 1.11 falls into the class of compounds called acceptor-porphyrin cyclophanes. It was thought that the electron-donating character of the pyromellitic diimide 'cap', which is linked over the top of the porphyrin, would add steric restrictions and influence the behaviour of the central metal ion in the porphyrin and thus affect its chemistry at both faces of the metal. From this crystal structure, however, it was observed that the 'cap' lies too far away from the central metal ion to affect its chemistry much.
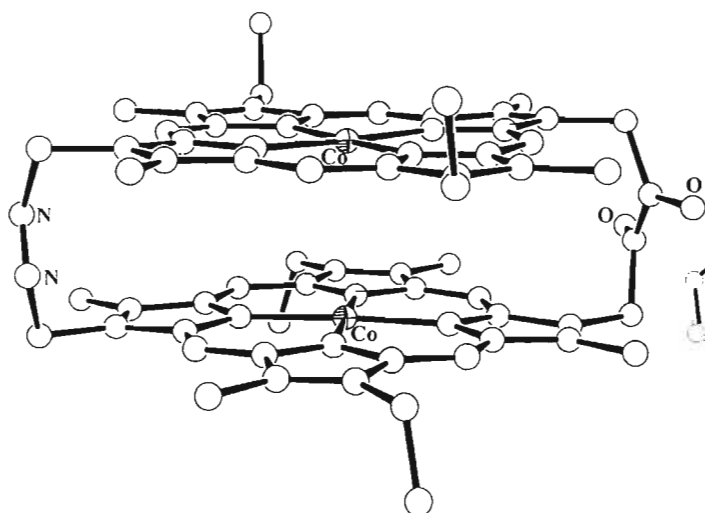
Figure 1.12: GETNEY[13]
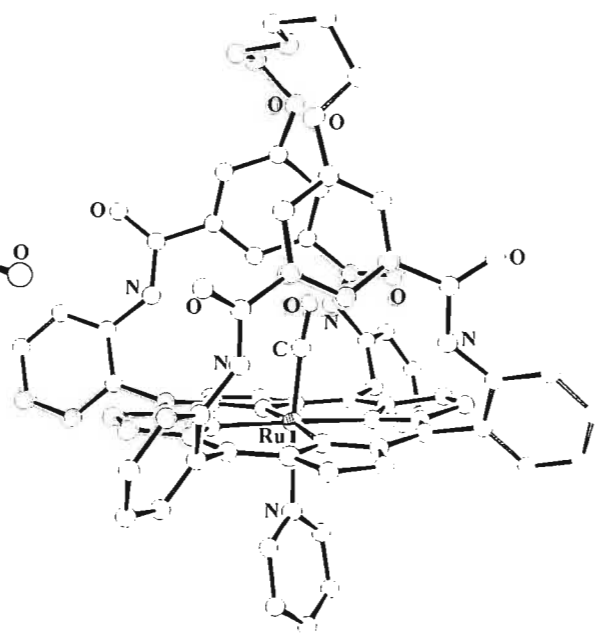
Figure 1.13: GETXAE[14]

Figure 1.12 shows a "face-to-face" porphyrin. As the name implies, this is a porphyrin macrocycle that is functionalised to form a bridge to another porphyrin. This results in an arrangement where the central metal ions are brought into close proximity to each other. In this situation the central metal ion is cobalt and this same compound was used as a catalyst in the four-electron reduction of dioxygen to water. Figure 1.13 shows the pioneering 'picnic-basket' porphyrin. These porphyrins were initially created to mimic biological systems that also have bulky sterically hindering appendages on the porphyrin macrocycle. Examples of the biological systems these researchers were attempting to mimic are the cytochrome P-450 enzymes.

1.3 Crystal Structures of Manganese, Cobalt and Rhodium Porphyrins

A survey of the published crystal structures of manganese, cobalt and rhodium porphyrins using the Cambridge Structural Database (CSD) has been performed to collect and illustrate structural and comformational trends in these groups of metalloporphyrins. Tables 1.4 to 1.26 summarise the coordination group and porphyrin core parameters for these compounds.

Those complexes for which there were no references available, or from which the relevant data were omitted, had the relevant data calculated from the CSD X-ray structure coordinates. Where no spin-states were given, the spin-state was assumed using conservative estimates. For 5-coordinate complexes the axial lengths contain the estimated standard deviation (esd) in parentheses after the value. For the 6-coordinate complexes the axial lengths were averaged and the value in parentheses after the averaged value is the average esd's of the individual lengths.

The metal to porphyrin-nitrogen lengths were averaged and inserted as a single value, the average esd's were inserted in parentheses after this value to give an indication of the spread in the individual datum. Out-of-plane deviations of the central metal were calculated from the 24 atom mean plane, and not the mean plane of the four pyrrole nitrogens. The out-of-plane deviations were rounded off to the nearest picometer (0.01 Å) and values below 1 pm were assigned to an 'in plane' status. In certain circumstances where more than one metalloporphyrin was present in an asymmetric unit, the average esd of the individual values was included in paretheses after the averaged value. Each metalloporphyrin complex was observed for conformational distortions of the 24 atom porphyrin core. Conformations stated within the corresponding publications were ignored as too many errors were noticeable. These conformations were assigned by careful scrutiny with *Mercury 1.0* distributed by the Cambridge

Structural Database Centre. Where there is more than one metalloporphyrin center per asymmetric unit, each porphyrin core conformation is assigned.

1.3.1 Omitted CSD Structures

Certain CSD entries were excluded from the tables appearing below. Complexes for which references could not be obtained, and no X-ray coordinates were present, were omitted for obvious reasons. The purpose of this extensive literature survey is to compile a database of all crystallographically crystallized complexes and to summarise the immediate coordination geometry within these complexes. Those complexes which displayed forced distortions of the porphyrin core, and are thus an artificial reflection of the coordination geometry, have been treated as outliers and, as such, N-(porphyrin)-oxo, N-alkylated porphyrins, sandwich porphyrin dimers, 'capped' porphyrins or 'picnic basket' porphyrins, and fullerene complexes were ommitted. CSD reference codes of the omitted complexes and the reasons for their exclusion are tabulated in Tables 1.1 to 1.3

Table 1.1: Omitted Manganese CSD Entries

REFCODE	Reason for ommission	Ref.
CMPOMN	N-methylated	15
JEDSAM	N-oxide	16
NOCWOR	Sandwich dimer	17
YEKHIF	Sandwich dimer	18

Table 1.2: Omitted Cobalt CSD Entries

REFCODE	Reason for ommission	Ref.
AXBYCZ	N-alkylated	19
BOJNIX	Fullerene	20
CELTIW	Fullerene	21
CELVUK	Fullerene	21
CELWAR	Fullerene	21
CELZAU	Fullerene	21
CMPORC10	N-alkylated	22
DASXOK	No core data	23

10

Table 1.2: Contd.

REFCODE	Reason for ommission	Ref.
FULBAP	N-oxide	24
GEPGAJ	Capped porphyrin	25
GETNEY	Sandwich dimer	13
KUZZIO	Sandwich dimer	26
KUZZOU	Sandwich dimer	27
LADGEC	No core data	28
LADGEC01	No core data	28
LOMLAA	Sandwich dimer	29
LOMLEE	Sandwich dimer	29
NOCWIL	Sandwich dimer	30
PEPOCO10	Publication unavailable	31
POYPUO	Sandwich dimer	32
QOFZIU	Fullerene	33
REDGUC	No core data	34
TEFSUT	Publication unavailable	35
TEFSUV	Publication unavailable	35
TEFSUX	Publication unavailable	35
TPORCP02	No core data	36
VIYFEO	No core data	37
WOSZOT	Capped porphyrin	38
WOSZUZ	Capped porphyrin	38
WOTBAI	Capped porphyrin	38

Table 1.3: Omitted Rhodium CSD Entries

REFCODE	Reason for ommission	Ref.
CIXPII	Sandwich dimer	166
DIWREG	Rh–In dimer	39

1.3.2 Manganese Porphyrins

A literature survey of the crystal structures of manganese porphyrins to date reveals a rather limited range of electron donors. The complexes that have been characterised consist mainly of O-donors (Table 1.5), N-donors (Table 1.6), two C-bound cyano (C≡N) derivatives (Table 1.7), a few halogen-donors (Table 1.8), 8 mixed-ligand complexes (Table 1.12) and relatively few 4-coordinate complexes (Table 1.13). To complete the survey, dimerised and polymerized

porphyrin complexes where the bridging ligands have μ-N-, μ-O- and μ-O/N-donor atoms, have also been included (Tables 1.9, 1.10, and 1.11, respectively). The extracted and averaged bond lengths for each class of donor atom are tabulated below in Table 1.4. The chemistry of the μ-dimer class of porphyrin complexes is deemed relatively irrelevant to this research work and, as such, the bond length data from these compounds has been excluded from Table 1.14.

Table 1.4: Summary of Bond Length Ranges For Manganese Porphyrins[a]

Bond	Mn–L$_{ax}$ Range	Mn–N$_{porph}$ Range
Mn^{III}–O	2.078–2.320	1.995–2.019
Mn^{IV}–O	1.839	2.012
Mn^{II}–N	1.641–2.192	2.004–2.128
Mn^{III}–N	2.029–2.309	2.003–2.017
Mn^{IV}–N	1.926	1.970
Mn^{III}–C	2.015–2.166	2.000–2.008
Mn^{II}–Cl	2.364	2.160
Mn^{III}–Cl	2.296–2.369	1.974–2.014
Mn^{III}–Br	2.490	2.008
Mn^{III}–I	2.749	2.011
Mn^{II} (4 coord)	NA	2.083–2.097

[a] Mixed ligand complexes and esd's excluded. All complexes are five- and six-coordinate coordinate unless otherwise stated.

Manganese porphyrins with axial O-donor ligands. The oxophilic nature of manganese results in a substantial record of O-donor atom X-Ray crystal structures. The most common O-donor is the aqua species, which is to be expected since it is one of the smaller O-donor ligands in terms of steric factors and is abundant in most solvents. Both 5-coordinate and 6-coordinate aqua species exist with the 5-coordinate species being the most commonly crystallized.[40–44] Structures with solvent ligands such as ethanol and methanol exist as well as DMF, DMSO and THF. A fairly limited array of μ-O-dimers exists with bridging oxo-, hydroxyl, formate and sulfate ligands being the scope to date.

All of the O-donor complexes of manganese(III) surveyed contain manganese in a d^4 high-spin electronic state, but for the Mn(IV) high-spin six-coordinate d^3 complex with methoxy axial ligands [1] shown in Figure 1.14. The Mn^{IV}–O bond length is 1.839(2) and 2.012(9) Å for the average Mn^{IV}–N$_{porph}$ bonds. In general the 5-coordinate aqua complexes of Mn [2 and 3] have Mn–O bond lengths in the range 2.105(4) to 2.149(3) Å, with the latter limit being the most common. The Mn–N$_{porph}$ bond lengths are at a more consistent value of 1.996(4) Å. 6-

Coordinate complexes of the aqua-type [4 and 5] have axial bond lengths in the range 2.220(1) to 2.271(2) Å, and Mn–N$_{porph}$ bond lengths in the range 1.998(0) to 2.012(3) Å.
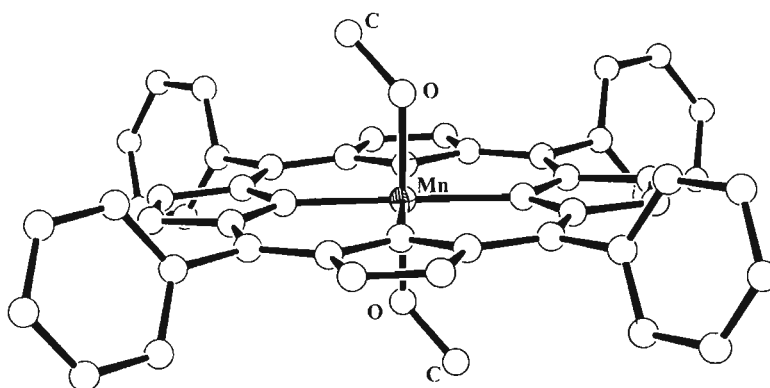
Figure 1.14: BOPWAE [1].

An example of a 6-coordinate aqua complex is shown in Figure 1.15. It is noticeable that the Mn–N$_{porph}$ bond length differences between 5- and 6-coordinate complexes are relatively insignificant (to within 0.004 Å), but what is significant is that the Mn–O bond lengths are slightly longer for the 6-coordinate complexes and this may be attributed to the slightly out of plane displacements of metals in 5-coordinate porphyrin complexes.
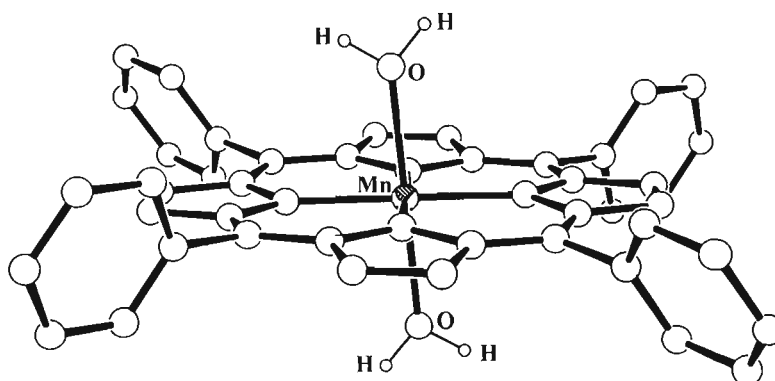
Figure 1.15: ZUTNAD [4].

The difference between 5- and 6-coordinate axial and metal–N$_{porph}$ bond lengths is again displayed in the 6 coordinate complexes with axial methanol [6] and the single 5 coordinate complex with axial ethanol [7]. Here the bis(methanol) complexes have axial bond lengths in the range 2.261(9) – 2.283(1) Å while the 5-coordinate ethanol complex has an axial bond length of 2.145(1) Å. This is a rather significant difference in bond lengths. The bis(methanol) Mn–N$_{porph}$ bond lengths are in the range 2.002(3) – 2006(2) Å. In comparison the single axial ethanol

13

complex has a Mn–N$_{porph}$ distance of 1.996(4) Å. This difference in lengths, although not vast, shows, as with the aqua species, that the 5-coordinate systems produce smaller Mn–N$_{porph}$ bond lengths.

A search for additional solvent complexes of Mn(III) porphyrins reveals a bis(DMF) complex [9] which has an axial bond length of 2.217(4) Å, a bis(THF) complex [10] that has an axial bond length of 2.320(2) Å and a bis(DMSO) complex [19] that has an axial bond length of 2.219(1) Å. This longer bond length for the THF species is presumably as a result of its larger steric bulk relative to DMF and DMSO. The Mn–N$_{porph}$ bond lengths are all reasonably similar at 2.010(8), 2.004(2) and 2.006(7) Å for the DMF, THF and DMSO species, respectively. It is noteworthy that there is only one complex of each donor available in the database, and thus these trends are not conclusive.

The two lutidine-*N*-oxide complexes produce axial bond lengths amongst the longest observed for O-donor complexes of Mn(III) porphyrins with 2.282(17) and 2.264(4) Å for the 5- [13] and 6-coordinate [12] complexes, respectively. The 6-coordinate complex is shown in Figure 1.16. This is not surprising as this axial ligand is one of the more sterically hindered O-donors. Surprisingly, these complexes produce Mn–N$_{porph}$ bond lengths which are amongst the shortest of the O-donor complexes at 1.984(9) and 1.996(5) Å for the 5- and 6-coordinate species, respectively. This may be attributed to the ruffled porphyrin conformations in these derivatives and the concomitant shortening of the Mn–N$_{porph}$ bonds as a result of this core distortion.
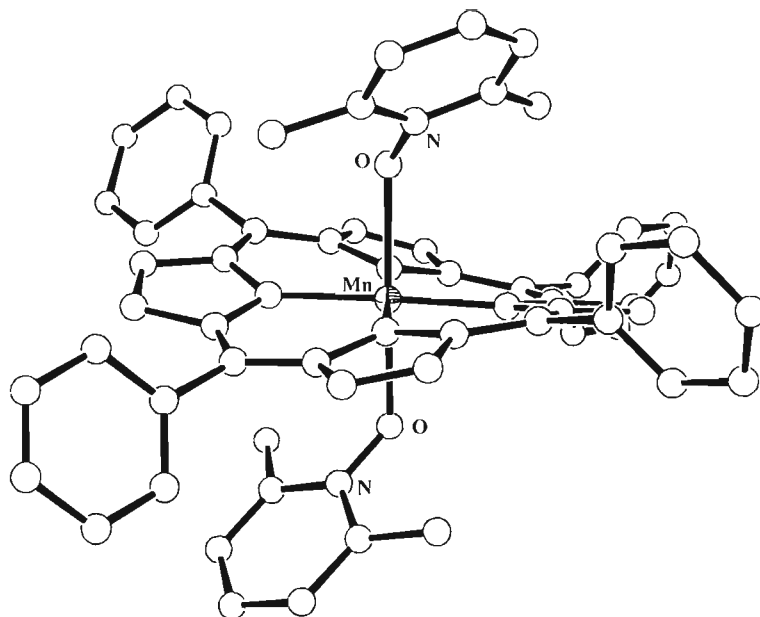
Figure 1.16: DIBBAR [12].

The 5-coordinate complexes of NO_2^- [16] and NO_3^- [17] display axial bond lengths of 2.059(4) and 2.101(3) Å, respectively, and Mn–N$_{porph}$ bond lengths of 2.012(2) and 2.007(7) Å, respectively. The NO_2^- complex shown has one of shortest axial Mn–O bond lengths, which is substantially shorter than the 5-coordinate aqua complexes. These Mn–N$_{porph}$ bond lengths are also surprisingly similar to those observed for 6-coordinate complexes of general O-donors.

Interestingly, although ClO_4^- is usually regarded as a weakly coordinating ion, the 5-coordinate perchlorato complex [18] has a Mn–O bond length of 2.183(1) Å and an average Mn–N$_{porph}$ bond length of 2.000(3) Å. These values do not lie outside the expected coordination group distances for O-donor complexes.

The only complex, other than [19], with a sulfur-containing O-donor is the HSO_4^- derivative shown in Figure 1.17, which forms a 5-coordinate complex [20] and has a Mn–O bond length of 2.078(5) Å, which is not unusual, and a Mn–N$_{porph}$ bond length of 1.991(6) Å, which appears to be consistent with most 5-coordinate O-donor systems.

15
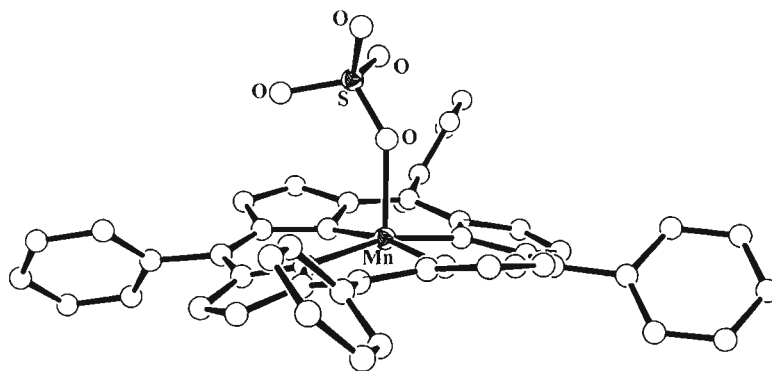
Figure 1.17: VIXKAO [20].

Manganese porphyrins with axial N-donor ligands. Tetracyanoethenide (TCNE) complexes form a large proportion of the structures to date. An extensive range of μ-N-dimers exists with this compound as a bridging ligand. Complexes with cyanate and thiocyanate donors have been synthesized as well as isolated examples of imidazole, azide and pyridine complexes.

The single case of manganese in a +5 oxidation state occurs in a Mn≡N complex [21], where the shortest Mn–N bond length of 1.515(3) Å is observed. This is indeed the shortest Mn axial bond length of any other donor in this survey of manganese complexes, consistent with a metal–nitrogen bond order of 3. The Mn–N$_{porph}$ bond lengths are consistent with most manganese complexes at 2.003(19) Å.

A Mn^{IV} bis (N=C=O) complex [22] does exist which is the only such oxidation state amongst the N-donors. The axial bond lengths are very short for a 6-coordinate system at 1.926(3) Å. The Mn–N$_{porph}$ bond lengths are also significantly shorter at 1.970(1) Å. The Mn–N$_{porph}$ bond length recorded for this complex is the shortest amongst all the manganese complexes surveyed. The short axial and Mn–N$_{porph}$ bonds clearly reflect the high oxidation state of the metal and its small ionic radius. This axial ligand is also coordinated in a 5-coordinate complex of Mn^{III} [27], as shown in Figure 1.18, where the axial and Mn–N$_{porph}$ bond lengths are significantly longer at 2.029(1) and 2.014(4) Å, respectively. A comparable complex of a 5-coordinate Mn^{III} system with an axial N=C=S ligand [28], as shown in Figure 1.19, produces a longer axial bond length of 2.070(3) Å, and a shorter Mn–N$_{porph}$ length of 2.003(9) Å.

16
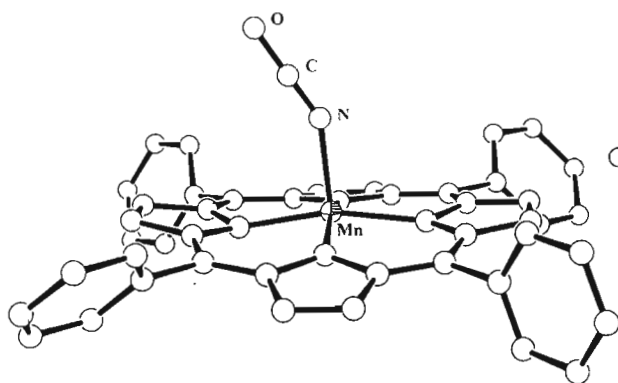
Figure 1.18: GISHIZ [27]. **Figure 1.19: GISJEX [28].**
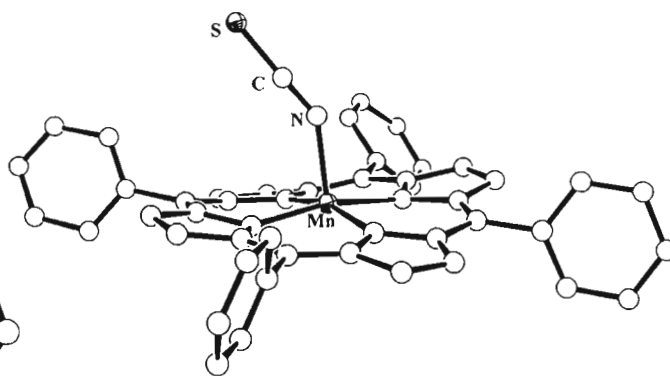
The tetracyanoethenide (TCNE) complexes [23–26] of manganese form the relative bulk of the N-donor section with 4 such structures in the database (excluding bridged dimers and polymers). This ligand forms an anionic radical and mostly bridges manganese centers to form dimers and polymers. This ligand has been reacted with Mn^{III} in various types of porphyrin macrocycles, and axial bond lengths vary between 2.285(9) and 2.309(12) Å. The $Mn–N_{porph}$ lengths vary between 2.008(7) and 2.017(1) Å. Both these lengths are not extraordinary and fall within the average range for Mn^{III} complexes.

A complex of 5-coordinate Mn^{III} with an axial pyridine [29] has an axial bond length of 2.216(8) Å and 2.007(2) Å for the $Mn–N_{porph}$ bond length. The axial bond length is fairly consistent with a relatively bulky axial ligand, and the $Mn–N_{porph}$ bond length is a consistent figure with the data surveyed thus far.

A single 5-coordinate complex of N_3 exists [30] with an axial and $Mn–N_{porph}$ bond lengths of 2.045(4) and 2.005(6) Å respectively. These lengths are consistent with the 5 coordinate $N=C=O^-$ and $N=C=S^-$ systems, but for the N_3^- axial length being marginally longer.

The only low-spin complex of either Mn^{II} or Mn^{III} with a N-donor exists as a Mn^{II} 5-coordinate complex with an axial $N\equiv O$ [31]. A very short axial length of 1.641(2) Å is observed for this low-spin system and is significantly shorter than that observed (2.192(2) Å) for a high-spin Mn(II) complex with a single axial 1-methylimidazole ligand [32]. The $Mn–N_{porph}$ length of the former complex is 2.004(4) Å, which is short for Mn(II) and falls in the range observed for Mn(III) porphyrins, while the latter complex displays a domed configuration with the metal protruding from the plane of the porphyrin, resulting in a long $Mn–N_{porph}$ bond length of 2.128(3) Å.

Manganese porphyrins with axial C-donor ligands. Both C-donor complexes are 5- [33] and 6-coordinate [34] cyano complexes of Mn^{III} with the 6-coordinate complex producing a low-spin state. The 6-coordinate complex is shown in Figure 1.20. The 5-coordinate and 6 coordinate systems display axial bond lengths of 2.166(6) and 2.015(20) Å. This difference reflects depopulation of the d_{z^2} orbital in the 6-coordinate Mn(III) ion, consistent with a low-spin state for this derivative. The Mn–N_{porph} lengths are quite normal at 2.008(8) and 2.000(20) Å for the 5- and 6-coordinate complexes, respectively. The reason for this is that the $d_{x^2-y^2}$ orbital is not significantly populated in either LS or HS Mn(III) porphyrins.
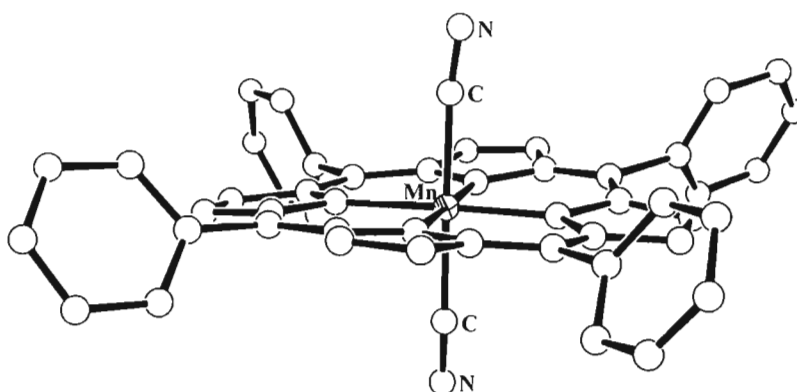
Figure 1.20: NEXSOY [34].

Manganese porphyrins with axial halogens. Crystal structures of complexes with chloride, bromide and iodide coordinated to manganese exist. Chloride is the most commonly used halide derivative and chloro manganese (III) complexes of a range of porphyrins are known.

The differences in atomic radius between the halogens as they descend down the Periodic Table may be clearly observed in Table 1.8. The range of axial bond lengths varies between 2.296(1) and 2.369(3) Å for chloride complexes [35–39] and the individual values for bromide [40] and iodide [41] complexes are 2.490(1) and 2.749(19) Å, respectively. An example of a chloride complex is shown in Figure 1.21. The Mn–N_{porph} bond length range is 1.990(10) – 2.014(15) for Mn^{III} and an unusually long 2.160(7) Å for Mn^{II}.
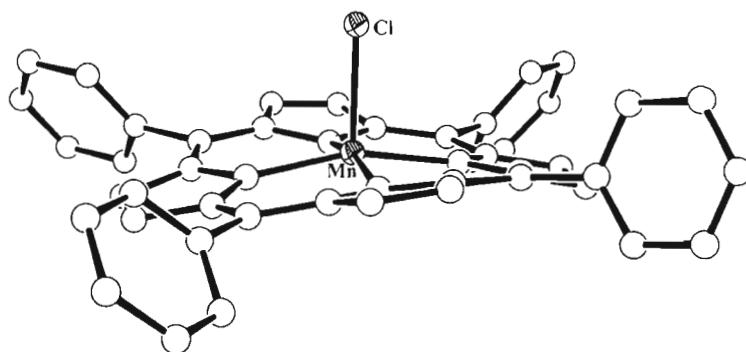
Figure 1.21: TPPMNA [36].

The long Mn–N$_{porph}$ bond in the Mn^{II} complex is due, in part, to the protrusion out of the porphyrin plane of the central ion and a general doming of the porphyrin. Furthermore, the HS d^5 configuration leads to population of the $d_{x^2-y^2}$ orbital and thus a significant M–L electrostatic repulsive interaction for the equatorial bonds in the complex. The Mn–N$_{porph}$ bond length for the bromide complex is 2.008(14) Å; a similar distance is observed for the iodide complex (2.011(7) Å).

***μ*-Dimers of manganese**. Dimerised and polymerised complexes of Mn^{III} are numerous and the most common bridging ligands, as shown in Table 1.9, are N-donors (TCNE and TCNQ derivatives). The complete range of the axial bond lengths is not substantially wide (2.228(47) to 2.440(79) Å), with the most common value at around 2.3 Å. These lengths are significantly longer than normally observed for 5-coordinate Mn^{III}, and comparisons can not accurately be made against the single 6-coordinate N-donor complex of Mn^{IV} bis(N=C=O) [22] which has substantially shorter axial bonds (1.926(3) Å). No dimerised complexes of Mn(II) porphyrins exist.

The TCNQ-type complexes [42–45] exhibit axial lengths between 2.271(7) and 2.332(13) Å, and Mn–N$_{porph}$ lengths between 1.998(2) and 2.016(4) Å. All of these complexes are high-spin, but for the DMTCNQ-bridged and imidazolate-bridged complexes, which show alternating high-spin / low-spin configurations between metal centers. In the former complex, this accounts for the high average standard deviation for this complex from the average axial length of 2.332(14) Å. The TCNE-bridged complexes [46–51], an example of which is shown in Figure 1.22, display a wider range of axial bond lengths, i. e., 2.268(1) to 2.440(79) Å, and a wide range of Mn–N$_{porph}$ lengths (1.993(5) to 2.012(7) Å).

19
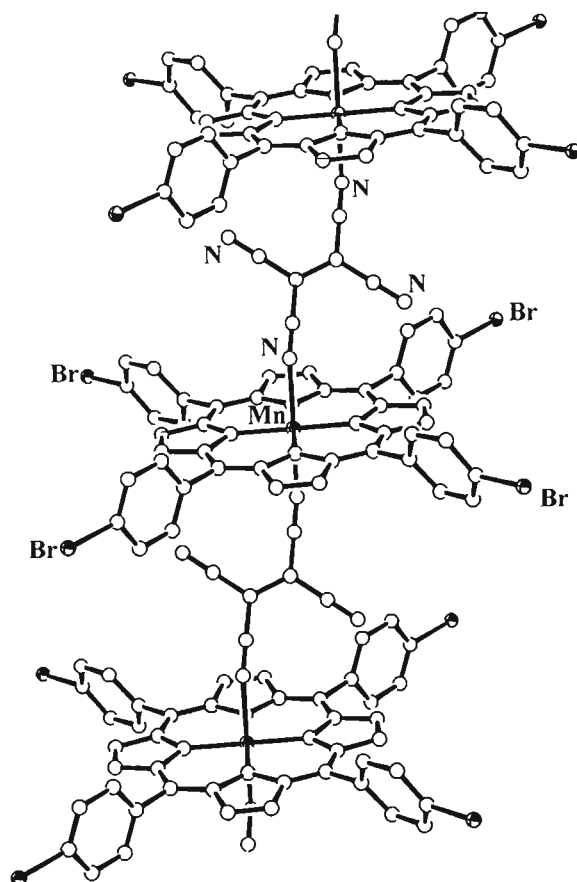
Figure 1.22: XASHEE [47].

The HCPD- [52] and HCBD-bridged [53–55] complexes display axial bond lengths between 2.315(8) and 2.420(1) Å and Mn–N$_{porph}$ lengths in the range 1.998(6) to 2.007(3) Å. These axial bond lengths appear to be consistent within the domain of N-bridged dimers and polymers. The C$_3$(CN)$_5$-bridged complex [56] exhibits an axial bond length of 2.352(1) Å and a short average Mn–N$_{porph}$ bond length of 1.976(10) Å.

Two 4, 4′-bipyridine- [57] and imidazolate-bridged [58] complexes exhibit axial lengths of 2.364(43) and 2.228(47) Å, respectively, with Mn–N$_{porph}$ lengths of 2.011(2) and 2.015(3) Å, respectively. While the latter bond lengths, and the bipyridyl dimer axial Mn–N lengths, remain consistent with the other bridged complexes, the imidazolate complex displays shorter than average axial lengths with a large average standard deviation. The short Mn–N$_{Im}$ distances reflect the fact that the imidazolate ion is a very strong σ-donor, while the large esd in the axial Mn–N distances reflect the fact that there are alternating high-spin and low-spin centers in the polymer.

An interesting porphyrin-bridged cluster-complex [59], shown in Figure 1.23, has also been included in this section as the species still displays N-donor bridging. The TpyrP-bridged metal centers exhibit axial bond lengths of 2.356(17) Å and Mn–N$_{porph}$ lengths of 2.007(18) Å – both of which are consistent with the coordination group distances observed for μ-N-dimers.
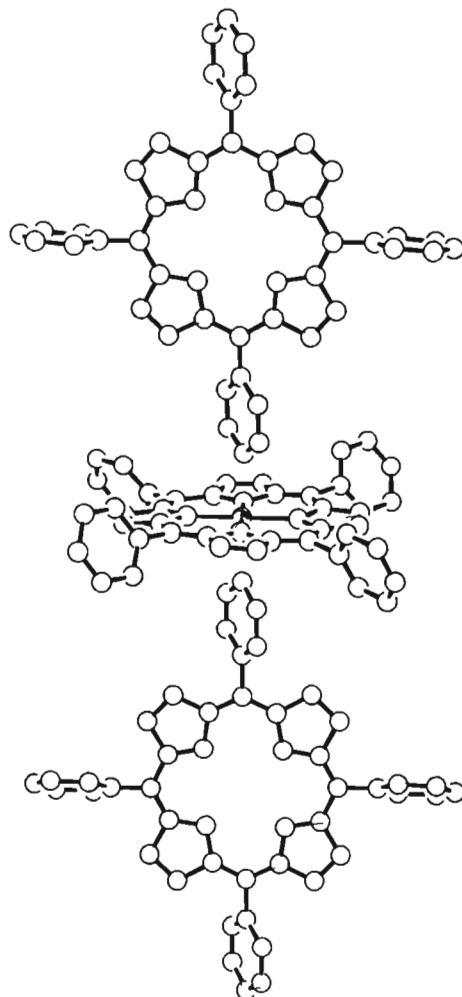
Figure 1.23: SIZSOJ [59].

Showing slightly shorter axial bond lengths are the μ-O-dimerised and polymerized complexes. The formate bridged complexes [61] display axial lengths of 2.189(2) and 2.239(55) Å, with Mn–N$_{porph}$ lengths of 2.015(1) and 1.997(7) Å. The latter bond-type lengths are of average dimension for the typical Mn^{III} complexes thus far. All of the μ-O-dimers are Mn^{III} complexes but for a Mn^{IV} μ-oxo-dimer [60] with N$_3^-$ bound to the outer faces of the metal centers. This complex shows very short axial bond lengths (1.769(26) Å) to the bridging oxygen atom and a very short 1.996(8) Å distance to the azide ligand. The only other azide complex is the Mn^{III} 5-coordinate complex [30] mentioned previously in the N-donor section. In that complex the Mn–N$_3^-$ bond length is 2.045(4) Å, which is substantially longer than this bond in the dimerised

complex.

Two μ-hydroxy-dimers [**63** and **64**] of Mn[III] produce very short (for O-donors) axial bond lengths of 2.012(14) and 2.028(13) Å, and relatively average Mn–N$_{porph}$ lengths of 2.008(1) Å. An example of a μ-hydroxy-dimer is shown in Figure 1.24.
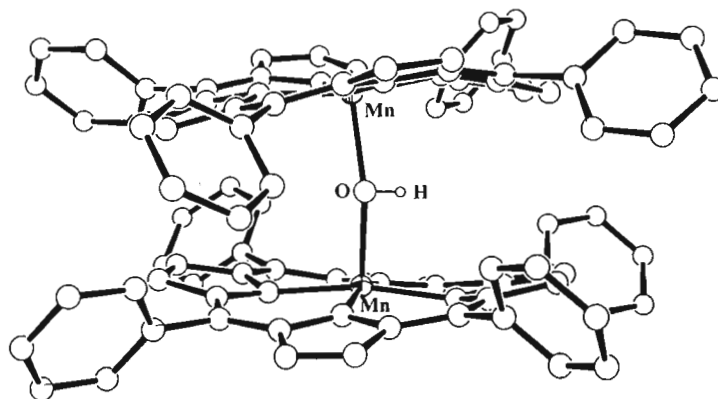
Figure 1.24: ZOVREH [64].

The only sulfur-containing bridging ligand, SO_4^{2-}, produces a dimer [**62**] with axial lengths of 2.004(10) Å, which are once again quite low for an O-donor. The Mn–N$_{porph}$ bond lengths appear to be relatively comparable to most complexes of Mn[III] (2.012(2) Å).

Only two complexes exist with axial ligands bearing an O-donor on one end and an N-donor on the other. The first is a TCNEO-bridged complex [**65**] with a Mn–O length of 2.371 Å, which is long for a Mn[III]–oxygen bond. Interestingly, the Mn–N bond at 2.010 Å is amongst the shorter Mn–N bonds reported thus far for Mn[III] systems. No X-ray coordinates and neither the esd's nor the Mn–N$_{porph}$ lengths were provided for this complex in the publication. The second complex is a [$C_4(CN)_5O^-$]-dimerised Mn[III] system [**66**] with fairly common Mn–N, and Mn–O lengths of 2.313(6) and 2.278(5) Å respectively. The Mn–N$_{porph}$ lengths are the same for every second metal center at 2.022(10) and 2.006(18) Å.

Mixed ligand complexes. All of the mixed ligand complexes are high-spin and are of the +3 oxidation state, but for a low-spin +2 electronic state occurring in a N≡O/4-Mepip complex [**69**] with axial bond lengths of 1.644(5)/2.206(5) Å, and with a Mn–N$_{porph}$ length of 2.027(2) Å. The Mn–NO length matches that of this ligand in the 5-coordinate complex of Mn[II], while the Mn–Mepip length seems consistent with other such secondary amine ligands and does not appear to

22

be out of the ordinary. The Mn–N$_{porph}$ length is somewhat shorter than that expected for Mn^{II} low-spin systems, although there is not a substantial database from which to draw conclusions.

A N$_3^-$/MeOH complex [67] exhibits axial bond lengths of 2.176(9)/2.329(7) Å and a 2.031(10) Å Mn–N$_{porph}$ bond distance. Likewise, an OH$^-$/MeOH complex [73] displays 2.268(7)/2.251(7) Å axial lengths, and a Mn–N$_{porph}$ length of 2.003(9) Å. From these two complexes, the variation in Mn–MeOH bond lengths with the identity of the proximal axial ligand is evident. The Mn–N$_{porph}$ lengths are normal. Another hydroxo complex of OH$^-$/H$_2$O [74] displays Mn–O axial lengths of 2.256(1)/2.344(1) Å, and although the Mn–OH$^-$ length is shorter than in the OH/MeOH complex mentioned above, it is not known which bond length is the more expected value as these are the only two hydroxo complexes of Mn(III) porphyrins. From these two complexes, the variation in Mn–H$_2$O bond lengths with the identity of the proximal ligand is evident. This Mn–H$_2$O length is longer than that observed for both the 5-coordinate and 6-coordinate complexes of Mn^{III}.

Three pyridine-ligated complexes exist, namely py/HCBD [68], py/ClO$_4^-$ [70] and py/Cl$^-$ [71] with axial bond lengths of 2.281(4)/2.507(5), 2.334(1)/2.325(1) and 2.443(1)/2.468(1) Å, respectively. The Mn–py lengths therefore vary between 2.281(4) and 2.443(1) Å. The Mn–N$_{porph}$ lengths for these complexes are 2.009(2), 2.002(12) and 2.010(6) Å, respectively, all of which fall into the common range for Mn^{III} complexes.

A further perchlorato complex displaying axial ligation by acetone/ClO$_4^-$ [72] shows axial bond lengths of 2.357(2)/1.987(1) Å, and a Mn–N$_{porph}$ length of 1.993(8) Å. Thus, the two perchlorate axial bond lengths recorded are 1.987(1) and 2.325(1) Å; these are vastly different. These two results lie on either extreme of the single other axial length to this ligand (2.183(1) Å) recorded in the 5-coordinate Mn^{III} system [18] referred to in the O-donor discussion.

Four-coordinate Manganese porphyrins. Only two structures of 4-coordinate complexes exist, both with Mn^{II}; this lack of variety is presumably as a result of the increased reactivity of the +2 oxidation state and the lack of non-coordinating counter-ions for the +3 oxidation state.

The Mn–N$_{porph}$ lengths are 2.083(2) and 2.097(4) Å for the two complexes of TPP [75] (as shown in Figure 1.25) and TpyrP [76] respectively. These lengths seem significantly long compared to the other Mn^{II} complexes as the metal centers of the 4 coordinate complexes are in

the plane of the porphyrin. It appears a trend that Mn[II] 5-coordinate systems, in contrast, cause a protrusion of the metal from the porphyrin plane and a doming of the macrocycle resulting in longer Mn–N$_{porph}$ lengths.
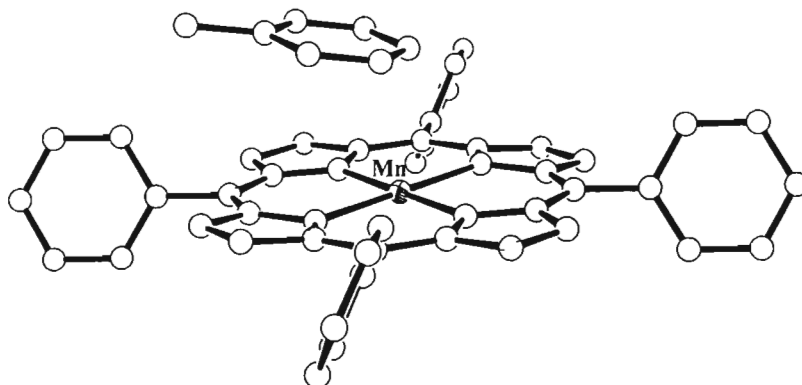
Figure 1.25: TPPMNT01 [75].

Table 1.5: Selected Structural Details of Published Crystal Structures of Mn Porphyrins with O-Donors[a]

No.	Metalloporphyrin	Mn–Ax (Å)	Mn–N$_p$ (Å)	Δ^b (Å)	Conformation[c]	Refcode[d]/[Ref.]
1	[Mn^{IV}(TPP)(OCH$_3$)$_2$][f]	1.839(2)	2.012(19)	In plane	Planar	BOPWAE/[45]
2	[Mn^{III}(OEP)(H$_2$O)]$^+$	2.149(3)	1.996(4)	0.17	Ruf	ZEKTOY/[41]
3	[Mn^{III}(TPP)(H$_2$O)]$^+$	2.105(4)	1.995(5)	0.17	Sad	FAVTOL/[43]
		2.145(4)[e]	1.995(4)	0.18	Ruf	FUWGAF/[16]
4	[Mn^{III}(TPP)(H$_2$O)$_2$]$^+$	2.271(2)	2.004(3)	In plane	Planar	FUWGEJ/[16]
		2.234(1)	2.003(5)	In plane	Sad/Ruf	HAMHEI/[18]
		2.258(1)	2.011(7)	In plane	Planar	ZUTMUW/[14]
		2.227(1)	2.012(3)	In plane	Planar	ZUTNAD/[14]
		2.220(1)	1.998(0)	In plane	Ruf	ZUTNEH/[14]
5	[Mn^{III}(TP$_{Mepyr}$P)(H$_2$O)$_2$]$^{5+}$	2.221(1)	2.012(1)	In plane	Planar	WANGAT/[46]
6	[Mn^{III}(TPP)(HOCH$_3$)$_2$]$^+$	2.261(9)	2.006(2)	In plane	Planar	BUFYOQ/[47]
		2.283(1)	2.002(3)	In plane	Planar	GEBPOS/[48]
7	[Mn^{III}(OEP)(HOCH$_2$CH$_3$)]$^+$	2.145(1)	1.996(4)	0.17	Ruf	ZOZKAA/[49]
8	[Mn^{III}(TPP)(O$_2$)]	1.895(7)	2.184(17)	0.76	Dom	FETJUJ/[50]
9	[Mn^{III}(TPP)(DMF)$_2$]$^+$	2.217(4)	2.010(8)	In plane	Wav	DERZIJ/[51]
10	[Mn^{III}{T(3′, 5′-DHP)P}(THF)$_2$]$^+$	2.320(2)	2.004(2)	In plane	Wav	NIPYEQ/[52]
11	[Mn^{III}(TPP)(CH$_3$COO)]	2.028(5)	2.019(9)	0.29	Sad	GISJAT/[53]

[a] All tabulated complexes are d^4 high-spin unless otherwise stated. [b] Out of plane displacements are deviations from the 24-atom mean plane of the porphyrin core. [c] Ruf = ruffled, wav = wave, dom = domed, sad = saddled. [d] Cambridge Structural Database reference codes. [e] Proximal benzene interaction. [f] d^3 (HS).

Table 1.5 Contd[a].

No.	Metalloporphyrin	Mn–Ax (Å)	Mn–N$_p$ (Å)	Δ^b (Å)	Conformation^c	Refcode^d/[Ref.]
12	[Mn^{III}(TPP)(Lut N-ox)$_2$]$^+$	2.264(4)	1.996(5)	In plane	Ruf	DIBBAR DIBBEV/[54]
13	[Mn^{III}(TPP)(Lut-N-ox)]$^+$	2.282(17)	1.984(9)	0.02	Ruf	DIBBEV10/[55]
14	[Mn^{III}(TPP)]$^+$ [QCl$_4$]$^{\bullet-}$	2.193(4)	2.010(see ref.)	In plane	Disordered	JANJEN/[56]
15	[Mn^{III}(TPP)(DEAPNO)$_2$]$^+$	2.210(1)	2.017(2)	In plane	Planar	PIXFUX/[57]
16	[Mn^{III}(TPP)(NO$_2$)]	2.059(4)	2.012(2)	0.22	Sad	SIYWEC/[58]
17	[Mn^{III}(TPP)(NO$_3$)]	2.101(3)	2.007(7)	0.21	Sad	SIYWAY/[58]
18	[Mn^{III}(OEP)(ClO$_4$)]	2.183(1)	2.000(3)	0.18	Planar	YOWHUN/[59]
19	[Mn^{III}(TPP)(DMSO)$_2$]$^+$	2.219(1)	2.006(7)	In plane	Planar	ZUTNIL/[40]
20	[Mn^{III}(TPP)(HSO$_4$)]	2.078(5)	1.991(6)	0.23	Sad	VIXKAO/[60]

[a] All tabulated complexes are d^4 high-spin. [b] Out of plane displacements are deviations from the 24-atom mean plane of the porphyrin core. [c] Ruf = ruffled, wav = wave, dom = domed, sad = saddled. [d] Cambridge Structural Database reference codes.

Table 1.6: Selected Structural Details of Published Crystal Structures of Mn Porphyrins with N-Donors

No.	Metalloporphyrin	Electron config.[a]	Mn–Ax (Å)	Mn–N$_p$ (Å)	Δ^b (Å)	Conformation[c]	Refcode[d]/[Ref.]
21	$[Mn^V(T(p\text{-}OCH_3)PP)\,(N)]$	d^2 (LS)	1.515(3)	2.003(19)	—	Planar	BORLAV/[61]
22	$[Mn^{IV}(TPP)(N=C=O)_2]$	d^3 (HS)	1.926(3)	1.970(1)	0.01	Ruf	CENRES/[62]
23	$[Mn^{III}(TF_4OMePP)]^+[tcne]^{\cdot-}$	d^4 (HS)	2.302(19)	2.017(1)	In plane	Planar	GOTBEW GOTBEW01/[63]
24	$[Mn^{III}(TIPP)]^+[tcne]^{\cdot-}$	d^4(HS)	2.285(9)	2.011(2)	In plane	Planar	XARCUO XARCOI/[64]
25	$[Mn^{III}(TFPP)]^+[tcne]^{\cdot-}$	d^4(HS)	2.309(12)	2.008(7)	In plane	Planar	SAQHAT/[65]
26	$[Mn^{III}(T(p\text{-}OCH_3)PP)]^+[tcne]^{\cdot-}$	d^4(HS)	2.289(2)	2.012(4)	In plane	Planar	SAQGUM/[35]
27	$[Mn^{III}(TPP)(N=C=O)]$	d^4 (HS)	2.029(1)	2.014(4)	0.34	Sad	GISHIZ/[53]
28	$[Mn^{III}(TPP)(N=C=S)]$	d^4 (HS)	2.070(3)	2.003(9)	0.23	Sad	GISJEX/[53]
29	$[Mn^{III}(TClPP)(Py)]^+$	d^4 (HS)	2.216(8)	2.007(2)	0.21	Sad	QIPPAG/[66]
30	$[Mn^{III}(TPP)(N_3)]$	d^4 (HS)	2.045(4)	2.005(6)	0.18	Ruf	ATPMBZ MNTPPZ10/[67]
31	$[Mn^{II}(TTP)(N\equiv O)]$	d^5 (LS)	1.641(2)	2.004(4)	0.40	Sad	NTPOMN/[68]
32	$[Mn^{II}(TPP)(MeIm)]$	d^5 (HS)	2.192(2)	2.128(3)	0.56	Dom+Sad/Ruf hybrid	MNTPPI10/[69]

[a] HS = high spin, LS = low spin and IS = intermediate spin. [b] Out of plane displacements are deviations from the 24-atom mean plane of the porphyrin core. [c] Ruf = ruffled, wav = wave, dom = domed, sad = saddled.
[d] Cambridge Structural Database reference codes. — No CSD data available and relevant data omitted from publication.

Table 1.7: Selected Structural Details of Published Crystal Structures of Mn Porphyrins with C-Donors

No.	Metalloporphyrin	Electron config.[a]	Mn–Ax (Å)	Mn–N$_p$ (Å)	Δ[b] (Å)	Conformation[c]	Refcode[d]/[Ref.]
33	[Mn^{III}(TPP)(C≡N)]	d^4 (HS)	2.166(6)	2.008(8)	0.25	Sad/Ruf hybrid	BUTVUH/[70]
34	[Mn^{III}(TPP)(C≡N)$_2$]$^-$	d^4 (LS)	2.015(20)	2.000(20)	In plane	Sad/Ruf hybrid	NEXSOY/[71]

Table 1.8: Selected Structural Details of Published Crystal Structures of Mn Porphyrins with Halogen Donors

No.	Metalloporphyrin	Electron config.[a]	Mn–Ax (Å)	Mn–N$_p$ (Å)	Δ[b] (Å)	Conformation[c]	Refcode[d]/[Ref.]
35	[Mn^{III}(DPPF$_{20}$)Cl]	d^4(HS)	2.369(3)	1.990(10)	0.24	Sad/Ruf hybrid	PURXAB/[72]
36	[Mn^{III}(TPP)Cl]	d^4(HS)	2.296(1)	2.002(0)	In plane	Planar	HIFMIS/[73]
		d^4(HS)	2.363(3)	2.009(13)	0.27	Sad/Ruf hybrid	TPPMNA/[74]
		d^4(HS)	2.381(1)	2.009(11)	0.27	Sad/Ruf hybrid	TPPMNA01/[53]
		d^4(HS)	2.345(1)	2.014(15)	0.69	Sad	JUKPIO/[75]
		d^4 (HS)	2.363(—)	—	0.27	—	CLPNMN/[76]
37	[Mn^{III}(TPP)(Cl)]$^+$	d^4 (HS)	2.320(10)	2.00(8)	In plane	Planar	DOJSOK/[77]
38	[Mn^{III}(TMCP)Cl]	d^4(HS)	2.348(9)	1.974(2)	0.44(1)	Highly Ruf	FEZXAJ/[78]
39	[Mn^{II}(TPP)Cl]$^-$	d^5(HS)	2.364(2)	2.160(7)	0.64	Dom	FETJOD/[50]
40	[Mn^{III}(TPP)Br]	d^4(HS)	2.490(1)	2.008(14)	0.67	Sad	GISHOF/[53]
41	[Mn^{III}(TPP)I]	d^4(HS)	2.749(19)	2.011(7)	0.21	Sad/Ruf hybrid	GISHUL/[53]

[a] HS = high spin, LS = low spin and IS = intermediate spin. [b] Out of plane displacements are deviations from the 24-atom mean plane of the porphyrin core. [c] Ruf = ruffled, wav = wave, dom = domed, sad = saddled.
[d] Cambridge Structural Database reference codes. — No CSD data available and relevant data omitted from publication.

Table 1.9: Selected Structural Details of Published Crystal Structures of Mn Porphyrin μ-N-Dimers

No.	Metalloporphyrin	Electron config.[a]	Mn–Ax (Å)	Mn–N$_p$ (Å)	Δ^b (Å)	Conformation[c]	Refcode[d]/[Ref.]
42	μ-(TCNQ)-[Mn^{III}(TMesP)]$_4$	d^4 (HS)	2.271(7)	2.016(4)	In plane	Planar	WARVEQ/[79]
43	μ-(TCNQ)-[Mn^{III}(TMesP)]$_2$	d^4 (HS)	2.331(13)	1.998(2)	In plane	wav	WASDEZ/[80]
44	μ-{(TFTCNQ)-[Mn^{III}(TMeOPP)]}$_n$	d^4 (HS)	2.321(1)	2.003(5)	In plane	Ruf	DORQIK/[81]
45	μ-{(DMTCNQ)-[Mn^{III}(TMesP)]}$_n$	d^4 (HS+LS)	2.332(14)	—	—	—	WASDEZ01/[82]
46	μ-{(TCNE)-[Mn^{III}(TCF$_3$PP)]}$_n$	d^4 (HS)	2.300(6)	2.006(4)	In plane	Wav	NURSUO/[83]
47	μ-{(TCNE)-[Mn^{III}(TBrPP)]}$_n$	d^4 (HS)	2.290(6)	2.008(1)	In plane	Wav	XASHEE/[84]
48	μ-{TCNE-[Mn^{III}(TP'P)]}$_n$	d^4 (HS)	2.299(10)	1.993(5)	In plane	Wav	TAVPUB/[85]
49	μ-{TCNE-[Mn^{III}(TPP)]}$_n$	d^4 (HS)	2.305(4)	1.998(1)	In plane	Planar	YAGJIZ/[86]
50	μ-{TCNE-[Mn^{III}(TClPP)]}$_n$	d^4 (HS)	2.268(1)	2.012(7)	In plane	Wav	VANDOD/[87]
		d^4 (HS)	2.277(1)	2.012(2)	In plane	Wav	VANFAR/[87]
51	μ-{TCNE-[Mn^{III}(OEP)]}$_n$	d^4 (HS	2.440(79)	1.997(7)	0.0350	Ruf	ZUFQEW/[88]
52	μ-{(HCPD)-[Mn^{III}(TBpP)]}$_n$	d^4 (HS)	2.323(3)	2.012(6)	In plane	Planar	NURSOI/[89]
53	μ-{HCBD-[Mn^{III}(TBrPP)]}$_n$	d^4 (HS)	2.315(8)	1.998(6)	In plane	Planar	QIPPIO/[66]
54	μ-{HCBD-[Mn^{III}(TtBuPP)]}$_n$	d^4 (HS)	2.353(1)	2.007(3)	In plane	Slight wav	REVKAE/[90]
55	μ-{HCBD-[Mn^{III}(OEP)]}$_n$	d^4 (HS	2.420(1)	2.004(2)	In plane	Planar	ZUFQIA/[88]
56	μ-{[C$_3$(CN)$_5$]-[Mn^{III}(TPP)]}$_n$	d^4 (HS)	2.352(1)	1.976(10)	0.0169	Ruf	PURTIF/[91]
57	μ-{(bipy)-[Mn^{III}(TPP)]$^+$}$_n$	d^4 (HS)	2.364(43)	2.011(2)	0.121(6)	Sad	PIKKID/[92]
58	μ-{(Im)-[Mn^{III}(TPP)]}$_n$	d^4 (HS+LS)	2.228(47)	2.015(3)	In plane	Sad/Ruf hybrid	IMTPMN/[93] IMTPMN10/[94]
59	μ-TpyrP-{[Mn^{III}(TPP)]$^+$}$_4$	d^4 (HS)	2.356(17)	2.007(18)	Mn1: 0.02 Mn2 & Mn3 in plane	Ruf	SIZSOJ/[95]

[a] HS = high spin, LS = low spin and IS = intermediate spin. [b] Out of plane displacements are deviations from the 24-atom mean plane of the porphyrin core. [c] Ruf = ruffled, wav = wave, dom = domed, sad = saddled.
[d] Cambridge Structural Database reference codes. — No CSD data available and relevant data omitted from publication.

Table 1.10: Selected Structural Details of Published Crystal Structures of Mn Porphyrin μ-O-Dimers

No.	Metalloporphyrin	Electron config.[a]	Mn–Ax (Å)	Mn–N$_p$ (Å)	Δ^b (Å)	Conformation[c]	Refcode[d]/[Ref.]
60	μ-{(O)-[Mn^{IV}(TPP)(N$_3$)]}$_2$	d^3 (HS)	Mn–[N$_3$]$^-$: 1.996(8) Mn–O: 1.769(26)	2.014(19)	0.09 ($\rightarrow$ O)	Sad/Ruf hybrid	BAHZAL/[96] BAHZAL10/[97]
61	μ-{(OCHO)-[Mn^{III}(TPP)]}$_n$	d^4 (HS)	2.189(2)	2.015(1)	In plane	Planar	KUKJOP/[98]
		d^4 (HS)	2.239(55)	1.997(7)	Mn1: 0.05 Mn2: In plane	Altern. Ruf/Wav	KUKJUV/[98]
62	μ-{(SO$_4$)-[Mn^{III}(TPP)]}$_2$	d^4 (HS)	2.004(10)	2.012(2)	0.20(1)	Sad	VIXKES/[60]
63	μ-{(OH)-[Mn^{III}(OEP)]$_2$}$^+$	d^4 (HS)	2.012(14)	2.007(1)	0.17	Ruf	ZEKTUE/[41]
64	μ-{(OH)-[Mn^{III}(TPP)]$_2$}$^+$	d^4 (HS)	2.028(13)	2.008(1)	0.20	Sad	ZOVREH/[99]

Table 1.11: Selected Structural Details of Published Crystal Structures of Mn Porphyrin μ-O/N-Dimers

No.	Metalloporphyrin	Electron config.[a]	Mn–Ax (Å)	Mn–N$_p$ (Å)	Δ^b (Å)	Conformation[c]	Refcode[d]/[Ref.]
65	μ-{(TCNEO)-[Mn^{III}(T(p-OCH$_3$)PP)]}$_n$	d^4 (HS)	Mn–O: 2.371(—) Mn–N: 2.010(—)	—	In plane	—	ZUGCUZ/[100]
66	μ-{[C$_4$(CN)$_5$O]-[Mn^{III}(TClPP)]}$_n$	d^4 (HS)	Mn–N: 2.313(6) Mn–O: 2.278(5)	Mn1: 2.022(10) Mn2: 2.006(18)	In plane	Mn1: Wav Mn2: Planar	QIPPOU/[66]

[a] HS = high spin, LS = low spin and IS = intermediate spin. [b] Out of plane displacements are deviations from the 24-atom mean plane of the porphyrin core. [c] Ruf = ruffled, wav = wave, dom = domed, sad = saddled.

[d] Cambridge Structural Database reference codes. — No CSD data available and relevant data omitted from publication.

Table 1.12: Selected Structural Details of Published Crystal Structures of Mn Porphyrins with Mixed Donors

No.	Metalloporphyrin	Electron config.[a]	Mn–Ax (Å)	Mn–N$_p$ (Å)	Δ[b] (Å)	Conformation[c]	Refcode[d]/[Ref.]
67	[Mn^{III}(TPP)(N$_3$)(HOCH$_3$)]	d^4 (HS)	Mn–N: 2.176(9) Mn–O: 2.329(7)	2.031(10)	0.09(→N)	Planar	MNTPAM10/[101]
68	[Mn^{III}(TClPP)(Py)(HCBD)]	d^4 (HS)	Mn–HCBD: 2.507(5) Mn–Py: 2.281(4)	2.009(2)	0.07	Sad	QIPPEK/[66]
69	[Mn^{II}(TPP)(N≡O)(4-Mepip)]	d^5 (LS)	Mn–NO: 1.644(5) Mn–Mepip: 2.206(5)	2.027(2)	0.08 (→ NO)	Sad	NTPIPM10/[68]
70	[Mn^{III}(TPP)(Py)(ClO$_4$)]	d^4 (HS)	Mn–N: 2.334(1) Mn–O: 2.325(1)	2.002(12)	0.03	Planar	ZUTMIK/[40]
71	[Mn^{III}(TPP)(Py)(Cl)	d^4 (HS)	Mn–N: 2.443(1) Mn–Cl: 2.468(1)	2.010(6)	0.93	Sad/Ruf hybrid	CTPMNP/[102]
72	[Mn^{III}(TPP)(Acetone)(ClO$_4$)]	d^4 (HS)	Mn–Acetone: 2.357(2) Mn–ClO$_4$: 1.987(1)	1.993(8)	0.01	Sad/Ruf hybrid	ZUTMOQ/[40]
73	[Mn^{III}(P*)(OH)(HOCH$_3$)]	d^4 (HS)	Mn–OH: 2.268(7) Mn–OHCH$_3$: 2.251(7)	2.003(9)	0.06	Ruf	PAQBAK/[103]
74	[Mn^{III}(TPP)(H$_2$O)(OH)]	d^4 (HS)	Mn–OH: 2.256(1) Mn–H$_2$O: 2.344(1)	2.012(15)	0.02	Sad	SUDVUI/[104]

[a] HS = high spin, LS = low spin and IS = intermediate spin. [b] Out of plane displacements are deviations from the 24-atom mean plane of the porphyrin core. [c] Ruf = ruffled, wav = wave, dom = domed, sad = saddled.
[d] Cambridge Structural Database reference codes.

Table 1.13: Selected Structural Details of Published Crystal Structures of 4-Coordinate Mn Porphyrins

No.	Metalloporphyrin	Electron config.[a]	Mn–Ax (Å)	Mn–N$_p$ (Å)	Δ[b] (Å)	Conformation[c]	Refcode[d]/|Ref.|
75	[Mn^{II}(TPP)]	d^5 (HS)	NA (toluene solvate at 2.299)	2.083(2)	In plane	Wav	TPPMNT01 TPPMNT10/[105]
76	[Mn^{II}(TPyrP)]	d^5 (HS)	NA	2.097(4)	In plane	Wav	CAYSOK CAYYEG/[106]

[a] HS = high spin, LS = low spin and IS = intermediate spin. [b] Out of plane displacements are deviations from the 24- atom mean plane of the porphyrin core. [c] Ruf = ruffled, wav = wave, dom = domed, sad = saddled.
[d] Cambridge Structural Database reference codes.

1.3.3 Cobalt Porphyrins

A literature survey of the cobalt porphyrins crystallized to date reveals a significantly lower percentage of O-donor complexes (Table 1.16) and an increase in the number of four-coordinate complexes (Table 1.21). The number of carbon donor complexes (Table 1.15) is more varied to include alkyl groups. Also reflected in this literature survey is the relative affinity that manganese has over cobalt in the formation of O-donor complexes, as the number of O-donor complexes of cobalt is significanly lower. The number of N-donor complexes (Table 1.17) is relatively similar to that of manganese with a very similar range of donors used. Another noteworthy point is the lack of halogen-donor complexes with only one such structure in the database (excluding mixed ligand species). The non-C/N/O-donor complexes have been tabulated in Table 1.19 and the mixed donor complexes in Table 1.20. The extracted and averaged bond lengths for each class of donor atom are tabulated below in Table 1.14.

Table 1.14: Summary of Bond Length Ranges For Cobalt Porphyrins[a]

Bond	Co–L_{ax} Range	Co–N_{porph} Range
Co^{II}–O	2.204–2.231	1.953–2.068
Co^{III}–O	1.933–1.936	1.916–1.964
Co^{III}–C	1.960–2.027	1.935–1.996
Co^{II}–N	1.833–2.386	1.960–1.992
Co^{III}–N	1.827–2.436	1.945–1.987
Co^{II}–S	2.497	1.969
Co^{III}–S	2.343	1.975
Co^{III}–Cl	2.149	1.985
Co^{0} (4 coord)	NA	1.971
Co^{I} (4 coord)	NA	1.942
Co^{II} (4 coord)	NA	1.929–1.986

[a] Mixed ligand complexes and esd's excluded. All complexes are five- and six-coordinate coordinate unless otherwise stated.

Cobalt porphyrins with axial C-donor ligands. As mentioned above, there are a slightly increased variety of C-donors with cobalt than with manganese. Where manganese C-donor complexes are limited to cyanide, the range with cobalt includes alkyl groups, i.e., methyl and ethyl groups, as well as acetone and formylmethyl ligands.

All the C-donor complexes are Co^{III} low-spin complexes, and the only 6-coordinate complex is the bis (cyano) system [81] shown in Figure 1.26. This complex displays an axial bond length of

1.960(20) Å and a Co–N$_{porph}$ distance of 1.935(7) Å. The axial bond lengths and Co–N$_{porph}$ distances are substantially shorter than that of the equivalent Mn^{III} system. This is due, in part, to the low-spin state of the Co^{III} center and the lack of electron density in the d$_{z^2}$ orbital. Also noticeable is the strongly ruffled conformation of the porphyrin core
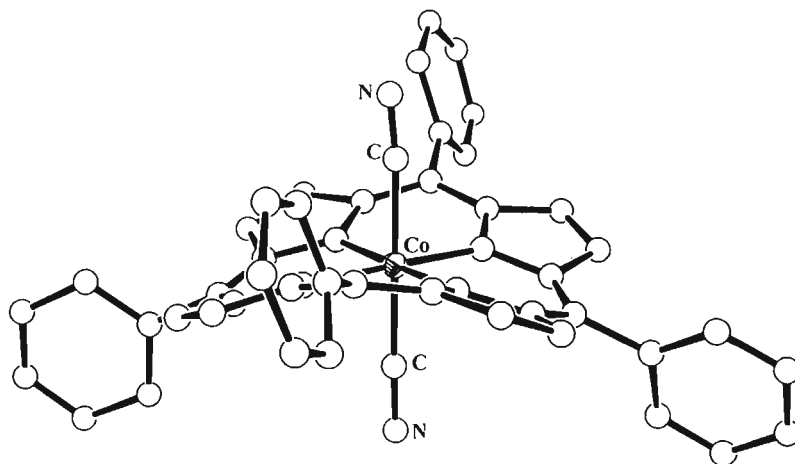
Figure 1.26: QOBXUA [81]

Two 5-coordinate complexes of acetone [77] and formylmethyl [78] produce axial bond lengths of 2.027(1) and 1.976(2) Å; the Co–N$_{porph}$ distances are 1.948(3) and 1.968(29) Å, respectively.

Two 5-coordinate alkyl complexes of methyl [79] and ethyl [80] ligands exist and have axial bond lengths of 1.976(2) and 1.988(2) Å, respectively, which are similar to those of the formylmethyl complex. These complexes are shown in Figures 1.27 and 1.28, respectively. These two derivatives exhibit Co–N$_{porph}$ lengths of 1.996(14) and 1.970(8) Å, respectively. The methyl complex shows an unusually long Co–N$_{porph}$ length compared to the other C-donor complexes.
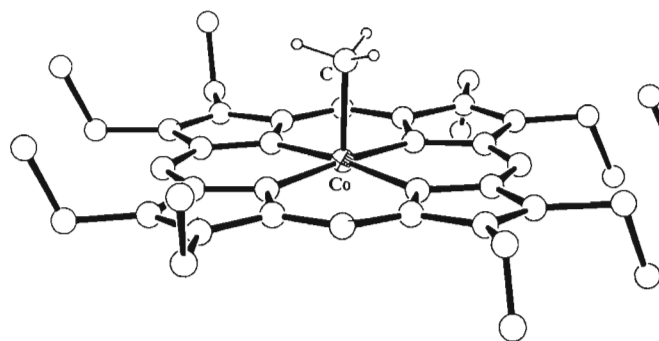
Figure 1.27: LIBCAA [79]   **Figure 1.28: ROQBEE [80]**
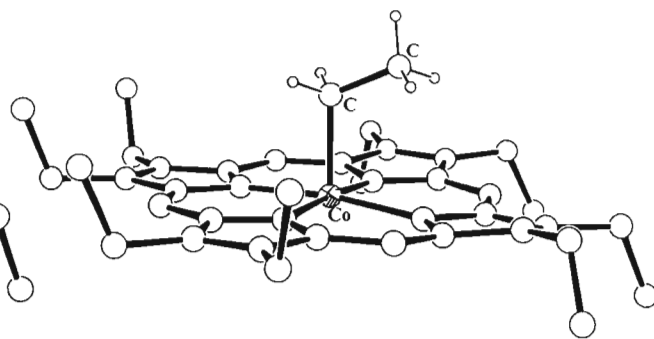
Cobalt porphyrins with axial O-donor ligands. A fairly limited array of O-donor complexes exists with only four examples, i.e., aqua, methanol and THF complexes, completing the entire range.

For Co^{II}, a 5-coordinate methanol complex [82] (shown in Figure 1.29) and a 6-coordinate bis(THF) complex [83] have been structurally characterized. The Co–O distances are 2.231(1) and 2.204(2) Å, respectively. The Co–N_{porph} lengths are significantly different at 1.953(3) and 2.068(4) Å, and apparently the dimensions of the bis(THF) complex indicate a high-spin configuration. $F_{28}TPP$ is known to be an electron-deficient σ-donor. Weak σ-donation from the porphyrin coupled with a weak axial ligand field from two THF ligands favours a high-spin state in this derivative.
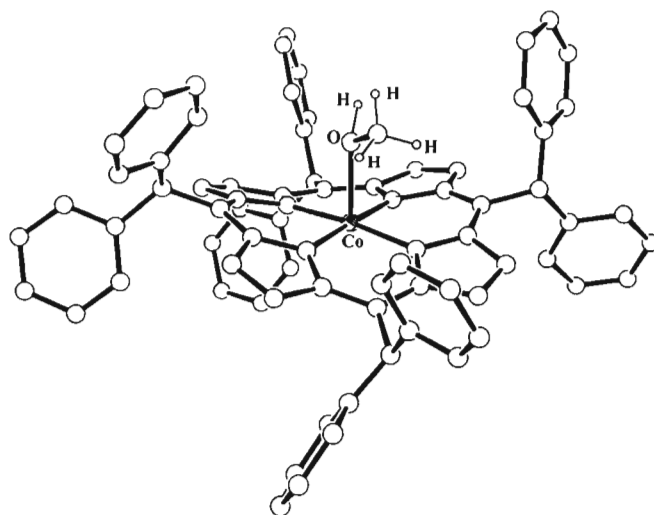
Figure 1.29: GOHJAO [82]

Two aqua complexes [85 and 86] exist with Co^{III} low-spin metal centers; both are 6-coordinate.

35

The axial bond lengths are similar at 1.936(5) and 1.933(4) Å. The Co–N_{porph} lengths do differ, however, at 1.964(4) and 1.916(4) Å. These axial and Co–N_{porph} lengths are significantly shorter than the equivalent complexes with Mn^{III}, which is consistent with the smaller ionic radius of the Co^{III} ion.

A 5-coordinate Co^{II} complex with axial trinitrobenzene [84] has an axial bond distance of 2.327(esd omitted from publication) Å, and a mean Co–N_{porph} distance of 1.968(4) Å. This is the longest of the O-donor axial lengths which probably reflects the fact that this is the bulkiest O-donor ligand in the series. The long Co–N_{porph} mean distance is due to 5-coordination and the out of plane location of the metal.

Cobalt porphyrins with axial N-donor ligands. The N-donor complexes of cobalt are mostly derivatives of the imidazole- and NO-type. Ten amine complexes have been structurally characterised and considering the vast array of amines available, there is certainly scope for research into this field.

One imidazole [107] and four 1-methylimidazole [87–89 and 99] complexes exist with Co – with the three 5-coordinate 1-methylimidazole complexes are Co^{II} derivatives. The range of axial bond lengths for these 5-coordinate 1-methylimidazole complexes is 2.132(3)–2.157(3) Å; the Co–N_{porph} lengths span the range 1.960(10)–1.986(5) Å. An example of 5-coordinate [Co(TPP)(1-MeIm)] is shown in Figure 1.30.
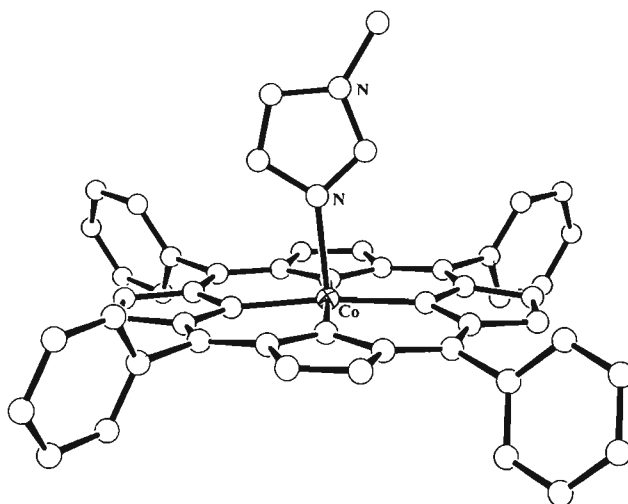
Figure 1.30: IMTPCO [87]

The 6-coordinate 1-methylimidazole complex [99] of Co^{III} displays a unique axial bond length of 1.942(6) Å and a mean $Co-N_{porph}$ distance of 1.977(5) Å. Although the $Co-N_{porph}$ bond lengths are comparable to those of Co^{II}, in this complex the axial bond lengths are far shorter than those of Co^{II}, which is expected as the Co^{II} state includes the occupation of the d_{z^2} orbital, forcing longer axial distances. The 6-coordinate imidazole complex [107] displays an axial bond length of 1.942(22) Å and a $Co-N_{porph}$ length of 1.935(3) Å. This axial bond length resembles that of the 6-coordinate 1-methylimidazole complex although the $Co-N_{porph}$ lengths in the imidazole complex are somewhat shorter.

The Co(II) complexes of phenethylamine [90], DMAP [91], 6-coordinate 3-picoline [92] and pyridine [93] exhibit axial bond lengths of 2.265(1), 2.191(2), 2.386(2) and 2.203(3) Å, respectively, with mean $Co-N_{porph}$ lengths of 1.992(5), 1.982(2), 1.992(1) and 1.988(3) Å, respectively. These axial lengths are distinctly greater than those of imidazole and methylimidazole and are once again characteristic of a longer Co^{II} bond length. The $Co^{II}-N_{porph}$ bond lengths appear to be similar to those of the Co^{III} N-donor systems, which may be explained by the fact that the $d_{x^2-y^2}$ orbital is not populated in either case.

One 5-coordinate NO complex of $[Co^{II}(TPP)]$ has been characterised [94]; the mean $Co-N_{ax}$ bond length is 1.833(53) Å and the mean $Co-N_{porph}$ length is 1.978(4) Å. One NO complex of $[Co^{II}(TPPBr_4NO_2)]$ is known [95]; the axial bond length is 1.827(21) and the mean $Co-N_{porph}$ length is 1.945(23)Å. Two 5-coordinate NO complexes of $[Co^{II}(OEP]$ have also been characterised and display a mean axial length of 1.844(2) Å and a mean $Co-N_{porph}$ length of 1.985(7) Å. There does not appear to be a noticeable trend in the bond lengths of these complexes. However, these are noticeably shorter axial lengths than the other N-donor complexes, as well as O-donor and C-donor complexes.

A single 5-coordinate NO_2 complex [97] exists with an axial bond length of 1.854(5) Å and a mean $Co-N_{porph}$ distance of 1.983(146) Å. This axial bond length is noticeably longer than the NO complexes yet still remains amongst the shorter of the Co-ligand axial bonds.

A mixed ligand NO_2/lutidine complex [98], shown in Figure 1.31, displays axial bond lengths of 1.948(1)/2.038(1) Å and a mean $Co-N_{porph}$ length of 1.953(7) Å. The slightly shorter than average $Co-N_{porph}$ length for this system reflects S_4-ruffling of the porphyrin core and contraction of the metal-binding cavity of the macrocycle.
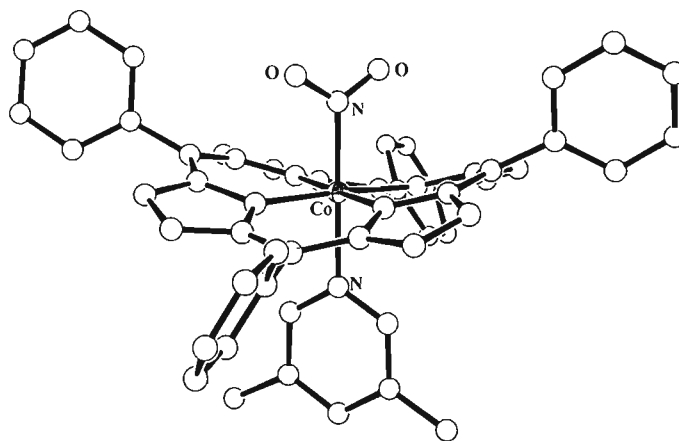
Figure 1.31: NTPOLC [98]

Six-coordinate complexes of prolinol [100], piperidine [101], 2-butylamine [102] and 1-methylpiperazine [106] display Co–N_{ax} distances of 2.049(3), 2.436(2), 2.004(19) and 2.040(1) Å, respectively, and mean Co – N_{porph} distances of 1.954(2), 1.987(2), 1.949(8) and 1.985(13) Å, respectively. The bis(piperidine) complex has a planar core conformation, while the prolinol complex shows S_4-ruffling and thus compressed Co–N_{porph} distances. The 1-methylpiperazine complex displays a hybrid sad/ruf conformation. The long Co–N_{ax} bonds in the bis(piperidine) system reflect the fact that the 2° amine is sterically hindered and that there is no core distortion to alleviate porphyrin–ligand steric interactions.

6-Coordinate 1° amine complexes of 1-butylamine [103], benzylamine [104] and phenethylamine [105] display Co–N_{ax} distances of 1.980(2), 1.983(2) and 1.978(8) Å, respectively. The mean Co–N_{porph} distances are 1.987(4), 1.987(4) and 1.986(3) Å, respectively. As can be expected, these axial bond lengths are substantially shorter and consisitent than those observed for the sterically hindered 2° amines.

Other donors. Two sulfur, one tin, and an anionic phosphorus-bound phosphorane form the limit of the non-C/N/O donor complexes.

Two axial sulfur-coordinated complexes exist, one of which is a 5-coordinate Co^{II} system, shown in Figure 1.32, with an axial F_4BzS [108] which shows an axial bond length of 2.497(1) Å and a mean Co–N_{porph} distance of 1.969(17) Å. This relatively long axial bond length reflects the fact that sulfur, compared to oxygen, carbon and nitrogen, and Co(II), compared to Co(III), have relatively large ionic radii. The mean Co–N_{porph} bond length is once again indicative of the Co^{II} center.

38

The second sulfur complex is of a 6-coordinate Co^{III} system with the same axial ligand [109], which displays an axial bond length of 2.343(7) Å and a mean Co–N$_{porph}$ length of 1.975(1) Å. The difference in the Co–S$_{ax}$ distances of the two complexes is readily explained by the Co^{II} and Co^{III} electronic state of each metal center. The Co–N$_{porph}$ distances are equivalent within the error limits of the experiment even though the metal is displaced out of the porphyrin mean plane in the 5-coordinate complex.
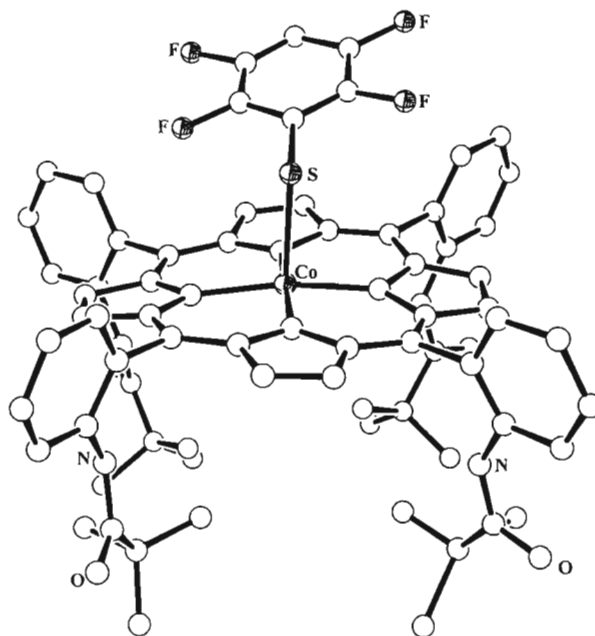
Figure 1.32: FOLWIM [108]

Two porphyrin-dimerised complexes exist with *meso*-substituted pyridine (N-donor) [110] and nitro (O-donor) [111] functionalities. These coordinating functionalities form dimers with axial bond lengths of 2.292(5) and 2.423(5) Å, respectively. The Co–N$_{porph}$ bond lengths are 1.994(5) and 1.964(5) Å. Both of these complexes contain Co(II). The significantly different Co–N$_{porph}$ distances reflect the differences in the porphyrin core conformations, i.e., wave *versus* saddled. The axial bond length for the tetrapyridyl complex is substantially longer than that of the single 5-coordinate Co^{II} pyridine complex mentioned in the N-donor discussion. The axial bond length of the nitro-functionalised complex cannot be compared to the nitro-coordinated complex referred to in the N-donor discussion as the nitro group is O-bound in this case.

The only reported halide derivative is that of a 5-coordinate chloro Co(III) complex [112] with an axial Co–Cl distance of 2.149(6) Å and a mean Co–N$_{porph}$ length of 1.985(9) Å. These axial and Co–N$_{porph}$ bond lengths are of relatively moderate dimension and are typical of the low-spin

Co^{III} metal center, even though the complex is 5-coordinate.

Figure 1.33 shows a tin-donor in the form of $SnPh_3$ bound in a Co^{III} complex [113]. This complex displays a very long axial bond length of 2.510(2) Å and a mean $Co-N_{porph}$ length of 1.966(5) Å. This is by far the longest of all the axial bond lengths for cobalt in this survey, and is long even when compared to Co^{II} bond-length records. The large size of the Sn donor atom clearly leads to the exceptional bond length in this case.
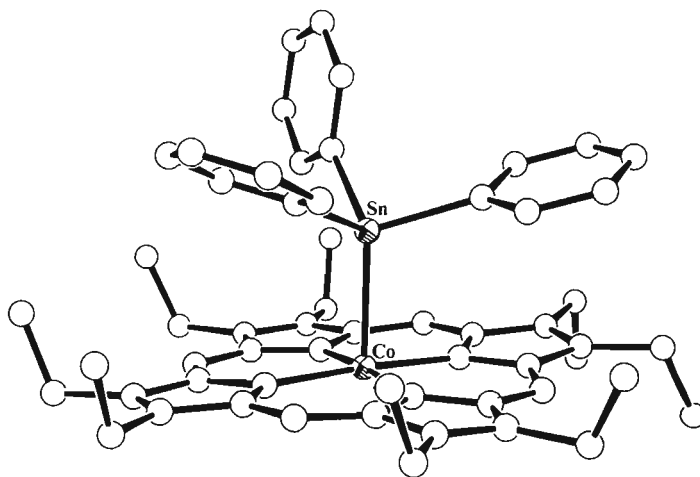
Figure 1.33: GIZTIS [113]

The only reported phosphine containing structure is that of a single $PO(NMe_2)_2$ [114] bound to Co^{III} to produce an axial bond length of 2.265(1) Å and a mean $Co-N_{porph}$ length of 1.972(4) Å. This complex is shown in Figure 1.34.
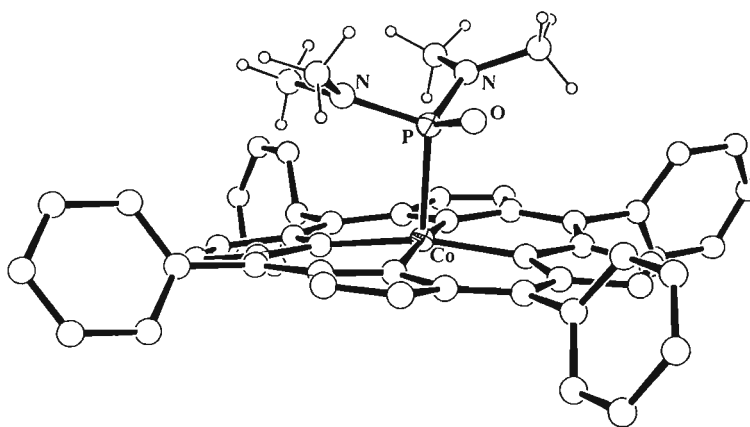
Figure 1.34: ZONQOI [114]

Mixed ligand complexes. All but one of the mixed ligand systems are Co^{III} complexes and most

have at least one nitrogen donor. The Co^{II} complex [115] bears F_4BzS/O_2 axial ligands with axial bonds of 2.363(1)/1.917(1) Å and a mean $Co–N_{porph}$ length of 1.968(11) Å. This Co–S bond length is comparable to the 6-coordinate complex of this ligand even though there is a difference in the oxidation state of the metal.

Four NO_2^- containing complexes exist with the axial ligand combinations MeIm/NO_2 [116], diMeIm/NO_2 [117], pip/NO_2 [119] and H_2O/NO_2 [123]. These complexes have axial bond lengths of 1.995(4)/1.898(4), 2.091(4)/1.917(4), 2.044(10)/1.897(11) and 1.963(1)/1.963(1) Å, respectively, and mean $Co–N_{porph}$ lengths of 1.964(5), 1.983(1), 1.953(4) and 1.982(1) Å, respectively. The last complex is disordered, as explained in the original work. Of these four complexes the H_2O/NO_2 complex shows the longest $Co–NO_2$ length and the pip/NO_2 complex shows the shortest $Co–NO_2$ length. However, the former complex cannot be commented on in depth owing to the uncertainty in the coordination distances resulting from the disorder in this structure. With respect to the MeIm/NO_2 and diMeIm/NO_2 complexes, the $Co–NO_2$ lengths are longer for the latter as there is a more exaggerated out-of-plane displacement of the metal in this complex away from the NO_2^- ion to the opposing ligand. All of these $Co–NO_2$ lengths are longer than the equivalent bond in the single 5-coordinate NO_2^- complex discussed under the N-donors.

A methyl/pyridine [118] complex displays axial bond lengths of 2.018(12)/2.214(9) Å and a mean $Co–N_{porph}$ bond distance of 1.983(19) Å. The Co–C bond length is longer for this complex than the distance reported for the 5-coordinate methyl complex (discussed under the C-donors), and, as for the $Co–N_{py}$ length, the axial Co–N distance is longer in this complex than it is in the 5-coordinate pyridine system discussed under the N-donors, due to 6-coordination of the metal, which requires placement of the metal ion more or less in the porphyrin plane.
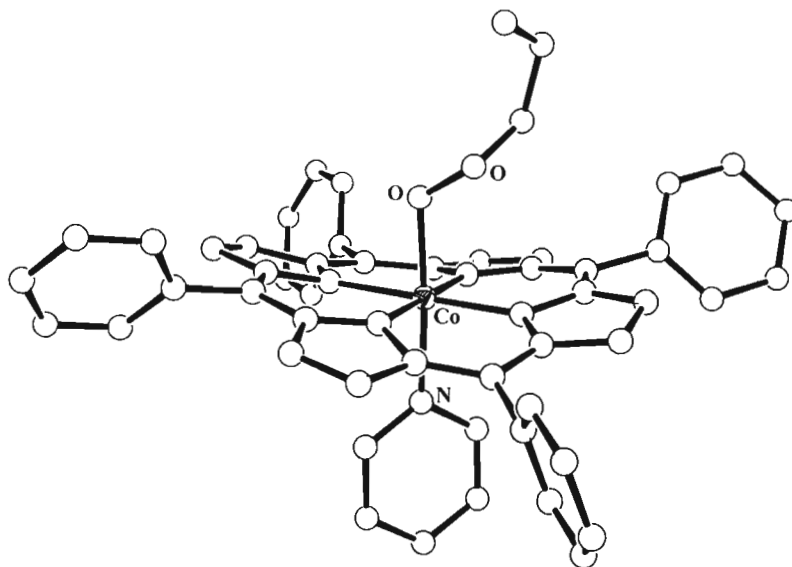
Figure 1.35: KEBMIN [120]

The only recorded peroxy ligand with cobalt exists in the form of an allylperoxy/pyridine complex [120], shown in Figure 1.35, with axial bond lengths of 1.920(10)/2.040(80) Å and a mean Co–N_{porph} length of 1.988(13) Å. This Co–N_{py} bond length is distinctly shorter than that of the equivalent bond in the methyl/pyridine complex mentioned above, which is interesting as both complexes have metal centers in the plane of the porphyrin. This short Co–N_{py} distance is consistent with the S_4-ruffled porphyrin core conformation in [120] since this allows bulky axial ligands to more closely approach the metal.

There are two mixed ligand chloro Co(III) complexes with ethanol/Cl^- [121] and H_2O/Cl^- [122] as the axial ligands. The axial bond lengths for both are 2.048(8)/2.211(3) and 1.979(3)/2.216(1) Å, respectively. The Co–Cl lengths are substantially longer than the equivalent bond in the 5-coordinate chloride complex discussed in the 'other'-donor section above, which is quite surprising since the metal centers of both mixed-ligand complexes are out of the porphyrin plane towards the axial chloride ion. The Co–O length in the aqua complex is slightly longer than the equivalent bond in the bis(aqua) complexes discussed in the O-donor section above. This is due, as mentioned above, to the out-of-plane position of the metal towards the trans Cl^- ion.

4-Coordinate species. The relatively large abundance of 4-coordinate species, mostly of the Co(II) oxidation state demonstrates the relatively stable nature of the Co^{II} ion.

The single Co⁰ complex [124], shown in Figure 1.36, displays a mean Co–N$_{porph}$ length of 1.971(3) Å. The single Co^I complex [125] shows a slightly shorter Co–N$_{porph}$ length of 1.942(3) Å.
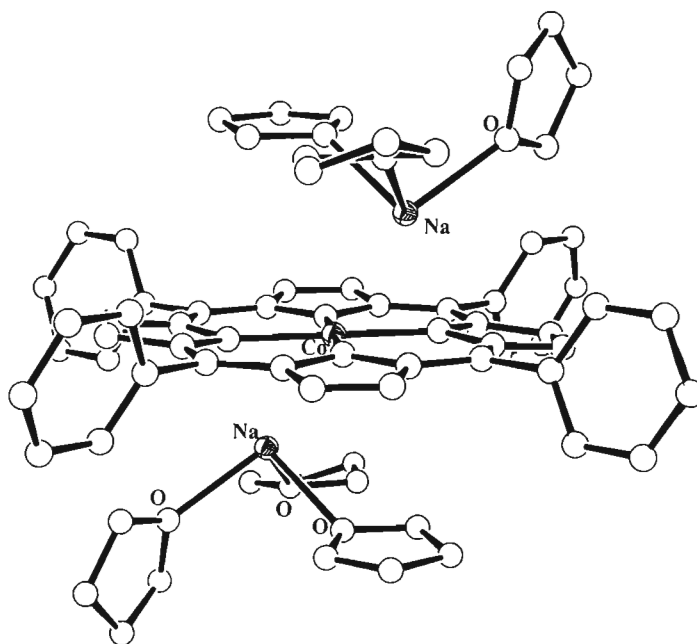
Figure 1.36: FAGCIZ [124]

The remaining 4-coordinate complexes [126–136] all vary in their Co–N$_{porph}$ lengths from 1.929(3) to1.986(2) Å. Amongst these Co^{II} 4-coordinate complexes are a few interesting cases of solvate molecules coordinating at lengths of 3.05 Å for a toluene solvate [133] to 3.28 Å for a benzene solvate [130]. The vast majority of these complexes have in-plane metal centers and almost half show conformational distortions away from planarity.

Table 1.15: Selected Structural Details of Published Crystal Structures of Cobalt Porphyrins with C-Donors

No.	Metalloporphyrin	Electron config.[a]	Co–Ax (Å)	Co–N$_p$ (Å)	Δ^b (Å)	Conformation[c]	Refcode[d]/[Ref.]
77	[Co^{III}(TPP)(acetonyl)]	d^6(LS)	2.027(1)	1.948(3)	0.17	Sad	ACPORC/[107]
78	[Co^{III}(TPP)(formylmethyl)]	d^6(LS)	1.976(2)	1.968(29)	0.10	Planar	COTWEN/[108]
79	[Co^{III}(OEP)(CH$_3$)]	d^6(LS)	1.976(6)	1.996(14)	0.08	Planar	LIBCAA/[109]
80	[Co^{III}(OEP)(CH$_2$CH$_3$)]	d^6(LS)	1.988(2)	1.970(8)	0.06	Sad	ROQBEE/[110]
81	[Co^{III}(TPP)(C≡N)$_2$]$^-$	d^6(LS)	1.960(20)	1.935(7)	In plane	Ruf	QOBXUA/[111]

Table1.16: Selected Structural Details of Published Crystal Structures of Cobalt Porphyrins with O-Donors

No.	Metalloporphyrin	Electron config.[a]	Co–Ax (Å)	Co–N$_p$ (Å)	Δ^b (Å)	Conformation[c]	Refcode[d]/[Ref.]
82	[Co^{II}(TDPMP)(HOCH$_3$)]	d^7 (LS)	2.231(1)	1.953(3)	0.11	Ruf	GOHJAO/[112]
83	[Co^{II}(F$_{28}$TPP)(THF)$_2$]	d^7 (HS)	2.204(2)	2.068(4)	In plane	Planar	HEQZIM/[113]
84	[Co^{II}(TPP)(TNB)]	d^7 (LS)	2.327(—)	1.968(4)	—	Ruf	HAVPEZ/[114]
85	[Co^{III}(TPP)(H$_2$O)$_2$]$^+$	d^6 (LS)	1.936(5)	1.964(4)	0.01	Ruf	BEKPIQ/[115]
86	[Co^{III}(TMcP)(H$_2$O)$_2$]$^+$	d^6 (LS)	1.933(4)	1.916(4)	0.01	Ruf	WIDZAK/[116]

[a] HS = high spin, LS = low spin and IS = intermediate spin. [b] Out of plane displacements are deviations from the 24-atom mean plane of the porphyrin core. [c] Ruf = ruffled, wav = wave, dom = domed, sad = saddled. [d] Cambridge Structural Database reference codes. — No CSD data available and relevant data omitted from publication.

Table 1.17: **Selected Structural Details of Published Crystal Structures of Cobalt Porphyrins with N-Donors**

No.	Metalloporphyrin	Electron config.[a]	Co–Ax (Å)	Co–N_p (Å)	Δ^b (Å)	Conformation[c]	Refcode[d]/[Ref.]
87	[Co^{II}(TPP)(MeIm)]	d^7 (LS)	2.157(3)	1.977(3)	0.14	Ruf	IMTPCO IMTPCO01/[117]
88	[Co^{II}(OC$_2$OPor)(MeIm)]	d^7 (LS)	2.132(3)	1.986(5)	0.13	Sad	WOTBEM/[118]
89	[Co^{II}(OEP)(MeIm)]	d^7 (LS)	2.150(10)	1.960(10)	0.16	Planar	OEPCOI10/[119]
90	[Co^{II}(TPP)(Phenethylamine)]	d^7 (LS)	2.265(1)	1.992(5)	0.06	Planar	HAMBAY/[120]
91	[Co^{II}(OEP)(DMAP)]	d^7 (LS)	2.191(2)	1.982(2)	0.16	Ruf	LIBBUT/[121]
92	[Co^{II}(OEP)(3-pic)$_2$]	d^7 (LS)	2.386(2)	1.992(1)	In plane	Planar	OEPCOP/[122]
93	[Co^{II}(OEPOH)(Py)]	d^7 (LS)	2.203(3)	1.988(3)	0.15	Planar	PIBNUJ/[123]
94	[Co^{II}(TPP)(NO)]	d^7 (LS)	1.833(53)	1.978(4)	0.10	—	NTPPCO/[124]
95	[Co^{II}(TPPBr$_4$NO$_2$)(NO)]	d^7 (LS)	1.827(21)	1.945(23)	0.21	Sad	CONQOL/[125]
96	[Co^{II}(OEP)(NO)]	d^7 (LS)	1.844(2)	1.985(7)	0.15	Planar	NEYCAV01/[126]
		d^7 (LS)	1.844(1)	1.984(8)	0.16	Planar	NEYCAV/[127]
97	[Co^{III}{T(p-OCH$_3$)PP}(NO$_2$)]	d^6 (LS)	1.854(5)	1.983(146)	0.20	ruf	TUBJOP/[128]
98	[Co^{III}(TPP)(NO$_2$)(3, 5-Lutidine)]	d^6 (LS)	Co–N(Lut): 2.038(1) Co–N(NO$_2$): 1.948(1)	1.953(7)	In plane	Ruf	NTPOLC/[129]
99	[Co^{III}(TDCPP)(MeIm)$_2$]$^+$	d^6 (LS)	1.942(6)	1.977(5)	0.01	Ruf	PACLIO/[130]

[a] HS = high spin, LS = low spin and IS = intermediate spin. [b] Out of plane displacements are deviations from the 24-atom mean plane of the porphyrin core. [c] Ruf = ruffled, wav = wave, dom = domed, sad = saddled.
[d] Cambridge Structural Database reference codes. — No CSD data available and relevant data omitted from publication.

Table 1.18: Contd

No.	Metalloporphyrin	Electron config.[a]	Co–Ax (Å)	Co–N$_p$ (Å)	Δ^b (Å)	Conformation[c]	Refcode[d]/[Ref.]
100	[Co^{III}(TMcP)(R/S-Prolinol)$_2$]$^+$	d^6 (LS)	2.049(3)	1.954(2)	0.02	Ruf	POZQIE, POZQOK/[131]
101	[Co^{III}(TPP)(Pip)$_2$]	d^6 (LS)	2.436(2)	1.987(2)	In plane	Planar	PTPORC/[132]
102	[Co^{III}(TMcP)(2-butylamine)$_2$]$^+$	d^6 (LS)	2.004(19)	1.949(8)	0.01	Ruf	PUCPAE/[133]
103	[Co^{III}(TPP)(1-butylamine)$_2$]$^+$	d^6 (LS)	1.980(2)	1.987(4)	In plane	Planar	IBIVIY/[134]
104	[Co^{III}(TPP)(benzylamine)$_2$]$^+$	d^6 (LS)	1.983(2)	1.987(8)	0.02	Planar	IBIVOE/[134]
105	[Co^{III}(TPP)(phenethylamine)$_2$]$^+$	d^6 (LS)	1.978(8)	1.986(3)	0.01	Planar	IBIVUK/[134]
106	[Co^{III}(TPP)(1-MePipz)$_2$]$^+$	d^6 (LS)	2.040(1)	1.985(13)	In plane	Sad/Ruf	IBIWAR/[134]
107	[Co^{III}(TMe$_3$AP)(Im)$_2$]	d^6 (LS)	1.942(22)	1.935(3)	In plane	Sad/Ruf	VEGRAA/[135]

Table 1.19: Selected Structural Details of Published Crystal Structures of Cobalt Porphyrins with Other Donors

No.	Metalloporphyrin	Electron config.[a]	Co–Ax (Å)	Co–N$_p$ (Å)	Δ^b (Å)	Conformation[c]	Refcode[d]/[Ref.]
108	[Co^{II}(TpivPP)(Fl$_4$BzS)]	d^7 (LS)	2.497(1)	1.969(17)	0.17	Sad/Ruf	FOLWIM/[136]
109	[Co^{III}(TPP)(Fl$_4$BzS)$_2$]$^-$	d^6 (LS)	2.343(7)	1.975(1)	In plane	Ruf	COSJOJ COSJUP/[137]
110	{[Co^{II}(TpyrP)]}$_n$	d^7 (LS)	2.292(5)	1.994(5)	0.02	Wav	CAYSIE/[138]
111	{[Co^{II}(OETNP)]}$_2$	d^7 (LS)	Co–O: 2.423(5)	1.964(5)	0.06(1)	Sad	LIYFII/[139]
112	[Co^{III}(TPP)(Cl)]	d^6 (LS)	2.149(6)	1.985(9)	In plane	Planar	CTPOCO/[140]
113	[Co^{III}(OEP)(SnPh$_3$)]	d^6 (LS)	2.510(2)	1.966(5)	0.08	Planar	GIZTIS/[141]
114	[Co^{III}(TPP){PO(NMe$_2$)$_2$}]	d^6 (LS)	2.265(1)	1.972(4)	0.20	Planar	ZONQOI/[142]

[a] HS = high spin, LS = low spin and IS = intermediate spin. [b] Out of plane displacements are deviations from the 24-atom mean plane of the porphyrin core. [c] Ruf = ruffled, wav = wave, dom = domed, sad = saddled.

[d] Cambridge Structural Database reference codes. — No CSD data available and relevant data omitted from publication.

Table 1.20: Selected Structural Details of Published Crystal Structures of Cobalt Porphyrins with Mixed Donors

No.	Metalloporphyrin	Electron config.[a]	Co–Ax (Å)	Co–N$_p$ (Å)	Δ[b] (Å)	Conformation[c]	Refcode[d]/[Ref.]
115	[Co^{II}(TpivPP)(Fl$_4$BzS)(O$_2$)]	d^7 (LS)	Co→S: 2.363(1) Co→O: 1.917(1)	1.968(11)	0.07	Sad/Ruf	FOLWOS/[136]
116	[Co^{III}(TpivPP)(MeIm)(NO$_2$)]	d^6 (LS)	Co–N(MeIm): 1.995(4) Co–N(NO$_2$): 1.898(4)	1.964(5)	0.04(→MeIm)	Sad/Ruf	XAFJIX/[143]
117	[Co^{III}(TpivPP)(DiMeIm)(NO$_2$)]	d^6 (LS)	Co–N(DiMeIm): 2.091(4) Co–N(NO$_2$): 1.917(4)	1.983(1)	0.09(→DiMeIm)	Sad/Ruf	XAFJOD/[143]
118	[Co^{III}(OEP)(CH$_3$)(Py)]	d^6(LS)	Co–C: 2.018(12) Co–N: 2.214(9)	1.983(19)	In plane	Planar	LIBCEE/[109]
119	[Co^{III}(TPP)(Pip)(NO$_2$)]	d^6 (LS)	Co–Pip: 2.044(10) Co-NO$_2$: 1.897(11)	1.953(4)	—	Ruf	KENFOY/[144]
120	[Co^{III}(TPP)(Allylperoxy)(Py)]	d^6 (LS)	Co–O: 1.920(10) Co–N: 2.040(80)	1.988(13)	In plane	Sad/Ruf	KEBMIN/[145]
121	[Co^{III}(TMcP)(OHCH$_2$CH$_3$)(Cl)]	d^6 (LS)	Co–O: 2.048(8) Co–Cl: 2.211(3)	1.925(3)	0.06(→Cl)	Ruf	PUCNUW/[146]
122	[Co^{III}(TPP)(H$_2$O)(Cl)]	d^6 (LS)	Co–O: 1.979(3) Co–Cl: 2.216(1)	1.955(3)	0.02	Ruf	GAMTAP/[147]
123	[Co^{III}(TPP)(H$_2$O)(NO$_2$)]	d^6 (LS)	1.963(1) disorder see ref	1.982(1)	In plane	Planar	XEGRIK/[148]

[a] HS = high spin, LS = low spin and IS = intermediate spin. [b] Out of plane displacements are deviations from the 24-atom mean plane of the porphyrin core. [c] Ruf = ruffled, wav = wave, dom = domed, sad = saddled.

[d] Cambridge Structural Database reference codes. — No CSD data available and relevant data omitted from publication.

Table 1.21: Selected Structural Details of Published Crystal Structures of 4-Coordinate Cobalt Porphyrins

No.	Metalloporphyrin	Electron config.[a]	Co–Ax (Å)	Co–N_p (Å)	Δ^b (Å)	Conformation[c]	Refcode[d]/[Ref.]
124	$[Co^0(TPP)]^{2-}$	$d^7 s^2$ (LS)	NA	1.971(3)	In plane	Planar	FAGCIZ/[149]
125	$[Co^I(TPP)]^-$	$d^7 s^1$	NA	1.942(3)	In plane	Wav	CUPPEI/[150]
126	$[Co^{II}(TPP)]$	d^7 (LS)	NA	1.949(3)	In plane	Ruf	TPORCP/[151]
		d^7 (LS)	NA	1.949(1)	In plane	Ruf	TPORCP11/[152]
127	$[Co^{II}(OETPP)]$	d^7 (LS)	NA	1.929(3)	0.02	Sad	WADRIC/[153]
128	$[Co^{II}(TpivPP)]$	d^7 (LS)	NA	1.966(4)	0.02	Planar	XAFJET/[143]
129	$[Co^{II}(TF_7PropP)]$	d^7 (LS)	NA	1.936(2)	In plane	Sad(small ruf)	ZAWFEI/[154]
130	$[Co^{II}(TF_5PP)]$	d^7 (LS)	NA (benzene at 3.28)	1.976(5)	In plane	Co2: Planar	SIRRUG/[159]
131	$[Co^{II}(T(p\text{-}OCH_3)PP)]$	d^7 (LS)	NA	1.948(56)	0.01	Ruf	TEFPEZ/[155]
		d^7 (LS)	NA	1.963(7)	In plane	Wav	TEFPID/[155]
132	$[Co^{II}(OEP)]$	d^7 (LS)	NA	1.971(6)	In plane	Wav	HECZIY/[156]
133	$[Co^{II}(F_{28}TPP)]$	d^7 (LS)	NA (toluene solvate at 3.05)	1.986(2)	In plane	Planar	HEQZEI/[113]
134	$[Co^{II}(TBP)]^+$	d^7 (LS)	NA	1.984(5)	In plane	Planar	JURFOR/[157]
135	$[Co^{II}(T(o\text{-}OCH_3)PP)]$	d^7 (LS)	NA	1.960(24)	In plane	Planar	NUWPOK/[158]
136	$[Co^{II}\{T(p\text{-}Me_2N)F_4PP\}]$	d^7 (LS)	NA (benzene at 3.07)	1.971(6)	In plane	Co1: Wav	SIRROA/[159]

[a] HS = high spin, LS = low spin and IS = intermediate spin. [b] Out of plane displacements are deviations from the 24-atom mean plane of the porphyrin core. [c] Ruf = ruffled, wav = wave, dom = domed, sad = saddled.

[d] Cambridge Structural Database reference codes.

1.3.3 Rhodium Porphyrins

Of the three metals observed in this literature survey, rhodium has by far the least number of successfully crystallized complexes. Also noticeable is that rhodium has the highest number of carbon-donor complexes (Table 1.23) of the three metals and virtually, but not entirely, no O-donor complexes. There are relatively few N-donor complexes (Table 1.24) and very few non-C/O/N-donor complexes (Table 1.25). There are two μ-dimers and a handful of mixed-ligand complexes (Table 1.26).

Table 1.22 contains a further summary of the surveyed data, from which the axial bond length ranges and the Rh–N$_{porph}$ bond length ranges have been extracted.

Table 1.22: Summary of Bond Length Ranges For Rhodium Porphyrins[a]

Bond	Rh–L$_{ax}$ Range	Rh–N$_{porph}$ Range
Rh^{III}–C	1.896–2.078	2.017–2.038
Rh^{III}–N	2.090–2.260	2.021–2.038
Rh^{III}–Si	2.305–2.316	2.016–2.033

[a] Mixed ligand complexes and esd's excluded.

Rhodium porphyrins with axial C-donor ligands. A substantial number and variety of C-donor ligands exist with the range extending from methyl to substituted phenyl derivatives. Of the three metals, rhodium is the only metal where carbene complexes have been crystallized. All of the C-donor complexes are 5-coordinate and contain rhodium in its +3 oxidation state. The axial bond lengths range from 1.896(6) to 2.078(1) Å, while the Rh–N$_{porph}$ distances are less varied with a range of 2.017(8) to 2.038(18) Å.

Three 5-coordinate methyl complexes exist with rhodium [137–139]. These complexes exhibit axial bond lengths in the range 1.975(1) to 2.031(6) Å and Rh–N$_{porph}$ distances of 2.028(11) to 2.032(4) Å. Although these axial bond lengths are dramatically shorter than those of the N-donor and 'other'-donor complexes, the Rh–N$_{porph}$ bond lengths are quite similar and do not show much deviation from one complex to the next. The values for the Rh–C axial bond lengths are ~2 % larger than that of the Co(III) analogue due to the larger ionic radius of Rh(III). This observation holds for all of the data in Tables 1.23–1.26.

A C(O)Ph [140] and a *meta*-cyanophenyl [141] complex display axial bond lengths of 1.963(7) and 2.001(2) Å, respectively. Complex [140] is shown in Figure 1.37 below. The mean Rh–N_{porph} distances are 2.032(4) and 2.035(8) Å, respectively.
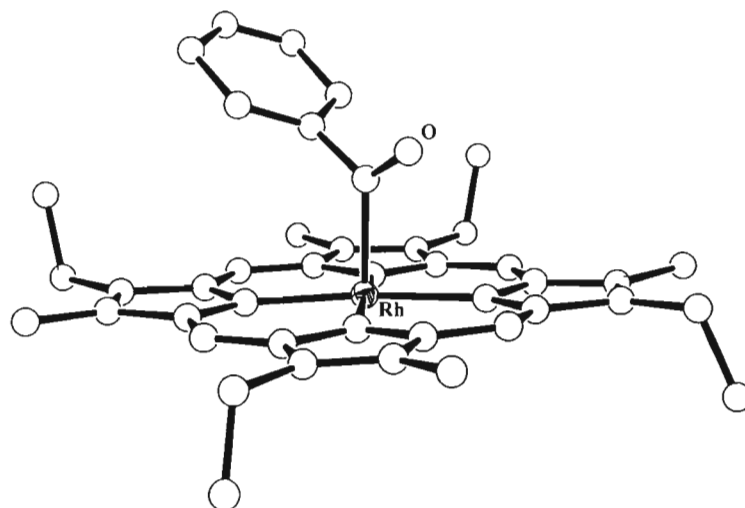
Figure 1.37: BINNUH [140]

Figure 1.38 shows the only carbene complex recorded for rhodium, which exists as a 6-coordinate complex of $CNCH_2Ph/$:$C(NHCH_2Ph)_2$ [142] with axial bond lengths of 2.064(13)/2.030(11) Å and a mean Rh–N_{porph} distance of 2.038(18) Å. The carbene–Rh(III) distance is only minimally shorter than that of the opposing ligand. Once again, the Rh–N_{porph} lengths do not show much deviation those of the other C-donor complexes.
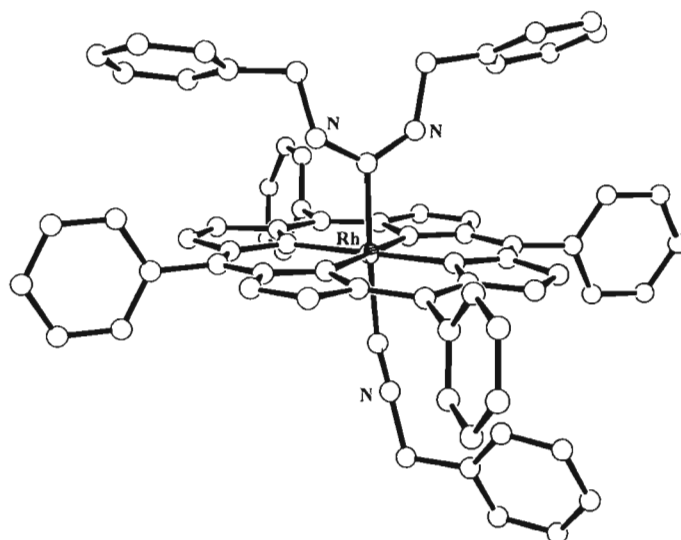
Figure 1.38: JAFXAP [142]

50

A C(O)OEt complex [143] and a C(O)NH(C$_6$H$_3$(CH$_3$)$_2$) complex [144] display axial bond lengths of 1.918(9) and 1.988(5) Å, respectively. The increased steric bulk of the latter ligand may account for the slightly longer axial bond length. In this derivative the Rh–N$_{porph}$ distances average 2.025(8) and 2.023(3) Å.

The increase in axial bond length with the steric size differences between primary and secondary alkyl ligands may be observed in the two 5-coordinate Rh(III) complexes of primary – CH$_2$CH$_2$Ph [145] and secondary –CH(CH$_3$)Ph [146] whose axial bond lengths measure 2.026(1) Å and 2.078(1) Å, respectively. The Rh–N$_{porph}$ distances for these two complexes, however, are similar at 2.019(11) and 2.017(8) Å, respectively.

An axial ligand derived from benzonitrile CNHPh [147] exhibits a short axial Rh(III)–C bond length of 1.963(5) Å; the Rh–N$_{porph}$ distance of 2.035(21) Å is more normal. A chloromethyl complex [148] displays a slightly longer than average axial bond of 2.010(4) Å and a normal Rh–N$_{porph}$ length of 2.020 (3)Å.

An unusual complex with axial 5-norbornen-2-yl methyl [149] has an axial bond length of 2.052(6) Å and a normal Rh–N$_{porph}$ distance of 2.022(4) Å. This complex is shown in Figure 1.39. This is one of the longer Rh(III)–C bonds recorded to date and reflects the steric bulk of the axial ligand.
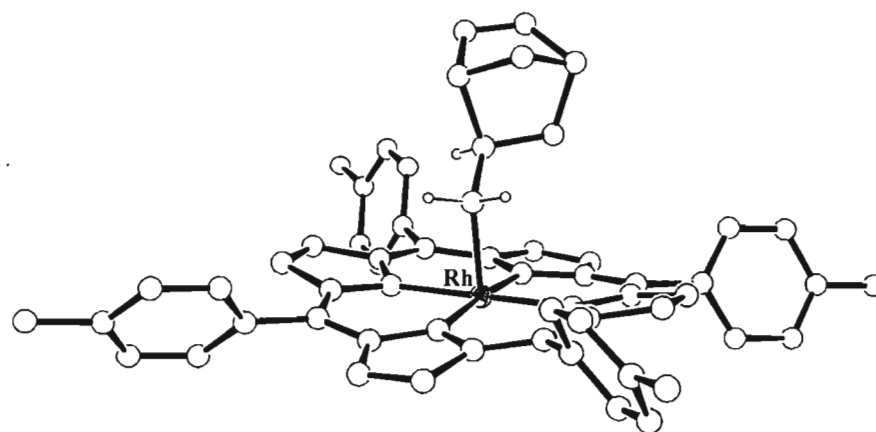
Figure 1.39: WOJFAC [149]

The only reported formyl complex of a rhodium(III) porphyrin [150] displays the shortest axial bond distances of all the complexes surveyed at 1.896(6) Å. The Rh–N$_{porph}$ lengths were omitted

from the publication and CSD coordinates were unavailable.

Rhodium porphyrins with axial N-donor ligands. With the larger portion of the crystal structures being C-donor complexes, the research into N-donor complexes has been minimal with pyridine and dimethyl amine complexes forming the bulk of this class of donor.

Two complexes of bis(dimethyl amine) [151 and 152] exist which exhibit axial bond lengths of 2.090(8) and 2.110(esd's omitted from publication) Å and Rh–N$_{porph}$ distances of 2.038(6) and 2.030(esd's omitted from publication) Å, respectively. These axial coordination distances appear to be very similar to those found for Co^{III}, while the Rh–N$_{porph}$ bond lengths are somewhat longer than the equivalent bonds in Co^{III} amine complexes.

A 5-coordinate benzonitrile complex [153] displays an axial Rh(III)–N bond length of 2.260(1) Å and a Rh–N$_{porph}$ distance of 2.021(9) Å. This nitrile ligand is N-bound and thus cannot be compared to any cobalt structures of similar composition. The axial bond length is substantially longer than those of the dimethylamine complexes, yet the Rh–N$_{porph}$ distance is virtually the same.
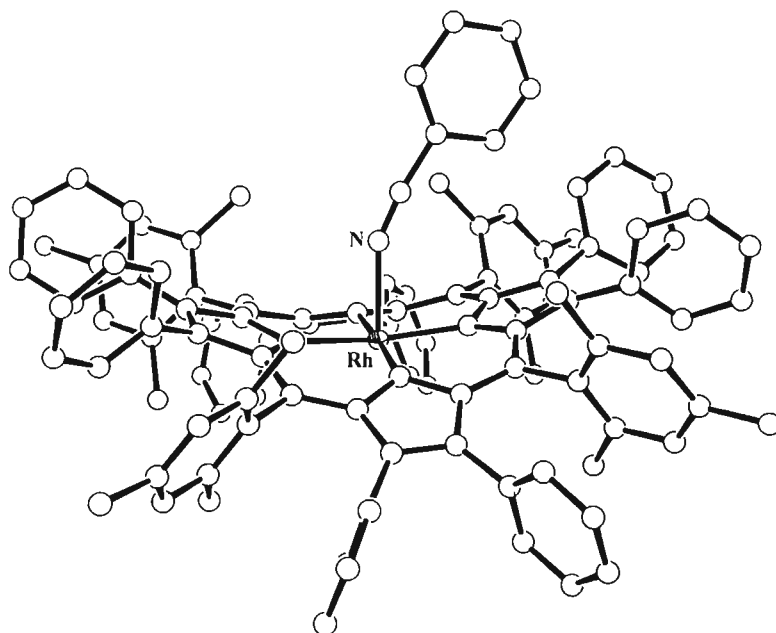
Figure 1.40: WOFPEM [153]

Other donors. The non-C/N-donor complexes of rhodium are once again quite limited with silicon-, tin- and a relevant phosphorus-donor forming the scope of this potentially broad

category.

Two 5-coordinate silicon-donor complexes exist in which SiEt$_3$ [154] and SiMe$_3$ [155] are coordinated to Rh(III) and which display axial bond lengths of 2.316(10) and 2.305(2) Å, and Rh–N$_{porph}$ distances of 2.033(2) and 2.016(5) Å, respectively. These axial bonds are somewhat longer than in the N-donor and C-donor complexes, yet the Rh–N$_{porph}$ distances are very similar. The long Si–Rh(III) distances reflect the larger size of Si relative to C or N.

The single 5-coordinate trichloro-tin complex [156], shown in Figure 1.41, displays an elongated axial bond length of 2.450(1) Å and a normal Rh–N$_{porph}$ distance of 2.017(8) Å.
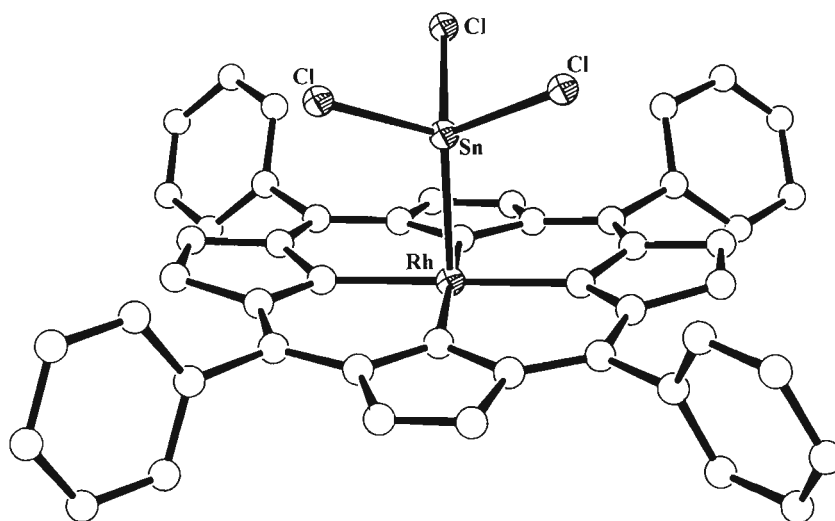
Figure 1.41: YOWJID [156]

Mixed donor complexes of rhodium. Only two bridged complexes have been structurally characterised; the first is a bipy-bridged species with iodine in the opposite position [157] and the second is a cyanopyridine-bridged species with a methyl group [158] in the opposite position. The axial bond lengths for the former complex are 2.121(4) Å for the Rh–bipy bond and 2.635(1) Å for the Rh–I bond. The axial bond lengths for the latter complex are 2.273(4) Å for the Rh–N bond of the N-bound cyanopyridine and 2.033(4) Å for the Rh–CH$_3$ bond. The Rh–N$_{porph}$ lengths are 2.049(6) Å and 2.032(3) Å for the former and latter complexes, respectively.

The only phosphine-containing complex, as shown in Figure 1.42, is that of a PPh$_3$/Cl$^-$ system [159], where the axial bond lengths measure 2.306(3)/2.442(2) Å, respectively. This Rh–P distance is one of the longest axial bonds for rhodium thus far, yet is perhaps unexpectedly short

considering the huge steric bulk of the PPh_3 axial ligand. The Rh–N_{porph} length is normal at 2.024(28) Å.
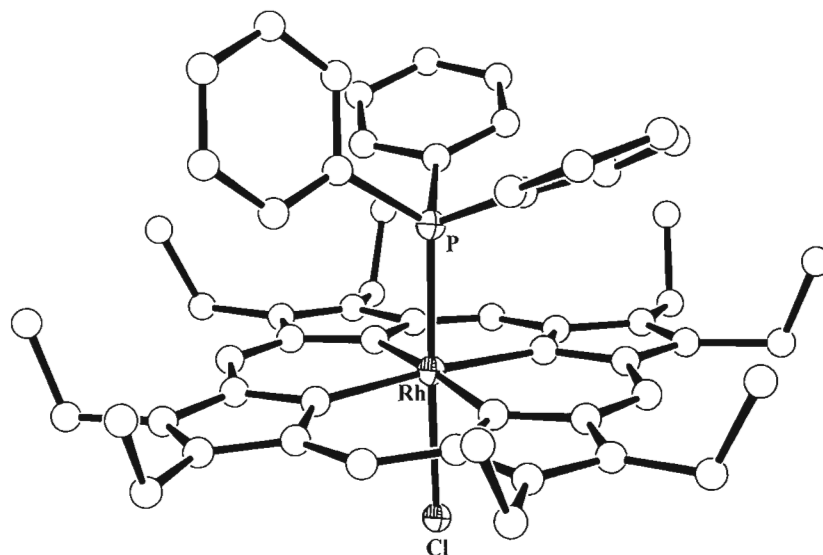
Figure 1.42: FIGVUM [159]

Two py/I⁻ complexes [160 and 161] have axial bond lengths of 2.139(3)/2.631(1) Å and 2.102(1)/2.633(1) Å, respectively. The former complex has significantly longer Rh–N_{py} bond distances than the latter, presumably as a result of the former porphyrin having a larger steric bulk and the latter porphyrin having adopted a more distorted conformation. The Rh–N_{porph} lengths are 2.048(2) and 2.030(4) Å, respectively.

The remaining complexes of *meta*-cyanophenyl/ethanol [162] and Ph/Cl [163] display axial bond lengths of 1.985(9)/2.349(7) and 2.050(esd's omitted from publication)/2.350(esd's omitted from publication) Å, respectively, with Rh–N_{porph} distances of 2.032(28) and 2.040(esd's omitted from publication) Å, respectively. The Rh–C distance in [162] is slightly shorter than the equivalent bond in the 5-coordinate complex of this ligand discussed in the C-donor section; likewise the Rh–Cl distance in [163] is shorter than the equivalent bond in [159].

An interesting observation is that there are no 4-coordinate complexes of Rh. This implies the instability of the +2 oxidation state and the lack of non-coordinating counter-ions to produce the 4-coordinate complexes of Rh(III).

Table 1.23: Selected Structural Details of Published Crystal Structures of Rhodium Porphyrins with C-Donors

No.	Metalloporphyrin	Electron config.[a]	Rh–Ax (Å)	Rh–N_p (Å)	Δ^b (Å)	Conformation[c]	Refcode[d]/[Ref.]
137	[Rh^{III}(DPTHTMP)(CH$_3$)]	d^6 (LS)	2.010(5)	2.032(4)	0.02	Ruf	CIXQEF/[160]
138	[Rh^{III}(F$_{28}$TPP)(CH$_3$)]	d^6 (LS)	2.027(4)	2.030(3)	0.10	Sad	LOSGAB/[161]
139	[Rh^{III}(OEP)(CH$_3$)]	d^6 (LS)	2.031(6)	2.031(8)	0.05	Wav	OEPMRH/[162]
		d^6 (LS)	1.975(1)	2.028(11)	0.01	Ruf	OEPMRH01/[163]
140	[Rh^{III}(etio-I){C(O)Ph}]	d^6 (LS)	1.963(7)	2.032(4)	0.07	Ruf	BINNUH/[164]
141	[Rh^{III}(OEP)(mcPh)]	d^6 (LS)	2.001(2)	2.035(8)	0.05	Ruf	GEQBOT/[165]
142	[Rh^{III}(TPP)(CNCH$_2$Ph){:C(NHCH$_2$Ph)$_2$}]$^+$	d^6 (LS)	Rh–CNCH$_2$Ph: 2.064(13) Rh–:C(NHCH$_2$Ph)$_2$: 2.030(11)	2.038(18)	0.02	Planar	JAFXAP/[166]
143	[Rh^{III}(OEP){C(O)OEt}]	d^6 (LS)	1.918(9)	2.025(8)	0.01	Ruf	JUZSUS/[167]
144	[Rh^{III}(OEP){C(O)NH(C$_6$H$_3$(CH$_3$)$_2$)}]	d^6 (LS)	1.988(5)	2.023(3)	0.03	Sad/Ruf hybrid	LAXBER/[168]
145	[Rh^{III}(TTP)(CH$_2$CH$_2$Ph)]	d^6 (LS)	2.026(1)	2.019(11)	0.02	Sad	LEZKOQ/[169]
146	[Rh^{III}(TTP){CH(CH$_3$)Ph}]	d^6 (LS)	2.078(1)	2.017(8)	0.11	Planar	LEZLAD/[169]
147	[Rh^{III}({(TPP)(Ph)$_4$})(CNHPh)]	d^6 (LS)	1.963(5)	2.035(21)	0.07	Sad	QENJOI/[182]
148	[Rh^{III}(TPP)(CH$_2$Cl)]	d^6 (LS)	2.010(4)	2.020(3)	0.04	Sad	QESHEB/[170]
149	[Rh^{III}(TTP)(5-norbornen-2-yl methyl)]	d^6 (LS)	2.052(6)	2.022(4)	0.02	Sad	WOJFAC/[171]
150	[Rh^{III}(OEP)(CHO)]	d^6 (LS)	1.896(6)	—	—	—	BEGDIA/[172]

[a] HS = high spin, LS = low spin and IS = intermediate spin. [b] Out of plane displacements are deviations from the 24-atom mean plane of the core. [c] Ruf = ruffled, wav = wave, dom = domed, sad = saddled. [d] Cambridge Structural Database reference codes. . — No CSD data available and relevant data omitted from publication.

Table 1.24: Selected Structural Details of Published Crystal Structures of Rhodium Porphyrins with N-Donors

No.	Metalloporphyrin	Electron config.[a]	Rh–Ax (Å)	Rh–N_p (Å)	Δ^b (Å)	Conformation[c]	Refcode[d]/[Ref.]
151	[Rh^{III}(etio-I){HN(CH$_3$)$_2$}$_2$]$^+$.	d^6 (LS)	2.090(8)	2.038(6)	In plane	Planar	RHETPR10/[173]
152	[Rh^{III}(TPP){HN(CH$_3$)$_2$}$_2$]$^+$	d^6 (LS)	2.11(—)	2.03(—)	—	—	PHPORPH/[174]
		d^6 (LS)	2.109(2)	2.036(2)	In plane	Wav	Own work
153	[Rh^{III}(OPTMP)(cyanophenyl)]	d^6 (LS)	2.260(1)	2.021(9)	0.05	Sad	WOFPEM/[175]

Table 1.25: Summary of Selected Structural Details of Published Crystal Structures of Rhodium Porphyrins with Other Donors

No.	Metalloporphyrin	Electron config.[a]	Rh–Ax (Å)	Rh–N_p (Å)	Δ^b (Å)	Conformation[c]	Refcode[d]/[Ref.]
154	[Rh^{III}(OEP)(SiEt$_3$)]	d^6 (LS)	2.316(10)	2.033(2)	In plane	Planar	YIXVIK/[176]
155	[Rh^{III}(TPP)(SiMe$_3$)]	d^6 (LS)	2.305(2)	2.016(5)	—	—	MAVMEB/[177]
156	[Rh^{III}(TPP)(trichloro-tin^{II})]	d^6 (LS)	2.450(1)	2.017(8)	0.01	Sad	YOWJID/[178]

[a] HS = high spin, LS = low spin and IS = intermediate spin. [b] Out of plane displacements are deviations from the 24-atom mean plane of the core. [c] Ruf = ruffled, wav = wave, dom = domed, sad = saddled. [d] Cambridge Structural Database reference codes. — No CSD data available and relevant data omitted from publication.

Table 1.26: Selected Structural Details of Published Crystal Structures of Rhodium Porphyrins with Mixed Donors

No.	Metalloporphyrin	Electron config.[a]	Rh–Ax (Å)	Rh–N_p (Å)	Δ^b (Å)	Conformation[c]	Refcode[d]/[Ref.]
157	μ-{(bipy)-[Rh^{III}(DPTHTMP)(I)]}$_2$	d^6 (LS)	Rh–N: 2.121(4) Rh–I: 2.635(1)	2.049(6)	0.05	Sad	CIXPOO/[180]
158	μ-{(CNpyr)-[Rh^{III}(TTP)(CH$_3$)]}$_2$	d^6 (LS)	Rh–C: 2.033(4) Rh–N: 2.273(4)	2.032(3)	0.01	Planar	WOJDUU/[171]
159	[Rh^{III}(OEP)(PPh$_3$)(Cl)]	d^6 (LS)	Rh–P: 2.306(3) Rh–Cl: 2.442(2)	2.024(28)	0.15	Domed	FIGVUM/[179]
160	[Rh^{III}(DPTHTMP)(Py)(I)]	d^6 (LS)	Rh–N: 2.139(3) Rh–I: 2.631(1)	2.048(2)	0.06	Sad	CIXQAB/[180]
161	[Rh^{III}(TPP)(Py)(I)]	d^6 (LS)	Rh–N: 2.102(1) Rh–I: 2.633(1)	2.030(4)	In plane	Sad/Ruf hybrid	QIJXEM/[181]
162	[Rh^{III}{(TPP)(Ph)$_4$}(mcPh)(EtOH)]	d^6 (LS)	Rh–C: 1.985(9) Rh–O: 2.349(7)	2.032(28)	0.03	Planar	QENJIC/[182]
163	[Rh^{IV}(TPP)(Ph)(Cl)]	d^5 (LS)	Rh–C: 2.05(—) Rh–Cl: 2.35(—)	2.04(—)	—	—	PRHTPP/[183]

[a] HS = high spin, LS = low spin and IS = intermediate spin. [b] Out of plane displacements are deviations from the 24-atom mean plane of the core. [c] Ruf = ruffled, wav = wave, dom = domed, sad = saddled. [d] Cambridge Structural Database reference codes. — No CSD data available and relevant data omitted from publication.

1.4 Vacant Research Fields

Manganese. The result of our literature survey shows a distinct lack of variety in ligand donors for Mn in a variety of oxidation states. Carbon, oxygen and nitrogen donors form the majority of the complexes, apart from a few halogen-donor complexes. Sulfur donors immediately spring to mind, since the oxygen affinity of manganese has been proven. There are no sulfur-donor complexes of manganese in the CSD, which surely provides a large scope for research. The lack of phosphines is also noticeable – with a large range of phosphine derivatives commercially available, this exposes a vast area of research to exploitation. The carbon-donor complexes are also noticeably lacking since the only successes within this category are two bis(cyanide) complexes. There are no recorded structures with alkyl axial ligands or any of the many other possibilities that have been successfully coordinated or bonded to rhodium.

Cobalt. Since a representative sample of N-donors already exists one would be loathe recommending any further research into this class of ligand. But what is noticeable is the lack, once again, of any phosphines apart from the anionic bis(dimethylamine)phosphorane. A larger number of halogen-donor complexes would be of use, since the halogens play a role as intermediates in metathesis reactions, and obviously in counter-ions. Also warranting a comment is that the current range of carbon-donor complexes of cobalt is in need of a few samples of cyano-type derivatives, both C- and N-bound.

Rhodium. In contrast to the comments on the cobalt complexes, there are noticeably few examples of amine complexes of rhodium. Since there is a large array of commercially available amines, the synthesis of such complexes should be pursued. There is a lack of sulfur-donor ligand complexes of rhodium, as with manganese. Examples of phosphine complexes are also limited, with rhodium being the only metal of the three metals surveyed where a neutral phosphine has been coordinated.

1.5 The Electronic Structures of Manganese, Cobalt and Rhodium Centres in Porphyrins

The diagram in Figure 1.43 shows the σ-symmetry orbitals of the central metal ion, namely the dz^2 and the dx^2-y^2 orbitals, and their orientation in a porphyrin macrocycle. The dx^2-y^2 orbital overlaps with the σ-symmetry orbitals of the porphyrin nitrogens, and the dz^2 orbital protrudes above and below the plane of the porphyrin.
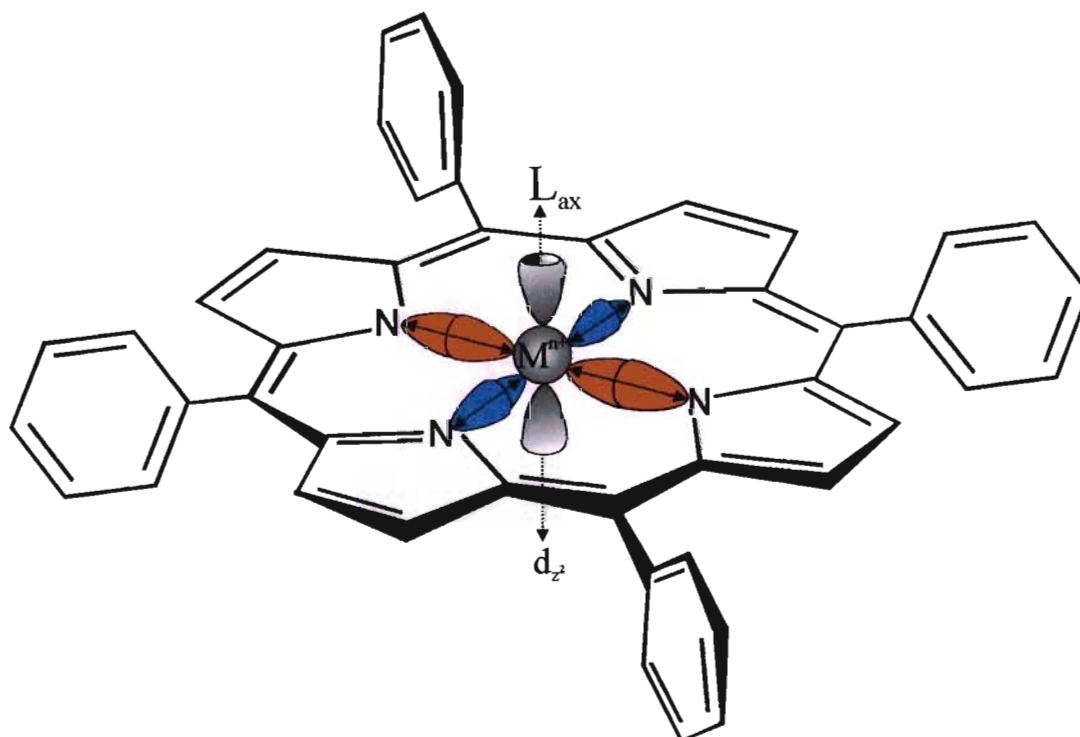
Figure 1.43: σ-Symmetry orbitals involved in M–L bonding in metalloporphyrins. Atomic orbitals have been shown for simplicity.

The drawing in Figure 1.44 shows the orientation of the π-symmetry orbitals of the central metal ion and their orientation in the porphyrin macrocycle. It is shown that the dxz and dyz orbitals protrude out towards the π-symmetry orbitals of the porphyrin nitrogens, which in turn interact with the π-symmetry orbitals of the alpha-carbon, which then interact with the next atom etc. When looking at the π-symmetry orbital interactions of the central metal ion with the π-symmetry orbitals of the macrocycle, one can see how the electronic character of the metal may influence the electronic character of the macrocycle. This is shown in the ^{1}H NMR of high spin paramagnetic manganese (III) porphyrins where the unpaired spin density of the manganese affects the porphyrin protons to such an extent that the spectrum is almost immeasurable. Thus,

the unpaired spin density of the manganese is delocalised over the porphyrin macrocycle.
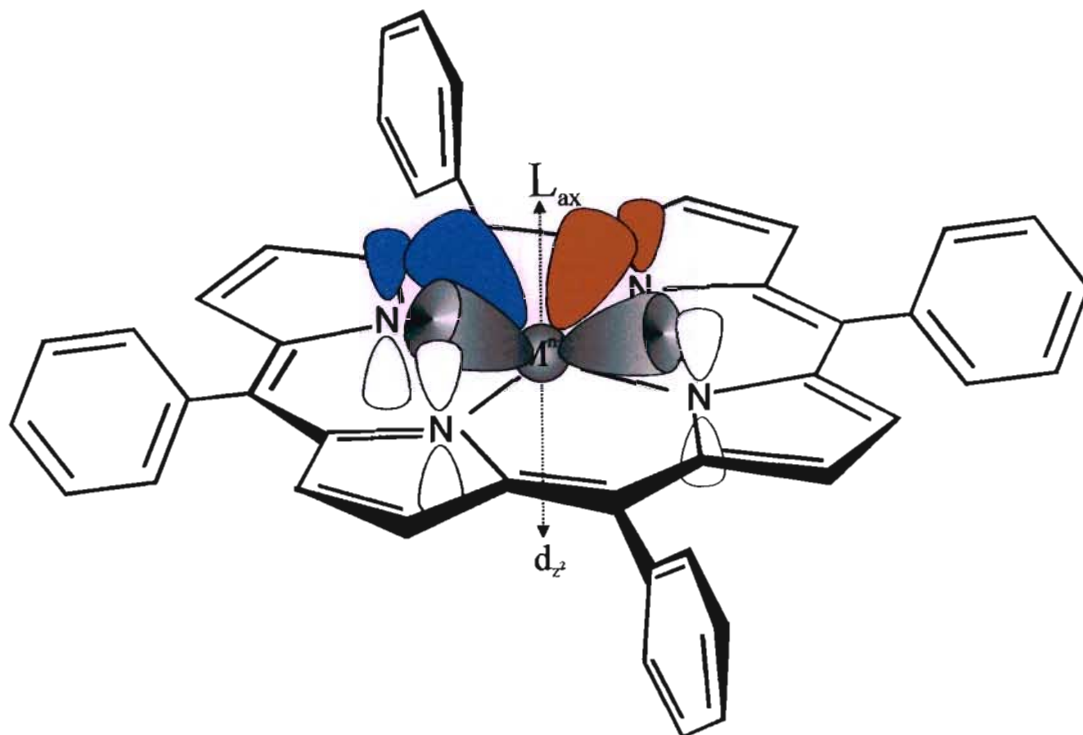
Figure 1.44: **Drawing of metalloporphyrin showing d_π-symmetry orbitals of metal and orbitals of π–symmetry of porphyrin nitrogens**

Manganese.[184]   The highest oxidation state of manganese is VII, which corresponds to its valence electron count. The VII oxidation state occurs predominantly in the oxides of the metal, and is a strong oxidizing agent. Mn(IV) is a relatively rare oxidation state, the most stable being Mn(II).

The more relevant oxidation state in this line of research is the Mn(III) state which is the more stable form of the ion in a porphyrin ligand. Both Mn(III) and Mn(II) will most commonly form octahedral complexes. In order to demonstrate the relative stability of the Mn(III) and Mn(II) metal centres in a porphyrin environment an attempt was made to reduce the Mn(III) porphyrin to Mn(II) without strong-field axial ligands, but rather with a $Zn/HgCl_2$ amalgam. Where the solution colour of dark green-black for the Mn(III) centre in [Mn(TPP)Cl] became dark blue-black corresponding to the presence of the Mn(II) centre in [Mn(TPP)]. However on standing under nitrogen the solution after a few hours re-oxidised back to the colour corresponding to the [Mn(TPP)Cl] Mn(III) colour. The electronic spectra of [Mn(TPP)Cl] and [Mn(TPP)] can be seen in Figure 1.50.

Mn(III) in the case of metalloporphyrins is d^4 high-spin, even in complexes with relatively strong-field ligands such as primary amines and phosphines, at least at room temperature. Low-spin Mn(III) metalloporphyrins have been synthesized using anionic and stronger-field ligands such as imidazolate and cyanide as the axial ligands in dimethyl sulfoxide.[185] What has recently been discovered in our laboratory is a temperature dependence of this spin-state with primary amines in the axial positions. This serendipitous discovery was observed when looking at the temperature-dependant NMR spectra of these systems. When looking at the variable temperature electronic spectra of these compounds one may track the spectral progression of the spin-state from low-spin at a higher temperature to high-spin at a lower temperature.

High-spin Mn(III) porphyrins have an unoccupied dx^2-y^2 orbital and a singly occupied dz^2 orbital.[186] The single electron occupation of the dz^2 orbital results in a lengthening, and thus weakening, of the bonds to the axial ligands due to electron-electron repulsion between this electron and the electrons of the lone-pair of the donor ligand atoms.

In high spin manganese(II) porphyrins, the dx^2-y^2 orbital is singly occupied. In the older literature[186] it was believed that this was responsible for a substantial out-of-plane displacement of the metal center from the plane of the nitrogen atoms of the porphyrin. It was thought this displacement favoured the coordination of a single sterically hindered axial ligand in this direction to form a five coordinate complex, and severely retarded the formation of a six coordinate species as a result of substantially increased bond lengths. However, no such relationship is recognized in the current literature and it has been shown that out of plane displacements are caused by a variety of factors and not simply orbital occupation.

Cobalt.[184] The highest oxidation state of cobalt is +4, although the cobalt atom has nine valence electrons. This is a result of the tendency of the second half of the d-block elements not to use all their valence electrons for bonding. The most stable oxidation states are +2 and +3 and the most stable in a metalloporphyrin complex such as [Co(TPP)Cl] is the +3 state. Evidence of the stability of the +3 state is its presence in the corrin ring system of vitamin B_{12}. The +2 state of cobalt is more stable in the simpler coordination compounds of cobalt.

Co(III) forms octahedral complexes and has a d^6 electronic configuration. Most complexes of Co(III) are low spin as even relatively weak field ligands induce spin-pairing in the d-orbitals. The exception to this is the cobalt hexafluoride anion which is high spin and thus paramagnetic.

The NMR spectra of Co(III) porphyrins are relatively straightforward to acquire as the complexes are diamagnetic. As a result of the spin pairing in the dxy, dyz and dxz orbitals, the dx^2-y^2 and dz^2 orbitals of the cobalt in a metalloporphyrin are unoccupied and thus fully available for coordination of the macrocycle and axial ligands. Cobalt (III) shows a particular affinity for nitrogen donors and these complexes are well known and numerous.

Rhodium.[184] The highest oxidation state of rhodium is +6, the reasoning for this not being higher follows that of cobalt. The most stable oxidation states are +3 and +4, with the +3 state being the most stable in a metalloporphyrin such as [Rh(TPP)Cl]. Complexes of Rh(III) have a d^6 electronic configuration and are usually stable, octahedral, low-spin, and diamagnetic. Rh(II) compounds are very rare, yet a few complexes of Rh(II) are known. The Rh(II) complexes are mostly binuclear and contain Rh–Rh bonds.

1.6 Applications of Manganese, Cobalt and Rhodium Porphyrins

Transition metal porphyrins have applications dependent mostly on the type of metal and its reactivity. The porphyrin macrocycle has an added benefit of the possibility of functionalisation. With specific functional groups on the macrocycle, the porphyrin may be polymerised, mostly electrocatalytically, onto supports. The heterogeneous activity of a catalyst is a significant reason for research into this field and the commonly occurring research drive in cobalt and manganese seems to be the reduction of O_2 to H_2O for applications in fuel-cell technology.

Manganese Porphyrins. These porphyrins have a variety of uses from biological applications to the synthesis of molecules and catalysis. Their use seems to be limited, however, to reaction mechanisms involving oxygen donors. This demonstrates the reactivity of the manganese center in these metalloporphyrins. The biological applications of manganese porphyrins include the catalytic scavenging of superoxide, hydrogen peroxide and peroxynitrite in biological tissue,[187,188] thus trapping this toxin for reduction by natural antioxidants and thus saving healthy tissue from damage.

Manganese porphyrins are also used extensively as catalysts in olefin oxidation[189] and epoxidation[190-193] reactions. μ-Oxo dimanganese systems have been used in the reduction of O_2 to H_2O.[194] It has been reported that manganese porphyrins have been used in the oxidation of cyclic alcohols to ketones[195] in aqueous solutions.

Tetracationic manganese porphyrins are being successfully investigated for DNA cleavage activity.[196] Anionic manganese porphyrins may be supported on polymers of poly(vinylpyridinium) where they are used in the potassium monopersulfate oxidation of lignin model molecules in the absence of an excess of free pyridine,[197] which is usually required for efficient manganese porphyrin-catalysed reactions. It has also been reported[198] that manganese porphyrins may be used as heterogeneous catalysts in the hydroxylation of cyclo-octane by NaOCl. For this function, the anionic porphyrin is immobilised onto a cross-linked polymer resin through coordinate linkages.

Cobalt Porphyrins. Research performed on water-soluble cobalt porphyrins has shown they may be used in the photocatalytic autooxidation[199] of $S_4O_6^-$ and $S_2O_3^{2-}$. Along a similar vein, these porphyrins have also been used heterogeneously in the oxidation of thiols,[200] by

intercalation into a phosphato-antimonic acid host. Cobalt porphyrins have been found to successfully reduce O_2 to H_2O.[201] This has, more significantly, been performed heterogeneously by the covering[202,203] or electropolymerisation of functionalised cobalt porphyrins onto vitreous carbon electrodes.[204] The same heterogeneous electrode-support concept has been used in the electrocatalysis of the reduction of trichloro-acetic acid[205] and the oxidation of 2-mercaptoethanol.[206] In an interesting study,[207] Castellani and Gushikem reported the *in situ* metallation option in creating porphyrin-coated electrodes for use in electrocatalysis. Here the porphyrin macrocycle is immobilised onto the surface of a $SiO_2/TiO_2/$phosphate matrix using ion-exchange techniques and then metallated with cobalt(II). Tetra-ruthenated cobalt porphyrins coated onto electrode surfaces have been used analytically in the detection of reducing analytes, such as nitrite and sulphite ions. This method is extremely efficient even at ppb concentrations.

Rhodium Porphyrins. Research on rhodium porphyrins appears to be substantially less than that of the manganese and cobalt porphyrins. This may, in part, be due to the high cost of the metal. Thus, the viability of using this metal as a reagent is limited to those complexes where exceptional reactivity is shown. Research into the uses of these porphyrins has revealed their applications in the enolisation of simple ketones[208] such as acetone. The generation of this class of reactive intermediates usually requires strongly basic conditions. Rhodium porphyrins also serve as efficient catalysts in the aerobic reduction of ketones with borane (BH_3).[209] Here the porphyrin generates borane from $NaBH_4$ despite the presence of an oxygen-rich environment, which usually quenches borane before it can react. The possibility that Rh(III) porphyrins may act as agents in the insertion of carbon monoxide into M–R (R = alkyl/aryl) bonds and possibly M–X (X = another transition metal) bonds has also been investigated.[210] The success of this research remains unclear. Another use of rhodium porphyrins has been in the modeling of biological amino-acid receptors[211] in an attempt to increase the specificity of coordination of amino-acid types to biological proteins in molecular-recognition research.

1.7 Complexes of Phosphines and Phosphonites

Due to the extensive research incorporating the substituted derivatives of triphenylphosphine to date, the scope of this discussion will be limited to phosphines and phosphonites with phenyl and alkyl substituents. For the sake of clarity, it must be noted that PR_3 (where R can be any combination of aryl or alkyl groups) phosphorous ligands are referred to as phosphines, $P(OR_1)_x(R_2)_{3-x}$ (where $R_1 \neq R_2$) phosphorous ligands are referred to as phosphonites and $P(OR)_3$

(where R is the same) is phosphorous ligands are more commonly referred to as phosphites.

Research involving bipyridine- and pyridine-substituted triphenylphosphine has little bearing on porphyrin chemistry as bidentate ligands are largely left to the domain of dimerisation or bridging attempts.

It is a classic teaching that trivalent phosphines are capable of back-bonding in their complexes with transition-metals. This is a result of phosphines having vacant π-symmetry d-orbitals. Phosphines are categorised as Lewis bases as they are capable of donating an electron pair to the metal, this they do through their full σ-symmetry p-orbitals. In many transition metals the metal has vacant σ-symmetry d-orbitals. The drawing in Figure 1.45 shows the interaction of the orbitals of a phosphorus(III) ligand with the central metal ion.
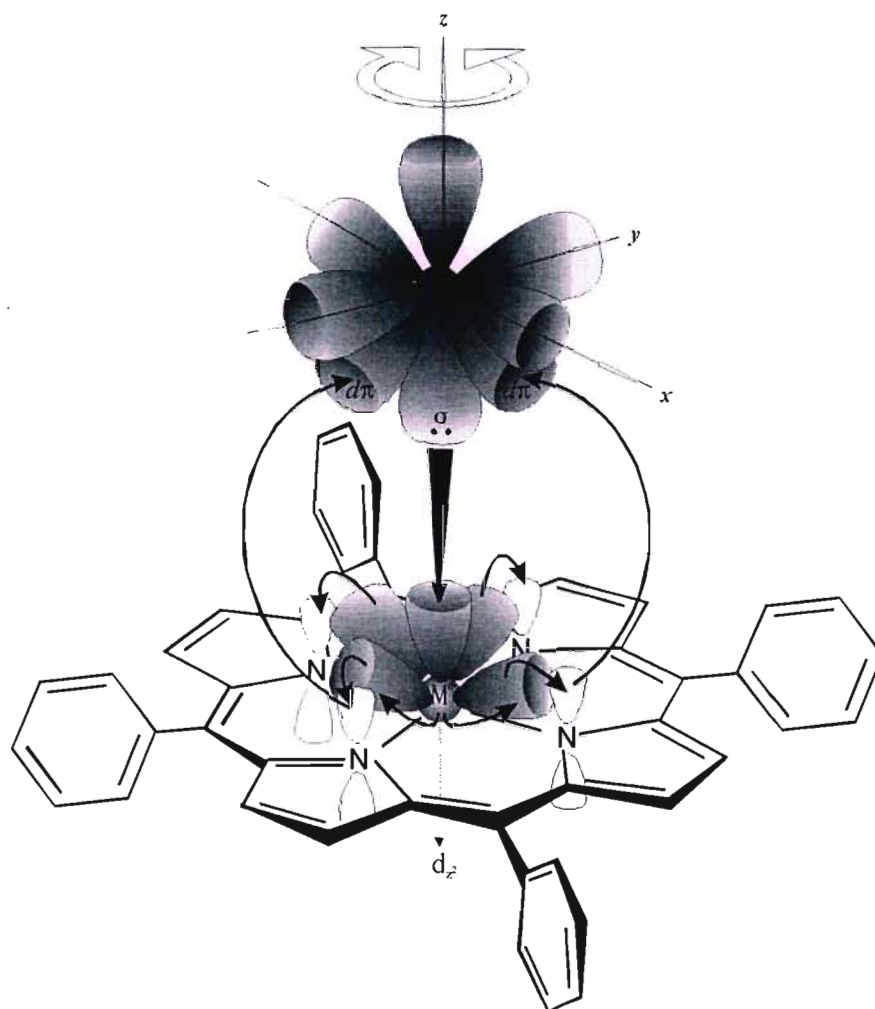
Figure 1.45: Drawing of a metalloporphyrin showing d_π-symmetry orbitals of metal and d_π-symmetry orbitals of an axial phosphine. Orbital phases are not shown.

65

The substituents of the phosphine overlap with the σ-symmetry orbitals of P. Protruding out of the phosphorus atom are the empty $d\pi$ orbitals which have the correct symmetry to overlap with the π-symmetry d-orbitals of the metal. Thus the phosphine has the ability to provide electron density in the correct symmetry orbital to the metal. The phosphine's vacant π-symmetry p-orbitals are capable of accepting excess electron density from the metal. Thus the phosphine-metal bonding can be roughly described as follows: (1) The phosphine with its full σ-symmetry p-orbitals overlap and form a bond with the vacant same-symmetry d-orbitals on the metal. Electron density flows from P→M. (2) The excess electron density now on the metal then bleeds off the metal back onto the phosphine (back-bonding) via the overlapping π-symmetry orbitals of both.[184] As a result of this approach it makes sense to determine what would affect the Lewis basicity of a phosphine and thus try and predict the relative binding strengths of a range of phosphines and phosphonites.

Studies performed by Wayland *et al.* showed that the presence of electronegative substituents results in a larger contribution of the phosphorous $3s$ orbital character to the σ-donor orbital.[212] Their calculations showed these contributions to be in the percentage range 27 to 68 %. This, they concluded, played a greater role in governing M–P bond lengths than back-bonding. Significantly, as the $3s$ character in the σ-donor orbital increases, so the metal–P bond distance decreases.

Thus, of the phosphine ligands used in this thesis one would want to assign an approximate order of Lewis basicity. Phosphonites have electron-withdrawing oxygen substituents, resulting in a decrease in σ-donor strength relative to the corresponding phosphines. The more phenyl substituents bound to the phosphine the poorer its donor strength, as phenyl substituents are electron withdrawing. With the addition of phenyl and similarly bulky substituents comes a larger steric hindrance also, presumably, lowering the binding strength. Inserting an oxygen into a P–C bond reduces the steric bulk of the tertiary phosphine, especially in the case of triphenylphosphine and triphenylphosphite. All of these factors make the binding strengths of each tertiary phosphine unique, and thus more challenging to predict.

Thus it is well accepted that π-back bonding plays a relatively insignificant role in the bonding character of the metal–phosphine bond in sterically hindered complexes such as porphyrins.[184] Steric factors and Lewis-base strength play an apparently more substantial role in the bonding. With an array of crystal structures and thus bond-lengths in the solid-state, attempts will be made

herein to determine the full effects of the substituents on the bonding character and bond-lengths between the metal and phosphine ligands. Figure 1.46 contains ORTEP[213] diagrams of the phosphines and related phosphonites used in this research work.

Triphenylphosphine (PPh₃)

Triphenylphosphite (PPh₃t)

Ethyldiphenylphosphine (Edpp)

Ethyldiphenylphosphonite (Edppt)

Diethylphenylphosphine (Depp)

Diethylphenylphosphonite (Deppt)

Triethylphosphine (Tep)

Triethylphosphite (Tept)
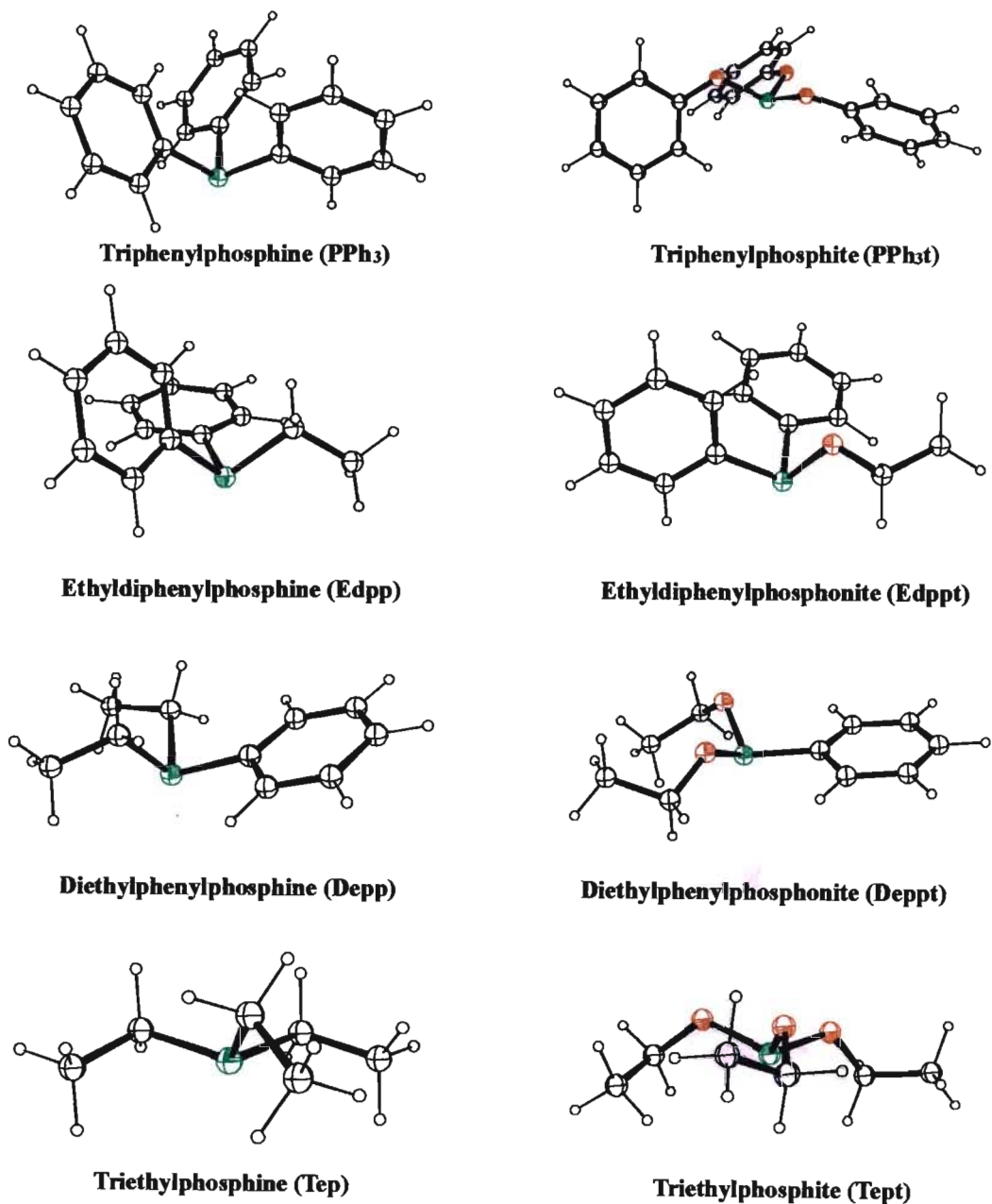
Figure 1.46: ORTEP diagrams of relevant phosphines and phosphonites.

1.8 ^{1}H NMR Spectroscopy

Of primary significance in the ^{1}H NMR spectra of diamagnetic metallopophyrins is the understanding of the 'ring current' induced perturbation of the porphyrin and axial ligand protons. The protons of the porphyrin are all shielded from the applied magnetic field to various degrees depending on their orientation relative to the main areas of delocalised electron density. These areas primarily exist where there is a large concentration of π-symmetry orbitals and thus increased π-electron density. These regions provide a shielding effect on the nearby protons and results in them having a lower effective local magnetic field and thus an upfield shift.[214]
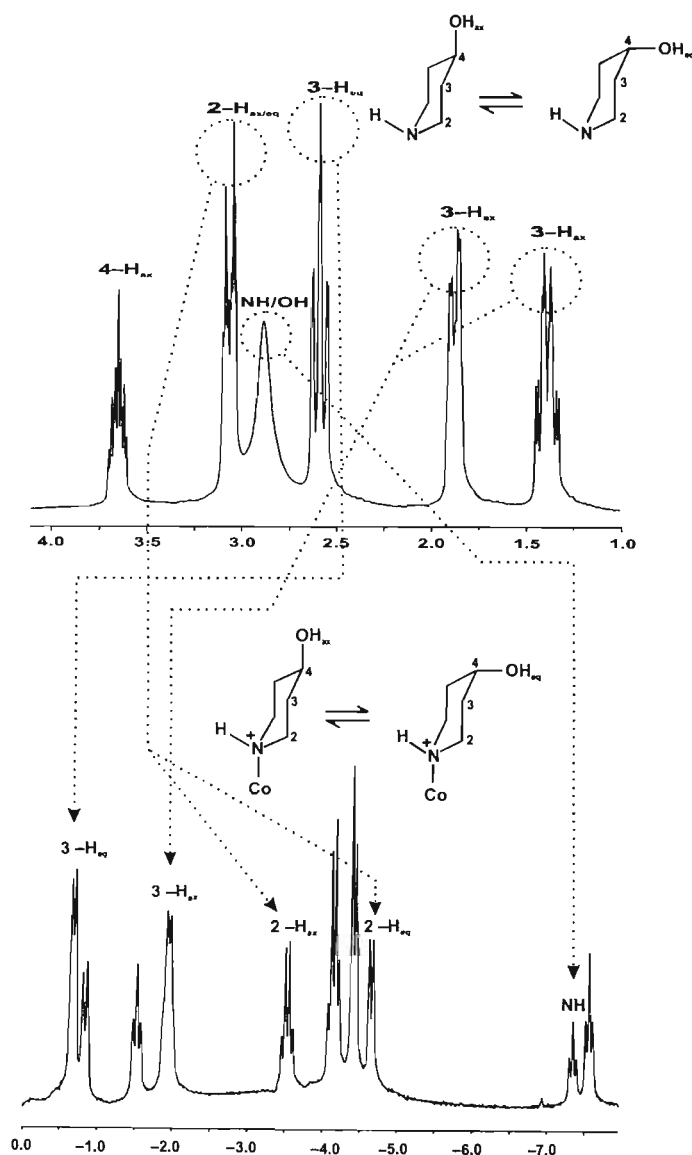
Figure 1.47: Diagram showing the effects of a porphyrin's 'ring current' on the ^{1}H NMR spectrum of [Co(TPP)(4-hydroxypip)$_2$]Cl (from ref. 214) and free 4-hydroxypiperidine.

A graphic example of this effect is given in Figure 1.47.[215] This diagram illustrates the upfield shifts of the 4-hydroxypiperidine proton signals upon coordination to a cobalt center in Co(TPP)Cl. The most noticeable ring-current effect is on the NH proton, where the corresponding signal has moved upfield by ~10 ppm relative to the uncoordinated 4-hydroxypiperidine. Also noticeable is that the ring current effect decreases as the distance from the coordinating atom increases. A simple representation of this effect is shown in Figure 1.48, where the "+" and "–" regions denote a shielding and deshielding of the protons in those environments, respectively.

The attributes of the proton NMR of porphyrins are largely dependent on the spin state and oxidation state of the metal centre as well as the nature of the axial ligands. The porphyrin macrocycle's "ring current effect" produces ring current induced shifts (RIS), which may result in wide spectral windows as shifts are spread out up to more than 15 ppm. In paramagnetic systems the observed proton chemical shifts are an additive result of diamagnetic and paramagnetic contributions. The diamagnetic contribution is the shift that would have been observed if there were no unpaired electrons in the molecule. The paramagnetic contribution (a. k. a. the hyperfine shift) is observed for molecules or ions where electron spin relaxation times are short. The hyperfine shift has two contributions: the contact and the dipolar terms. These terms arise due to the spin delocalisation from the unpaired electrons of the high-spin metal centre onto the porphyrin protons.[216]

The ring current is located in the plane of the macrocycle as well as slightly above and below it. This effect is diminished the further from the porphyrin's centre the proton is. Thus the typical free porphyrin has the pyrrole protons resonating further downfield and the phenyl protons (in the case of TPP) resonating at slightly lower frequencies. The *ortho* protons are downfield of the *meta* and *para* protons of the phenyl substituents. The *meta* and *para* protons are very similar with respect to chemical shifts, which are reasonably simply explained in terms of the ring current effect. When one looks at the *ortho*-protons, their closer proximity to the center of the macrocycle results in a downfield shift as expected. Likewise one would presume that the *meta* protons would be further downfield relative to the *para* protons because of the increasing distance from the center of the macrocycle, yet the *meta* protons are further away from the plane of the ring current which is also strongest in the plane of the macrocycle. Thus the *meta* protons are less deshielded and lie in very close proximity to the shifts of the *para* protons.

The splitting patterns for the protons of the TPP macrocycle are relatively easily understood, with the beta-protons typically producing a singlet because of their equivalence. The ortho protons couple with the meta protons which results in a doublet, the meta protons couple to both the ortho and para protons and thus display a multiplet. The para protons couple to the meta protons and this normally also results in a multiplet. Often the chemical shifts of the meta and para protons occur in a very similar region of the spectrum, resulting in the formation of large multiplets. The coupling constants for these aromatic protons are typically in the region of 6 – 10 Hz.
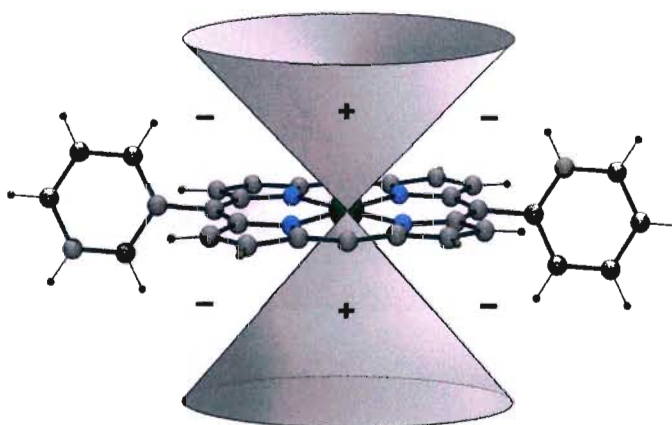
Figure 1.48: Diagram showing the ring current effect in porphyrins.

1.9 ^{31}P NMR Spectroscopy

^{31}P NMR remains a valuable tool in this field of research. The signals in the ^{31}P NMR spectra of the free ligands, given in Table 1.27, were singlets, which showed line broadening on coordination to the metal centres. In the spectra of the Rh(III) porphyrins the phosphorus nucleus of the phosphine/phosphonites in [Rh(TPP)(edpp)$_2$]SbF$_6$, [Rh(TPP)(deppt)$_2$]SbF$_6$ and [Rh(TPP)(edppt)$_2$]SbF$_6$ showed coupling to the rhodium centre to produce doublets. In the initial measurement of the ^{31}P NMR spectra of the free phosphine ligands in deuterated solvents the spectra showed a significant ratio of oxidised phosphine present. This proved invaluable as proof that the solvent degassing and drying techniques were crucial and were to be thoroughly carried out in order to prevent coordination of unwanted oxidation products.

An interesting trend in the ^{31}P NMR spectra of the free ligands is the movement either upfield or downfield of the signal depending on whether the compound is a phosphine or a phosphonite derivative.

Table 1.27: Summary of ^{31}P NMR Shifts for Related Phosphine and Phosphonite Ligands in CDCl$_3$^{a}:

Phosphine/Phosphonite	Free Ligand Shift (ppm)
depp	−14.52
depp(=O)	+44.61
deppt	+157.11
deppt(=O)	+25.64
edpp	−10.41
edpp(=O)	+35.48
edppt	+112.14
edppt(=O)	+22.44
PPh$_3$	−5.8
PPh$_3$(=O)	+28.1
PPh$_3$t	+129.1
PPh$_3$t(=O)	−16.4

^{a} Measurements from this work. Calibrated with H$_3$PO$_4$

The phosphines (depp, edpp and PPh$_3$) produce a signal far upfield and are all negative values (−14.52 ppm, −10.40 ppm, and −5.8 ppm, respectively). The corresponding phosphonites (deppt, edppt and PPh$_3$t) produce a signal far downfield (+157.11 ppm, +112.14 ppm and +129.1 ppm, respectively). Furthermore, on oxidation of a phosphine ligand to a phosphine oxide the ^{31}P signal moves downfield. In contrast, upon oxidation of a phosphonite ligand to a phosphonite oxide, the ^{31}P signal moves upfield.

1.10 ^{103}Rh NMR Spectroscopy

Rhodium occurs exclusively as one isotope with a nuclear spin I = ½. This nucleus[217] has a low magnetogyric ratio and thus low relative (to ^{1}H) resonance frequency of 3.16 MHz compared, for example, to 23.6 for ^{59}Co or 21.4 MHz for ^{195}Pt. This is unfortunately below the frequency obtainable with normal NMR probes. Additionally, this nucleus also has a low receptivity of 3.2 × 10^{-5}. Yet ^{103}Rh NMR spectra may be recorded indirectly via ^{31}P NMR of the sample since double resonance methods may be employed. This is a feasible option since the ^{103}Rh nucleus and ^{31}P nucleus both occur in absolute (100%) abundance. The presence of an axial phosphine and phosphonite in these complexes of Rh porphyrins allows probing of the Rh(III) center.

Since ^{103}Rh NMR of porphyrin complexes is unprecedented, attempts have been made to establish as comprehensive a range of ^{103}Rh NMR shifts with commercially available phosphines and phosphonites as possible.

In a brief survey of the literature to determine the range of ^{103}Rh chemical shifts commonly observed for Rh(III) complexes, it was observed that the rhodium(III) bis(phosphine) and bis(phosphonite) complexes synthesized in this research work exhibited ^{103}Rh chemical shifts far upfield (2365–2558 ppm) to those of the complexes generally observed in the literature. The O-donor hydroxo-bridged *aqua* complexes of rhodium(III) generally produce the most down-field chemical shifts in the range 9671 to 10 049 ppm.[218, 219] Likewise, the octahedral *aqua* complex [Rh(H$_2$O)$_6$]$^{3+}$ displays a ^{103}Rh chemical shift of 9924 ppm.[220]

The halogen-donor hexachloro and hexabromo complexes display more up-field shifts of 8025 and 7051 ppm, respectively. The N-donor complexes [Rh(NO$_2$)$_6$]$^{3-}$ and [Rh(NH$_3$)$_6$]$^{3+}$ display ^{103}Rh chemical shifts of 5580 and 4776 ppm, respectively. Two sulfur-donor complexes, [Rh{S$_2$P(Oet)$_2$}$_3$] and [Rh(SCN)$_6$]$^{3-}$ display ^{103}Rh chemical shifts of 3665 and 2726 ppm, respectively.[220]

These briefly surveyed spectroscopic data outline the progression of the ^{103}Rh chemical shift to more upfield chemical shifts with an increase in the electron-withdrawing strength of the coordinated ligands.

Work done by Leitner *et al.* has elucidated the relationship between rhodium chemical shifts and the electronic character of chelating bidentate phosphine ligand complexes.[221] The results of this work show that the degree of electon-donating strength of the axial ligand has a relatively minimal effect on the range of ^{103}Rh chemical shifts in Rh(I) cation complexes. Instead, it has been determined that the bulky substituents on these phosphines cause a deformation of the square planar coordination geometry around the central rhodium. This type of distortion causes a far more significant deshielding of the Rh nucleus, and thus a larger variation in chemical shifts is observed.

1.11 Infrared Spectroscopy

Table 1.28 contains the literature values of expected infrared absorption frequencies for the more

73

relevant bonds to phosphorus. These absorption bands have been used where possible to characterise the novel compounds synthesized in this research work.

Table 1.28: Literature Infrared Absorption Frequencies of Applicable P–X Bonds: [222]

P–X	Frequencies (cm^{-1})*
P=O	1310-1170(vs)
P–C (Ph)	1450-1425(s) and 1000
P–C (Alkyl)	750-650
P–O–C (Alkyl)	1050-1030 (s, br with ethyl/sharp with methyl)
P–O–C (Ar)	950-850
P–O–C (Et)	1090-1030
P–H	2440-2350 (stretching) and 1121-990 (bending)

* vs = very strong, s = strong, br = broad

1.12 Electronic Spectroscopy

The electronic spectra of porphyrins are well documented and largely regarded as a crucial means of quick and accurate characterization of both metallated and unmetallated porphyrins. The absorbance spectra, in brief, are representative of three major types of electronic transitions: (1) Intraligand $\pi \rightarrow \pi^*$ (bonding to antibonding) molecular orbital transitions. These transitions result in an intense B (Soret) band, a weaker Q band and two other bands, N and L. (2) d-d transitions within the $3d$-orbital manifold of the central metal, usually obscured by the $\pi \rightarrow \pi^*$ transitions. (3) Charge-transfer transitions which occur between the $3d$-orbitals of the metal and the molecular orbitals of the axial ligands and porphyrin.

The electronic spectra of metalloporphyrins may be categorized as either normal, hyper or hypso, which is characteristic of the arrangement of electrons in the d orbitals of the metal center. Before a porphyrin (the example used here will be H_2TPP) is metallated there are characteristically six significant absorption bands: (1) a shoulder at 373 nm; (2) an intense Soret band at 417 nm; and (3) four absorption bands at 515(IV), 552(III), 594(II) and 650(I) nm, respectively. The last four absorption bands experience the most dramatic and diagnostic perturbations with metallation. It is the perturbation, upon metallation, of this region of the spectrum that results in the possible classification of metalloporphyrin spectra[186,223] into the three-

abovementioned categories. Examples of each type of electronic spectrum are shown in Figure 1.49 below.
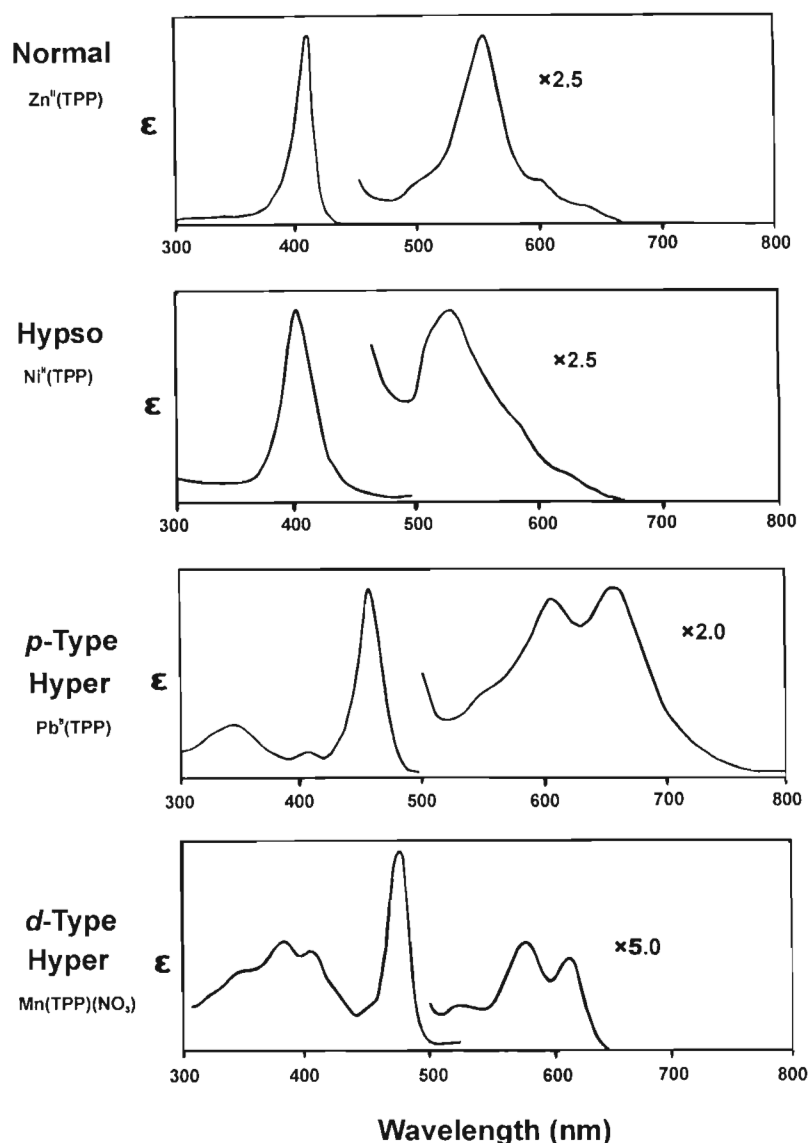
Figure 1.49: Examples of 'normal', 'hypso' and 'hyper' electronic spectra of metalloporphyrins.[223]

'Normal' **Spectra.** Characteristically, these spectra have one intense Soret/B-band between 320 and 450 nm and one or two absorbances (Q-bands) between 450 and 700 nm. As far as spectral differences between porphyrins and metalloporphyrins are concerned, the four bands become 2 bands in the visible region and are known as the α and β bands which fall into the same region as absorption bands I and III, respectively, of H_2TPP. These lower energy bands often show merging with *meso*-substitution. The Soret band may move but usually deviations are on a smaller level. The colour of this class of compound in solution is purple. This 'normal'

spectrum is characteristic of all metals of groups 1 to 5 with oxidation states of I to V respectively, as well as all other d^0 and d^{10} systems.

Non-metallated porphyrins also display *normal* spectra, but have four-banded spectra in the 450 to 700 nm region. These extra bands are a result of the lowering of the symmetry of the porphyrin from D_{4h} to D_{2h} symmetry due to the presence of protons on the pyrrole nitrogens.

'*Hyper*' Spectra. The *hyper* spectra are further categorized into *p*-type and *d*-type. These spectra show additional absorption bands when compared to the *normal* and *hypso* spectra. Generally, these bands appear to the blue of the *Q*-band and are of moderate intensity. The *p*-type spectra occur with main group elements in a low oxidation state, and the extra bands are a result of metal-to-ligand charge transfer. The *d*-type spectra are characteristic of d^1–d^6 systems only and usually these porphyrins are brown or green in solution. The extra bands in this class of spectra are as a result of porphyrin ligand-to-metal charge transfer transitions. Manganese(III) metalloporphyrins fall into this class of spectra. The electronic spectra for manganese porphyrins vary dramatically between oxidation and spin states, but the 6-coordinate porphyrin complexes characteristically display single, relatively sharp Soret bands in the region 470 – 480 nm. There are typically two or three relatively high-intensity *N* bands in the approximate range 375 – 425 nm, as well as three well-defined *Q* bands in the range 500 – 630 nm.[47, 58, 93]

'*Hypso*' Spectra. These spectra closely resemble *normal* spectra and differ only in the *Q*-bands, which are typically blue-shifted to wavelengths less than 570 nm. According to Gouterman[224] as the *d*-electron count increases with the late first-row transition metal ions, the spectra become less blue-shifted. These spectra only occur in d^6–d^9 systems. Cobalt(III) and rhodium(III) metalloporphyrins fall into this class of spectra. However, the 6-coordinate cobalt(III) porphyrins typically display *d*-type *hyper* spectra. In 1984, Doppelt *et al.* described an unprecedented "split" Soret band for a cobalt (III) porphyrin, with two absorption bands at 384 and 465 nm and three apparent *Q*-bands at 520, 585 and 640 nm.[137]

Rhodium porphyrins show spectra more consistent with the *hypso* spectra. They typically display a single Soret band that varies generally within a very limited range around 420 nm. There is also a lack of *N* bands, or if they are present they are generally weak and in the region of 340 – 365 nm. Consistent with this class of spectra, there are one to three *Q* bands to a higher wavelength, typically in the range 530 – 565 nm, to the Soret band.[179, 160]

Figure 1.50 below highlights the sensitivity of the electronic spectrum to the solvent system utilised. The figure shows the electronic spectrum of Mn^{III}(TPP)Cl and it's dependence on solvent and the oxidation state of the metal. The blue and green spectra correspond to a solution of the complex in dichloromethane and chloroform, respectively. Noticeable is the substantial shift of the Soret band to that of a shorter wavelength. The red spectrum corresponds to the reduction of Mn(III) to Mn(II). In this case the reduction process is easily identifiable using electronic spectroscopy and thus this method provides valuable assistance with characterisation in areas where other methods fail.
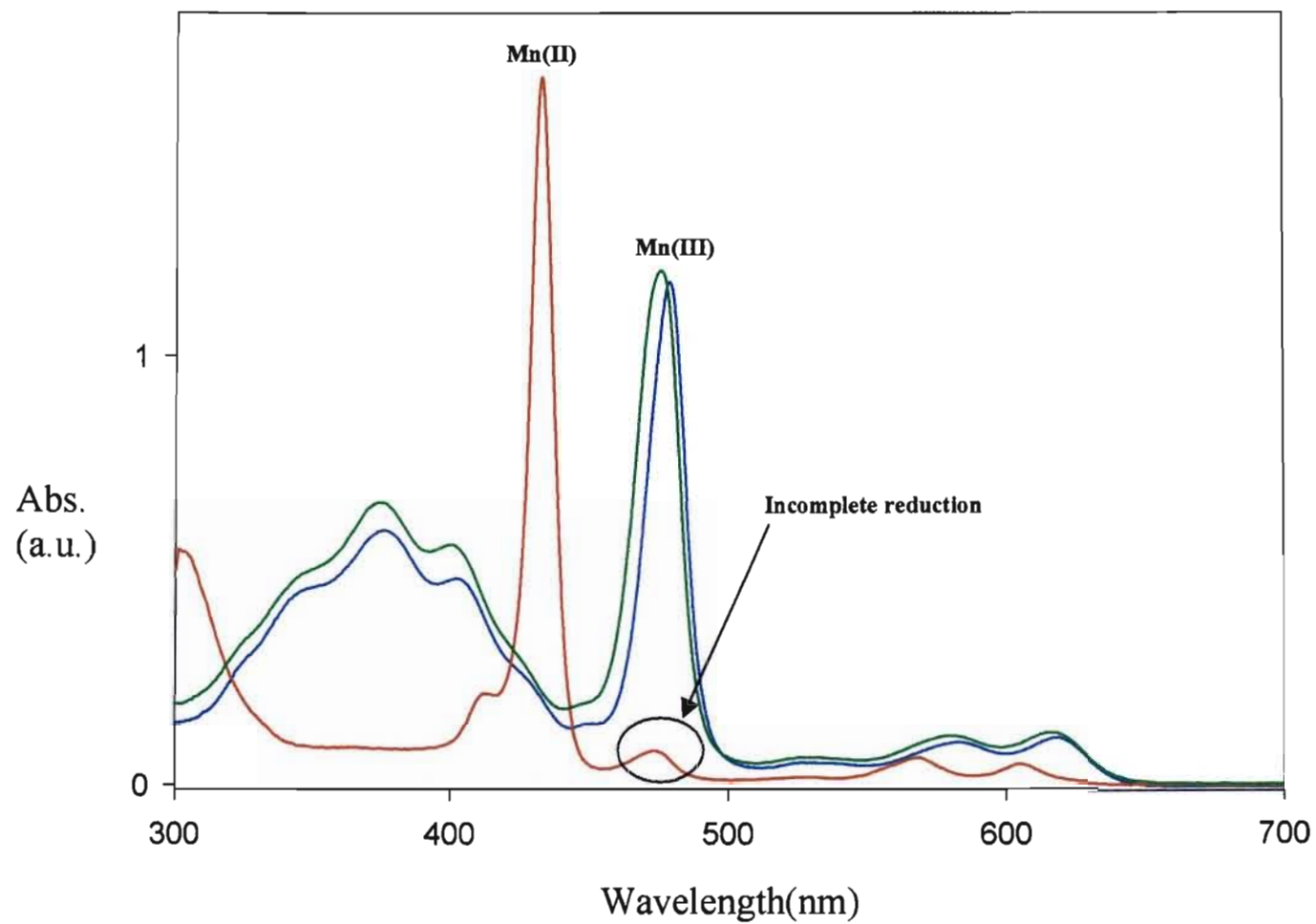
Figure 1.50: Electronic Spectra of [Mn$^{(III)}$(TPP)Cl] in CH$_2$Cl$_2$ and CHCl$_3$ and [Mn$^{(II)}$(TPP)]

CHAPTER TWO

PHOSPHINE AND PHOSPHONITE COMPLEXES OF Mn(III) PORPHYRINS

2.1 Reaction of Phosphines with Manganese (III) Porphyrin Precursors

In this Chapter, the coordination of phosphines and phosphonites to a manganese(III) porphyrin will be discussed. Very little is known about the behaviour of these compounds. To date there are no reported X-ray crystal structures of bis(phosphine) or bis(phosphonite) complexes of manganese(III) porphyrins. Large molar excesses (>20) of phosphine and phosphonite ligands were used in the synthesis of the complexes and when preparing samples for characterisation. This method was adopted because of the steric bulk of the phosphines and phosphonites used and to ensure 6-coordinate species were synthesized in preference to the 5-coordinate analogues. The intention in this investigation was to synthesize novel complexes of Mn(III) porphyrins with axial ligands related to triphenylphosphine and triphenylphosphite.

2.1.1 Synthesis and Characterization of [Mn(TPP)(PPh$_3$)$_2$](SbF$_6$)

Manganese has a strongly oxophilic character; extra precautions were therefore taken to ensure that solvents were thoroughly degassed and dried before use. A 50 molar excess of PPh$_3$ was added to the metathesis product, [Mn(TPP)(SbF$_6$)], in order to ensure coordination of the phosphine to the manganese centre. The reaction procedures are shown in equations 1 and 2 below.

$$[Mn(TPP)Cl] + AgSbF_6 \xrightarrow{\text{THF}} [Mn(TPP)FSbF_5] + AgCl(s) \dots\dots\dots(1)$$

$$[Mn(TPP)FSbF_5] + \text{excess } PPh_3 \xrightarrow{\text{CH}_2\text{Cl}_2} [Mn(TPP)(PPh_3)_2](SbF_6) \dots\dots\dots(2)$$
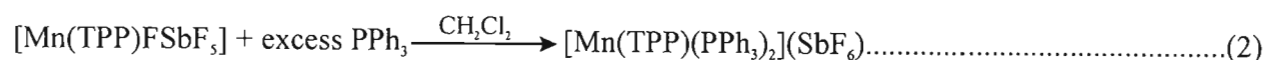
The solution of [Mn(TPP)(PPh$_3$)$_2$](SbF$_6$) was dark green/black, indicating a Mn(III) complex. The synthesis was repeated a number of times without successful isolation of X-ray quality crystals. After rigorous degassing procedures and saturation of the hexane layer with excess PPh$_3$, an X-ray quality crystal was isolated from a polycrystalline reaction product.

The Mn(III) ion in $[Mn(TPP)(PPh_3)_2](SbF_6)$ is paramagnetic (high-spin d^4). ^1H NMR studies reported by Goff and Hansen on manganese porphyrins with N-donors showed that dramatic increases in line broadening occurred in the change of spin state from low-spin to high-spin.[185] A significant observation is that P-donor ligands characteristically cause considerably shorter relaxation times for the hydrogen nuclei in manganese(III) porphyrin complexes. A transformation from an S = 1 state to an S = 2 state results in a dramatic increase in the unpaired-spin density on the porphyrin, the relaxation times of the nucleus being probed are thus shortened. This explains the lack of assignable signals observed for the ^1H, ^{13}C and ^{31}P NMR spectra for this compound, despite repeated attempts.

Thus ^1H NMR, ^{13}C NMR and ^{31}P NMR measurements of the manganese complexes are largely ignored in this Chapter and emphasis is placed on X-Ray, IR and UV-vis characterisation. The IR and UV-vis spectral data for $[Mn(TPP)(PPh_3)_2](SbF_6)$ are given in Table 2.1. Elemental analysis was also omitted as the crystals of pure $[Mn(TPP)(PPh_3)_2](SbF_6)$ could not be isolated from the bulk material which evidently contained unreacted PPh_3 (excess).

Table 2.1 Spectroscopic data for $[Mn(TPP)(PPh_3)_2](SbF_6)$

Infrared ^{a}	1434.8 (s, $\nu(P–C_{Ph})$) and 1025.8 (m, $\nu(P–C_{Ph})$)
UV-vis ^{b}	620 (6.6×10^3), 584 (5.8×10^3), 532 (2.5×10^3), 478 (7.8×10^4), 448 (8.5×10^3), 401 (3.0×10^4), 374 (3.7×10^4)

^{a} $\bar{\nu}$ (cm^{-1}). KBr disk. ^{b} λ_{max}/nm (ε/$dm^3 mol^{-1} cm^{-1}$). Measured at 298 K in dried and degassed dichloroethane.

Figure 2.1 shows the electronic spectrum of $[Mn(TPP)(PPh_3)_2](SbF_6)$ in the range 800–350 nm. The electronic spectrum and molar extinction coefficient measurements were run in solutions of excess PPh_3 ligand to ensure negligible dissociation of the complex to form the unwanted 5-coordinate species in solution. At higher PPh_3 concentrations, the sampling wavelength range becomes immeasurable below 430–350 nm due to the dominant absorption of the phenyl substituents of the PPh_3 ligand.

The electronic spectrum appears consistent with that expected for a six-coordinate manganese(III) porphyrin, as is discussed in Chapter 1.12. The profile of the Soret, or B(0, 0), band at 478 nm is sharp and intense and one can presume that there is a single 6-coordinate

species in solution. There are two N bands in the lower wavelength region of the spectrum, namely, the $N(1, 0)$ and $N(0, 0)$ bands at 374 and 401 nm, respectively. The three Q bands, $N(0, 0)$, $N(1, 0)$ and $N(1, 0)$, are at 620, 584 and 532 nm, respectively.

All drying and degassing precautions were taken in order to eliminate the possibility of inaccurate spectra due to oxidation products of PPh$_3$. The infrared spectrum was recorded with the compound suspended in a KBr disk in the range 4000–450 cm^{-1}.
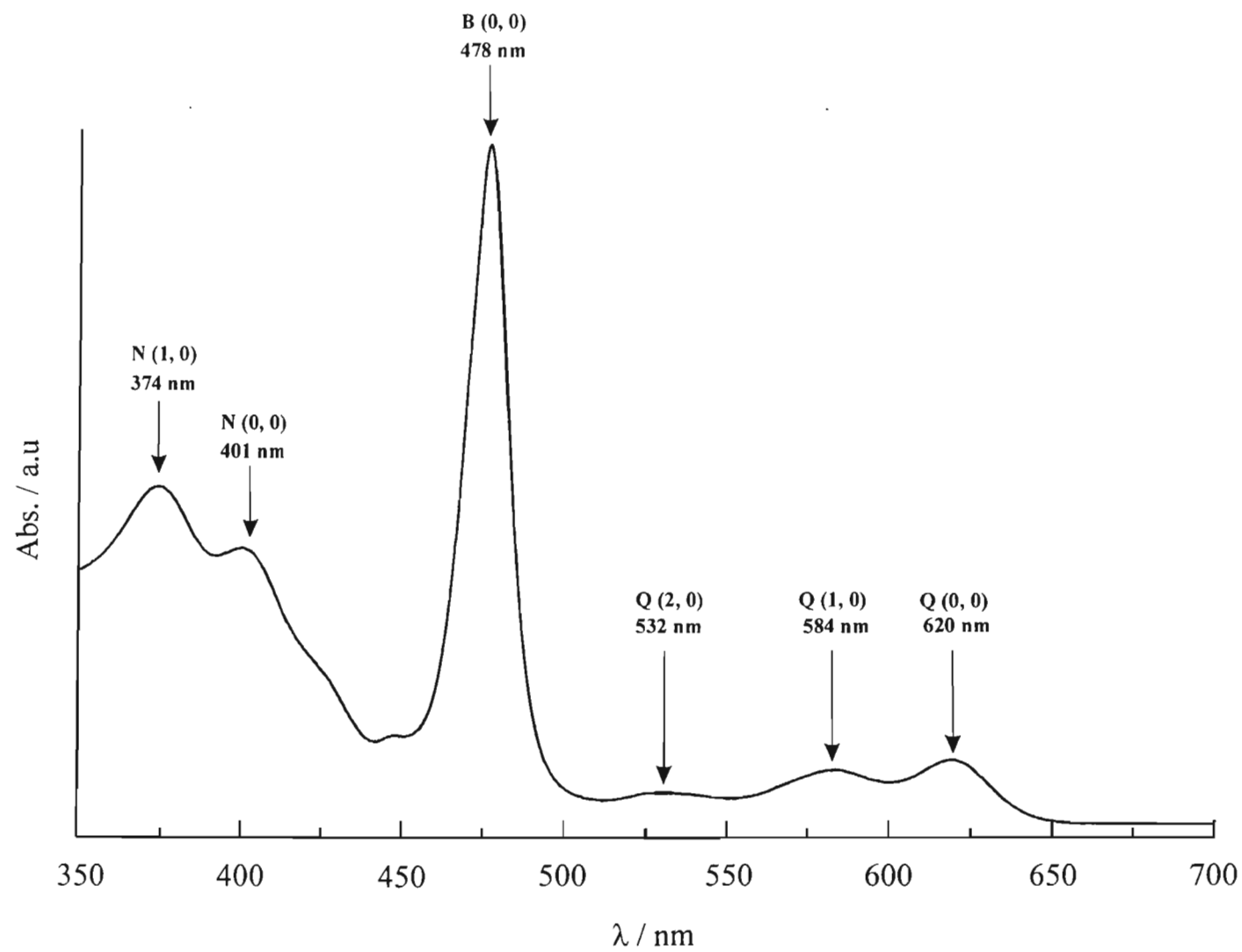
Figure 2.1: Electronic spectrum of [MnTPP)(PPh$_3$)$_2$](SbF$_6$) in dichloroethane at 25 °C.

2.1.2 Crystal Structure Determination of [Mn(TPP)(PPh₃)₂](SbF₆)

X-ray quality crystals of [Mn(TPP)(PPh₃)₂](SbF₆) were withdrawn from the supernatant CH_2Cl_2 / hexane solvent system in the Schlenk tubes using Paratone® oil on a stainless steel spatula. The single crystals were covered in Paratone® oil and then mounted onto thin glass fibres for X-Ray structure determination. The data collection was performed at 210 K in anticipation of substantial thermal motion of the sterically hindered PPh₃ ligands. The resulting X-ray crystal structure is shown in the ORTEP diagram in Figure 2.2. It must be noted that the bulk of the sample was a polycrystalline mixture of excess triphenylphosphine and [Mn(TPP)(PPh₃)₂](SbF₆) and thus unsuitable for elemental analysis.

The compound crystallizes in the monoclinic crystal system in the $P2_1/c$ space group. There are four asymmetric units per unit cell. The asymmetric unit contains no center of inversion, and thus no symmetry operations were needed to generate the full complex. The final R_1 index is 0.0803. The crystal structure shows significant thermal motion within the phenyl substituents of the PPh₃ as well as the TPP macrocycle. In the crystal structure of [Mn(TPP)(PPh₃)₂](SbF₆) the average Mn–P bond length is 3.088(2) Å. The average Mn–N bond length is 1.998(6) Å. These axial bond lengths are substantially greater than those observed for any of the complexes surveyed in Chapter 1. The axial bond length of the 5-coordinate iodine complex [41] at 2.749 Å is the closest to this figure.

The P–Mn–P angle is 170° due to the off-axis tilting of the axial triphenylphosphine ligands. The reasons for the off-axis tilt are the contacts between the phenyls of the coordinated triphenylphosphine ligand and the triphenylphosphine phenyls of the adjacent complex. The contacts are between the phenyl carbon C66 and the proton on carbon C75 in a neighbouring complex. This interaction distance is 2.796 Å. The opposing axial triphenylphosphine has a contact between the proton on carbon C94 and the proton on carbon C73 of a neighbouring complex. This interaction distance 2.325 Å.

The Mn(III) ion is located slightly out of the mean plane of the macrocycle by 0.027 Å and a moderate degree of saddling of the porphyrin ring is also evident from Figure 2.6. The β-carbons display the largest displacements from the 24-atom mean plane, with the two largest deviations being Cb2 and Cb4 at 0.20 and 0.21 Å, respectively, on alternate sides of the mean plane.
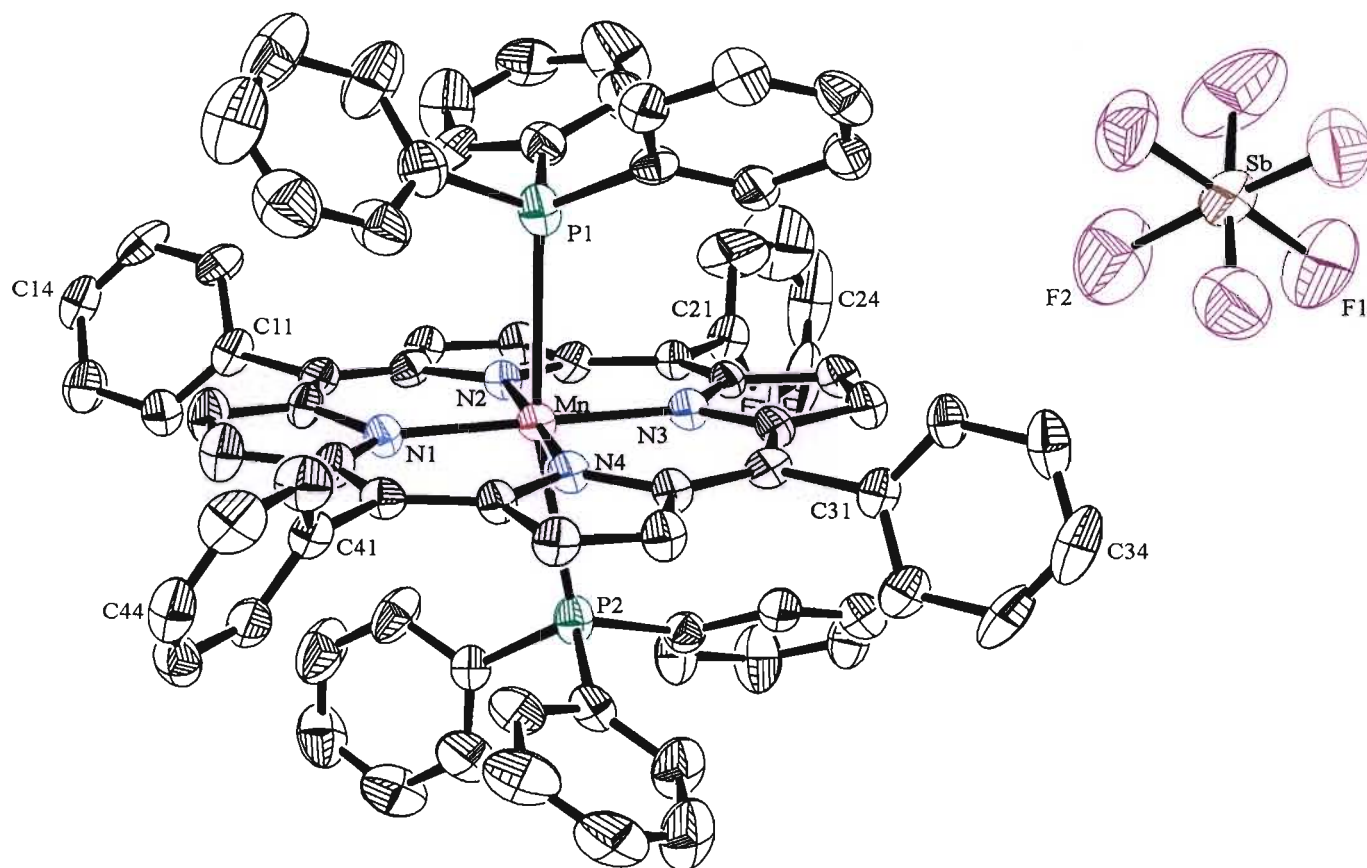
Figure 2.2: Selectively labelled ORTEP diagram of the X-Ray crystal structure of [Mn(TPP)(PPh₃)₂](SbF₆). H-atoms have been omitted for clarity. Thermal ellipsoids are drawn at the 30% probability level.

The disorder of one of the phenyl substituents within one of the axial triphenylphosphine ligands is shown in Figure 2.3.
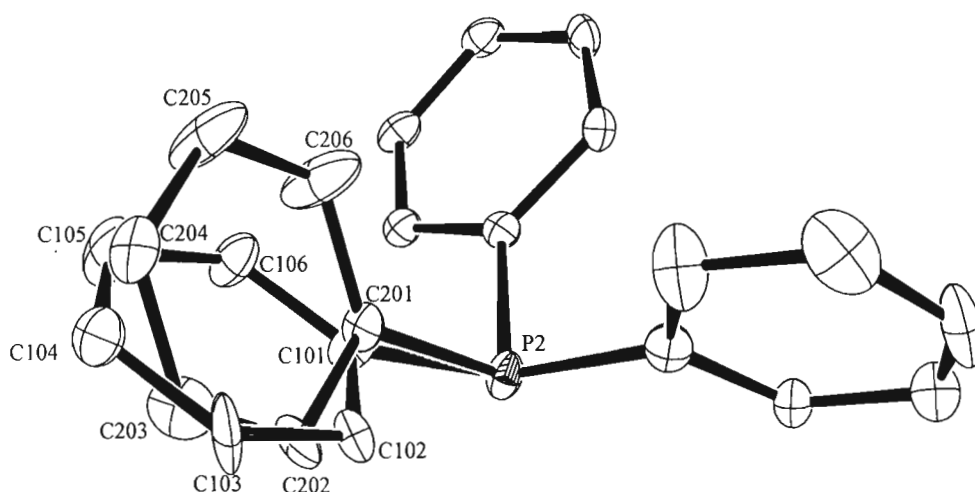
Figure 2.3: **ORTEP diagram of the disordered triphenylphosphine ligand in [Mn(TPP)(PPh₃)₂](SbF₆).**

It is obvious from Figure 2.3 that there are predominantly two positions of this phenyl group with atoms C101 to C106 forming one phenyl ring orientation and atoms C201 to C206 forming the other phenyl ring orientation. Atoms C101 and C201 are 0.270 Å away from each other, and the furthest deviations of the atoms, within these phenyl groups, from each other are 1.512 Å for atoms C105 and C205 followed by 1.244 Å for atoms C106 and C206. The angle between the planes of these two phenyl groups is 42.90°, which means that these phenyls do not only deviate from each other by a movement away from a porphyrin pyrrole (N2, Ca3, Ca4, Cb3 and Cb4), but also by rotation.

In order to identify and quantify these intramolecular contacts between the axial triphenylphosphine and the porphyrin a close-contacts diagram was drawn using Mercury 1.1. Figure 2.4 shows the atoms C201 to C206 with their corresponding protons and their spatial contacts within their van der Waal's radii. From this figure it may be observed how the proton on C202 (H202) displays obvious contacts with the N2 pyrrole of the porphyrin. These contacts thus justify the second orientation for this phenyl as shown in Figure 2.5.

85

C201 to C206

2.517 Å (H202–N2)
2.427 Å (H202–Ca3)
2.875 Å (H202–Cb3)
2.806 Å (H202–Ca4)

H202
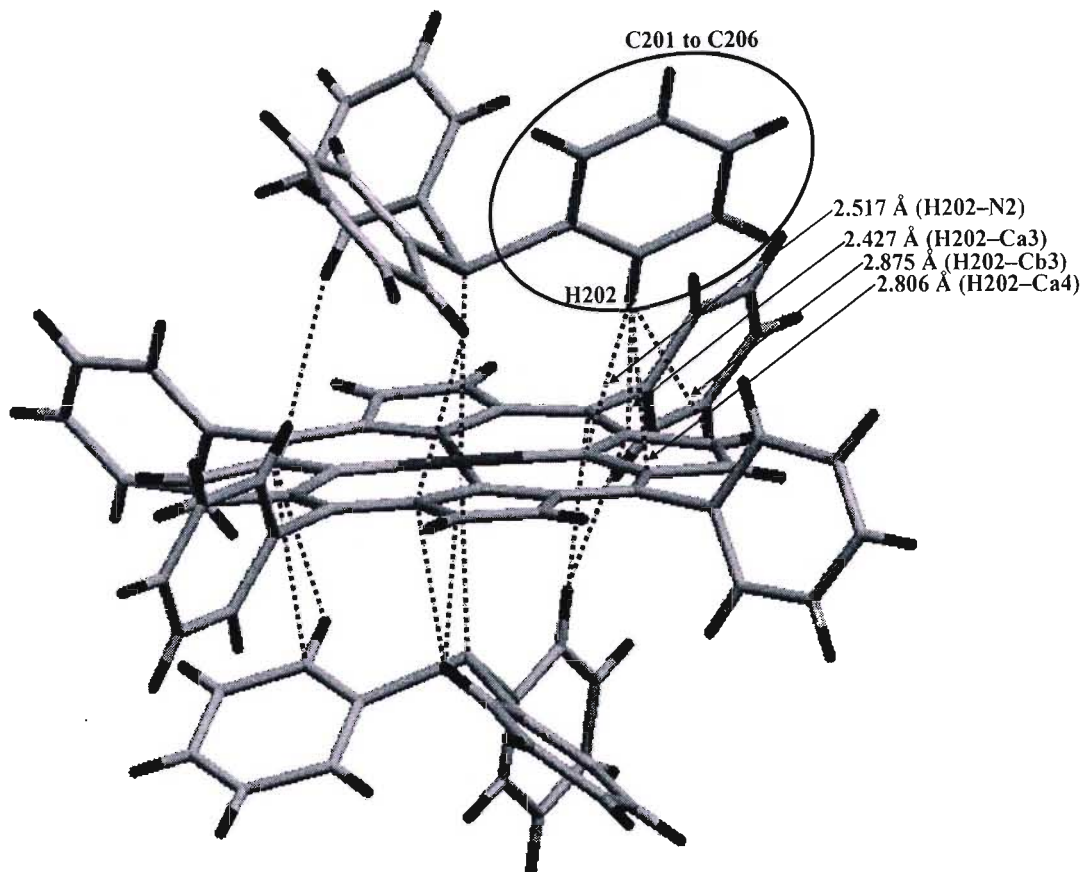
Figure 2.4: Diagram (Mercury 1.1) of the close contacts within the X-ray crystal structure of [Mn(TPP)(PPh₃)₂](SbF₆). Close contacts of atoms C201 to C206 of the disordered axial triphenylphosphine are shown.

Figure 2.5 shows the contacts for the second phenyl orientation (C101 to C106) and also the remaining close-contacts within the X-ray crystal structure. It is noticeable how this orientation of the disordered phenyl within the triphenylphosphine displays no contacts with the porphyrin, and that in Figure 2.4 each phenyl in the axial ligand has an atom with a close contact with the porphyrin. This emphasises the large steric bulk of the triphenylphosphine ligand.
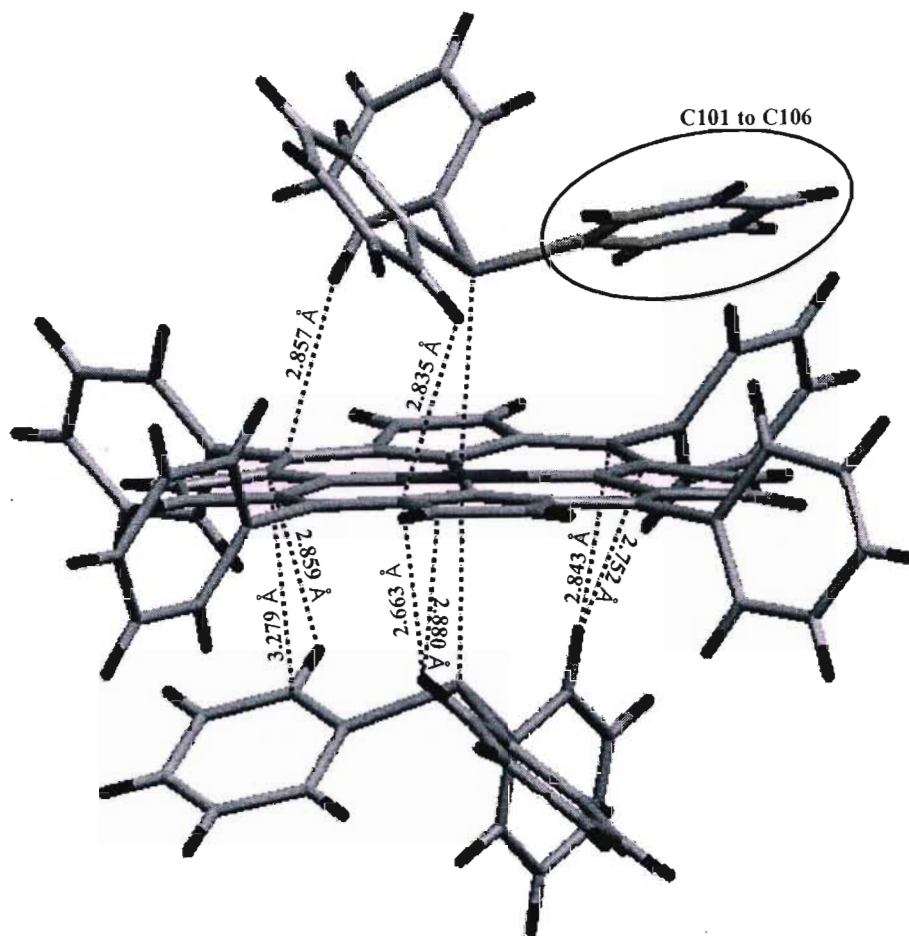
Figure 2.5: Diagram (Mercury 1.1) of the close contacts within the X-ray crystal structure of [Mn(TPP)(PPh₃)₂](SbF₆).

The axial ligand orientations, porphyrin core geometry and mean plane deviations have been summarised in Figure 2.6. The macrocycle bond lengths and angles are also summarised in Figure 2.6.

The dihedral angles of the phenyl substituents relative to the mean plane of the porphyrin macrocycle are: C11–C16 = 61.01°; C21–C26 = 77.04°; C31–C36 = 72.02° and C41–C46 = 66.41°. These acute angles are likely to be responsible for the weakly saddled porphyrin core conformation as a result of intramolecular van der Waals repulsion between the tipped aryl rings and the adjacent pyrrole rings.

Figure 2.6: Crystallographic information for [Mn(TPP)(PPh₃)₂](SbF₆). Displacements from the 24-atom mean plane are given in pm; bond lengths are in Å.

The individual separations of the atoms in the disordered phenyls (where C101 to C106 form the first phenyl ring orientation and C201 to C206 from the second phenyl ring orientation) from each other are: C101···C201 = 0.270 Å; C102···C202 = 0.548 Å; C103···C203 = 0.465 Å; C104···C204 = 0.853 Å; C105···C205 = 1.512 Å and C106···C206 = 1.244 Å.

A view of the unit cell packing diagram is shown in Figure 2.7. The packing pattern is quite elegant when the unit cell is viewed down the *a*-axis.
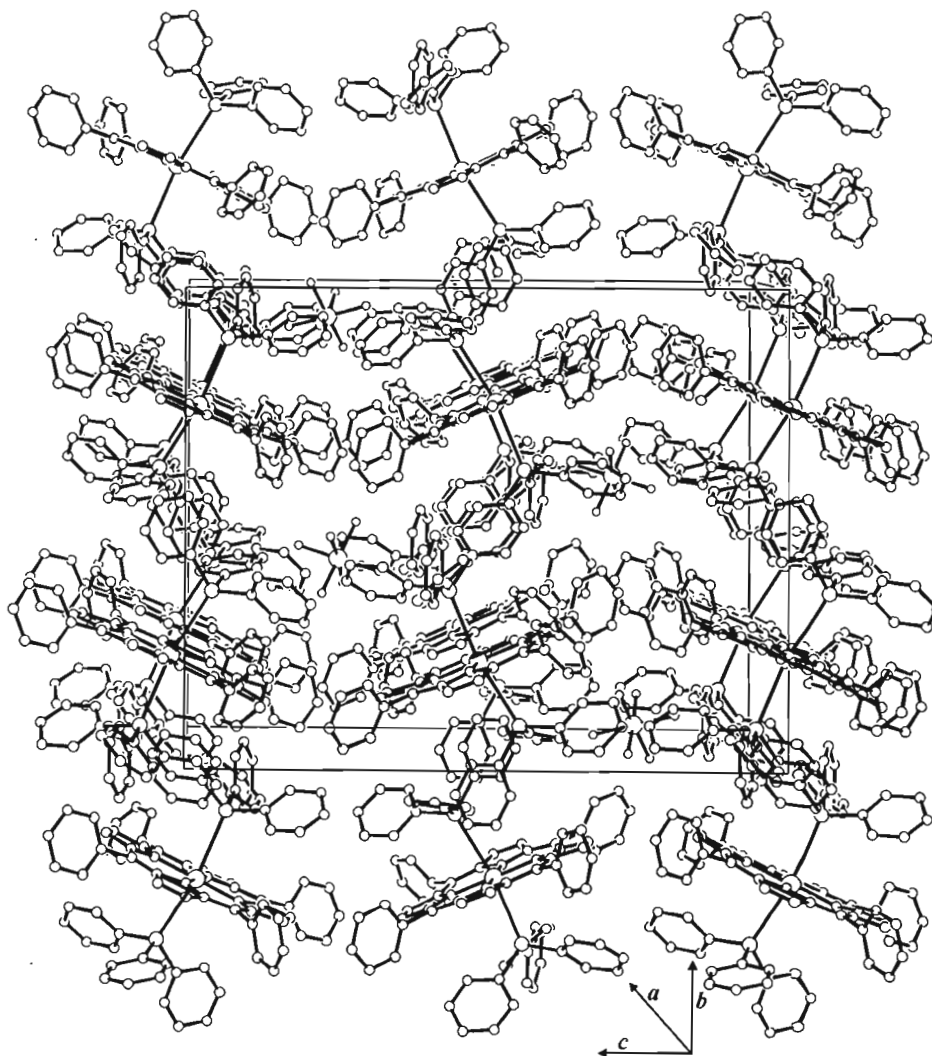
Figure 2.7: ORTEP diagram of unit cell (along the *a*-axis).

In Figure 2.7, a distinct pattern of arrangement of the porphyrin complexes within the unit cell is noticeable. This repeated pattern is simplified in Figure 2.8 and may be likened to a 'herringbone' arrangement.
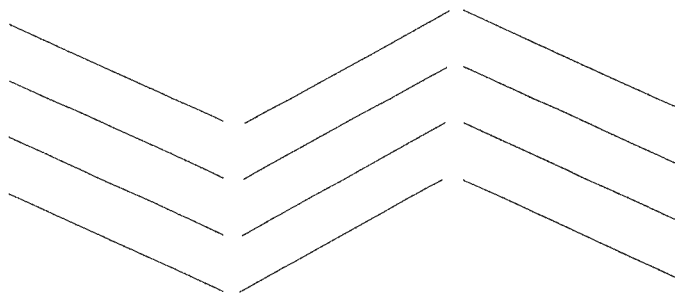
Figure 2.8: 'Herringbone'-type arrangement of [Mn(TPP)(PPh₃)₂](SbF₆) within unit cell.

A view of the complex perpendicular to the porphyrin plane and roughly down the P–Mn–P axis is shown in Figure 2.9. The torsion angles of the axial phenyls of the triphenylphosphine are summarized pictorially in the upper diagram in Figure 2.6. Note that there is no inversion symmetry in this molecule and the opposing phosphorus centers do not exactly eclipse each other. This is due, in part, to the large number of inter-atomic contacts between the axial triphenylphosphine ligands and the porphyrin causing an off-axis tilt.
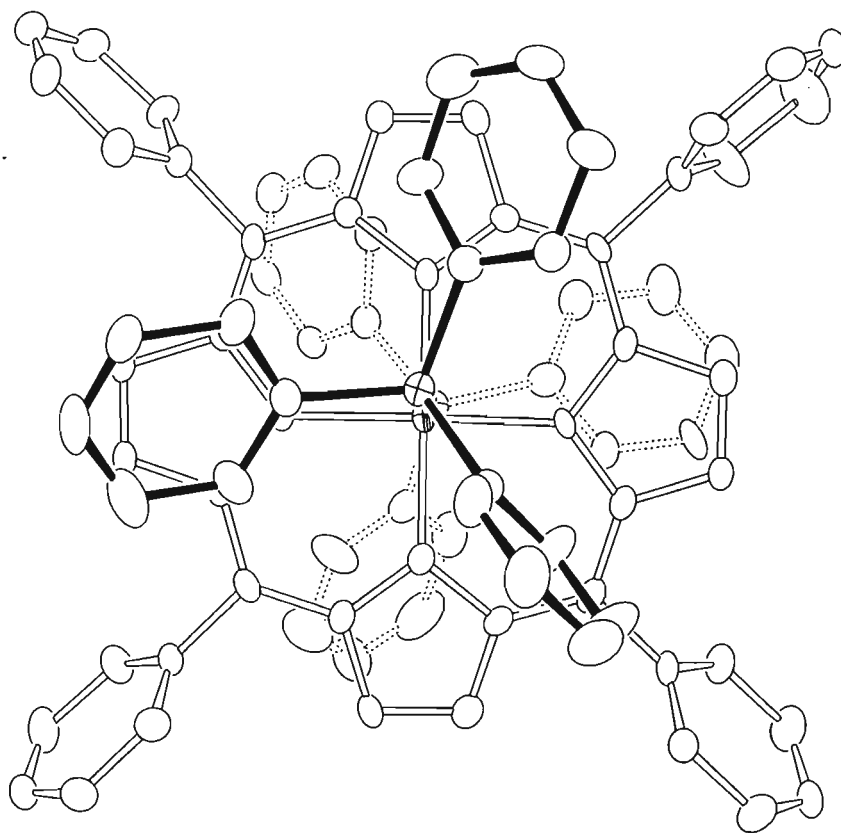
Figure 2.9: ORTEP diagram of the [Mn(TPP)(PPh₃)₂]⁺ cation perpendicular to the porphyrin mean plane. H-atoms have been omitted for clarity. Thermal ellipsoids are drawn at the 30 % probability level.

2.2 Reaction of Diphenylphosphonate with [Mn(TPP)(FSbF$_5$)]

The intention of this specific reaction was to synthesize a bis(triphenylphosphite) complex of Mn(III), according to reaction scheme 1 and 2 below, to be compared structurally with the bis(triphenylphosphine) complex in Section 2.1.

$$[Mn(TPP)Cl] + AgSbF_6 \xrightarrow{\text{THF}} [Mn(TPP)FSbF_5] + AgCl(s) \dots\dots\dots\dots\dots\dots\dots(1)$$

$$[Mn(TPP)FSbF_5] + \text{excess } P(OPh)_3 \xrightarrow{\text{CH}_2\text{Cl}_2} [Mn(TPP)\{P(OPh)_3\}_2](SbF_6) \dots\dots\dots\dots\dots(2)$$

However, reaction 2 was not observed and the resulting complex was an unexpected oxygen-bound 5-coordinate species [Mn(TPP){(O)PH(OPh)$_2$}](SbF$_6$). This phosphine oxide ligand, more specifically known as diphenylphosphonate (shown in Figure 2.10), was initially presumed to be an oxidation product derived from the presence of oxygen in the solvents used. However, after extensive investigation via GC/GC-MS, it was discovered that the phosphine oxide is a contaminant in the commercial reagent PPh$_3$t. Thus, the crystallization of the bis(triphenylphosphite) complex remains to be optimised. It is noteworthy, however, that even with a 20 molar excess of the PPh$_3$t ligand in solution the preferred reaction product contains the phosphine-oxide. This confirms the oxophilic nature of Mn(III) and further suggests a low binding constant for triphenylphosphite, possibly due to steric factors. The stability constants of a range of [Mn(TPP)(PR$_3$)$_2$](SbF$_6$) derivatives will be measured in a separate work.

2.2.1 Synthesis and Characterisation of [Mn(TPP){(O)PH(OPh)$_2$}](SbF$_6$)

Since the desired reaction product was different to the actual complex obtained experimentally, the experimental method mentioned in Section 2.3.3 is not the recommended synthetic route for the synthesis of [Mn(TPP){(O)PH(OPh)$_2$}](SbF$_6$). It is recommended that the bottled PPh$_3$t (shown in Figure 2.11) be either distilled or reacted with a Mn(III) salt in a non-coordinating solvent and filtered off as an oxide-free reagent in order to synthesize [Mn(TPP)(PPh$_3$t)$_2$}](SbF$_6$). Neither of these two methods of purification was utilised in this specific synthesis.
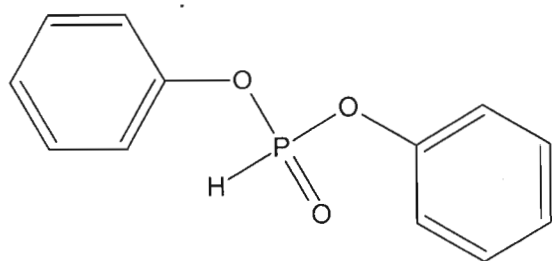
Figure 2.10: Diphenylphosphonate   **Figure 2.11: Triphenylphosphite**
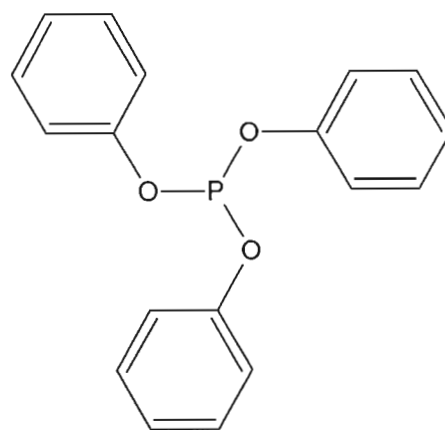
Characterisation of this compound outside of X-ray crystallography has been limited, as the compound is notably an undesired product. The NMR sample was made up of the crystallized material resulting from the crystallization attempt; thus the majority of the material is presumably the correct compound [Mn(TPP)(PPh3t)2](SbF6). This naturally makes the characterisation of the oxide derivative extremely difficult. This is shown in the ^{31}P NMR spectrum where the major product, at 116.91 ppm, in the sample corresponds to bound PPh3t ligand.

Table 2.2: Spectroscopic Data for [Mn(TPP){(O)PH(OPh)2}](SbF6)

^{1}H NMR[a]	Ligand: 4.31 (br s, *o*-H), 3.83 (br s, *m*-H), 3.43 (br s, *p*-H)
^{31}P NMR[a]	116.91 (s w, bound PPh3t)
Infrared[b]	1195.9 (str, ν(P=O)) and 861.3 (str, ν(P–OPh))

[a] Chemical shifts in ppm. Measured at 294 K in CDCl3, s = singlet, d = doublet, t = triplet, m = multiplet, str = strong, m = medium, w = weak, sh = sharp, br = broad. [b] ṽ (cm^{-1}). KBr disk.

2.2.2 Crystal Structure Determination of [Mn(TPP){(O)PH(OPh)2}](SbF6)

As mentioned above X-ray crystallography has been the only method of characterisation for this compound. Single crystals were isolated from the supernatant CH2Cl2 / hexane solvent system and covered in Paratone® oil. The crystals were then mounted onto thin glass fibres for X-ray structure determination. The data collection was performed at room temperature.

The ORTEP diagram of the X-ray crystal structure of [Mn(TPP){(O)PH(OPh)$_2$}](SbF$_6$) is shown in Figure 2.12. This compound crystallized in the monoclinic crystal system in the $P2_1/n$ space group. There are four asymmetric units per unit cell. The compound crystallizes in a general position and does not exhibit any recognisable symmetry. The final R_1 index was 0.0593. The complex is 5-coordinate and the phosphine-oxide is oxygen-bound to the Mn(III) metal centre. The steric hindrance of the intended PPh$_3$t axial ligand within this class of compounds is substantially greater than that associated with the diphenylphosphonate ligand, as well as the inherent affinity manganese centers have for O-donors, probably explains the formation of [Mn(TPP){(O)PH(OPh)$_2$}](SbF$_6$). Since the steric hindrance contribution from the porphyrin macrocycle is primarily from the phenyl substituents, it is understandable that coordination by oxygen results in a larger spatial separation between the macrocycle phenyls and those phenyls of the axial phosphonate.

The saddling of the macrocycle is significantly larger than that observed in [Mn(TPP)(PPh$_3$)$_2$](SbF$_6$) and is summarised in Figure 2.13. This is attributed to the steric interaction of neighbouring molecules that are present in close proximity in the lattice. Since this compound is 5-coordinate it is susceptible to close back-to-back packing by other 5-coordinate species, in this situation the inter-manganese spacing is 5.242 Å which is short compared to 12.113 Å for the equivalent spacing in [Mn(TPP)(PPh$_3$)$_2$](SbF$_6$). This reduced spatial separation results in increased steric perturbation between phenyl substituents of neighbouring compounds.

The Mn–O bond length is 2.122(3) Å, which is significantly shorter than the Mn–P bond length of 3.088(2) Å observed in [Mn(TPP)(PPh$_3$)$_2$](SbF$_6$) The average Mn–N bond length is 2.002(3) Å. This axial bond length is amongst the shortest observed for Mn–O lengths in the literature surveyed and discussed in Chapter 1. The axial length of the 5-coordinate ethanol complex 7, at 2.145 Å, exhibits the closest length to that observed in this complex.

The Mn(III) ion protrudes from the 24 atom mean plane by 0.154 Å towards the oxygen of the axial ligand. The *beta*-carbons deviate the most from planarity with a range of 0.29 to 0.40 Å. The hydrogen bound (H100) to the phosphine, located in the difference Fourier map, has been left in the ORTEP diagram in Figure 2.11 in order to show the hydrogen-bonding between this proton and one of the fluorine atoms of the SbF$_6^-$ counter-ion. This proton is displaced from its tetrahedral-point position on the phosphine in a direction towards the counter-ion.
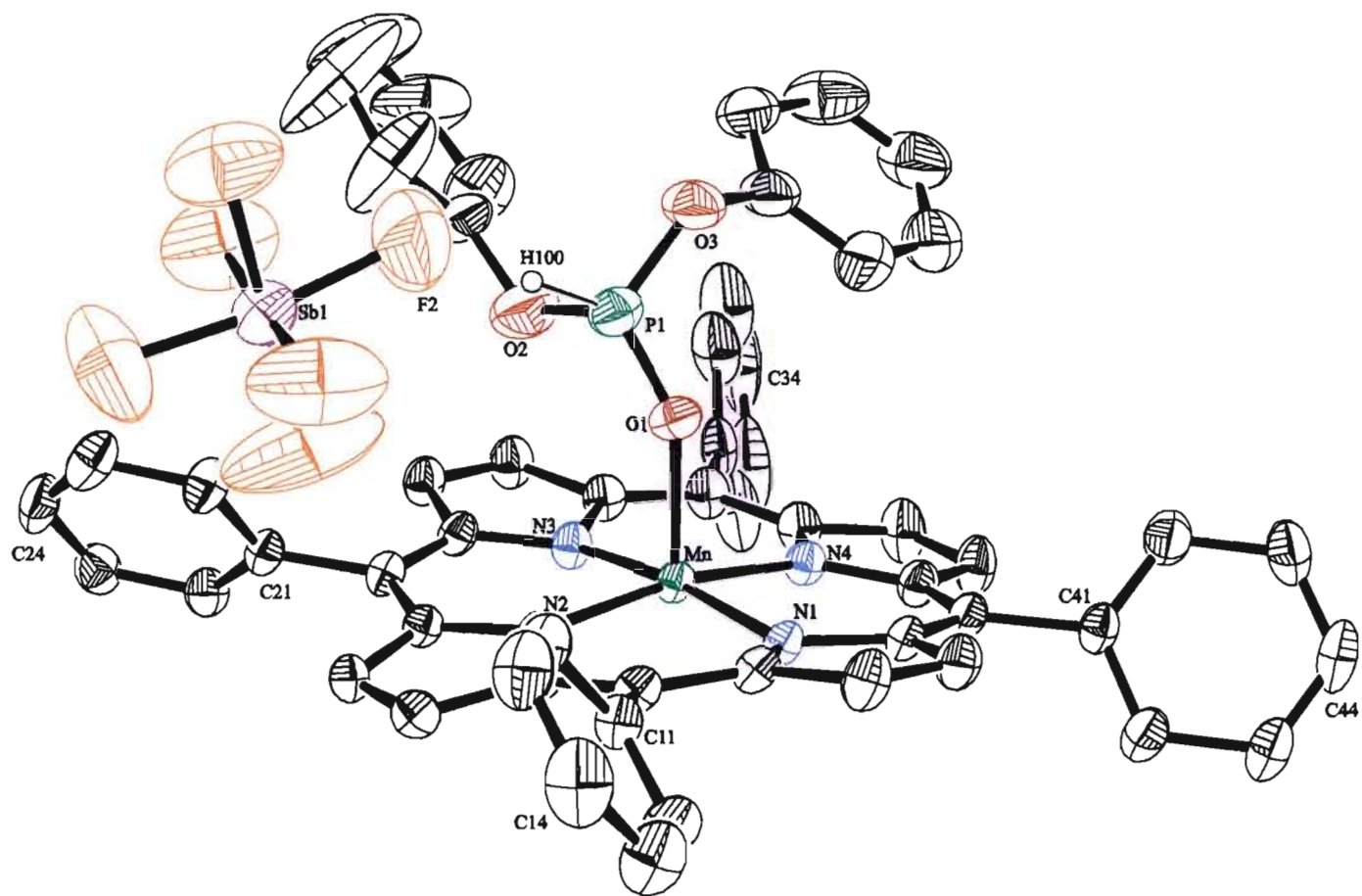
Figure 2.12: Selectively labeled ORTEP diagram of the X-ray crystal structure of [Mn(TPP){(O)HP(OPh)$_2$}](SbF$_6$). H-atoms have been omitted for clarity. Thermal ellipsoids are shown at the 30% probability level.
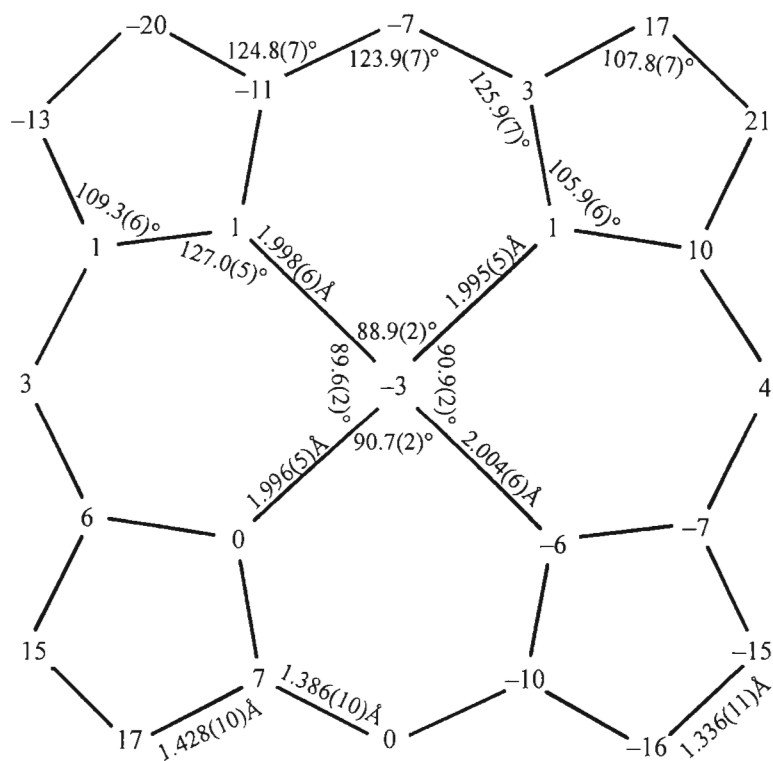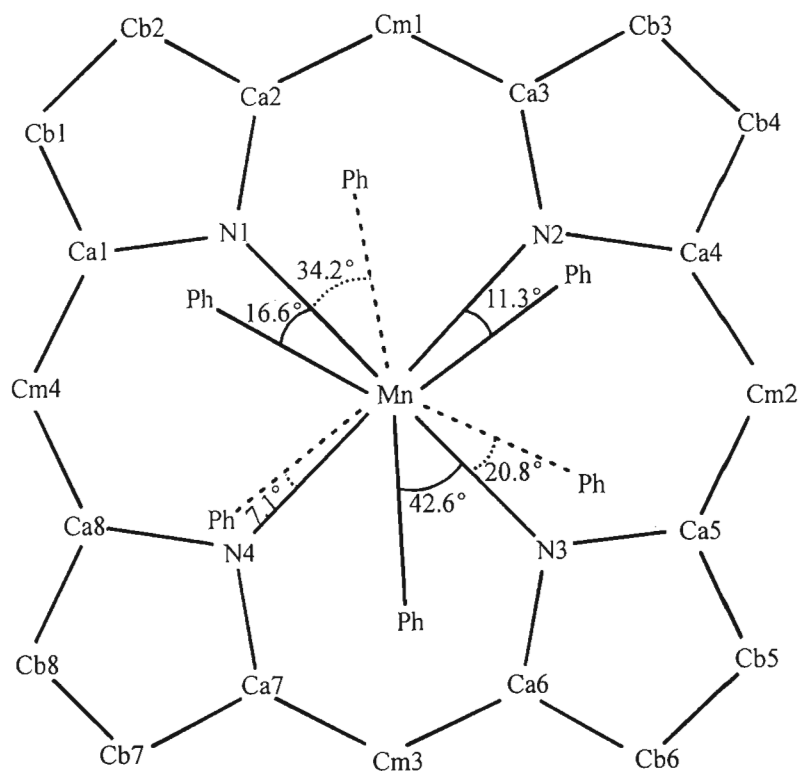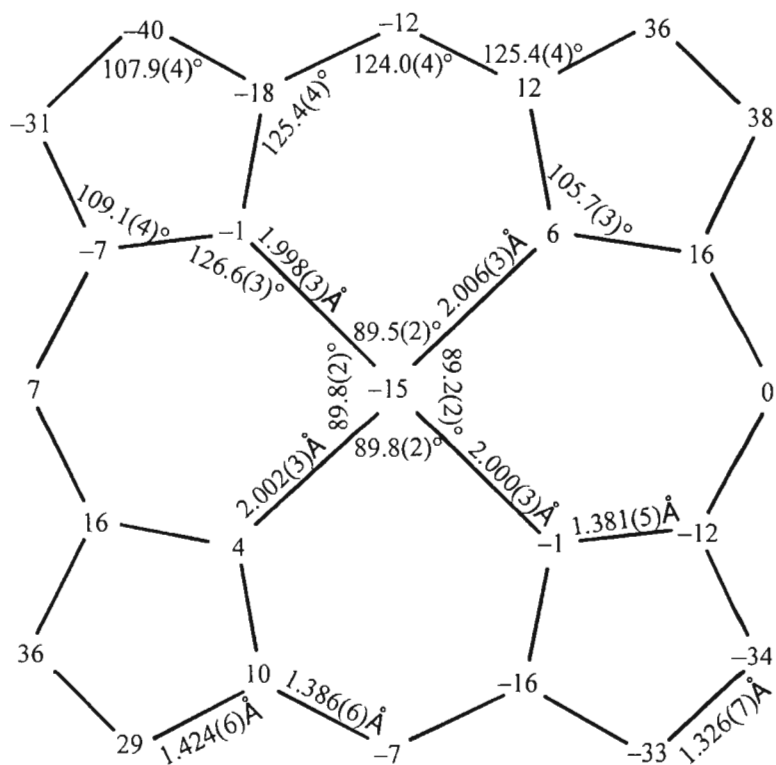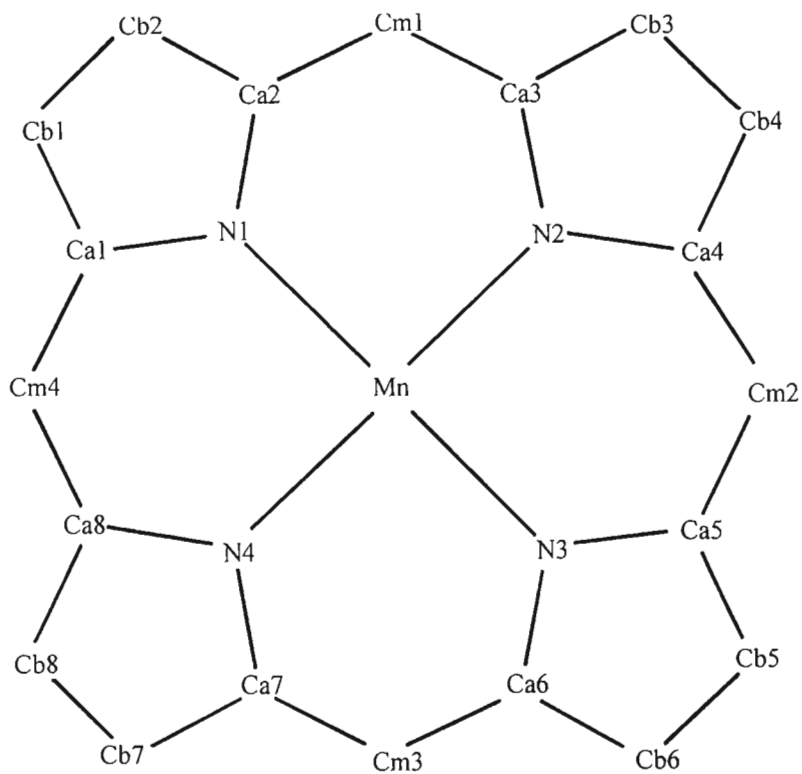
Figure 2.13: Crystallographic information for [Mn(TPP){(O)HP(OPh)₂}](SbF₆). Displacements from the 24-atom mean plane are given in pm.

The dihedral angles of the phenyl substituents relative to the mean plane of the porphyrin macrocycle are: C11–C16 = 53.91°; C21–C26 = 55.36°; C31–C36 = 81.82° and C41–C46 = 59.82°. These acute phenyl group angles lead to the significantly saddled porphyrin core conformation seen in Figure 2.12.

An interesting observation is the manner in which the phenyl substituents of the axial ligand are orientated away from each other as shown in the packing diagrams in Figure 2.14. In this figure diagram 'A' has been rotated by 90 ° along the Mn–P bond to produce diagram 'B'.
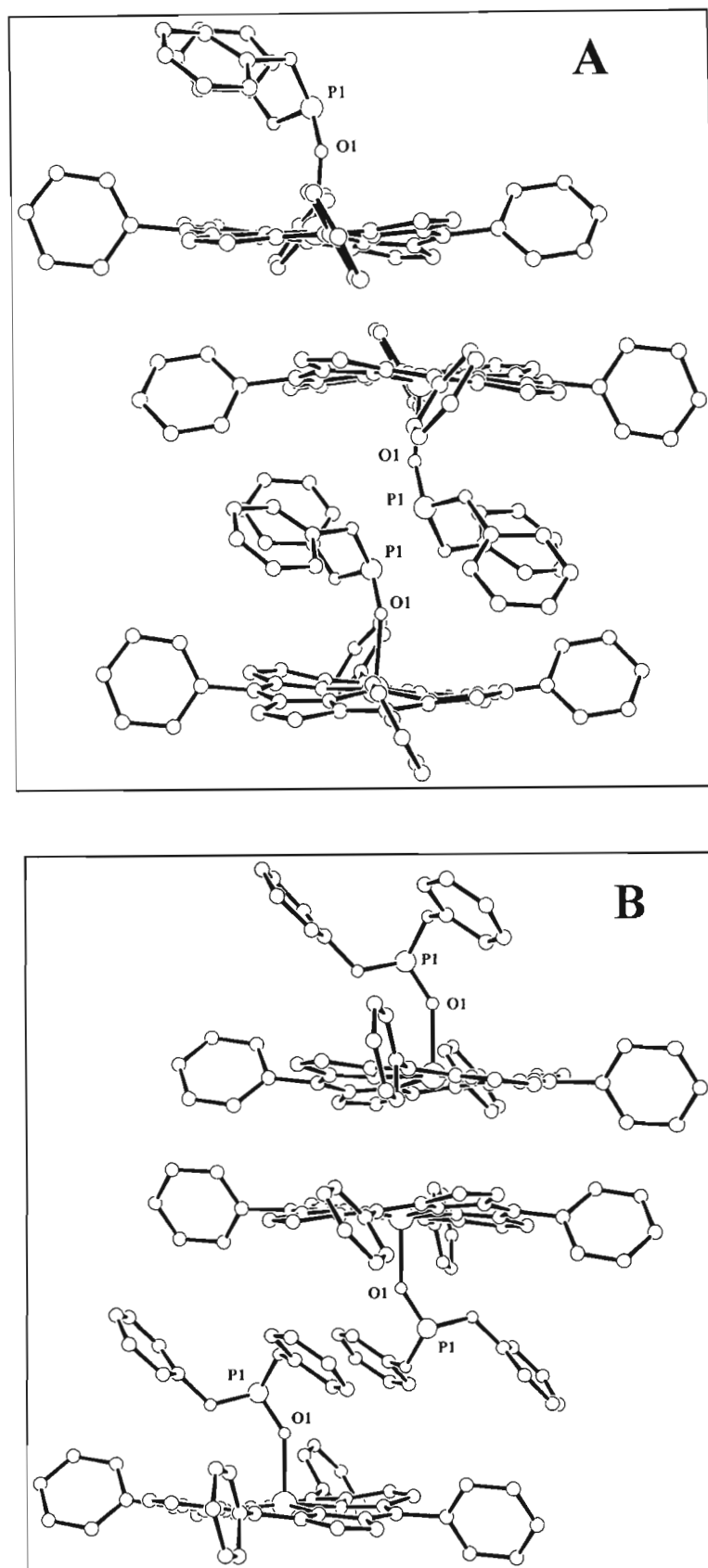
Figure 2.14. ORTEP diagram of the crystal packing arrangements of the [Mn(TPP){(O)PH(OPh)$_2$}] cation (view approximately perpendicular to P1–O1 axis, 'A', and rotated by approximately 90° to 'B').

A view perpendicular to the porphyrin plane is shown in Figure 2.15 where the relative orientation of the axial substituents may be observed.
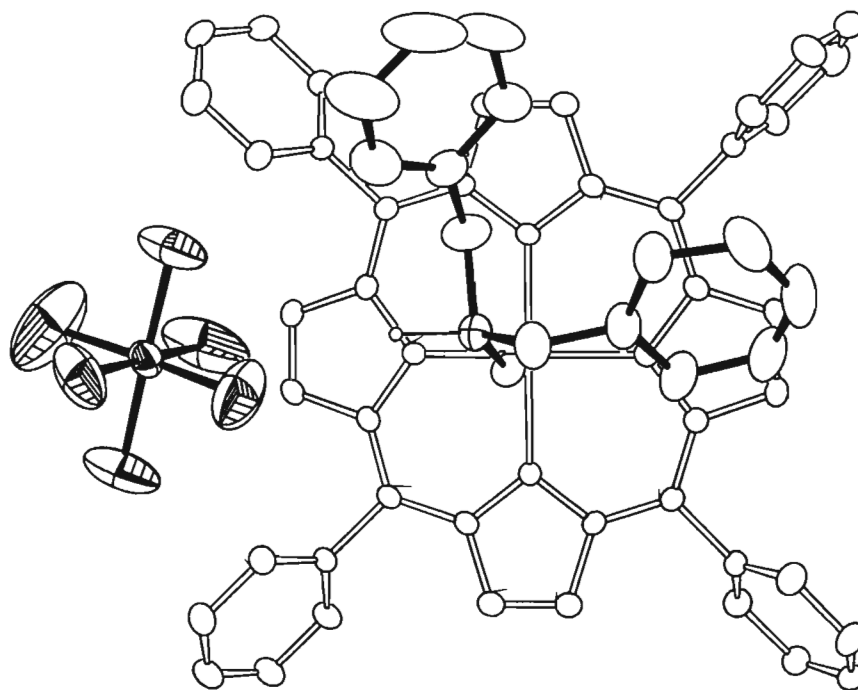
Figure 2.15: ORTEP diagram of [Mn(TPP){(O)PH(OPh)$_2$}](SbF$_6$) perpendicular to the porphyrin mean plane.

Figure 2.16 contains the summarized close-contacts within the X-ray crystal structure. These contacts were observed and drawn using Mercury 1.1. These close contacts are within the van der Waal's radii of the respective atoms and highlight the hydrogen bonding that exists between the protons of the phosphonate axial ligand as well as the porphyrin and the fluorine atoms of the antimony hexafluoride counter-ion. Also immediately noticeable is the lack of contacts between the phenyl substituents of the axial phosphonate ligand and the porphyrin. In the X-ray crystal structure of [Mn(TPP)(PPh$_3$)$_2$](SbF$_6$) there are numerous such contacts and thus one could conclude that the P=O and P–O bonds in [Mn(TPP){(O)PH(OPh)$_2$}](SbF$_6$) increase the separation between the porphyrin and the phenyls of the phosphonate ligand.
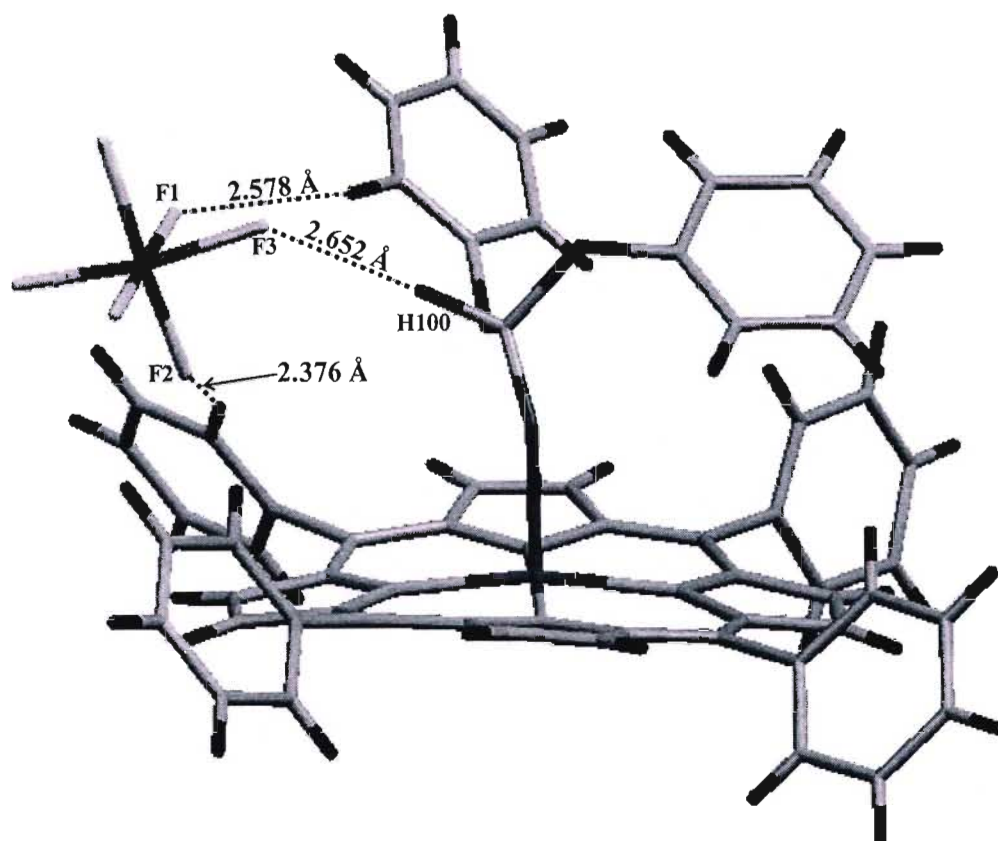
Figure 2.16: Diagram of close contacts within X-ray crystal structure of [Mn(TPP){(O)PH(OPh)$_2$}](SbF$_6$).

A view of the packing in the unit cell may be observed in Figure 2.17. 'Stacking' of the individual complexes over each other to form vaguely linear chains, may be observed (when the unit cell is viewed down the *a*-axis) to form separate channels of cations and anions.

In terms of 5-coordinate porphyrin complexes of Mn(III), this complex shows an axial bond length similar to that expected for primary and neutral O-donor axial ligand complexes. From Table 1.5, 8 such complexes exist and the axial bond lengths from these complexes average to 2.121 (35) Å. On average, these complexes also exhibit both saddled and ruffled conformations with only one of the 8 complexes displaying an in-plane conformation of the manganese metal center.
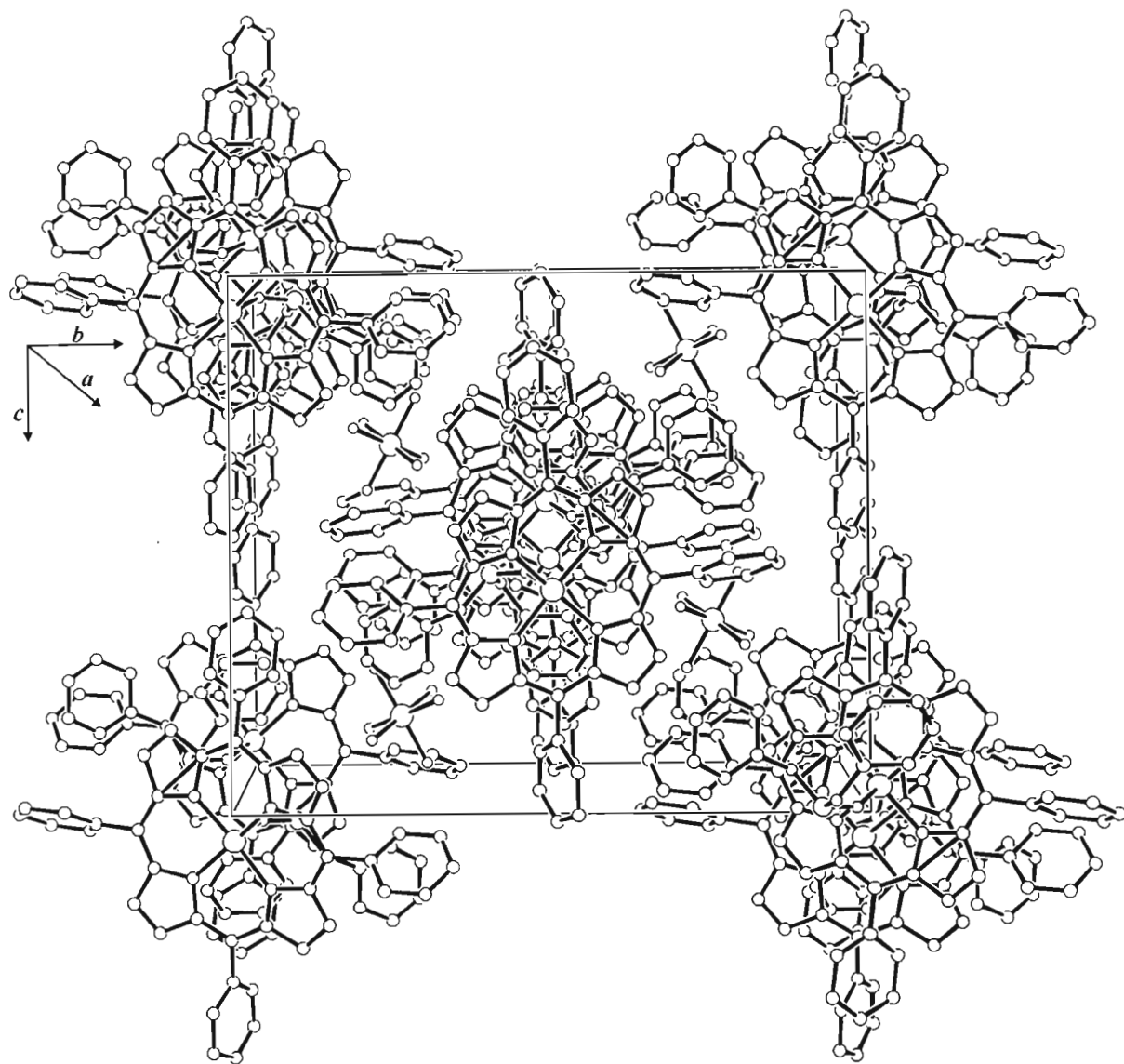
Figure 2.17: ORTEP diagram of the unit cell [Mn(TPP){(O)PH(OPh)$_2$}](SbF$_6$) (along a axis).

2.3 Experimental

General Information. See Appendix AIII.2.

2.3.1 Synthesis of [Mn(TPP)(PPh₃)₂](SbF₆)

To [Mn(TPP)Cl] (150 mg, 0.21 mmol) and AgSbF₆ (88 mg, 0.26 mmol) in a 250 ml Schlenk tube under nitrogen was added 50 ml of freshly distilled and degassed THF. The solution was allowed to stir for ~12 hr at room temperature. The THF was then removed *in vacuo* and the green-brown solid redissolved in dichloromethane (50 ml). The solution was then filtered, to remove precipitated silver chloride, into a 250 ml Schlenk tube into which PPh₃ (2.75 g, 11 mmol) had been added. The solution was left to stir at room temperature for ~10 min. The green solution was then transferred into 12 Schlenk tubes in ~4 ml portions and layered with hexane that had been saturated with triphenylphosphine. X-ray quality crystals were observed after 4 days. Yield: 0.3346 g (111 %). Yield exceeded 100 % as the sample contained a beige powder of precipitated excess triphenylphosphine.

2.3.2 Single Crystal X-ray diffraction study of [Mn(TPP)(PPh₃)₂](SbF₆)

As mentioned above, X-ray quality crystals of [Mn(TPP)(PPh₃)₂](SbF₆) were obtained by slow diffusion of hexane into a CH_2Cl_2 solution of the compound. The crystallographic data and structure refinement details are provided in Table 2.3. The most relevant inter-atomic angles and distances have been averaged and inserted into Figure 2.6. The original bond length and bond angle data have been tabulated in Table AI.1 in Appendix I. The atomic coordinates have been tabulated in Table AII.1 in Appendix II. Use was made of DIFABS absorption correction in order to improve the quality of the structure solution.

Table 2.3. Crystal data and structure refinement for [Mn(TPP)(PPh₃)₂](SbF₆).

Identification code	MnPPh$_3$
Empirical formula	C$_{80}$H$_{58}$MnN$_4$P$_2$SbF$_6$
Formula weight	1427.93
Temperature	210(2) K
Wavelength	0.71073 Å
Crystal system	Monoclinic
Space group	$P2_1/c$
Unit cell dimensions	a = 13.692(4) Å, α = 90.000(4)°
	b = 19.792(5) Å, β = 90.65(2)°
	c = 24.845(4) Å, γ = 90.00(2)°
Volume	6732(3) Å^3
Z	4
Density (calculated)	1.409 Mg/m^3
Absorption coefficient	0.701 mm^{-1}
$F(000)$	2904
Crystal size	0.45 × 0.25 × 0.25 mm
Theta range for data collection	2.06 to 24.97 °
Index ranges	$-16 \leq h \leq 16$; $0 \leq k \leq 23$; $0 \leq l \leq 29$
Reflections collected	9361
Independent reflections	9361 [R(int) = 0.0000]
Reflections observed (>2σ)	4698
Max. and min. transmission	0.8442 and 0.7432
Refinement method	Full-matrix least-squares on F^2
Data / restraints / parameters	9361 / 630 / 878
Goodness-of-fit on F^2	1.108
Final R indices [$I > 2\sigma(I)$]	R_1 = 0.0803 wR_2 = 0.2317
R indices (all data)	R_1 = 0.1409 wR_2 = 0.2661
Largest diff. peak and hole	1.214 and -0.640 e Å^{-3}

2.3.3 Synthesis of [Mn(TPP){(O)PH(OPh)₂}](SbF₆)

To [Mn(TPP)Cl] (150 mg, 0.21 mmol) and AgSbF₆ (88 mg, 0.26 mmol) in a 250 ml Schlenk tube under nitrogen was added 50 ml of freshly distilled THF. The solution was allowed to stir for ~12 hr at room temperature. The THF was then removed *in vacuo* and the green-brown solid redissolved in dichloromethane (50 ml). The solution was then filtered, to remove precipitated silver chloride, into a 250 ml Schlenk tube into which PPh₃t (1.1 ml, 4.3 mmol) had been added. The solution was left to stir at room temperature for ~10 min. The red–brown solution was then transferred into 12 Schlenk tubes in ~4 ml portions, and layered with hexane. X-ray-quality crystals were observed after 4 days. The yield was not calculated, as the material was not pure.

2.3.4 Single Crystal X-ray diffraction study of [Mn(TPP){(O)PH(OPh)₂}](SbF₆)

X-ray quality crystals of [Mn(TPP){(O)PH(OPh)₂}](SbF₆) were obtained by slow diffusion of hexane into a CH₂Cl₂ solution of the compound. The crystallographic data and structure refinement details are provided in Table 2.4. The most relevant inter-atomic angles and distances have been averaged and inserted into Figure 2.13. The original bond length and bond angle data have been tabulated in Table AI.2 in Appendix I. The atomic coordinates have been tabulated in Table AII.2 in Appendix II.

Table 2.4. Crystal data and structure refinement for [Mn(TPP){(O)PH(OPh)₂](SbF₆).

Identification code	MnPPh3t2
Empirical formula	$C_{56}H_{39}MnN_4O_3PSbF_6$
Formula weight	1137.57
Temperature	293(2) K
Wavelength	0.70930 Å
Crystal system	Monoclinic
Space group	$P2_1/n$
Unit cell dimensions	$a = 13.719(2)$ Å, $\alpha = 90°$
	$b = 20.817(3)$ Å, $\beta = 94.132(11)°$
	$c = 17.390(2)$ Å, $\gamma = 90°$
Volume	4953.7(12) Å³
Z	4
Density (calculated)	0.763 Mg/m³
Absorption coefficient	0.452 mm⁻¹
$F(000)$	1144
Crystal size	$0.5 \times 0.5 \times 0.5$ mm
Theta range for data collection	2.07 to 24.92 °
Index ranges	$-1 \leq h \leq 16; -1 \leq k \leq 24; -20 \leq l \leq 20$
Reflections collected	10668
Independent reflections	8694 [R(int) = 0.0179]
Reflections observed (>2σ)	6205
Refinement method	Full-matrix least-squares on F^2
Data / restraints / parameters	8694 / 0 / 653
Goodness-of-fit on F^2	1.182
Final R indices [$I > 2\sigma(I)$]	$R_1 = 0.0593$ $wR_2 = 0.1832$
R indices (all data)	$R_1 = 0.0826$ $wR_2 = 0.2075$
Largest diff. peak and hole	1.037 and -0.481 e Å⁻³

CHAPTER THREE

PHOSPHINE AND PHOSPHONITE COMPLEXES OF Co(III) PORPHYRINS

3.1 Reactions of Phosphines with Cobalt(III) Porphyrin Precursors

In this Chapter, the coordination of phosphines and phosphonites to a cobalt(III) porphyrin will be discussed. As with manganese(III) and rhodium(III) porphyrins, very little is known about the chemistry and behaviour of these compounds. There are no reported X-ray crystal structures of bis(phosphine) and bis(phosphonite) complexes of cobalt porphyrins in the literature to date. For synthetic purposes, however, it has been presumed that cobalt porphyrins have a lower affinity for O-donor ligands. This reduces the probability of coordinated oxidation products.

3.1.1 Synthesis and Characterization of [Co(TPP)(depp)₂](SbF₆)

The phosphine used in this reaction was diethylphenylphosphine, as shown in Figure 3.1 below.
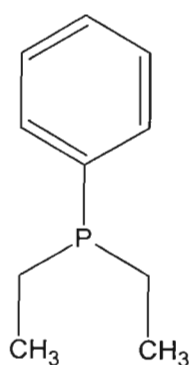
Figure 3.1: Structural diagram of diethylphenylphosphine.

Since Co(III) has a higher affinity for phosphorus as an electron donor than oxygen-bearing oxidation products, there were no complications in this synthesis due to preferred coordination by the former. All solvents and reagents used in this synthesis were nevertheless thoroughly dried and degassed before use. Because of the presumed increase in phosphine-affinity relative

to the Mn(III) porphyrins, a lower molar excess of the phosphine and phosphonite was added to the reaction mixture. A 20 molar excess of the phosphine was added as a precaution to unwanted 5-coordinate reaction products. As a result the product was indeed 6-coordinate.

The reaction procedures are shown in equations 1 and 2 below.

$$[Co(TPP)Cl] + AgSbF_6 \xrightarrow{\text{THF}} [Co(TPP)FSbF_5] + AgCl(s) \dots\dots\dots\dots(1)$$

$$[Co(TPP)FSbF_5] + \text{excess depp} \xrightarrow{\text{CH}_2\text{Cl}_2} [Co(TPP)(depp)_2](SbF_6) \dots\dots\dots(2)$$
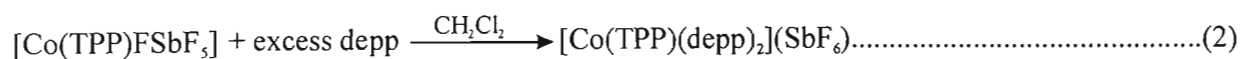
A THF solution of the product was maroon in colour. The spectroscopic data for $[Co(TPP)(depp)_2](SbF_6)$ are summarised in Table 3.1.

The ^{1}H NMR assignments are complicated by the presence of the excess phosphine signals, as is obvious in the spectrum in Figure 3.2 below.

The pyrrole protons produce a signal that is a singlet at 9.00 ppm and has been set as the reference integral at 8 protons. The phenyl *ortho* protons of the porphyrins macrocycle have been assigned to the broad doublet at 7.95 ppm. Substantiation of this is in the integration of this peak equating to 8 H's. This signal should ideally be a doublet, although in this situation there may be a coupling with the para protons to produce a multiplet state. The broad multiplet at 7.82 ppm has been tentatively assigned to the meta- and para-protons of the phenyl rings of the porphyrins. This set of signals integrates to 12 H's. As mentioned in Capter 1.8, the two signals corresponding to the meta and para protons may overlap in their chemical shifts, resulting in a broad signal which may be difficult to assign accurately.

The *para-*, *meta-* and *ortho*-phenyl protons of the bound phosphine ligand have been tentatively assigned to the three multiplets at 7.02 ppm, 6.54 ppm and 3.67 ppm, respectively. These three signals integrate relatively accurately to 2, 4 and 4 H's, respectively. These signals are quite substantially separated from one another, which illustrates the shielding cone effect on the proton signals of the coordinated phosphine. With an increase in the separation of the protons, on the phenyl substituents of the phosphine, from the center of the complex, the corresponding signals move upfield. The multiplicity of these signals may be influenced by the movement of these phenyl substituents within the shielding cone.

The broad irregular multiplet at −1.44 ppm has been tentatively assigned to the terminal methyl groups of the coordinated depp ligand and accurately integrates to 12 H's. Although not a triplet, as is expected for these protons, this may be explained by the possibility of limited movement of the $-CH_2CH_3$ moeity around the C–P bond resulting in more complicated coupling considerations.

The broad single peak at −2.27 ppm as well as the irregular multiplet at −3.04 ppm has been assigned to the $-CH_2-$ protons of the coordinated ligands. The peaks integrate to 4 H's each, which augers well for their assignments. It is apparent that a proton from the $-CH_2-$ linkage is 'dipping' into the shielding zone of the porphyrin and is being forced more up-field, resulting in the loss in the equivalence of these protons. Enhanced resolution of these signals would almost certainly produce two quartets.

In general, the signals produced by the coordinated axial ligand protons are broad and of low-intensity. The coupling constants are, as expected for aromatic systems, all around 6.5 to 7 Hz for the measurable signals.
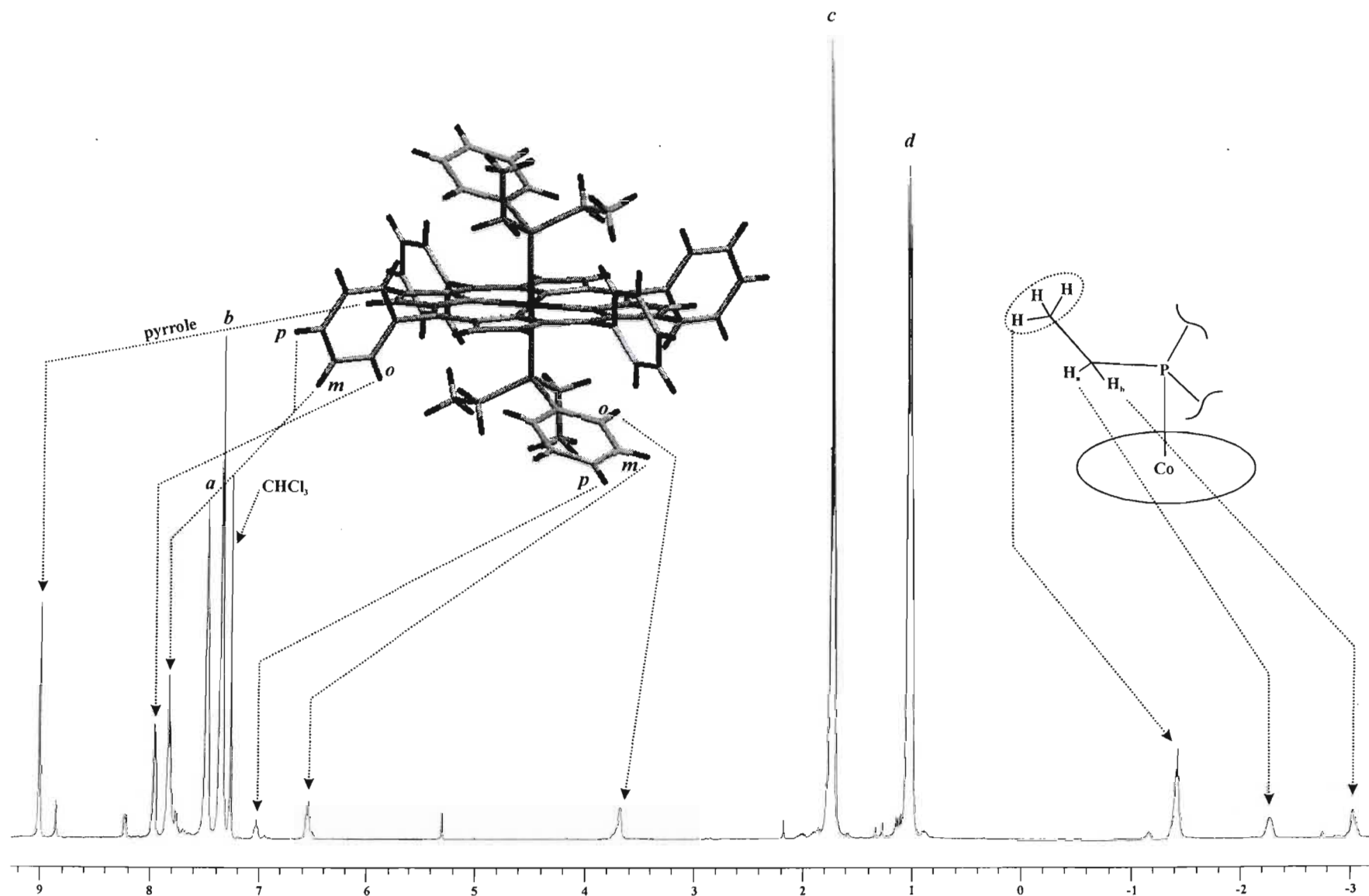
Figure 3.2: ^{1}H NMR spectrum of [Co(TPP)(depp)$_2$](SbF$_6$) at 25 °C.

The more intense signals in this spectrum are due to the excess free ligand. Signals a and b in the spectrum in Figure 3.2 form a doublet of doublets at 7.42 ppm that corresponds to the *phenyl* protons of the depp phenyl and the multiplets at 1.71 ppm (signal c) and 1.01 ppm (signal d) correspond to the $-CH_2$ and $-CH_3$ protons, respectively. Signals a, b, c and d integrate to 5, 4 and 6 H's, respectively.

The ^{31}P NMR spectrum shown in Figure 3.3 below includes 3 peaks; the free ligand signal is at $-$12.91 ppm. This signal is some 1.5 ppm up-field of that for the free ligand in a solution without the Co(III) porphyrin. The ^{31}P resonance of $PhEt_2P=O$ is observed at 45.33 ppm. The coordinated phosphine ligand resonance occurs at 18.30 ppm. The line shape is broad and of relatively low intensity and appears to be comprised of two separate signals. A likely explanation for this observation is that there are two different conformations of the complex in solution, on the ^{31}P NMR timescale.
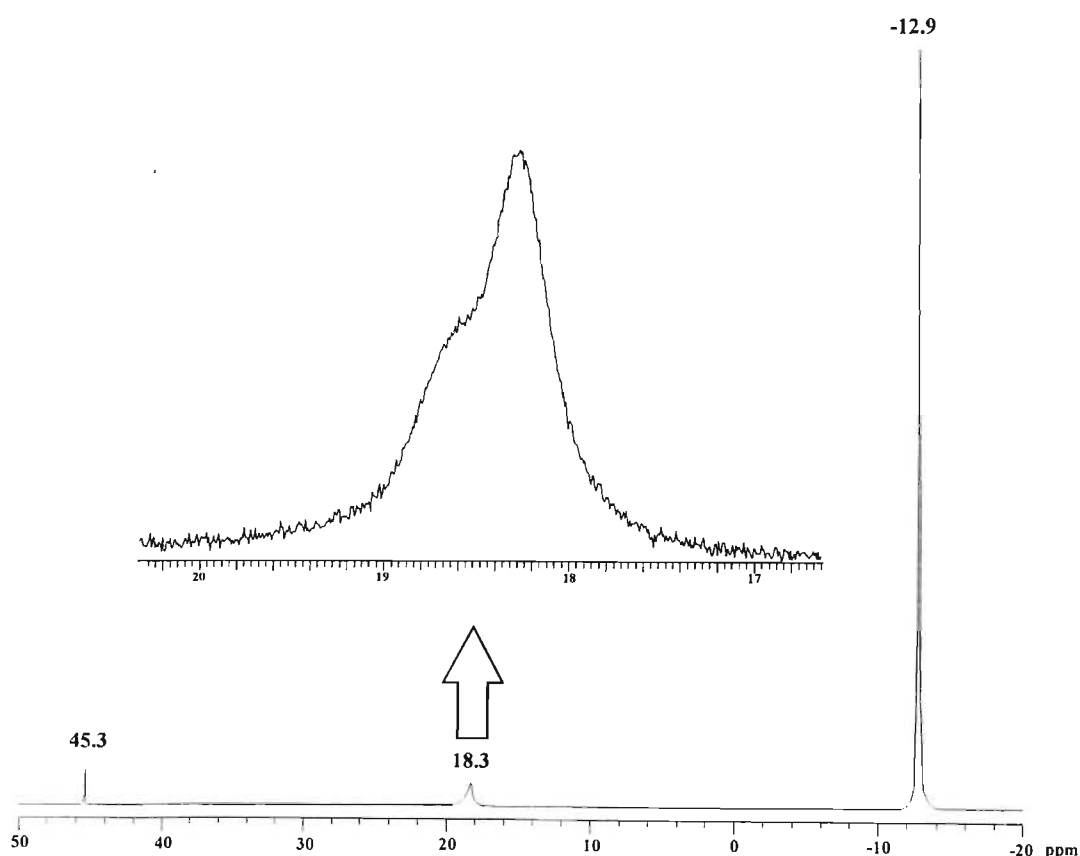
Figure 3.3: ^{31}P NMR spectrum of [Co(TPP)(depp)₂](SbF₆).

The electronic spectrum of [Co(TPP)(depp)₂](SbF₆) shown in Figure 3.4 shows a relatively sharp

and intense Soret band at 461 nm. The sharp profile of the Soret band may indicate the presence of a single species in solution, however, the shoulders at 418 and 349 nm suggest that a second species might also be present. It appears that if there is another species in solution, the Soret bands absorb at the same wavelength. Generally, the electronic spectrum for $[Co(TPP)(depp)_2](SbF_6)$ follows that described in Chapter 1.12 for a typical 6-coordinate cobalt(III) porphyrin, differing only in the presence of a shorter wavelength band. This band has been tentatively assigned as an N band, primarily due to the lower wavelength region in which this band is typically found. The $B(1, 0)$ band is found at 425 nm. This is an interesting characteristic as this band is usually obscured by the more intense Soret band, resulting in a broader profile of the Soret band. This "splitting" or resolution of the $B(1, 0)$ band appears to be a distinct characteristic of these Co(III) porphyrins as it is observed in all the Uv-vis spectra of the Co(III) porphyrins reported in this thesis. The Q bands are found in the range 543 nm to 633 nm. The complete band assignments are shown in Figure 3.4.

Table 3.1 Spectroscopic data for $[Co(TPP)(depp)_2](SbF_6)$

^{1}H NMR [a]	**TPP:** 9.00 (8H, sh s, pyrrole H's), 7.95 (8H, br d, ^3J = 6.9 Hz, o–H's), 7.82 (12H, br m, m,p–H's) **Depp:** 7.02 (2H, br t, ^3J = 6.9 Hz, p–H's), 6.54 (4H, br t, ^3J = 6.7 Hz, m–H's), 3.67 (4H, br m, o–H's), –1.44 (9H, br m, –CH$_3$), –2.27 (4H, br s, –CH$_a$–), –3.04 (4H, br t, ^3J = 7.0 Hz, –CH$_b$–)
^{31}P NMR [a]	18.30
^{13}C NMR [a]	^{13}C signal undetectable
Infrared [b]	1440.9 (med, ν(P–C$_{Ph}$)), 996.8 (med, ν(P–C$_{Ph}$)), 734.6 (med, ν(P–C$_{Et}$))
Uv-vis [c]	633 (8.9×10^3), 587 (5.5×10^3), 543 (4.6×10^3), 461 (9.5×10^4), 425 (4.5×10^4), 418 (3.8×10^4), 367 (4.3×10^4), 349 (3.1×10^4)

[a] Chemical shifts measured in ppm. Measured at 294 K in CDCl$_3$, s = singlet, d = doublet, t = triplet, m = multiplet, str = strong, med = medium, w = weak, sh = sharp, br = broad. [b] $\tilde{\nu}$ (cm^{-1}). KBr disk. [c] λ_{max}/nm (ε/dm^3 mol^{-1} cm^{-1}); measured at 298 K in dried and degassed dichloroethane.

Figure 3.4: Electronic Spectrum of [Co(TPP)(depp)₂](SbF₆) in dichloroethane at 25 °C.

3.1.2 Crystal Structure Determination of [Co(TPP)(depp)$_2$](SbF$_6$)

The compound was crystallized via slow-diffusion of hexane into a solution of the compound in CH$_2$Cl$_2$. Only cube-shaped crystals of the compound were isolated from the solution and X-ray quality crystals were mounted on glass microfibres. The X-ray diffraction data were collected at 176(2) K partly due to suspected solvation of the crystals. The compound crystallized in the monoclinic crystal system in the $P2_1/c$ space group. The asymmetric unit consists of a half porphyrin and half an antimony hexafluoride. There is a center of inversion at the Co metal center and at the Sb of the SbF$_6^-$ counter-ion. Each of these two atoms is thus half-occupied. The SbF$_6^-$ counter-ion showed severe disorder with three positions for the Sb center, only one of these being capable of generating the other half of the counter-ion using the inversion-symmetry operator.

The Co–P$_{ax}$ bond length is 2.312(1) Å and the averaged Co–N$_{porph}$ bond length is 1.980(3) Å. The latter mean bond length falls within the bond length range reported for the Co(III) N–donor complexes in Table 1.14. Also noticeable from this table is the similarity in axial bond length of this complex with that of the S–donor complexes.

The final R_1 = 0.0477 for the structure solution. The ORTEP diagram of the crystal structure is shown in Figure 3.5. The summarized data of the phosphine orientation as well as the mean plane deviations and bond-lengths and angles are given in Figure 3.6.

The inversion symmetry through the central cobalt ion implies that this metal centre lies in the plane of the 24-atom mean plane. The porphyrin core is mostly planar, with only minimal displacements from the mean plane. The existing mean plane deviations are vaguely consistent with a saddle/ruffle hybrid conformation. The asymmetric unit is shown in Figure 3.7. The relative orientations of the axial ligands are shown in Figure 3.8. In this diagram, the view down the P–Co–P axis is shown. Figure 3.9 is a diagram of the unit cell, where the view is down the b-axis, allowing the best possible view of the packing arrangement of this complex.

A diagram of the close-contacts, generated using Mercury 1.1, is shown in Figure 3.10. From this diagram the relative proximity of the SbF$_6^-$ counter-ion to the macrocycle is noticeable. Hydrogen bonding is observed between one of the fluorine atoms of the counter-ion and a proton of one of the phenyls of the TPP and also between a fluorine atom and the terminal methyl

protons of the axial phosphine. The distances between these atoms are 2.449 and 2.638 Å, respectively. The Co···Sb distance is 8.500 Å.

The dihedral angles of the phenyl substituents relative to the mean plane of the porphyrin macrocycle are: C11–C16 = 74.49° and C21–C26 = 74.25°.
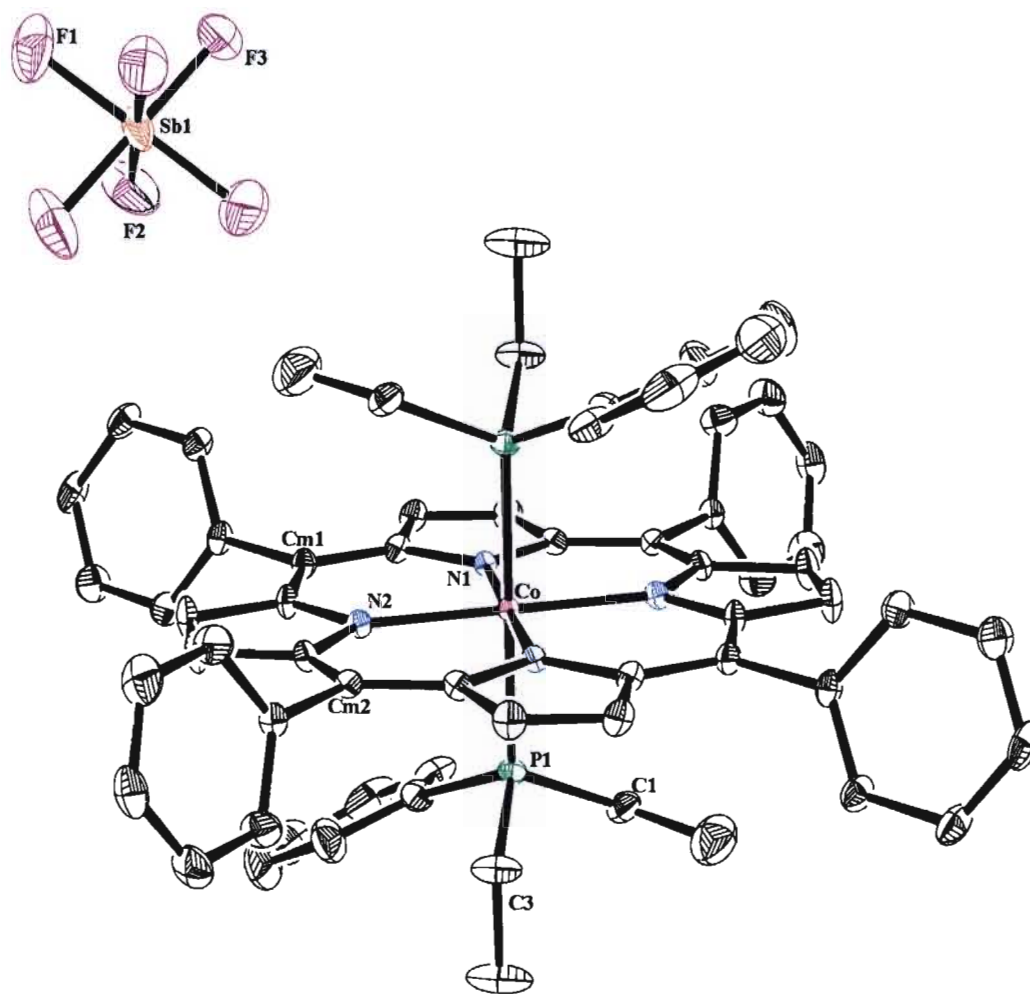
Figure 3.5: Selectively labeled ORTEP diagram of the X-ray crystal structure of [Co(TPP)(depp)$_2$](SbF$_6$). The thermal ellipsoids have been drawn at the 30% probability level. Hydrogen atoms are omitted for clarity.

Figure 3.6: Crystallographic information for [Co(TPP)(depp)₂](SbF₆). Prime symbols indicate symmetry-equivalent atoms. Displacements from the 24-atom mean plane are given in pm.
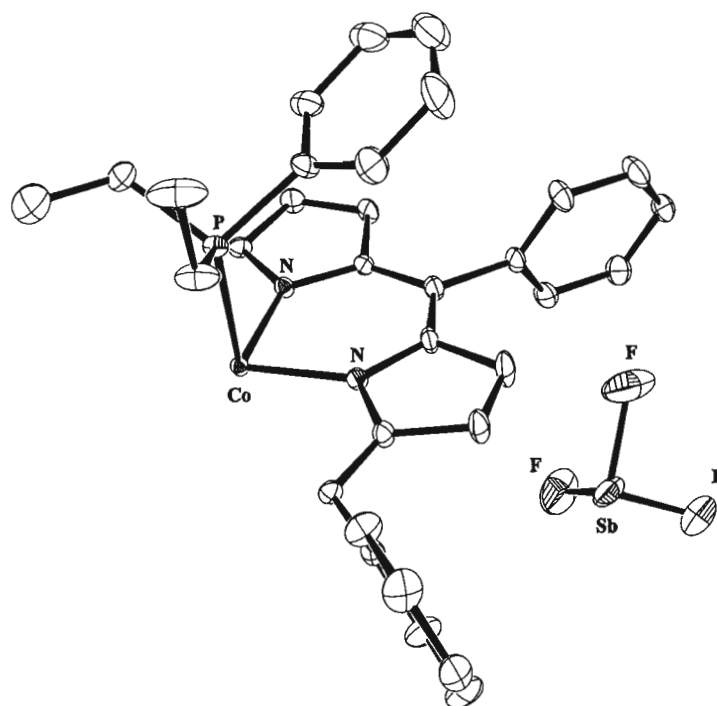
Figure 3.7: ORTEP diagram of the asymmetric unit of the X-ray crystal structure of [Co(TPP)(depp)₂](SbF₆). H atoms are omitted for clarity.
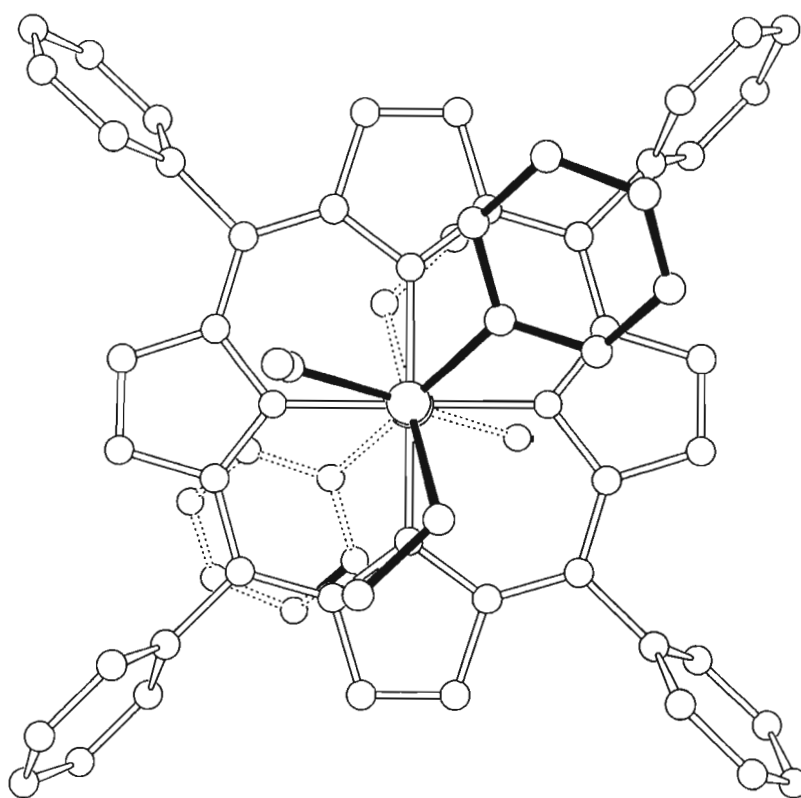
Figure 3.8: ORTEP diagram of [Co(TPP)(depp)₂](SbF₆) (view perpendicular to porphyrin plane along the P–Co–P axis).

Figure 3.9: ORTEP diagram of the unit cell contents of the monoclinic structure of [Co(TPP)(depp)$_2$](SbF$_6$) (view along the *b*-axis).
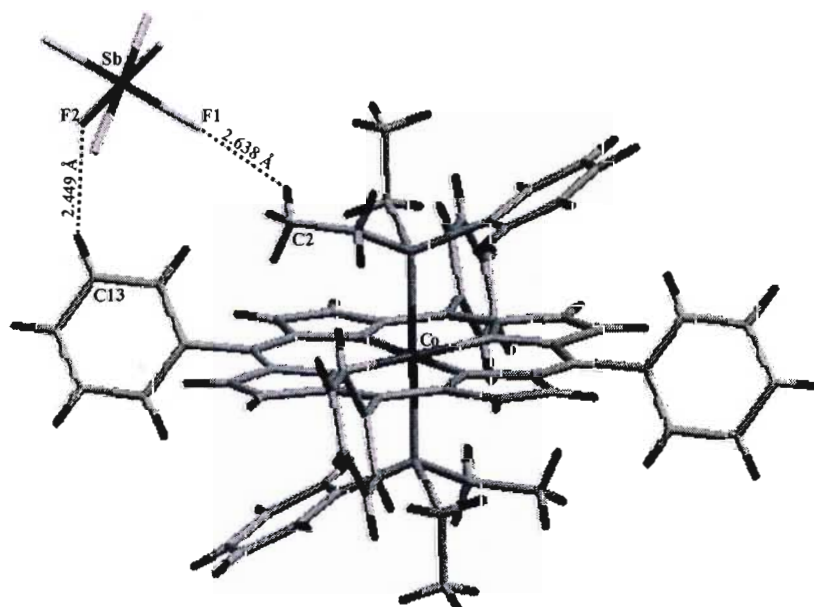
Figure 3.10: Diagram of close contacts within the X-ray crystal structure of [Co(TPP)(depp)$_2$](SbF$_6$).

3.1.3 Synthesis and Characterization of [Co(TPP)(edpp)₂](SbF₆)

The phosphine used in this reaction was ethyldiphenylphosphine, as shown in Figure 3.11 below.
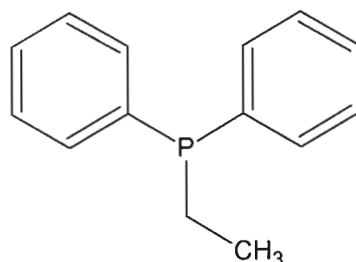
Figure 3.11: Structural diagram of ethyldiphenylphosphine.

The synthetic procedures and chemistry used in the synthesis of this compound are identical to those used in the synthesis of [Co(TPP)(depp)₂](SbF₆). The reaction scheme is similar in concept and the molar excesses were identical. This phosphine was treated as extremely air-sensitive and was thus handled under an inert atmosphere and all solvents were thoroughly dried and degassed before use.

The reaction procedures are shown in equations 1 and 2 below.

$$[Co(TPP)Cl] + AgSbF_6 \xrightarrow{\text{THF}} [Co(TPP)FSbF_5] + AgCl(s) \dots\dots(1)$$

$$[Co(TPP)FSbF_5] + \text{excess edpp} \xrightarrow{CH_2Cl_2} [Co(TPP)(edpp)_2](SbF_6) \dots\dots(2)$$

A THF solution of the product was maroon in colour. The spectroscopic data for [Co(TPP)(edpp)₂](SbF₆) are summarised in Table 3.2. The ^{13}C NMR spectrum is shown in Appendix IV in Figure AIV.1.

The ^{1}H NMR sample was made up of the same batch of crystals from which the X-ray crystal structure was obtained, thus no excess edpp ligand was added to the sample and there were no complications due to the presence of the excess phosphine signals, as is obvious in the spectrum in Figure 3.12 below. Dissociation of the axial ligands was not evident, consistent with the kinetic inertness of Co(III).

The sharp singlet at 8.94 ppm corresponds to the pyrrole protons and has been set as the reference integral at 8 protons. The phenyl *para* protons of the porphyrin macrocycle have been assigned to the triplet at 7.80 ppm. Substantiation of this is in the integration of this peak equating to 4 H's. The triplet at 7.74 ppm has been tentatively assigned to the *meta* protons of the phenyl rings of the porphyrin. This signal integrates to 8 H's. The doublet at 7.64 ppm corresponds to the *ortho* protons and also accurately integrates to 8 H's.

The *para-*, *meta-* and *ortho-*phenyl protons of the bound phosphine ligand have been tentatively assigned to the three broad singlets at 7.05 ppm, 6.60 ppm and 3.75 ppm, respectively. These three signals integrate relatively accurately to 4, 8 and 8 protons, respectively. The 'ring-current' effect is noticeable here, in that the protons nearer the apex of the shielding cone (i. e. the *ortho-*protons nearer the metal centre) are more shielded and are found in a more upfield position, relative to those protons further from the apex (i. e. the *para-*protons). Figure 1.48 in Chapter 1 illustrates this 'ring-current' shielding cone.

The explanation for the splitting patterns and chemical shifts for the pyrrole protons as well as the phenyl protons of the phosphine is similar to that of $[Co(TPP)(depp)_2]SbF_6$.

The sharp singlet at 1.55 ppm has been tentatively assigned to the terminal methyl groups of the coordinated depp ligand and accurately integrates to 6 H's.

The broad single signal at −1.39 ppm has been assigned to the −CH$_2$− protons of the coordinated edpp and accurately integrates to 4 H's. It must be emphasized that these two assignments are uncertain as the multiplicities expected for the −CH$_3$ and −CH$_2$− proton signals are a triplet and multiplet, respectively. The possibility of the signal assigned to the −CH$_2$− protons being a multiplet cannot be discounted as the broad nature of the suspected signal would cause an obcuring of the true multiplicity.

In general, as with $[Co(TPP)(depp)_2](SbF_6)$, the axial ligand protons produce broad, low-intensity signals with immeasurable coupling constants.

The ^{31}P NMR spectrum consists of a single "washed-out" signal at 10.8 ppm.

The electronic spectrum of $[Co(TPP)(edpp)_2](SbF_6)$ shown in Figure 3.13 shows a relatively

sharp and intense Soret band at 462 nm. The spectrum appears very similar to that of [Co(TPP)(depp)$_2$](SbF$_6$), exhibiting a similar "splitting" of the Soret band with the tentatively assigned $B(1, 0)$ band found at 419 nm. A shoulder is evident on the $B(1, 0)$ band at 425 nm, possibly indicating the presence of another species in solution. Likewise, the suspected N band (371 nm) appears reasonably broad and may be concealing a shoulder and supporting the possibility of a minor second species. It must be pointed out, though, that the Soret band for H$_2$TPP occurs at 417 nm, and as such this may be the minor species. Four Q-bands are also evident between 516 and 627 nm. The band at 516 nm may also correspond to an absorption band of H$_2$TPP. The complete band assignments are shown in Figure 3.13.

Table 3.2 Spectroscopic data for [Co(TPP)(edpp)$_2$](SbF$_6$)

^{1}H NMR ^{a}	**TPP:** 8.94 (8H, sh s, pyrrole H's), 7.80 (4H, t, ^3J = 7.4 Hz, p–H's), 7.74 (8H, t, ^3J = 7.4 Hz, m–H's), 7.64 (8H, d, ^3J = 7.4 Hz, o–H's) **Edpp:** 7.05 (4H, br s, p–H's), 6.60 (8H, br s, m–H's), 3.75 (8H, br s, o–H's), 1.55 (6H, sh s, –CH$_3$), –1.39 (4H, br s, –CH$_2$–)
^{31}P NMR ^{a}	10.80
^{13}C NMR ^{a}	144.57 (w s), 140.18 (w s), 136.16 (w s), 134.10 (med s), 136.16 (w s), 134.13 (w s), 128.66 (w s), 127.42 (med s), 77.42 (str s), 77.22 (str t)
Infrared ^{b}	1437.8 (med, ν(P–C$_{Ph}$)), 1005.8 (med, ν(P–C$_{Ph}$)), 754.4 (med, ν(P–C$_{Et}$))
Uv-vis ^{c}	627 (6.4×10^3), 582 (4.0×10^3), 541 (3.3×10^3), 516 (3.4×10^3), 462 (7.9×10^4), 425 (4.3×10^4), 419 (5.3×10^4), 371 (3.0×10^4)

^{a} Chemical shifts measured in ppm. Measured at 294 K in CDCl$_3$, s = singlet, d = doublet, t = triplet, m = multiplet, str = strong, med = medium, w = weak, sh = sharp, br = broad. ^{b} $\tilde{\nu}$ (cm^{-1}). KBr disk. ^{c} λ_{max}/nm (ε/dm^3 mol^{-1} cm^{-1}); measured at 298 K in dried and degassed dichloroethane.
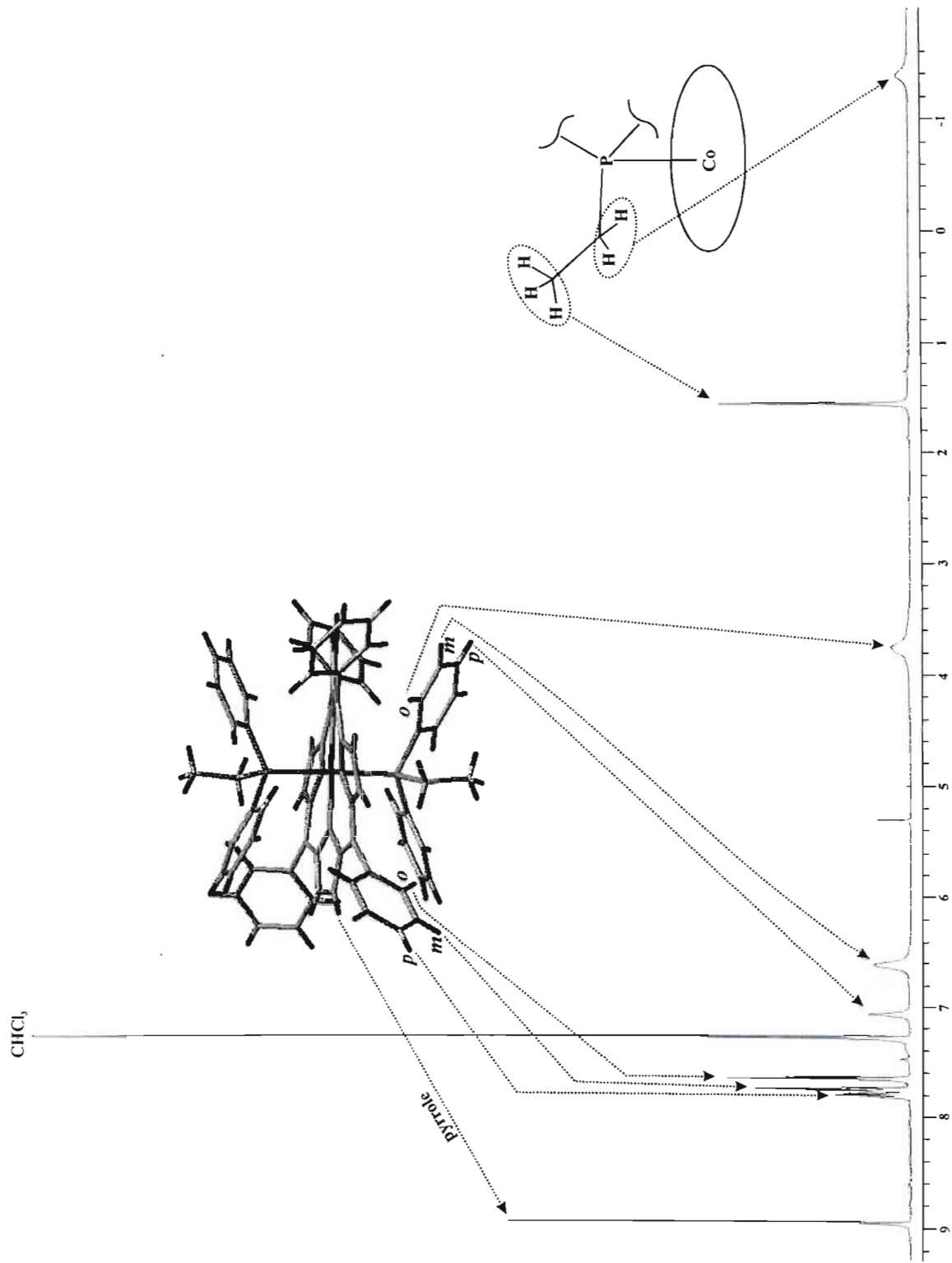
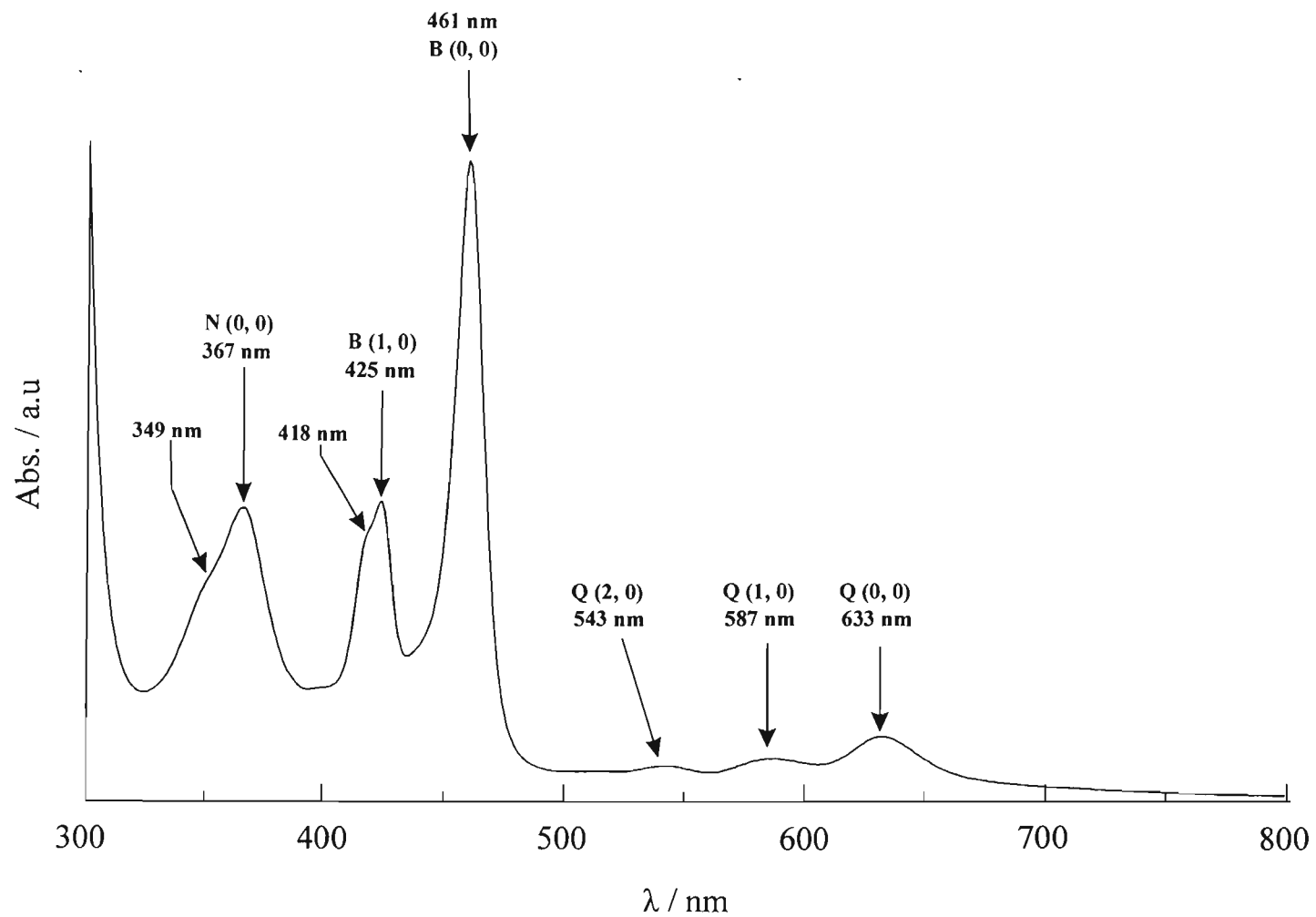Figure 3.12: ^{1}H NMR spectrum of [Co(TPP)(edpp)$_2$](SbF$_6$).
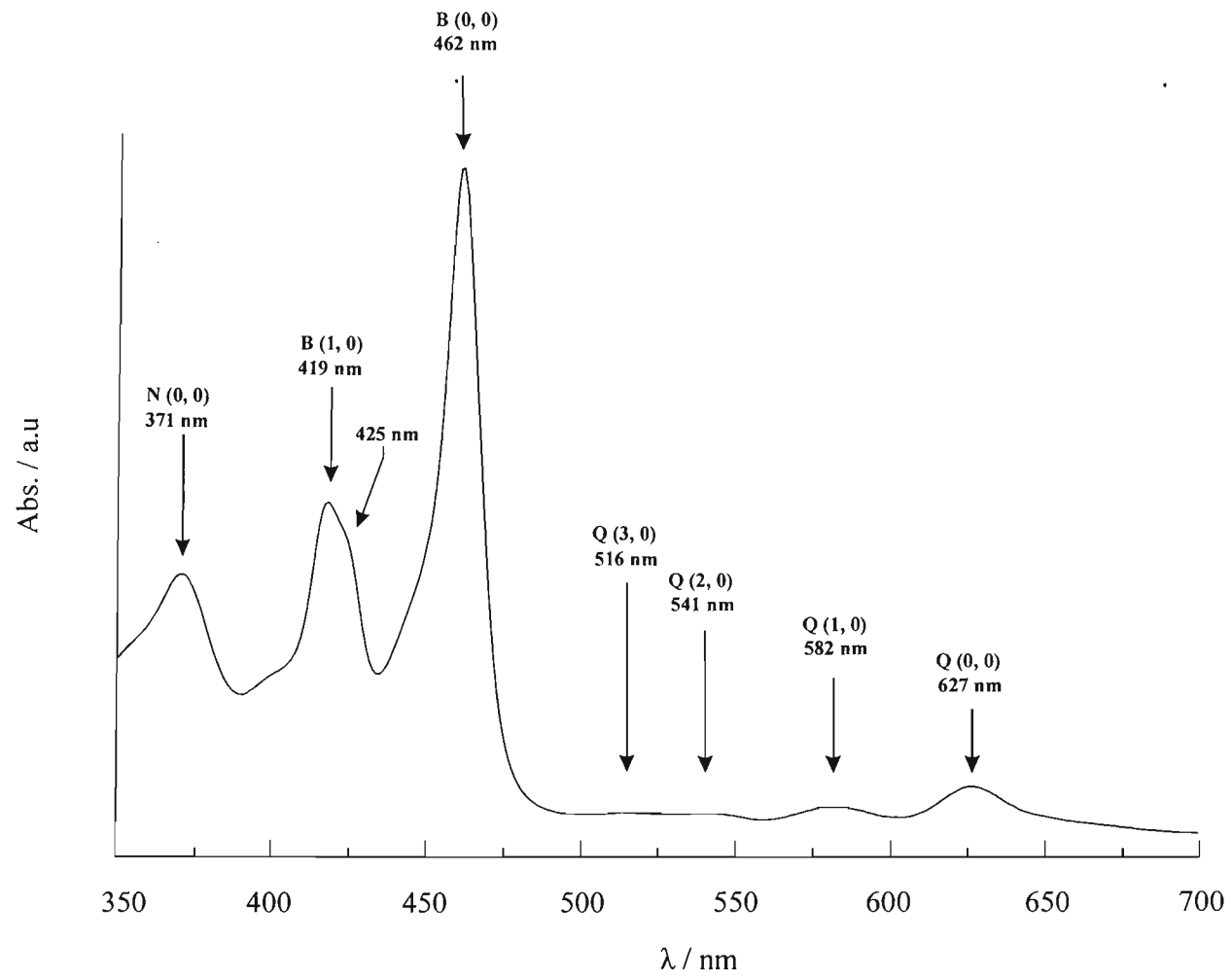
Figure 3.13: Electronic Spectrum of [Co(TPP)(edpp)₂](SbF₆) in dichloroethane at 25 °C.

3.1.4 Crystal Structure Determination of [Co(TPP)(edpp)₂](SbF₆)

The compound was crystallized via slow diffusion of hexane into a solution of the compound in CH_2Cl_2. Only cube-shaped crystals of the compound were isolated from the solution and X-ray quality crystals were mounted on glass microfibres. The X-ray diffraction data were collected at 100(1) K, partly due to suspected solvation of the crystals. The compound crystallized in the monoclinic crystal system in the $P2_1/n$ space group. The asymmetric unit consists of a full porphyrin, a dichloromethane solvate and an antimony hexafluoride ion.

The Co–P_{ax} bond lengths are 2.330(1) Å and 2.316(1) Å and the averaged Co–N_{porph} bond length is 1.972(7) Å. These axial and Co–N_{porph} bond lengths are similar to the 2.312(1) and 1.980 (3) Å reported for [Co(TPP)(depp)₂](SbF₆). It is noteworthy that the substitution of an ethyl moeity in the axial phosphine ligand with a phenyl group distinctly increases the axial bond length and thus has increased the effective steric bulk of the axial ligand. These axial bond lengths are, however, distinctly shorter than the Mn(III)–P bond length reported for [Mn(TPP)(PPh₃)₂](SbF₆) (3.088 Å).

The final R_1 = 0.0415 for the structure solution. The ORTEP diagram of the crystal structure is shown in Figure 3.14. Data summarizing the phosphine orientation as well as the mean plane deviations and bond lengths and angles are given in Figure 3.15.

The porphyrin core is highly ruffled. The reason for this distortion is obvious when looking at the axial ligand orientations summarized in Figure 3.15. The *meso*-carbons Cm3 and Cm4 both are spatially close to the phenyls of axial ligands on opposing sides of the porphyrin plane. Thus the two adjacent *meso*-carbons are induced into out of plane conformations in opposing directions. This ruffled conformation is then propagated through the porpyrin core so that the *meso*-carbons are alternately displaced above and below the mean plane. The largest deviations from the 24-atom mean plane are for atoms Cm1 and Cm3 (*meso*-carbons 1 and 3), both with a value of 39 pm. The central cobalt does, however, lie in the mean plane. The relative orientations of the axial ligands are shown in Figure 3.16 where the view of the complex is down the P1–Co–P2 axis. Figure 3.17 shows a diagram of the unit cell, where the view is down the *b*-axis, allowing the best possible view of the packing arrangement of this complex.

An interesting feature of this complex is how the opposing phenyls of the TPP alternate between

125

an eclipsed and staggered conformation. The phenyls C21–C26 and C41–C46 form a 'staggered' conformation and the C11–C16 and C31–C36 form an 'eclipsed' conformation, relative to each other. This is shown in Figure 3.18.

The dihedral angles of the phenyl substituents relative to the mean plane of the porphyrin macrocycle are: C11–C16 = 57.62°, C21–C26 = 61.65°, C31–C36 = 64.10° and C41–C46 = 68.10°.

The close contacts within the X-ray crystal structure are limited to the interactions between the SbF_6^- counterion and the solvate dichloromethane. Obvious hydrogen-bonding is observed between two of the fluorine atoms and the two protons of the solvate. The two hydrogen bonds cited here have lengths of 2.524 and 2.617 Å.

The cobalt to antimony distance is 8.1 Å, although the asymmetric unit contains the neighbouring unit cell's SbF_6^- counter-ion and this cobalt to antimony distance is 18.5 Å. The former distance is an average separation. This separation distinctly shows a non-interacting relationship between the ion pairs. Shown in Figure 3.19, is the existence of hydrogen bonding between the SbF_6^- and the protons of a solvate dichloromethane molecule. Here, this interaction brings the two atoms within 2.524 Å of each other.
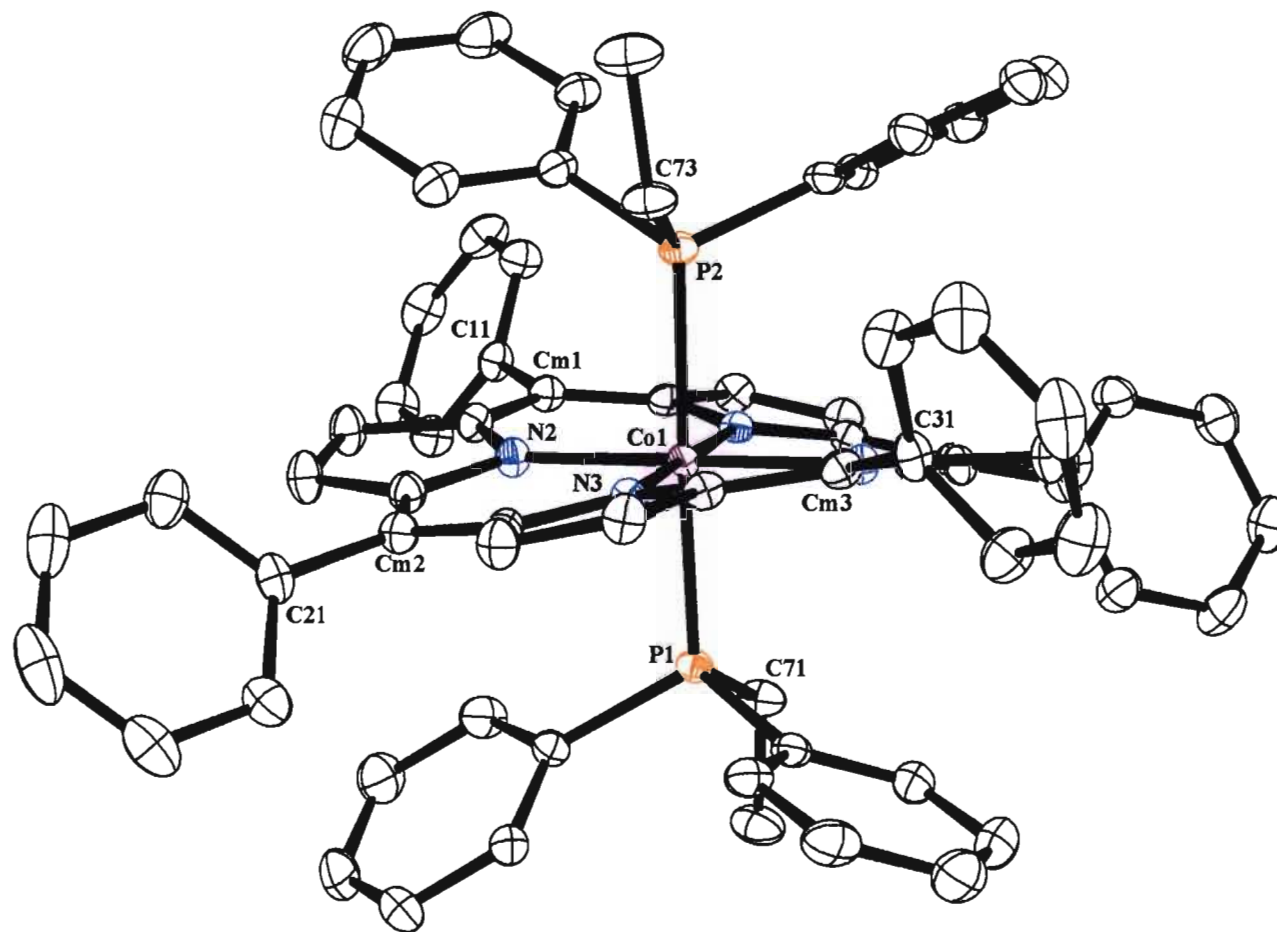
Figure 3.14: Selectively labeled ORTEP diagram of the X-ray crystal structure of [Co(TPP)(edpp)$_2$](SbF$_6$). The thermal ellipsoids have been drawn at the 70% probability level. Hydrogen atoms, solvent molecules and counterions are omitted for clarity.
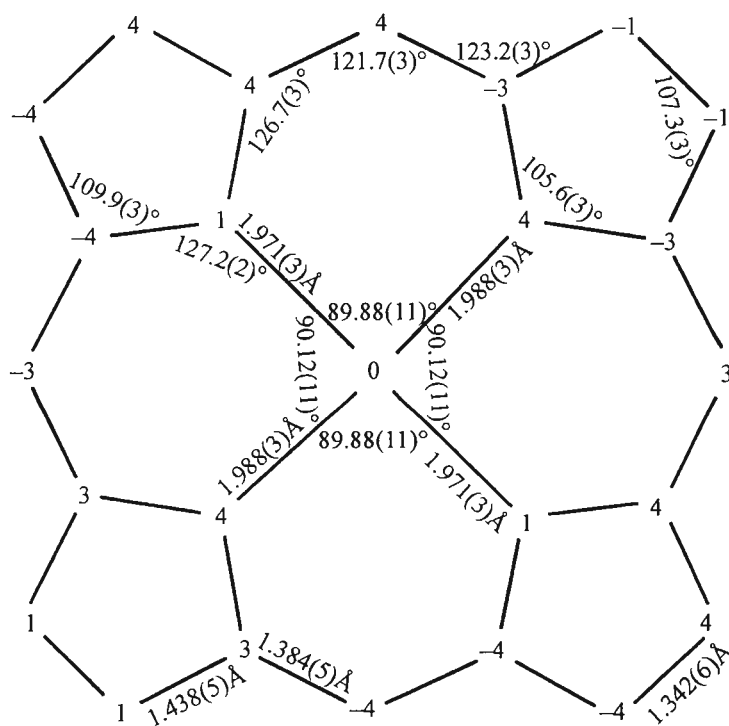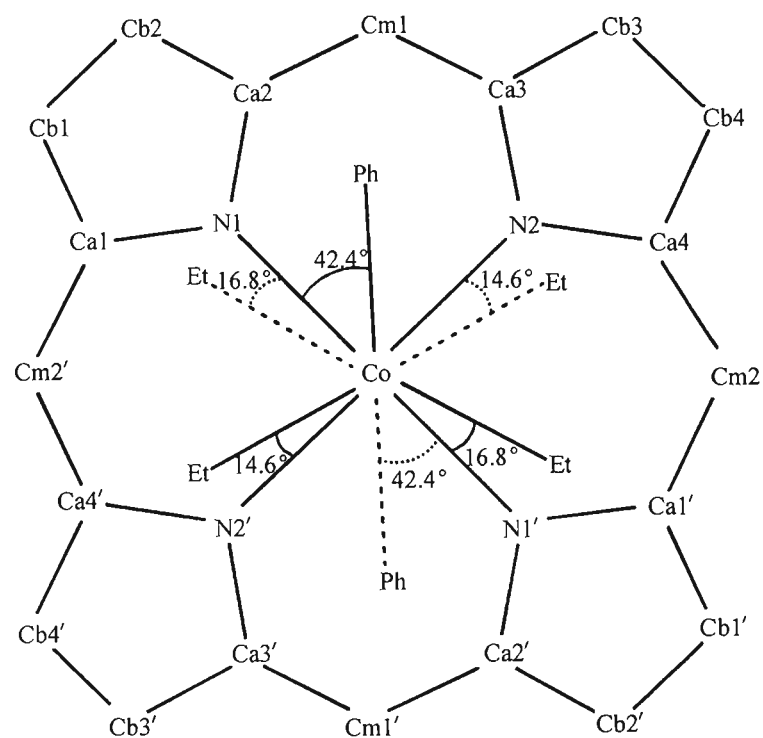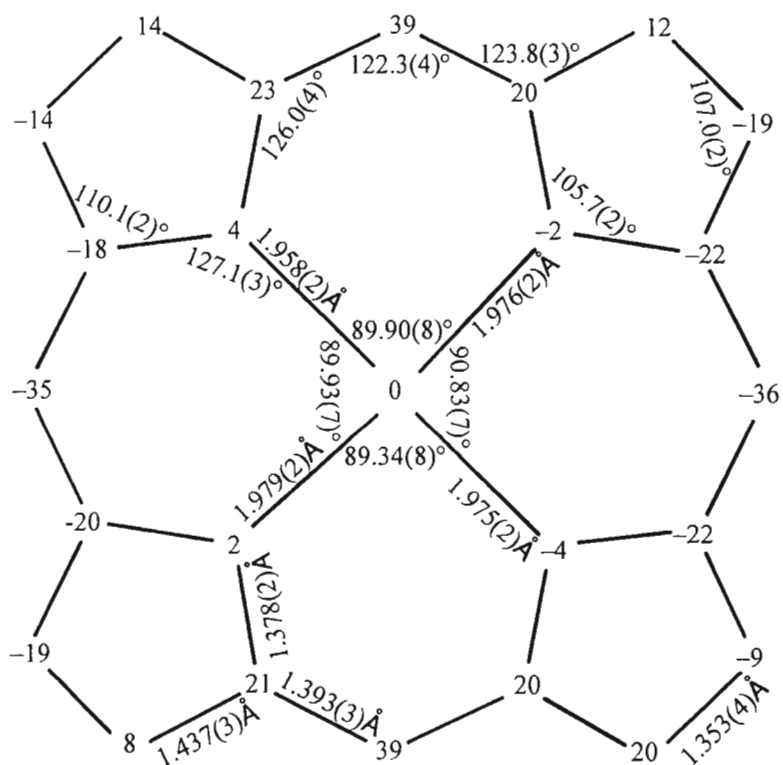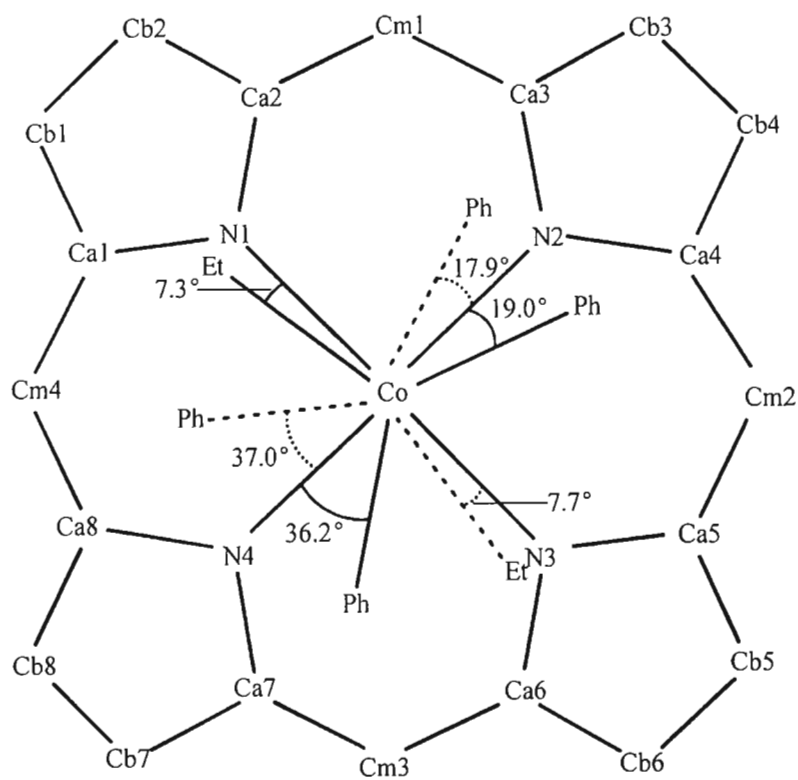
Figure 3.15: Crystallographic information for [Co(TPP)(edpp)₂](SbF₆). Displacements from the 24-atom mean plane are given in pm.
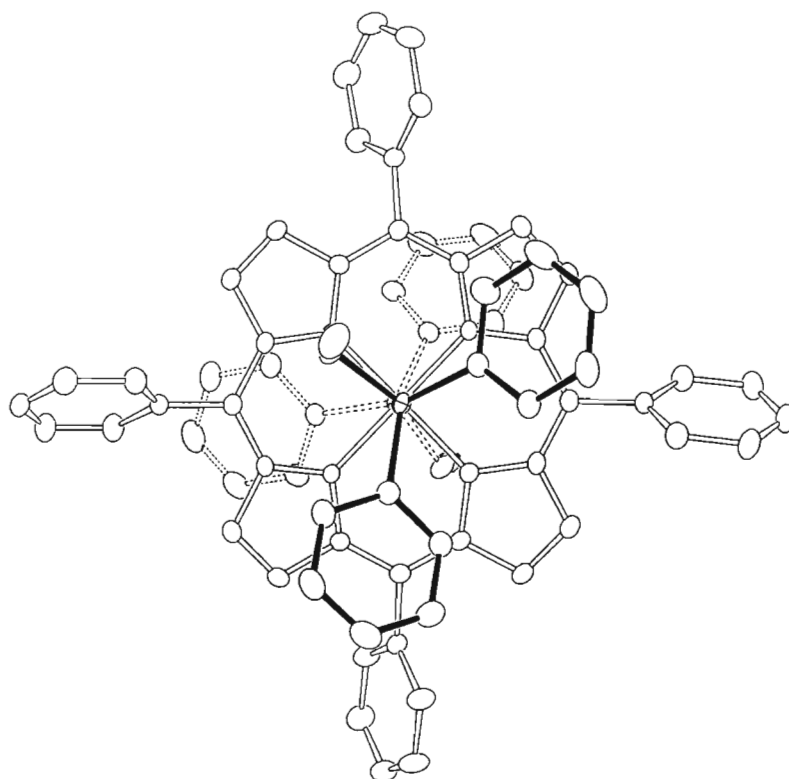
Figure 3.16: ORTEP diagram of [Co(TPP)(edpp)₂](SbF₆) (view perpendicular to porphyrin plane along P–Co–P axis).
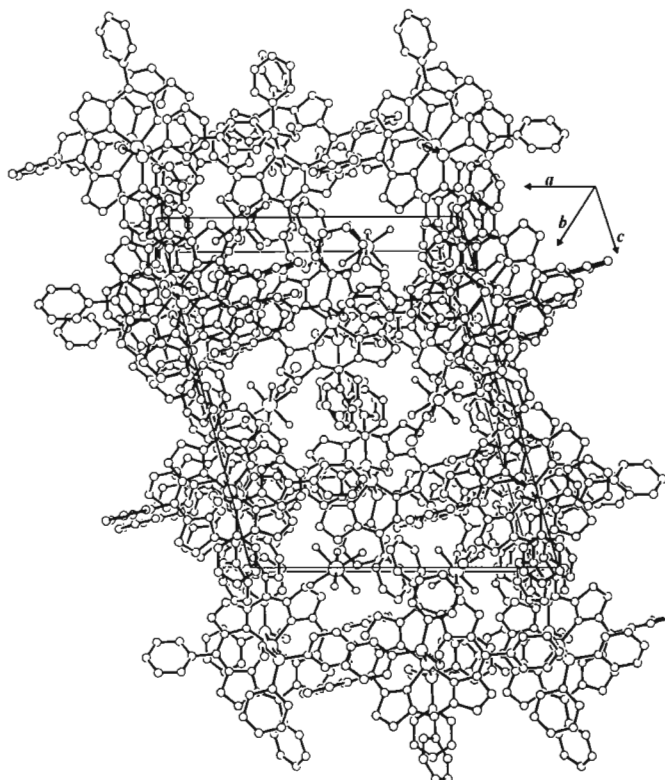
Figure 3.17: ORTEP diagram of the unit cell contents of the monoclinic structure of [Co(TPP)(edpp)₂](SbF₆) (view along *b* axis).
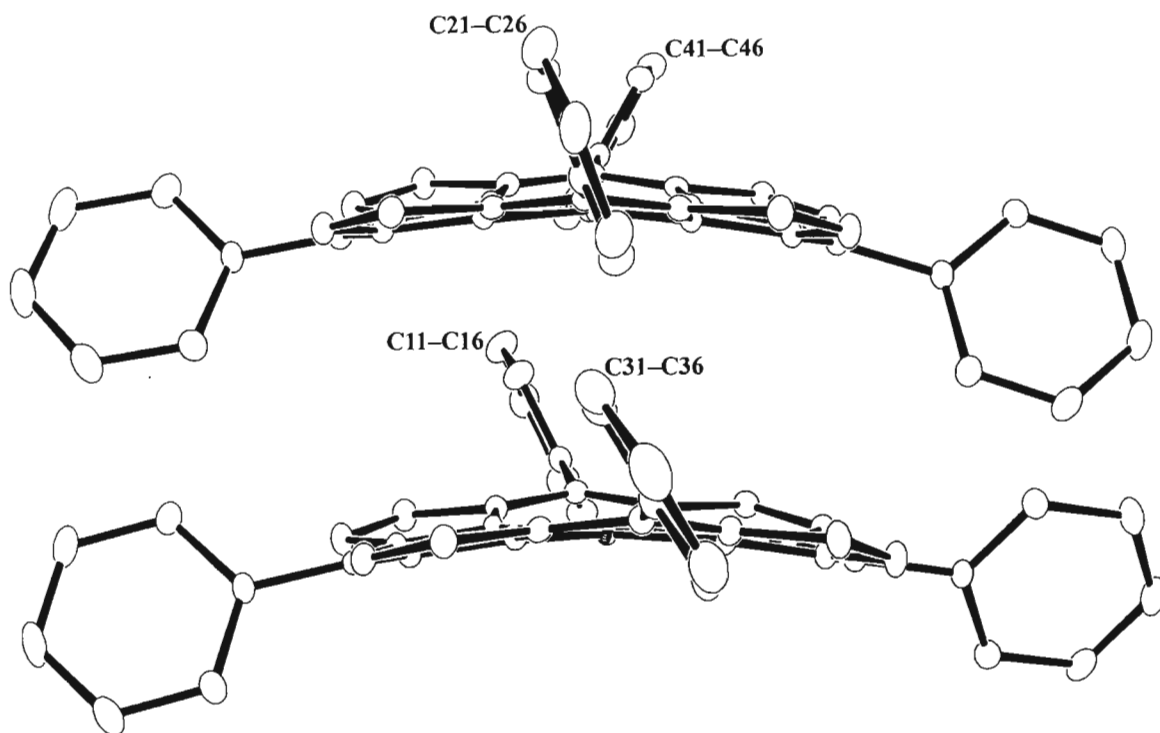
Figure 3.18: ORTEP diagram of the 'staggered' (upper) and 'eclipsed' (lower) orientations of the phenyl substituents within the X-ray crystal structure of [Co(TPP)(edpp)$_2$](SbF$_6$).
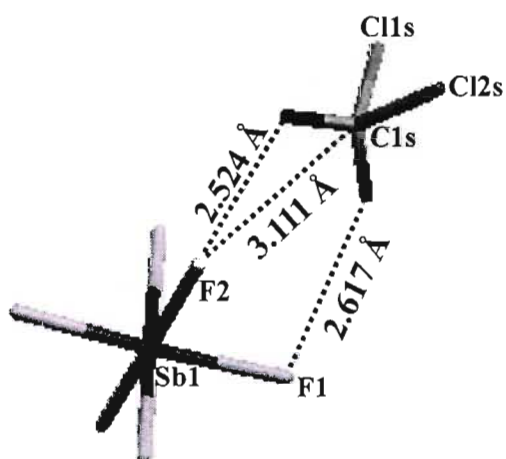
Figure 3.19: Diagram of the close contacts within the X-ray crystal structure of [Co(TPP)(edpp)$_2$](SbF$_6$). Close contacts occur between SbF$_6^-$ and solvate dichloromethane only.

3.2 Reactions of Phosphonites with Cobalt(III) Porphyrin Precursors

3.2.1 Synthesis and Characterisation of [Co(TPP)(deppt)$_2$](SbF$_6$)

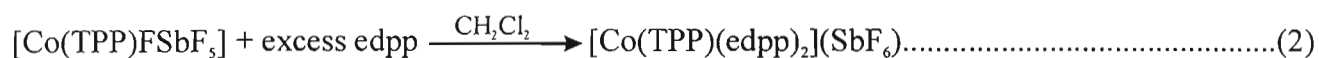The phosphonite used in this reaction was diethylphenylphosphonite, as shown in Figure 3.20 below.
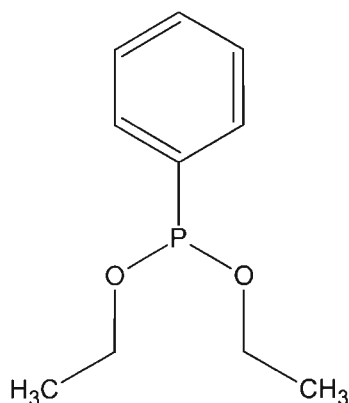
Figure 3.20: Structural diagram of diethylphenylphosphonite.

Routine precautions of degassing and drying of solvents were employed, both in the synthesis and in the preparation of NMR and UV-vis samples to ensure as non-oxidising an environment as possible. A 20 molar excess of the deppt was added to the [Co(TPP)(FSbF$_5$)] to ensure a six-coordinate product.

The reaction procedures are shown in equations 1 and 2 below.

$$[Co(TPP)Cl] + AgSbF_6 \xrightarrow{\text{THF}} [Co(TPP)FSbF_5] + AgCl(s) \dots\dots(1)$$

$$[Co(TPP)FSbF_5] + \text{excess deppt} \xrightarrow{\text{CH}_2\text{Cl}_2} [Co(TPP)(deppt)_2](SbF_6) \dots\dots(2)$$
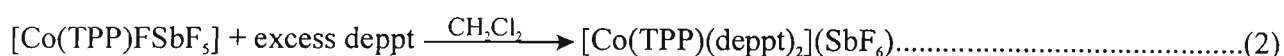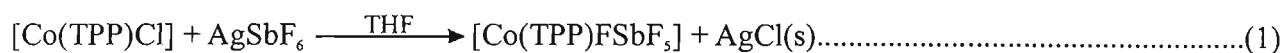
The product has a deep maroon colour in solution and yields dark maroon coloured crystals. The spectroscopic results are tabulated in Table 3.3. The ^{13}C NMR spectrum is shown in Appendix IV in Figure AIV.2.

The ^{1}H NMR spectrum of this compound, as shown in Figure 3.21 below, has been assigned with caution, as the excess ligand signals were broad and imposing. Thus the assignments made below are tentative and mention must be made of the resulting integration irregularities.

The singlet at 8.93 ppm has been assigned to the pyrrole protons and has been set as the reference integral as 8 H's. The sharp doublet at 7.93 ppm has been assigned to the *ortho*-protons of the porphyrin phenyls and integrates to 8 H's. The sharp multiplet at 7.78 ppm has been assigned to the *para*- and *meta*-protons of the porphyrins phenyls and integrates to 12 H's.

The signals corresponding to the bound ligands have been integrated separately to the porphyrin protons to enhance the accuracy of the assignments. The broad singlet at 7.02 ppm has been assigned to the *para*-protons and the broad singlet at 6.55 ppm has been assigned to the *meta*-protons of the bound phosphine ligand. The integrals of 2 and 4 H's, respectively, correspond with expected values. The signal from the *ortho*-protons is presumably within the broad irregular multiplet at 3.72 ppm, since for $[Co(TPP)(depp)_2](SbF_6)$ and $[Co(TPP)(edpp)_2](SbF_6)$, the chemical shifts for this signal had the values 3.67 and 3.75 ppm, respectively.

The splitting pattern of the above protons follows the same general character as that discussed for $[Co(TPP)(depp)_2](SbF_6)$.

The H_a and H_b signals of the co-ordinated ligand are assigned to the two low-intensity broad peaks at 0.89 ppm and 0.55 ppm. The integrals, being 4 H's each, of these two signals are relatively accurate and reflect the expected values. The broad, slightly higher intensity signal at-0.12 ppm has been assigned to the terminal methyl protons of the bound ligand and integrates relatively accurately to the expected value of 12 H's. The broad nature of these two sets of signals does not allow for the accurate determination of their multiplicity. The above splitting pattern suggests that the terminal $-CH_3$ groups, rather than the $-CH_2-$ groups, as was the case with $[Co(TPP)(depp)_2](SbF_6)$, are in a region less-exposed to the shielding cone, resulting in a more downfield position of these protons.

It must be emphasized that the expected signals corresponding to the two $-CH_2CH_3$ groups of the co-ordinated phosphine ligand will most likely produce two different sets of signals, corresponding to their different orientations within the shielding cone. Hence there may be signals corresponding to at least one of these orientations in the unassignable signals in the

region 1.1 to 2.9 ppm of the spectrum.

The protons of the coordinated axial ligands produce signals which are generally broad and of low intensity. No coupling constants were obtainable from these signals.

The signals a, b and c in this spectrum are due to the 4 excess moles of free ligand as a molar ratio of 5:1 of ligand to $[Co(TPP)(SbF_6)]$ was added. Signal a in the spectrum in Figure 3.21 corresponds to the *phenyl* protons of the uncoordinated deppt. The broad and irregular multiplet b corresponds to the $-CH_2-$ protons and the broad singlet c corresponds to the $-CH_3$ protons.
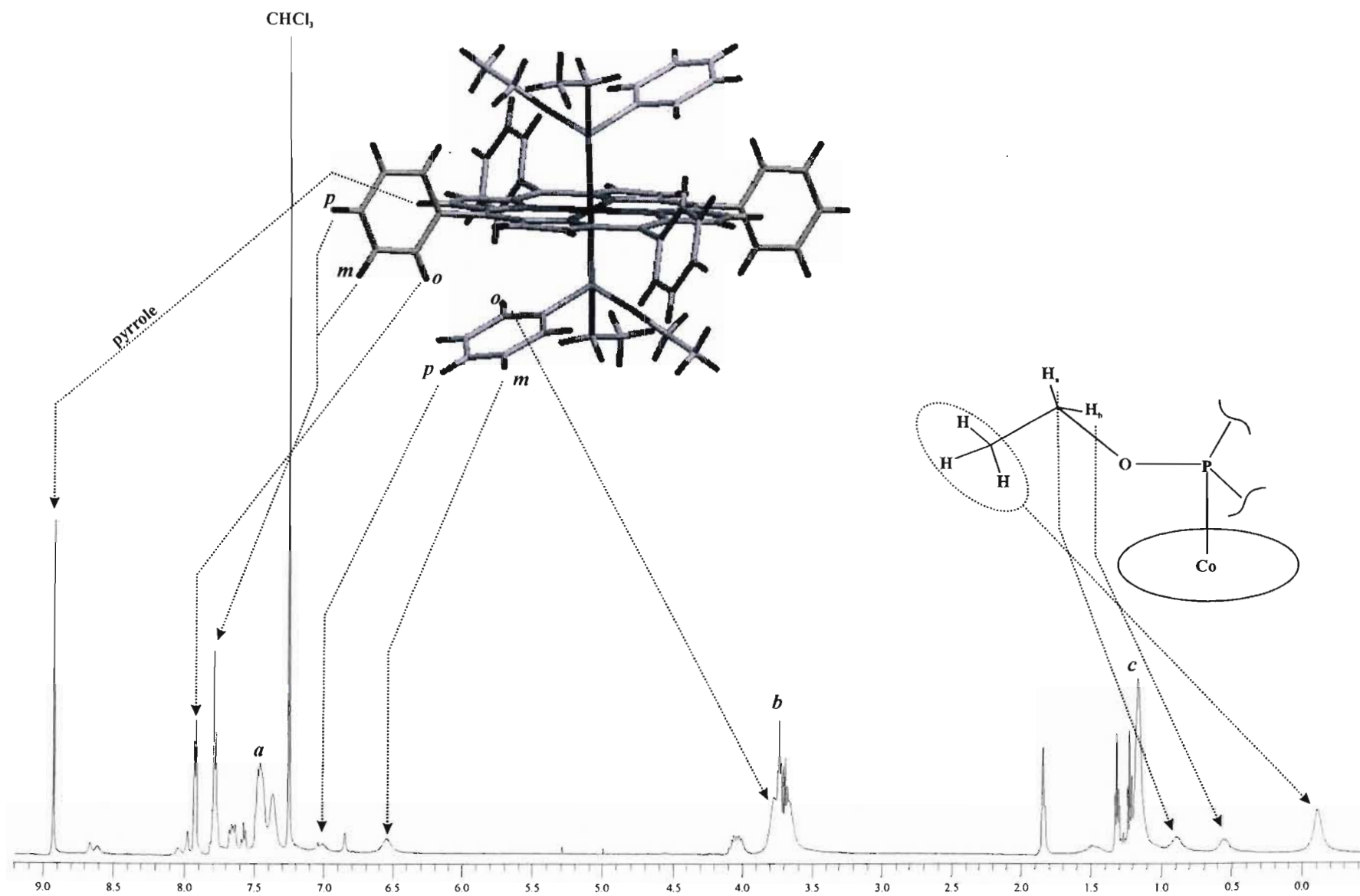
Figure 3.21: ^{1}H NMR spectrum of [Co(TPP)(deppt)$_2$](SbF$_6$) at 25 °C.

The proton-decoupled ^{31}P NMR spectrum in Figure 3.22 shows a major product and two minor products. The ^{31}P resonance of the free ligand occurs at 156.64 ppm and that of the co-ordinated ligand occurs at 114.80 ppm. The resonance of the oxidized phosphine occurs at 19.85 ppm. The signal at 25.85 ppm is an unknown contaminant.

The electronic spectrum for [Co(TPP)(deppt)$_2$](SbF$_6$) is shown in Figure 3.23. As with the previous two cobalt complexes, the Soret band at 457 nm is relatively sharp and intense. Immediately noticeable is the increased relative difference in intentensity between the "split" Soret bands, i.e., the $B(0, 0)$ and $B(1, 0)$, bands relative to the previous two bis(phosphine) Co(III) complexes reported on earlier in this chapter. The suspected $N(0, 0)$ band is found at 351 nm, and is broader than that reported for the two previous complexes. The three Q bands are found between 542 nm and 627 nm.
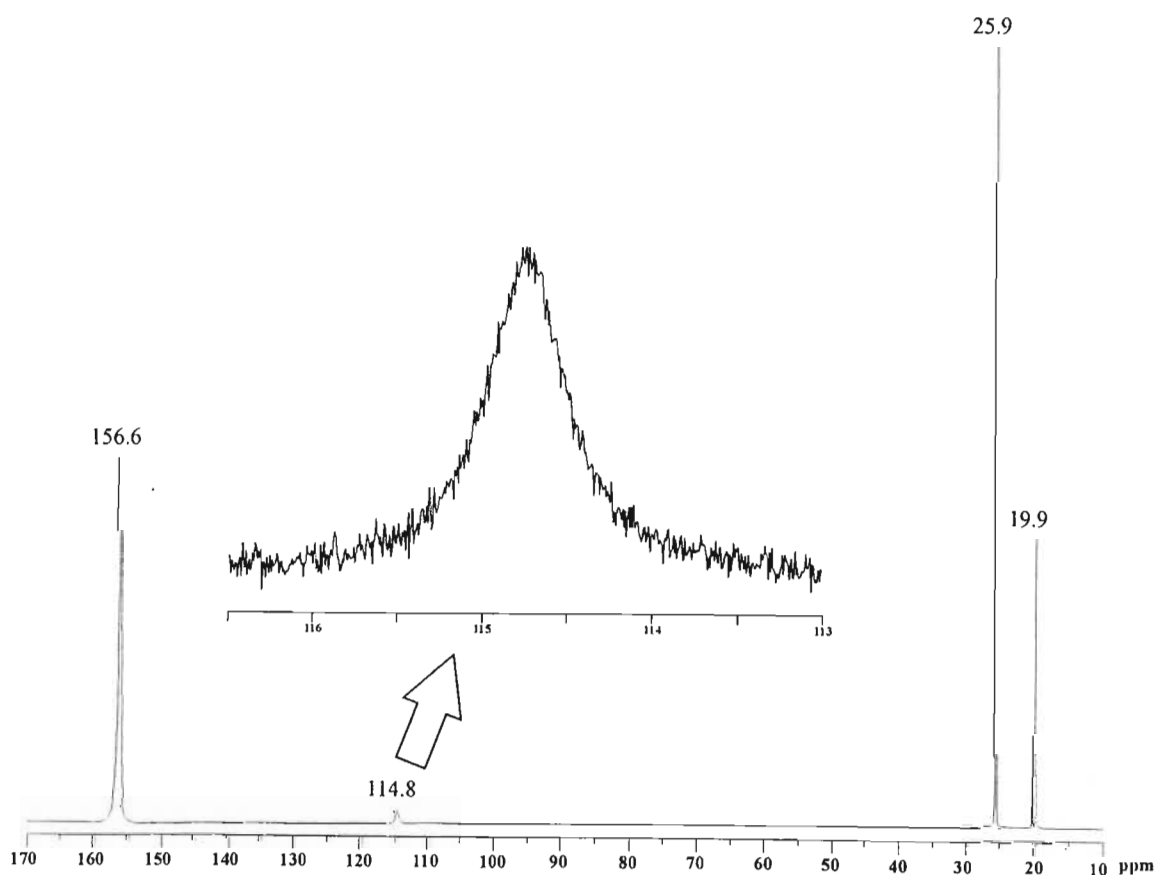
Figure 3.22: Proton-decoupled ^{31}P NMR spectrum of [Co(TPP)(deppt)$_2$](SbF$_6$) at 25 °C.
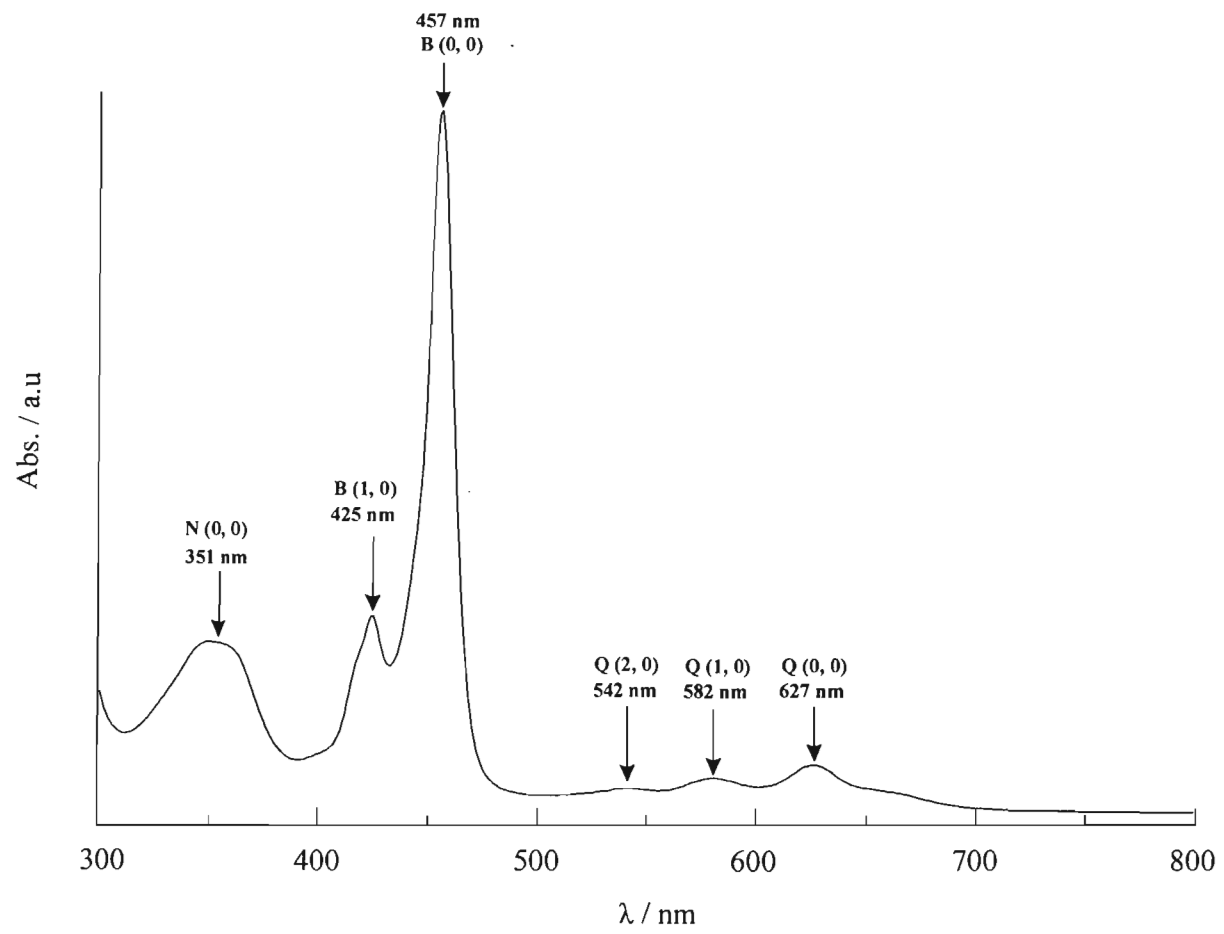
Figure 3.23: Electronic Spectrum of [Co(TPP)(deppt)₂](SbF₆) in dichloroethane at 25 °C.

Table 3.3 Spectroscopic data for [Co(TPP)(deppt)₂](SbF₆)

^{1}H NMR^a	**TPP:** 8.93 (8H, sh s, pyrrole H's), 7.93 (8H, sh d, $^3J = 6.9$ Hz, o–H's), 7.78 (12H, sh m, m,p–H's) **Deppt:** 7.02 (2H, br s, p–H's), 6.55 (4H, br s, m–H's), 3.72 (o–H's), 0.89 (4H, br s, H$_a$), 0.55 (4H, br s, H$_b$), –0.12 (12H, br s, –CH$_3$)
^{31}P NMR^a	114.80
^{13}C NMR^a	144.18 (s, str), 141.06(d, w), 134.99 (s, str), 134.09 (s, str), 133.06 (d, str), 132.35 (d, w), 131.71 (d, str), 129.65 (d, str), 128.73 (d, str), 128.49 (s, w), 128.33 (d, w), 128.12 (d, str), 127.19 (s, str), 77.10 (t, str), 62.48 (d, str), 62.05 (t, w), 18.36 (s, w), 17.05 (d, str), 16.31 (t, w)
Infrared^b	1072.8 (med, ν(P–O$_{OEt}$)), 1440.1 (med, ν(P–C$_{Ph}$)), 996.7 (str, ν(P–C$_{Ph}$))
Uv-vis^c	627 (1.2×10^4), 582 (8.3×10^3), 542 (6.0×10^3), 457 (1.7×10^4), 425 (4.7×10^4), 418 (3.4×10^4), 351 (4.1×10^4)

^{a} Chemical shifts in ppm. Measured at 294 K in CDCl₃, s = singlet, d = doublet, t = triplet, m = multiplet, str = strong, med = medium, w = weak, sh = sharp, br = broad. ^{b} $\bar{\nu}$ (cm^{-1}). KBr disk. ^{c} λ_{max}/nm (ε/dm³ mol^{-1} cm^{-1}); measured at 298 K in dried and degassed dichloroethane.

137

3.2.2 Crystal Structure Determination of [Co(TPP)(deppt)₂](SbF₆)

The compound was crystallized by slow diffusion of hexane into a solution of the compound in CH_2Cl_2. Cube-shaped crystals were isolated from the solution and X-ray quality crystals were mounted on glass microfibres. The X-ray data were collected at room temperature (293 K) and the final $R_1 = 0.0633$ for the structure solution. The compound crystallized in the monoclinic crystal system in the space group $P2_1/n$. There is inversion symmetry in the asymmetric unit and the Co center is thus half occupied. The asymmetric unit comprises two half porphyrins and a full antimony hexafluoride. The two porphyrin complexes are distinguished from each other by means of a prime symbol.

The average $Co-P_{ax}$ bond length is 2.258(2) Å and the averaged $Co-N_{porph}$ bond length is 1.980(4) Å. Likewise, the average $Co'-P'_{ax}$ bond length is 2.258(2) Å and the averaged $Co'-N'_{porph}$ bond length is 1.984(4) Å. These axial bond lengths are shorter than the axial bond lengths observed for the two phosphine complexes of cobalt. It appears that the ethoxy substituent in the phosphonite deppt minimizes the steric bulk of the ligand, relative to the corresponding phosphine. The predicted effect of replacing an ethoxy substituent with a phenyl would thus be a lengthening of the axial bonds as the steric bulk is increased accordingly.

The atomic displacements, within the porphyrin core, from the 24-atom mean plane are minimal and show only a vague hybrid saddle/ruffle conformation. The inversion symmetry through the central cobalt is consistent with the metal being in the plane of the 24-atom core. There is significant disorder of the alkoxy substituents of the phosphonite axial ligand as these fragments are capable of significant 'swiveling' in space and thus a low temperature data collection of this compound might well improve the quality of the structure solution.

The ORTEP diagram of the crystal structure is shown in Figure 3.24. The axial ligand orientations for the first complex within the asymmetric unit as well as the mean plane deviations of the porphyrin core atoms and bond-lengths and angles are summarized in Figure 3.25. The analogous data for the second complex within the asymmetric unit is given in Figure 3.26. The asymmetric unit itself is shown in Figure 3.27. The view of the two complexes within the asymmetric unit along the P–Co–P axis and P'–Co–P' axis is shown in Figures 3.28 and 3.29, respectively. The relative axial ligand orientations for each complex within the asymmetric unit are shown in these two figures.

Figure 3.30 shows that the only existing close-contacts within this X-ray crystal structure are between the phenyls of the two complexes making up the asymmetric unit. Here the proton on carbon C34 comes within 2.890 Å of carbon C16′ of the neighbouring complex. The Co···Sb distance measures 8.602 Å, consistent with a well separated ion pair.

The dihedral angles of the phenyl substituents relative to the mean plane of the porphyrin macrocycle are: C11–C16 = 88.56°; C21–C26 = 72.01°; C11′–C16′ = 68.75° and C21′–C26′ = 66.84°.

The ordered packing arrangement of the complex in the unit cell has been shown in Figure 3.31.
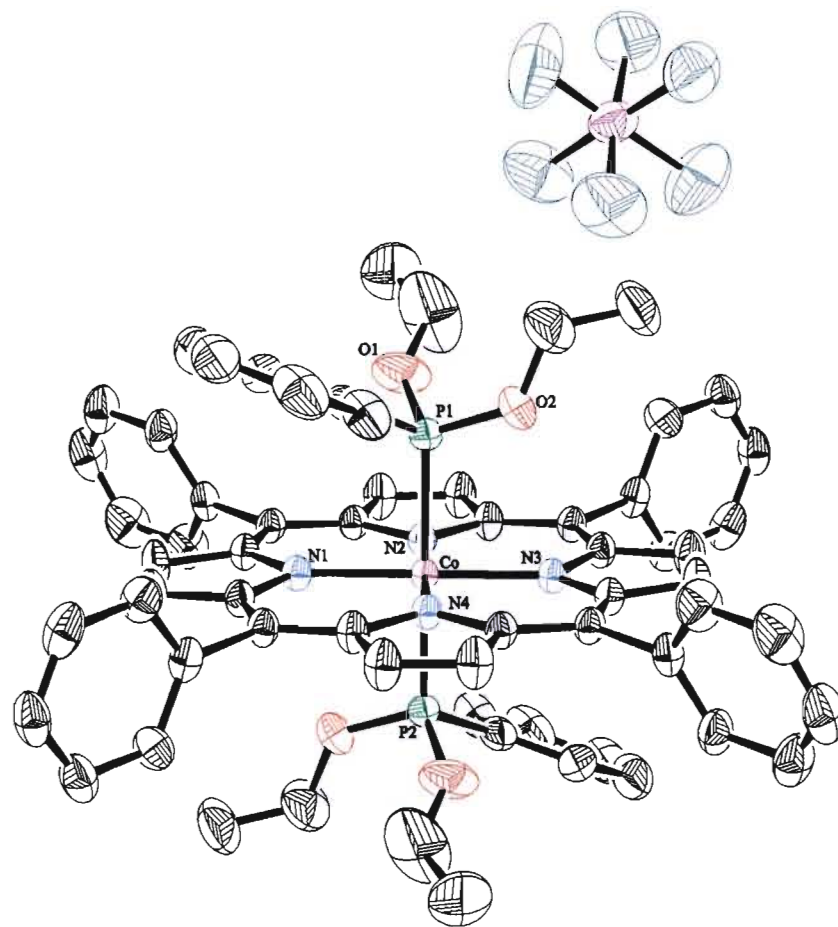
Figure 3.24: Selectively labelled ORTEP diagram of the X-ray crystal structure of [Co(TPP)(deppt)$_2$](SbF$_6$). Thermal ellipsoids have been drawn at the 30% probability level. H atoms are omitted for clarity.
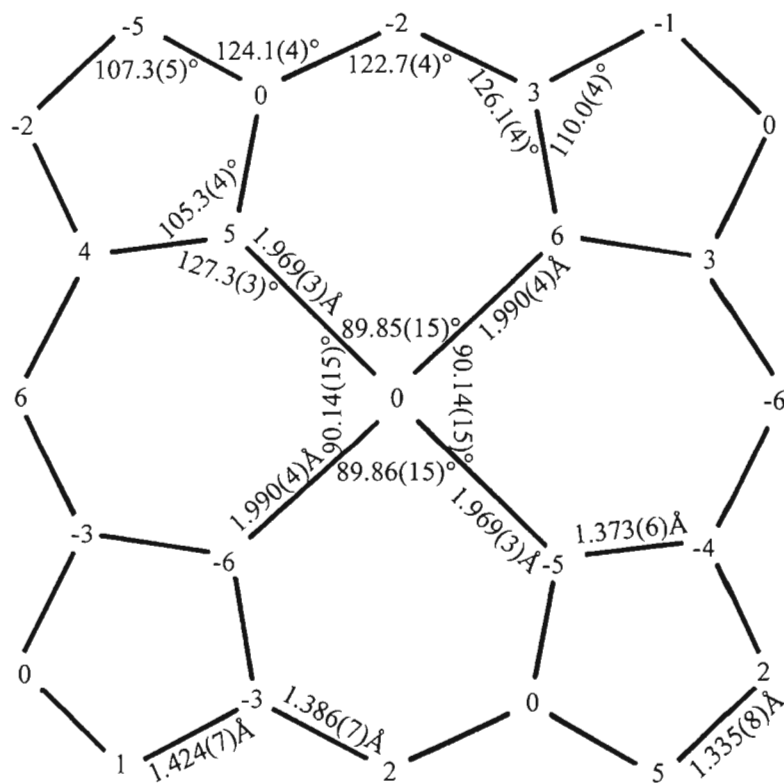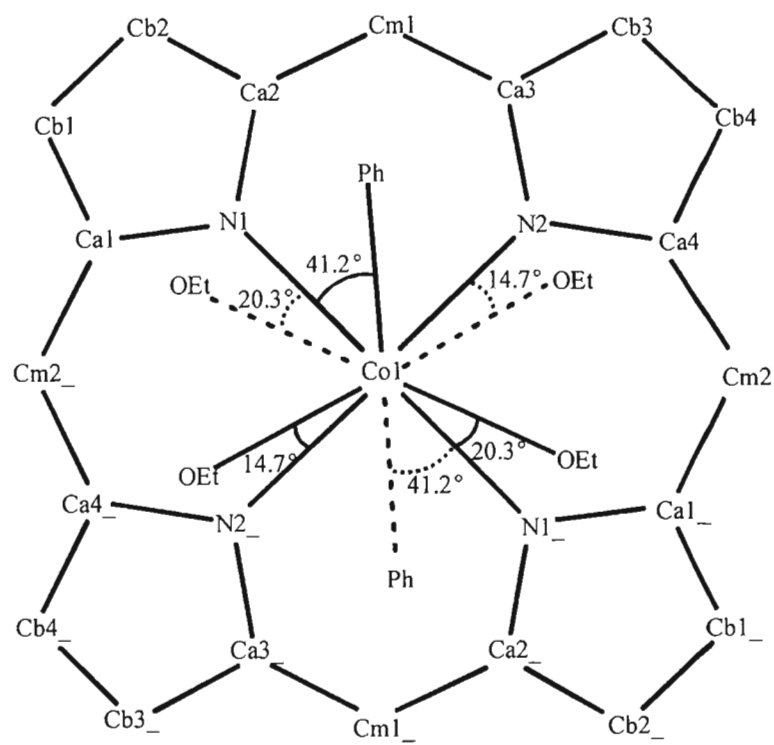
Figure 3.25: Crystallographic information for [Co(TPP)(deppt)₂](SbF₆). Underscores designate symmetry-equivalent atoms. Displacements from the 24-atom mean plane are given in pm.
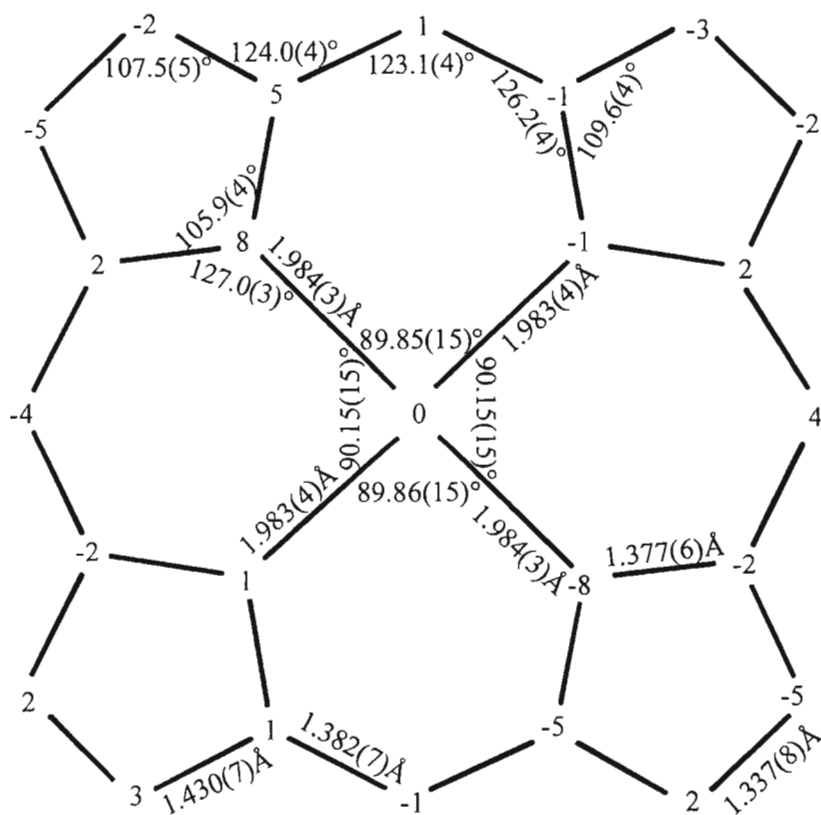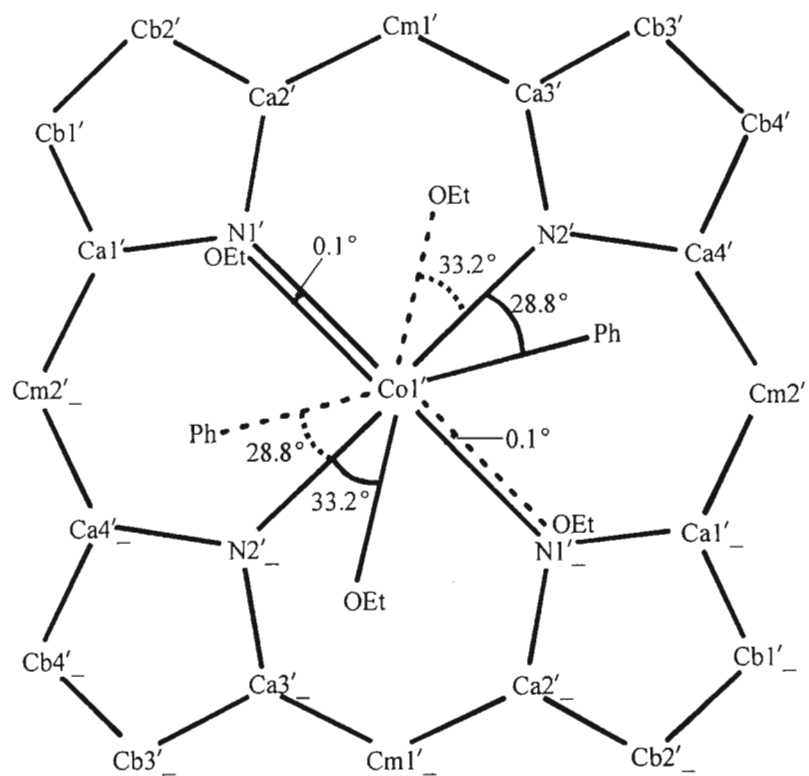
Figure 3.26: Crystallographic information for [Co′(TPP)(deppt)₂](SbF₆). Underscores designate symmetry-derived atoms. Displacements from the 24-atom mean plane are given in pm.

142
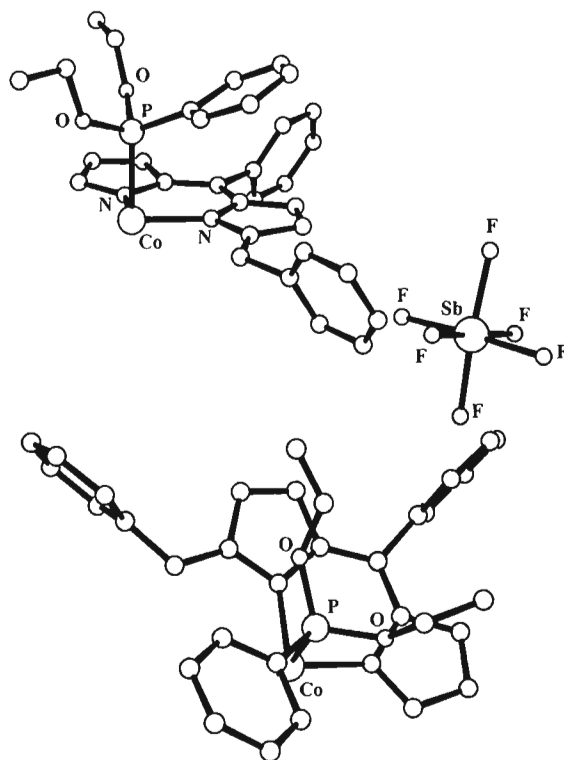
Figure 3.27: ORTEP diagram of the asymmetric unit of the X-ray crystal structure of [Co(TPP)(deppt)₂](SbF₆).
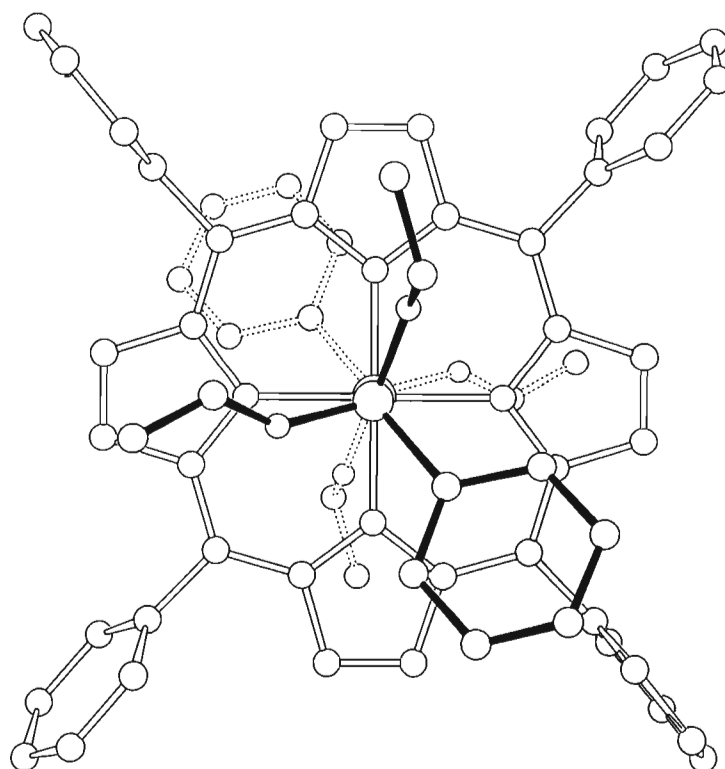
Figure 3.28: ORTEP diagram of the [Co(TPP)(deppt)₂]⁺ cation (view perpendicular to porphyrin plane along P–Co–P axis).
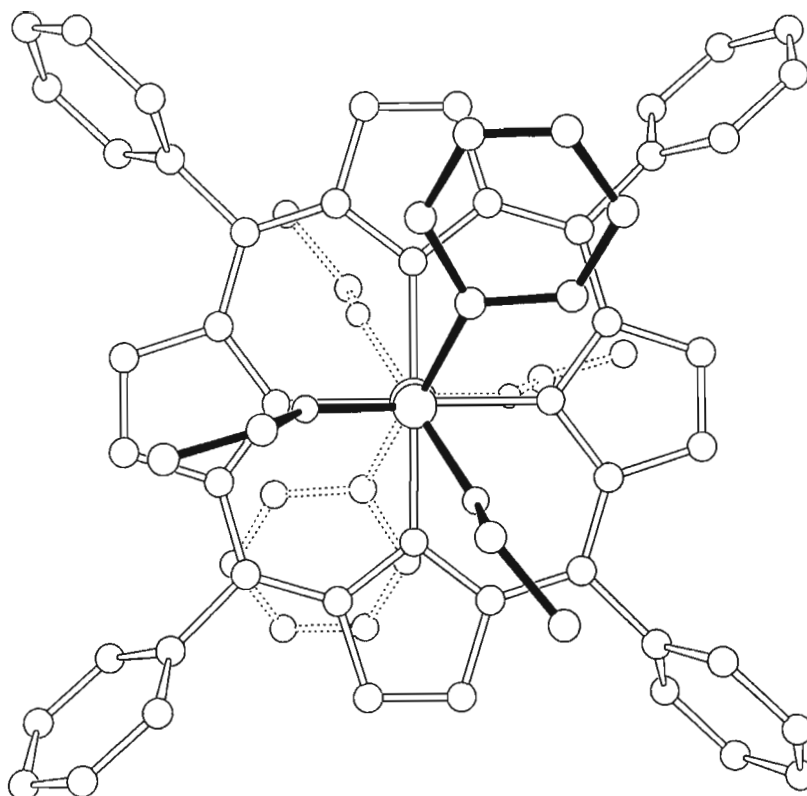
Figure 3.29: ORTEP diagram of the second independent [Co′(TPP)(deppt)₂]⁺ cation in the asymmetric unit (view perpendicular to porphyrin plane along P′–Co′–P′ axis).
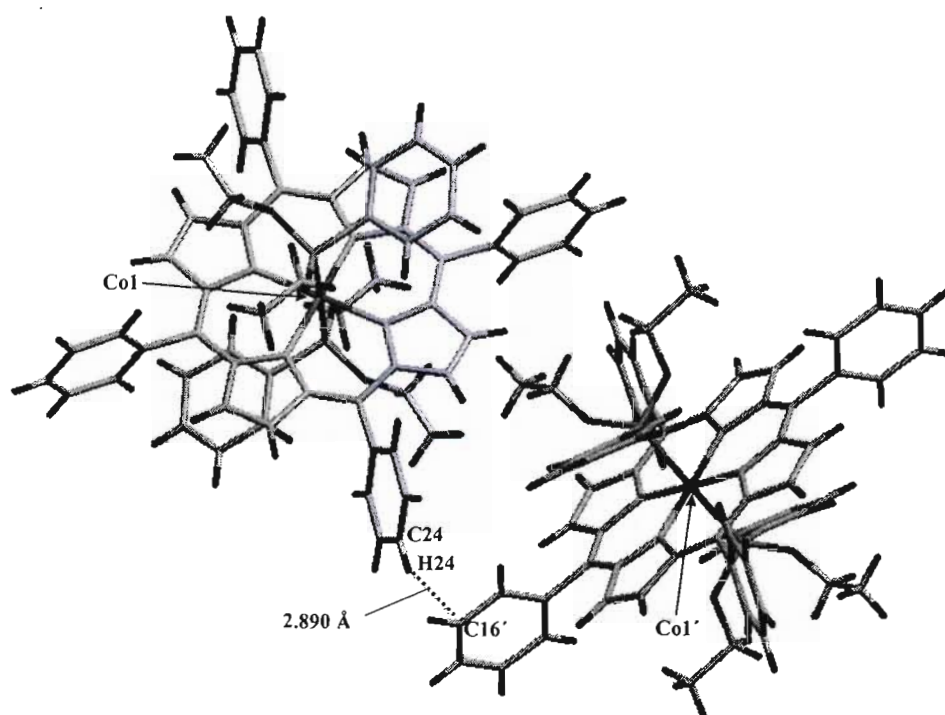
Figure 3.30: Diagram (Mercury 1.1) of the close contacts within the two independent porphyrins of the asymmetric unit in the X-ray crystal structure of [Co(TPP)(deppt)₂](SbF₆).
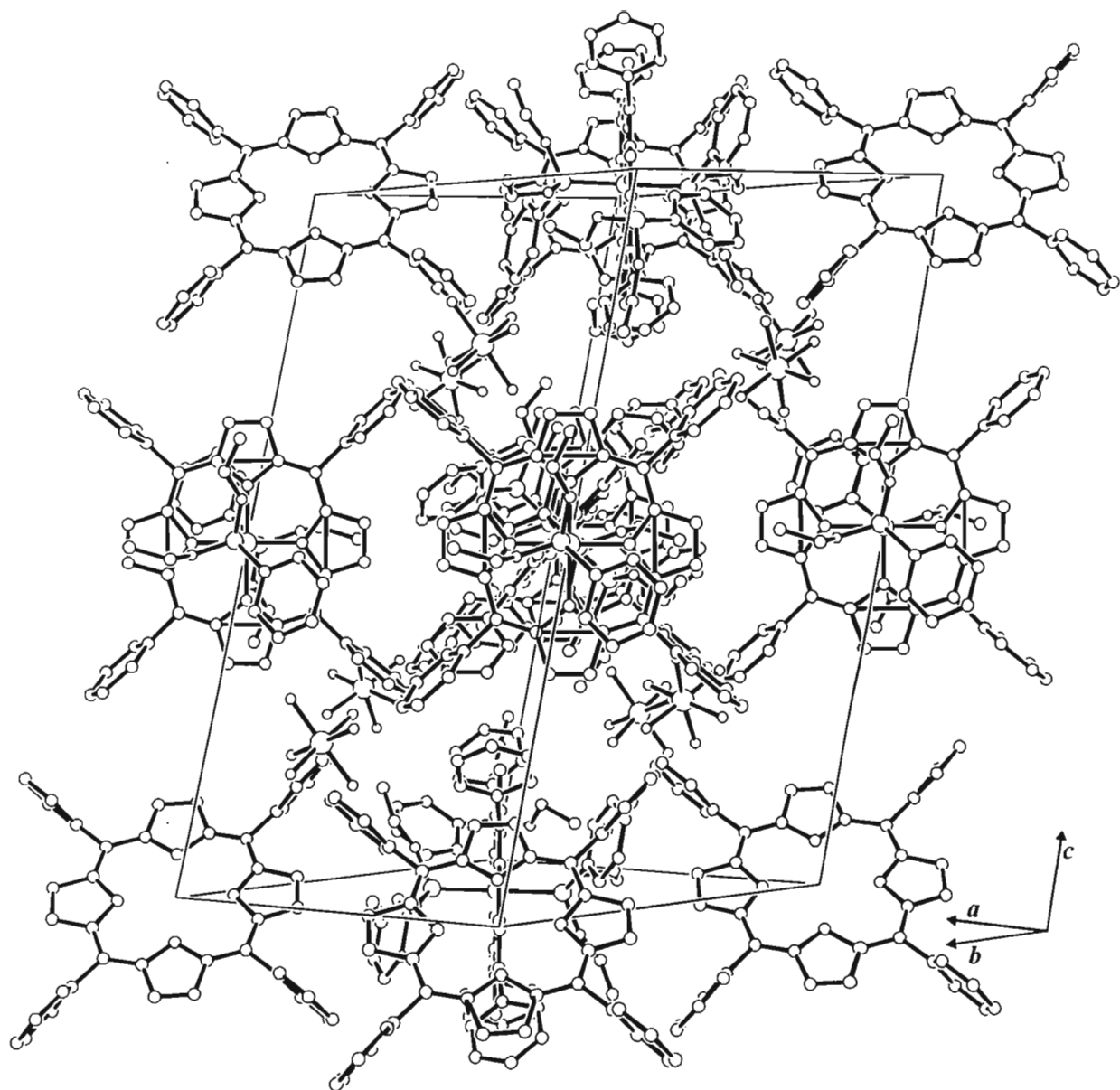
Figure 3.31: ORTEP diagram of the unit cell contents of the monoclinic structure of [Co(TPP)(deppt)₂](SbF₆). Selected axial ligands and metal ions have been removed for clarity.

3.3 Summary of Crystallographic and Spectroscopic Data for Bis(Phosphine) and Bis(Phosphonite) Complexes of Co(III) Porphyrins.

Crystallography. All three of the complexes studied are 6-coordinate and crystallize in the monoclinic crystal system. The bis(phosphine) complexes display axial Co–P bond lengths of 2.312(1) and 2.330(1)/2.316(1) Å for $[Co(TPP)(depp)_2](SbF_6)$ and $[Co(TPP)(edpp)_2](SbF_6)$, respectively, resulting in a mean Co–P axial bond length for this class of compound of 2.319(9) Å. The axial Co–P bond length for the single bis(phosphonite) complex $[Co(TPP)(deppt)_2](SbF_6)$ is 2.258 (2) Å and is substantially shorter than the equivalent bond observed in the bis(phosphine) complexes.

The conformations adopted by the porphyrin core are mostly planar but for $[Co(TPP)(edpp)_2](SbF_6)$, where a strongly ruffled conformation is observed. The central cobalt ion is positioned in the centre of the 24-atom mean plane in all three complexes, consistent with a six-coordinate geometry in each case.

Table 3.4: Summary of Important Crystallographic Data for Bis(Phosphine) and Bis(Phosphonite) Compexes of Co(III) Porphyrins

	$[Co(TPP)(depp)_2](SbF_6)$	$[Co(TPP)(edpp)_2](SbF_6)$	$[Co(TPP)(deppt)_2](SbF_6)$
Crystal System	Monoclinic	Monoclinic	Monoclinic
Spacegroup	$P2_1/c$	$P2_1/n$	$P2_1/n$
T (K)	176(2)	100(1)	293(2)
Co–P (Å)	2.312(1)	2.330(1)/2.316(1)	2.258(2)
Co–N$_{porph}$ (Å)	1.980(3)	1.972(7)	1.980(4) / 1.984(4)
Conformation	Planar	Ruffled	Planar
Δ_{Co} (pm)	0	0	0

a Δ_{Co} = displacement of Co(III) ion from 24-atom mean plane.

In a seach of the CSD for phosphine and phosphonite complexes of Co(III) of the type as shown in Figure 3.32 below, only two complexes were found. Both of the complexes were bis(phosphine) compounds, with triphenylphosphine as the P-donor ligand.
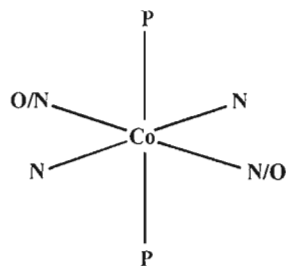
Figure 3.32: Search outline for related complexes.

The first compound is bis{bis(α-furyl)-glyoximato}-triphenylphosphine-cobalt(III) nitrate derivative, which is shown in Figure 3.33. This complex exhibits a unique Co–P bond length of 2.397(2) Å. The second compound, bis(1, 2-cyclohexanedionedioximato) bis(triphenylphosphine) Co(III) pentafluorosilicate, shown in Figure 3.34, displays a Co–P bond length of 2.371(10) Å. Both these Co–P bond lengths are distinctly longer than those observed for the complexes synthesized in this work. These longer axial bond lengths may be attributed to the large steric bulk of the tripenylphosphine ligand relative to the relatively unencumbered ligands used in this work.
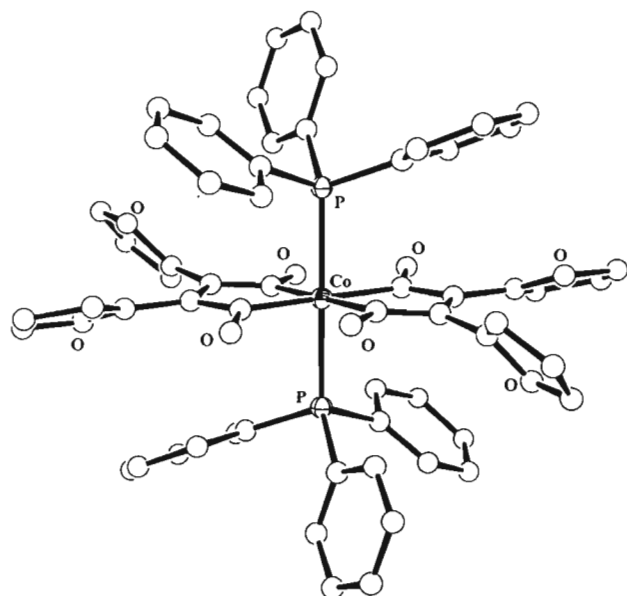
Figure 3.33: BEMVEU[225]
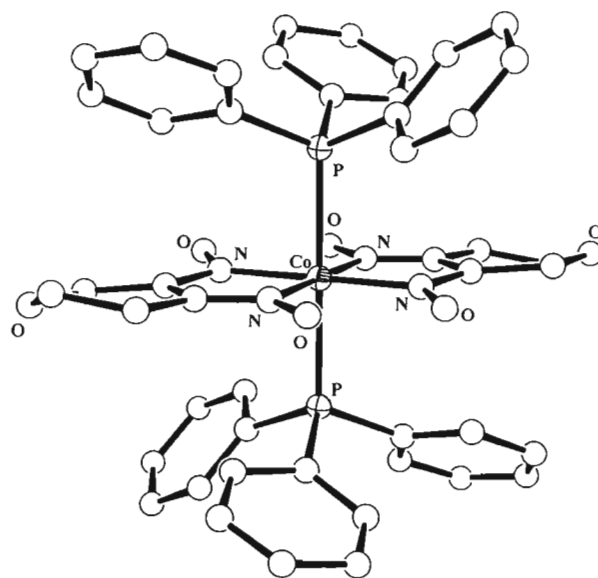
Figure 3.34: ECIDAV[226]

Spectroscopy. In the ^{1}H NMR spectra of the three Co(III) complexes, a loss of equivalence in the –CH$_2$– protons of the axial ligand may be observed in [Co(TPP)(depp)$_2$](SbF$_6$) and [Co(TPP)(deppt)$_2$](SbF$_6$). Where these protons should display a quartet, they instead display

147

two broad, single signals of equal intensity. This is explained by these protons having an orientation whereby one is 'dipping' further down into the shielding cone than the other, resulting in a difference in the magnetic shielding environment for each. In all three complexes, the protons of the ligands show a dramatic upfield shift upon coordination, consistent with the sizeable ring current of the porphyrin macrocycle.

The ^{31}P NMR signals for all three compounds are relatively broad singlets. The ^{31}P shifts were plotted against the Co–P bond lengths derived from the X-ray crystal structure of each complex, as shown in Figure 3.35.
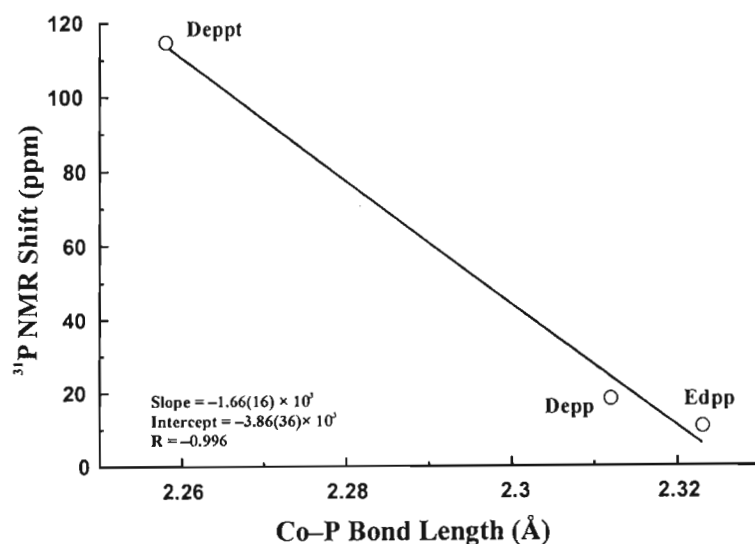
Figure 3.35: Graph of ^{31}P NMR shifts *versus* Co–P$_{ax}$ bond lengths for [Co(TPP)(depp)$_2$](SbF$_6$), [Co(TPP)(edpp)$_2$](SbF$_6$) and [Co(TPP)(deppt)$_2$](SbF$_6$).

In this plot, a possible inverse relationship exists between the axial Co–P bond lengths and the ^{31}P NMR shifts for these complexes. A plot of the Co–P bond lengths *versus* the ^{31}P NMR shifts of the free ligands also shows a similar trend. There are, however, too few data at present from which to draw any accurate correlations. The downfield shift for the deppt complex may reflect the lower charge on the P atom or the better M→L π backbonding due to a shorter Co–P distance.

The graph in Figure 3.36 shows the Co–P$_{ax}$ bond lengths versus the wavelength of the B(0, 0) or Soret band in the electronic spectra of the three complexes. An obvious linear relationship is observed which is an indication that the Co–P$_{ax}$ bond lengths of these complexes are actually indicative of the σ-donor strength of the respective phosphine or phosphonite. A stronger σ-

donor causes a shorter Co–P$_{ax}$ bond and has, correspondingly, caused a shift of the Soret band to a higher energy (shorter wavelength) region of the Uv-vis spectrum.
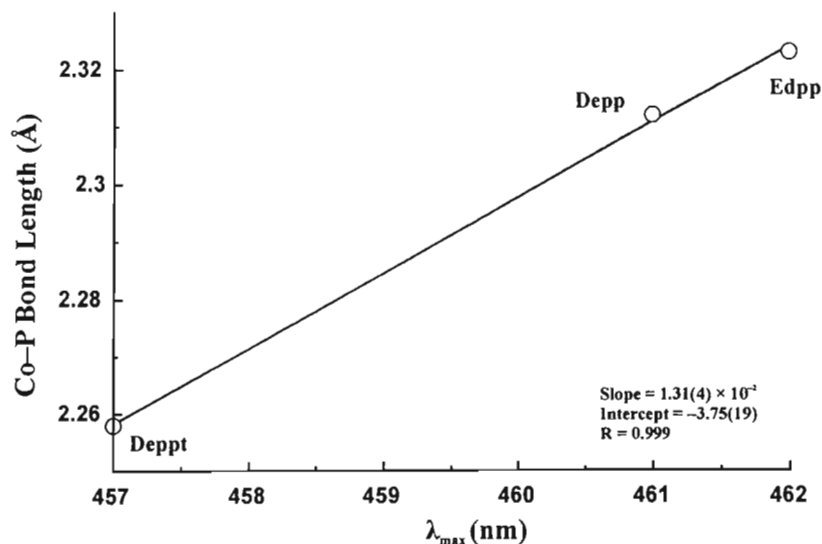
Figure 3.36: **Graph of the Co–P$_{ax}$ bond lengths *versus* the wavelength of the B(0, 0) band in the electronic spectra of (*a*) [Co(TPP)(deppt)$_2$](SbF$_6$), (*b*) [Co(TPP)(depp)$_2$](SbF$_6$), and (*c*) [Co(TPP)(edpp)$_2$](SbF$_6$).**

Although we have too few data at this stage to thoroughly confirm the trend evident from Figure 3.36, a possible explanation for the blue-shift in the B(0, 0) band with decreasing Co–P$_{ax}$ distance, is that the phosphonite derivative is a better π-acceptor ligand than the corresponding phosphines. Reduction of the Co(III) electron-density through M→L π-backbonding is expected to increase the HOMO-LUMO gap and thus raise the energies of transitions involving these two MO's. A possible test of this assumption would be to calculate the electronic spectra of the three complexes using the X-ray coordinates and the CI-singles (single-excitation configuration-interaction) method.

Interestingly, a nearly perfectly linear relationship exists, as is shown in Figure 3.37 below, between the Co–P bond length and Tolman's cone angle[230] (see Chapter 4.5) of the phosphine/phosphonite. This may highlight the importance of the phosphine/phosphonite's cone angle in determining the Co–P bond length in cobalt(III) systems, rather than the electronic character of the phosphorous donor atom. However, such a conclusion is weakened by the lack of X-ray structural data at this time.
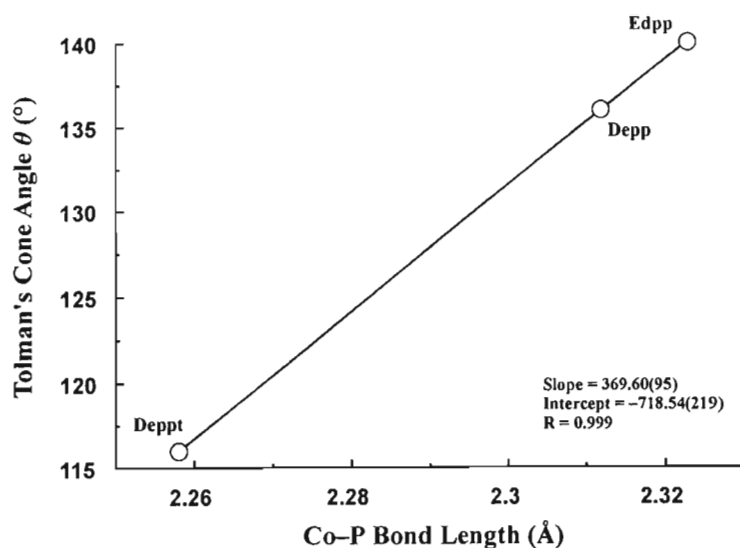
Figure 3.37: Graph of the Tolman's cone angle θ versus Co–P bond length.
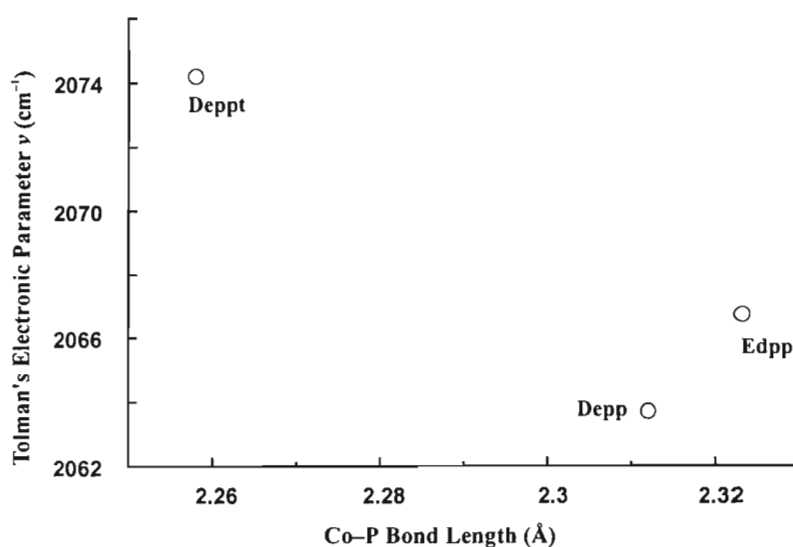
Figure 3.36: Graph of the Tolman's electronic parameter v versus Co–P bond length.

Figure 3.36 shows a plot of the Tolman's electronic parameter v versus Co–P bond length. No statistically significant relationship appears to exist within the current data. Thus, a tentative conclusion on the Co–P bond length dependence in cobalt(III) metalloporphyrin complexes is that the steric size of the phosphine/phosphonite plays a larger role in axial bond length determination than electronic factors do. This difference in behaviour relative to the analogous Rh(III) complexes may well reflect the poorer ability of the $3d\pi$ orbitals of Co(III) to overlap with the vacant d orbitals on the phosphine/phosphonite ligands owing to their contracted radii relative to the $4d\pi$ orbitals of Rh(III). Steric effects consequently dominate the Co–P bonding interaction in bis(P-donor ligand) complexes of Co(III) porphyrins.

150

3.4 Experimental

General Information. See Appendix AIII.2.

3.4.1 Synthesis of [Co(TPP)(depp)₂](SbF₆)

To [Co(TPP)(H₂O)₂Cl] (150 mg, 0.20 mmol) and AgSbF₆ (83 mg, 0.24 mmol) in a 250 ml Schlenk tube under nitrogen was added 50 ml of freshly distilled THF. The solution was allowed to stir for ~12 hr at room temperature. The THF was then removed *in vacuo* and the green-brown solid redissolved in dichloromethane (50 ml). The solution was then filtered, to remove precipitated silver chloride, into a 250 ml Schlenk tube into which depp (0.70 ml, 4.02 mmol) had been added. The solution was left to stir at room temperature for ~ 10 min. The red-brown solution was then transferred into 12 Schlenk tubes, in ~ 4 ml portions, and layered with hexane. X-ray-quality crystals were observed after 4 days. Yield: 0.2408 g (97 %).

3.4.2 Single Crystal X-Ray Diffraction Study of [Co(TPP)(depp)₂](SbF₆)

X-ray quality single crystals were isolated from the supernatant solvent mixture and the crystals were immersed in Paratone® oil before being mounted on thin glass micro fibres. The crystal data and structure refinement data are tabulated in Table 3.3. No significant decay in the crystal quality was observed. The original bond length and bond angle data have been tabulated in Table AI.3 in Appendix I. The atomic coordinates have been tabulated in Table AII.3 in Appendix II.

Table 3.3. Crystal Data and Structure Refinement for [Co(TPP)(depp)$_2$](SbF$_6$)

Identification code	Codepp2
Empirical formula	$C_{64}H_{58}CoN_4P_2SbF_6$
Formula weight	1239.76
Temperature	176(2) K
Wavelength	0.70930 Å
Crystal system	Monoclinic
Space group	$P2_1/c$
Unit cell dimensions	$a = 24.632(7)$ Å, $\alpha = 90°$
	$b = 15.333(3)$ Å, $\beta = 108.94(2)°$
	$c = 15.767(5)$ Å, $\gamma = 90°$
Volume	5633(2) Å^3
Z	2
Density (calculated)	1.462 Mg/m^3
Absorption coefficient	0.895 mm^{-1}
$F(000)$	2528
Crystal size	$0.5 \times 0.4 \times 0.2$ mm
Theta range for data collection	2.65 to 24.92°
Index ranges	$-1 \le h \ge 29; -3 \le k \ge 18; -18 \le l \ge 17$
Reflections collected	4563
Independent reflections	3866 [R(int) = 0.0268]
Reflections observed ($>2\sigma$)	3485
Refinement method	Full-matrix least-squares on F^2
Data / restraints / parameters	866 / 0 / 373
Goodness-of-fit on F^2	0.813
Final R indices [$I > 2\sigma(I)$]	$R_1 = 0.0477$ $wR_2 = 0.1867$
R indices (all data)	$R_1 = 0.0514$ $wR_2 = 0.1897$
Largest diff. peak and hole	0.915 and -0.846 e Å^{-3}

3.4.3 Synthesis of [Co(TPP)(edpp)₂](SbF₆)

To [Co(TPP)(H₂O)₂Cl] (150 mg, 0.20 mmol) and AgSbF₆ (83 mg, 0.24 mmol) in a 250 ml Schlenk tube under nitrogen was added 50 ml of freshly distilled THF. The solution was allowed to stir for ~12 hr at room temperature. The THF was then removed *in vacuo* and the green-brown solid redissolved in dichloromethane (50 ml). The solution was then filtered, to remove precipitated silver chloride, into a 250 ml Schlenk tube into which edpp (0.70 ml, 3.42 mmol) had been added. The solution was left to stir at room temperature for ~ 10 min. The red-brown solution was then transferred into 12 Schlenk tubes, in ~ 4 ml portions, and layered with hexane. X-ray-quality crystals were observed after 4 days. Yield: 0.248 g (93 %).

3.4.4 Single Crystal X-Ray Diffraction Study of [Co(TPP)(edpp)₂](SbF₆)

X-ray quality single crystals were isolated from the supernatant solvent mixture and the crystals were immersed in Paratone® oil before being mounted on thin glass microfibres. The crystal data and structure refinement data are tabulated in Table 3.4. No significant decay in the crystal quality was observed. The original bond length and bond angle data have been tabulated in Table AI.4 in Appendix I. The atomic coordinates have been tabulated in Table AII.4 in Appendix II.

Table 3.4. Crystal Data and Structure Refinement for [Co(TPP)(edpp)$_2$](SbF$_6$)

Identification code	Coedpp
Empirical formula	C$_{73}$H$_{60}$Cl$_2$CoF$_6$N$_4$P$_2$Sb
Formula weight	1420.77
Temperature	293(2) K
Wavelength	0.71073 Å
Crystal system	Monoclinic
Space group	$P2_1/n$
Unit cell dimensions	$a = 17.420(7)$ Å, $\alpha = 90.00(4)°$
	$b = 17.513(7)$ Å, $\beta = 105.22(4)°$
	$c = 20.902(12)$ Å, $\gamma = 90.00(3)°$
Volume	6153(5) Å^3
Z	4
Density (calculated)	1.534 Mg/m^3
Absorption coefficient	0.915 mm^{-1}
F(000)	2888
Crystal size	0.5 × 0.4 × 0.2 mm
Theta range for data collection	4.08 to 36.17°
Index ranges	$-26 \leq h \leq 28$; $-26 \leq k \leq 26$; $-32 \leq l \leq 32$
Reflections collected	74345
Independent reflections	25325 [R(int) = 0.0331]
Reflections observed (>2sigma)	17789
Data Completeness	0.858
Refinement method	Full-matrix least-squares on F^2
Data / restraints / parameters	25325 / 0 / 803
Goodness-of-fit on F^2	0.949
Final R indices [$I > 2\sigma(I)$]	$R_1 = 0.0415$ $wR_2 = 0.0914$
R indices (all data)	$R_1 = 0.0641$ $wR_2 = 0.0992$
Largest diff. peak and hole	1.476 and -1.563 e Å^{-3}

154

3.4.5 Synthesis of [Co(TPP)(deppt)₂](SbF₆)

To [Co(TPP)(H₂O)₂Cl] (150 mg, 0.20 mmol) and AgSbF₆ (83 mg, 0.24 mmol) in a 250 ml Schlenk tube under nitrogen was added 50 ml of freshly distilled THF. The solution was allowed to stir for ~12 hr at room temperature. The THF was then removed *in vacuo* and the green-brown solid redissolved in dichloromethane (50 ml). The solution was then filtered, to remove precipitated silver chloride, into a 250 ml Schlenk tube into which deppt (0.70 ml, 3.64 mmol) had been added. The solution was left to stir at room temperature for ~10 min. The red-brown solution was then transferred into 12 Schlenk tubes in ~4 ml portions, and layered with hexane. X-ray-quality crystals were observed after 4 days. Yield: 0.2582 g (99 %).

3.4.6 Single Crystal X-Ray Diffraction Study of [Co(TPP)(deppt)₂](SbF₆)

X-ray quality single crystals were isolated from the supernatant solvent mixture and the crystals were immersed in Paratone® oil before being mounted on thin glass microfibres. The crystal data and structure refinement data are tabulated in Table 3.5. No significant decay in the crystal quality was observed during the data collection. The original bond length and bond angle data have been tabulated in Table AI.5 in Appendix I. The atomic coordinates have been tabulated in Table AII.5 in Appendix II.

Table 3.5. Crystal data and structure refinement for [Co(TPP)(deppt)₂](SbF₆)

Identification code	Codeppt
Empirical formula	$C_{64}H_{58}CoN_4O_4P_2SbF_6$
Formula weight	1303.76
Temperature	293(2) K
Wavelength	0.70930 Å
Crystal system	Monoclinic
Space group	$P2_1/c$
Unit cell dimensions	$a = 14.872(6)$ Å, $\alpha = 90°$
	$b = 16.682(4)$ Å, $\beta = 106.34(6)°$
	$c = 25.15(2)$ Å, $\gamma = 90°$
Volume	5989(6) Å³
Z	4
Density (calculated)	1.446 Mg/m³
Absorption coefficient	0.851 mm⁻¹
$F(000)$	2656
Crystal size	$0.5 \times 0.4 \times 0.2$ mm
Theta range for data collection	2.08 to 24.95°
Index ranges	$-17 \leq h \leq 16; 0 \leq k \leq 19; 0 \leq l \leq 29$
Reflections collected	10522
Independent reflections	10522 [R(int) = 0.0000]
Reflections observed (>2σ)	6582
Refinement method	Full-matrix least-squares on F^2
Data / restraints / parameters	10522 / 0 / 742
Goodness-of-fit on F^2	1.086
Final R indices [$I > 2\sigma(I)$]	$R_1 = 0.0633$ $wR_2 = 0.1883$
R indices (all data)	$R_1 = 0.0996$ $wR_2 = 0.2057$
Largest diff. peak and hole	1.070 and −0.929 e Å⁻³

CHAPTER FOUR

PHOSPHINE AND PHOSPHONITE COMPLEXES OF RHODIUM(III) PORPHYRINS

4.1 Rh(III) Complexes with *Trans* P-Donor Ligands

In this Chapter, the coordination of phosphines and phosphonites to a rhodium(III) porphyrin will be discussed. As with these axial ligands in manganese and cobalt porphyrin complexes, very little is known about the behaviour of these compounds and as such there are currently no reported X-ray crystal structures of bis(phosphine) or bis(phosphonite) complexes of rhodium(III) porphyrins in the literature. In terms of X-ray crystal structures of phosphine and phosphonite complexes of rhodium of the structural type shown in Figure 4.38 (*vide infra*), only three such complexes exist, and are discussed in Section 4.4. Triphenylphosphine and triethylphosphine are the only two ligands used in these three complexes. Thus the field of research centred around phosphine and phosphonite complexes of rhodium is largely untapped and contains vacant areas of research which are touched on in this work.

Interestingly, ^{103}Rh NMR spectra of rhodium porphyrin systems have yet to be reported on in the literature. Since these complexes contain phosphorus donors, the indirect probing of the ^{103}Rh nucleus through the ^{31}P nucleus has been achieved in this work and the results discussed in Section 4.5. The ^{103}Rh and ^{31}P NMR spectra of these rhodium complexes were collected by Prof. Laurence Carlton of the University of the Witwatersrand(see Appendix AIII.1).

As with the previous porphyrins, large molar excesses (>20) of phosphine and phosphonite ligands were used in the synthesis of the complexes and when preparing samples for characterisation. This method was adopted because of the steric bulk of the phosphines and phosphonites used and to ensure 6-coordinate species were synthesized in preference to the 5-coordinate analogues. The intention of this investigation was to synthesize novel complexes of Rh(III) porphyrins with axial ligands related to triphenylphosphine and triphenylphosphite.

4.2 Reactions of Phosphines with Rhodium(III) Porphyrin Precursors

4.2.1 Synthesis and Characterisation of [Rh(TPP)(edpp)₂](SbF₆)

The phosphine used in this reaction was ethyldiphenylphosphine as shown in Figure 4.1 below.
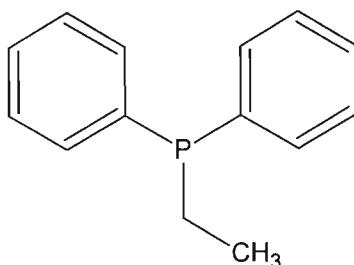
Figure 4.1: Structure of ethyldiphenylphosphine.

All solvents were thoroughly dried and degassed before use. A 20 molar excess of the phosphine was added to the rhodium precursor to ensure the crystallization of a 6-coordinate complex.

The reaction procedures are shown in equations 1 and 2 below.

$$[Rh(TPP)Cl] + AgSbF_6 \xrightarrow{\text{THF}} [Rh(TPP)FSbF_5] + AgCl(s) \quad \text{.....................................(1)}$$

$$[Rh(TPP)FSbF_5] + \text{excess edpp} \xrightarrow{\text{CH}_2\text{Cl}_2} [Rh(TPP)(edpp)_2](SbF_6) \quad \text{.............................(2)}$$
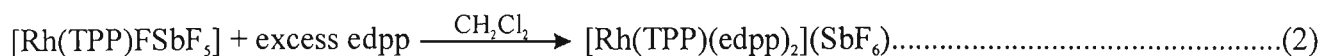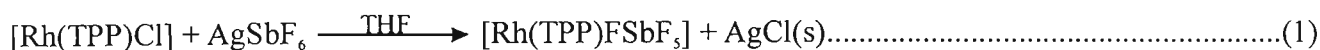
The colour of the complex in solution is a dark maroon. A summary of the spectroscopic data has been tabulated in Table 4.1. The ^{13}C NMR spectrum is shown in Appendix IV in Figure AIV.3.

The ^{1}H NMR spectrum is shown in Figure 4.2. The samples for NMR spectroscopy were made up from the same batch of crystals from which the X-ray crystal structure was obtained. No excess phosphine ligand was added to the sample and thus there are no signals from the un-coordinated phosphine. Assignments were thus relatively simplified.

The intense singlet at 8.8 ppm (signal y) has been assigned as the signal from the pyrrole protons of the porphyrin and has been set at the reference integral of 8 H's. The phenyl protons of the

porphyrin are all similarly found in the three closely spaced sets of multiplets at approximately 7.8 ppm. This set of signals, accordingly, integrates to 20 H's. The singlet at 9.0 ppm (signal *x*) has been assigned to the pyrrole protons of a second complex of unknown conformation. Signal *x* is present in a less significant proportion with a *x:y* ratio of 1:8. The ^{31}P NMR results also show a set of signals for a "minor" product at a smaller proportion to the "major" product. The logical assumption is that the minor signal corresponds to a 5-coordinate species since no excess edpp was added to the NMR sample, yet the Rh–P coupling constants for both species are the same, indicating a 6-coordinate geometry for both.

The triplet at 7.0 ppm corresponds to the *para*-protons of the phenyls of the coordinated edpp ligands and integrates to 4 H's. The triplet at 6.6 ppm corresponds to the *meta*-protons of the edpp phenyls and integrates to 8 H's, while the *ortho*-protons have been assigned to the quintet at 3.7 ppm (integral = 8 H).

The splitting of the phenyl protons of the porphyrin macrocycle and the co-ordinated phosphine ligand discussed above, follow the same generic pattern as discussed in Chapter 1.8 and for that of the cobalt complexes discussed in Chapter 2.

The terminal methyl protons of the axially coordinated edpp ligands correspond to the quintet at –1.4 ppm that integrates accurately to 6 H's. The weak quartet at –2.8 ppm corresponds to the methylene protons (integral = 4 H). The –CH$_2$– protons are in a more upfield position relative to the terminal methyl protons. This may be explained by the orientation of these protons towards a more shielding environment of the shielding cone. Note there is no splitting/inequivalence of these protons as was observed with these protons in the bis(phosphine/phosphonite) cobalt(III) porphyrins, consistent with exchange broadening of the signals.

From Table 4.1 it is noticeable that the coupling constants for the proton signals of the coordinated axial ligand are in the 7.3 to 7.7 Hz range, except for the signal assigned to the phenyl *ortho*-protons, which displays a coupling constant of 3.8 Hz.

The ^{31}P NMR spectrum shown in Figure 4.3 shows two doublets: an intense doublet, termed the 'major' product, at 10.79 ppm corresponding to the coordinated edpp ligand, and a relatively weak doublet, termed the 'minor' product, at 13.29 ppm corresponding to another isomer of unknown conformation. These values are quoted at 300 K. The ratio of 'major' to 'minor'

product of 21:1 does not appear to be temperature dependent over the temperature range 213 to 300 K.

The Rh–P coupling constant is 82.07(41) Hz for the two doublets over the three temperatures (213, 300 and 333 K). That both products have the same coupling constant is indicative of the 'minor' species having a 6-coordinate conformation and dispels the notion that it is a 5-coordinate dissociation product.

CHCl₃
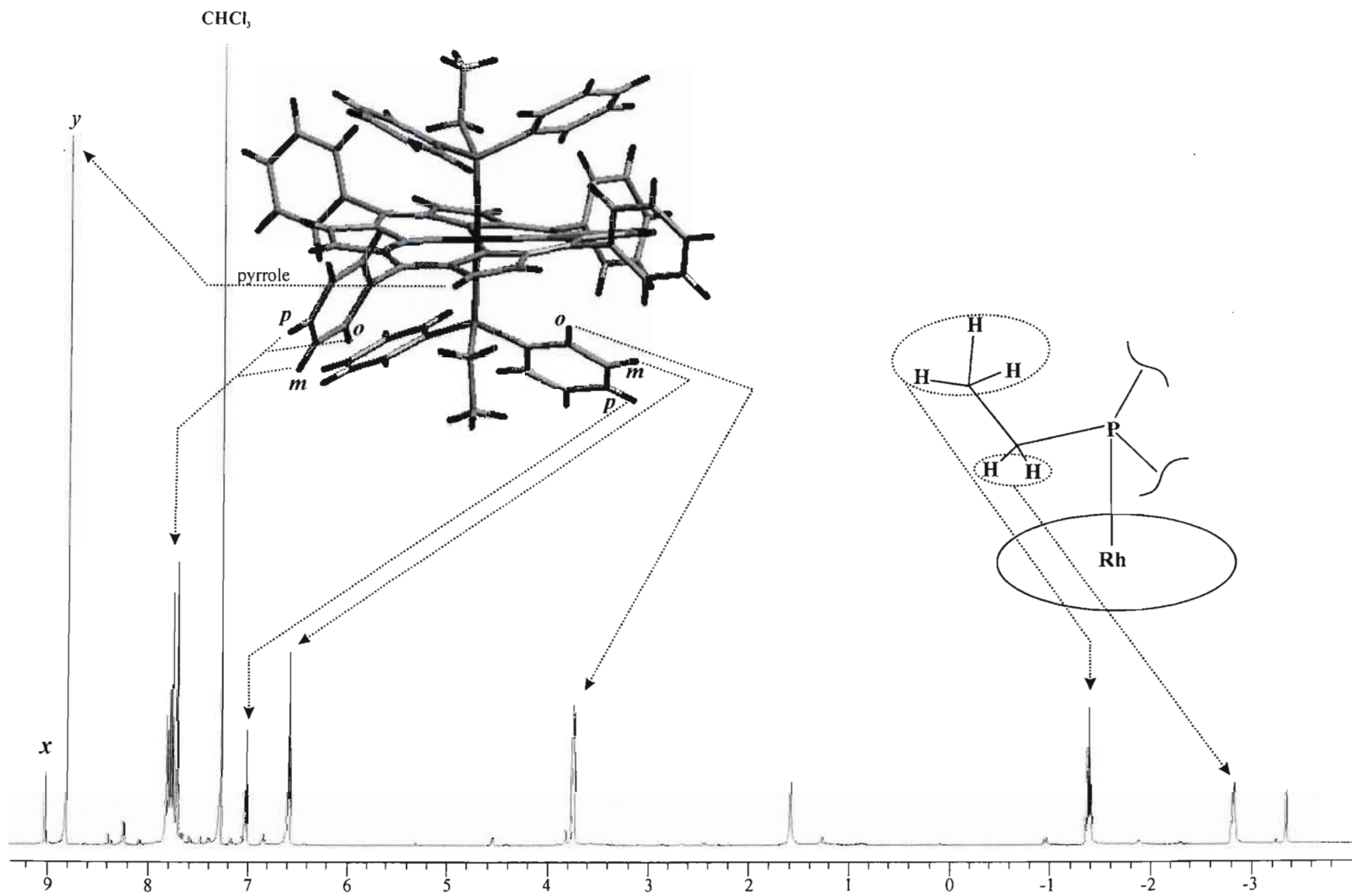
Figure 4.2: ¹H NMR spectrum of Rh(TPP)(edpp)₂](SbF₆).
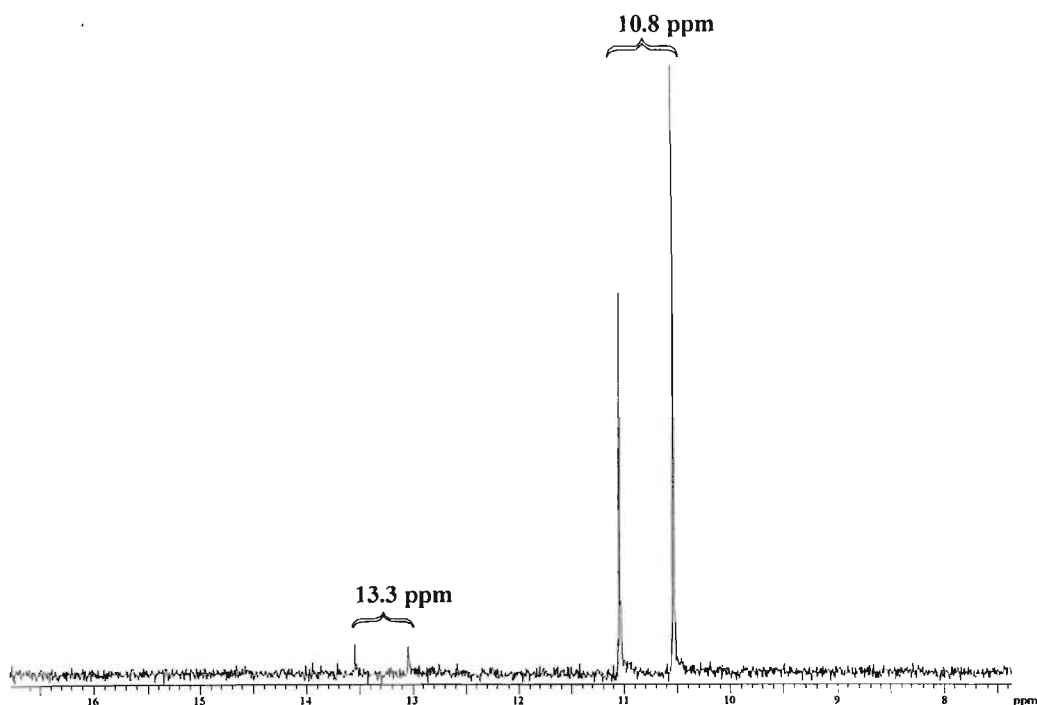
Figure 4.3: ^{31}P NMR spectrum of Rh(TPP)(edpp)$_2$](SbF$_6$) (300 K).

The temperature dependence of these signals at 213, 300 and 333 K has been plotted in Figure 4.4. The graph shows an approximate trend of possible convergence at higher temperatures out of the range of the data available.
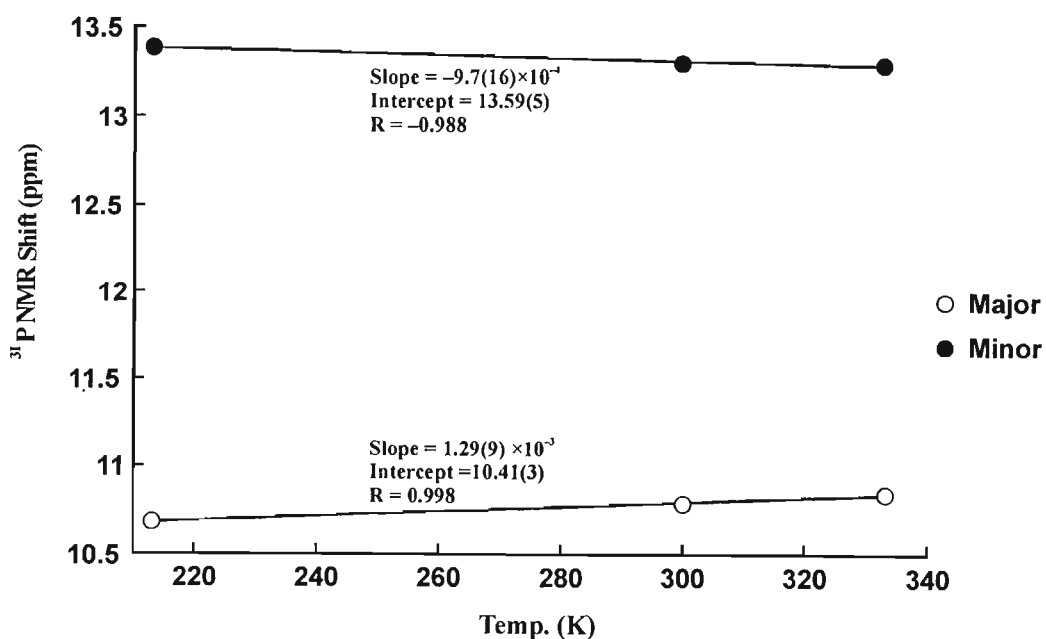
Figure 4.4: Graph showing the temperature dependence of the ^{31}P NMR signals for Rh(TPP)(edpp)$_2$](SbF$_6$).

Figure 4.5 shows the ^{31}P–^{103}Rh COSY NMR spectrum at 300 K. The ^{103}Rh NMR signal consists of a singlet at 2558 ppm.

The electronic spectrum is shown in Figure 4.6, and generally follows the pattern described for rhodium(III) porphyrins as discussed in Chapter 1.12.[160,179] Unlike the electronic spectra observed with the bis(phosphine/phosphonite) complexes of Co(III), the B(0, 0) and B(1, 0) bands are not resolved. Instead, a broad and intense single band results at 420 nm. The Q(0, 0), Q(1, 0) and Q(2, 0) bands are at 563, 529, and 492 nm, respectively. The Q(2, 0) band is broad and may be concealing another absorption band. A suspected N(0, 0) band is found at 345 nm. The low intensity band at 447 nm shows a deviation from Beers' Law, i.e., there is not a linear increase in absorption with concentration. This behaviour may be due to the band inheriting an increasing percentage of the Soret band character as the concentration of the porphyrin increases, and the Soret band broadens to include this wavelength region. However, this band plays a relatively minor role in the electronic spectrum of Rh(TPP)(edpp)$_2$](SbF$_6$), and as such, has not been assigned. The lowest intensity band at 600 nm is somewhat unusual and may be a Rh($d\pi$)→P($d\pi$) charge transfer band or Rh($d\pi$)→P(σ*) band since its intensity is too high for a Rh(III) d–d band (ε = 1.1 × 10^3 M^{-1} cm^{-1}).
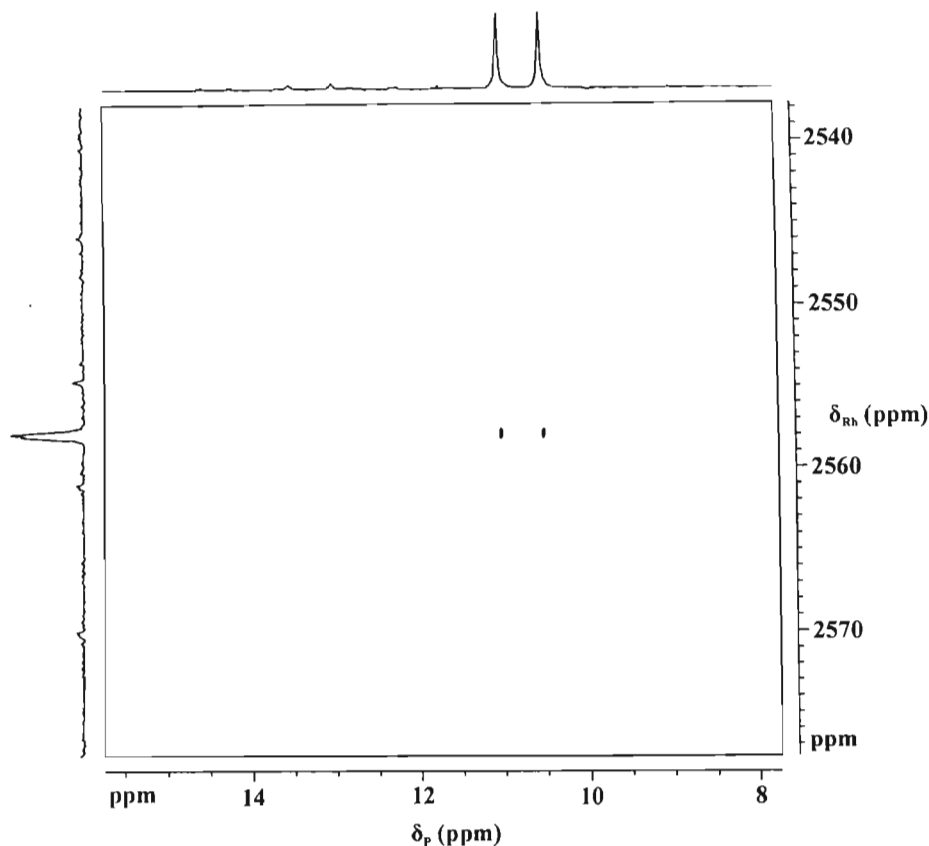
Figure 4.5: 2D ^{31}P–^{103}Rh COSY NMR spectrum of Rh(TPP)(edpp)$_2$](SbF$_6$) at 300 K.

Table 4.1 Spectroscopic Data for [Rh(TPP)(edpp)$_2$](SbF$_6$)

^{1}H NMR[a]	**TPP:** 8.78 (8 H's, sh s, pyrrole H's), 7.76 (20 H's, m, *o / m / p*–H's) **Edpp:** 7.01 (4 H's, t, ^3J = 7.3 Hz, *p*–H's), 6.57 (8 H's, t, ^3J = 7.5 Hz, *m*–H's), 3.73 (8 H's, r, ^3J = 3.8 Hz, *o*–H's), –1.40 (6 H's, r, ^3J = 7.7 Hz, –CH$_3$), –2.84 (4 H's, q, ^3J = 7.7 Hz, –CH$_2$–)			
^{31}P NMR	**Temp. (K)**	**213**	**300**	**333**
	Major (ppm)	10.68	10.79	10.84
	Minor (ppm)	13.39	13.29	13.28
^{13}C NMR[a]	137.86 (d, w), 132.57 (d, str), 128.55 (s, str), 128.33 (d, str), 77.00 (t, w), 30.81 (s, w), 20.51 (d, w), 9.88 (d, w)			
Infrared[b]	739.8 (w, ν(P–Et)), 1438.4 (w, ν(P–Ph)), 1001.8 (w, ν(P–Ph))			
Uv-vis[c]	600 (1.1 × 10^3), 563 (1.9 × 10^3), 529 (8.0 × 10^3), 492 (3.0 × 10^3), 447 (Beer's law violation), 420 (5.7 × 10^4), 345 (6.3 × 10^3)			
^{103}Rh NMR[d]	2558 (82)			

[a] Chemical shifts measured in ppm. Measured at 294 K in CDCl$_3$, s = singlet, d = doublet, t = triplet, r = quartet, p = quintet, m = multiplet, str = strong, w = weak, sh = sharp, br = broad. [b] $\bar{\nu}$ (cm^{-1}). KBr disk. [c] λ_{max}/nm (ε/dm^3 mol^{-1} cm^{-1}); measured at 298 K in dried and degassed dichloroethane. [d] ppm ($J\{^{103}$Rh–^{31}P$\}$/Hz)
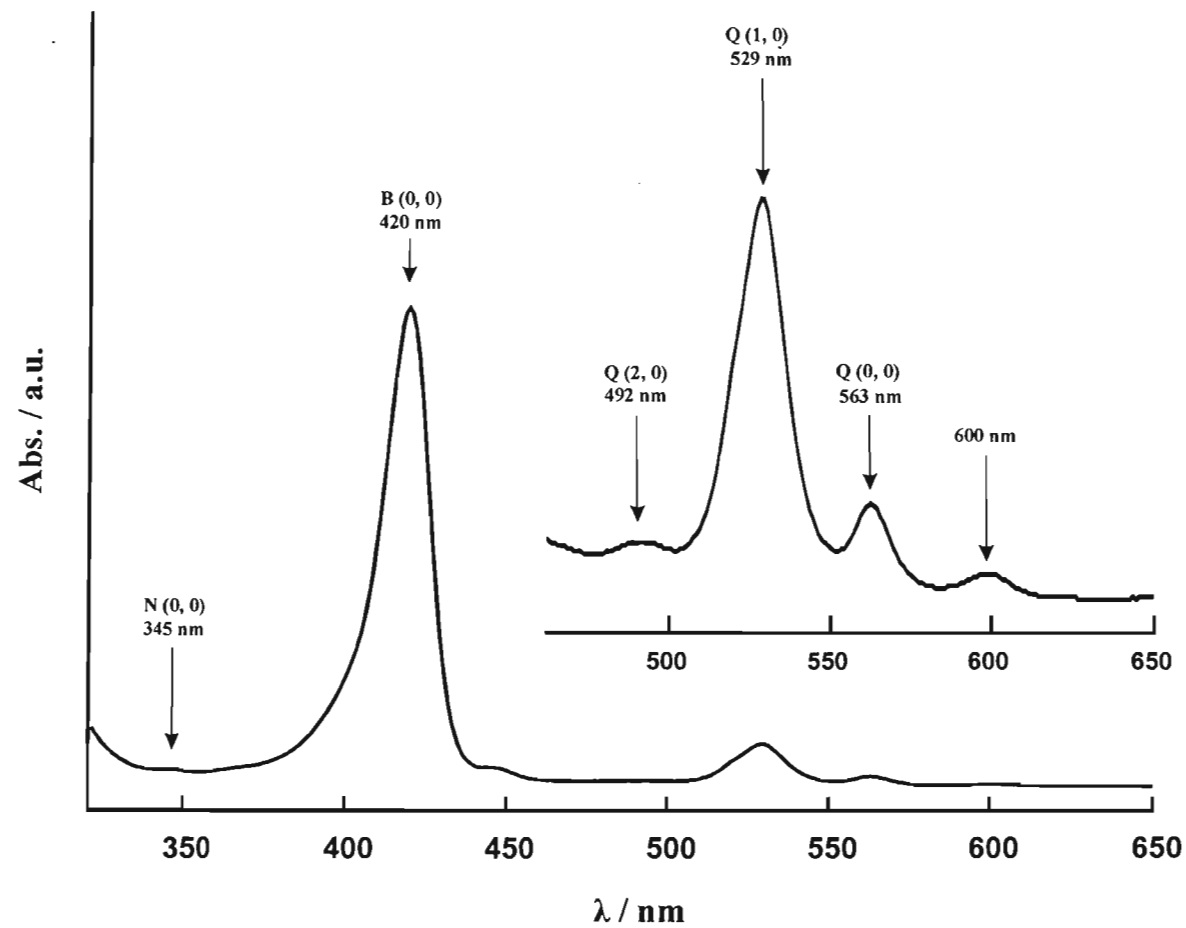
Figure 4.6: Electronic Spectrum of [Rh(TPP)(edpp)$_2$](SbF$_6$) in dichloroethane at 25 °C.

4.2.2 Crystal structure determination of [Rh(TPP)(edpp)₂](SbF₆)

The compound was crystallized via slow diffusion of hexane into CH_2Cl_2. The compound forms a deep red colour in solution; crystals of the compound are very deep red such that they appear black. Cube-shaped crystals of the compound were isolated and immersed in Paratone® oil immediately to prevent possible decomposition of the crystals if solvated. They were then mounted on glass microfibres for X-ray analysis. The X-ray data were collected at 259(2) K in order to, in part, prevent decay of the crystal if solvated and to improve the quality of the data collection. The compound crystallized in the monoclinic crystal system in the space group $P2_1/n$. The asymmetric unit is the full complex and full counter-ion as well as two dichloromethane molecules. There is no inversion symmetry.

The final R_1 = 0.0492 for the structure solution. An ORTEP diagram of the crystal structure is shown in Figure 4.7. From the X-ray crystal structure, the Rh–P_{ax} bond length is 2.401(2) Å and the Rh–N_{porph} bond length averages to 2.035(3) Å. The porphyrin core, as shown in Figure 4.8, displays significant deviations from planarity, with a moderate ruffled conformation. However, the central metal ion is roughly in the mean plane of the 24-atom core as it is only displaced from the mean plane by a minimal 0.015 Å.

The dihedral angles of the phenyl substituents relative to the mean plane of the porphyrin macrocycle are: C11–C16 = 65.65°; C21–C26 = 64.13°; C31–C36 = 82.77° and C41–C46 = 75.98°.

The Rh⋯Sb distance is 9.599 Å. A disordered phenyl substituent of the TPP ligand is shown in Figure 4.9. Constituting this disorder are two major positions for the phenyl substituent labelled C41 to C46 and C41′ to C46′. The two planes formed by each phenyl are tilted away from each other by 38.12° and the atoms C41 and C41′ are located 0.320 Å from each other. Thus, the phenyl group displays thermal rotation and movement in a plane roughly perpendicular to the plane of the porphyrin. The non-bonded separations of the individual atoms are: C41⋯C41′ = 0.320 Å; C42⋯C42′ = 1.024 Å; C43⋯C43′ = 1.248 Å; C44⋯C44′ = 0.932 Å; C45⋯C45′ = 1.008 Å and C46⋯C46′ = 0.870 Å.

A view of the complex perpendicular to the plane of the porphyrin is shown in Figure 4.10. In this figure the relative orientations of the axial phosphines are shown.
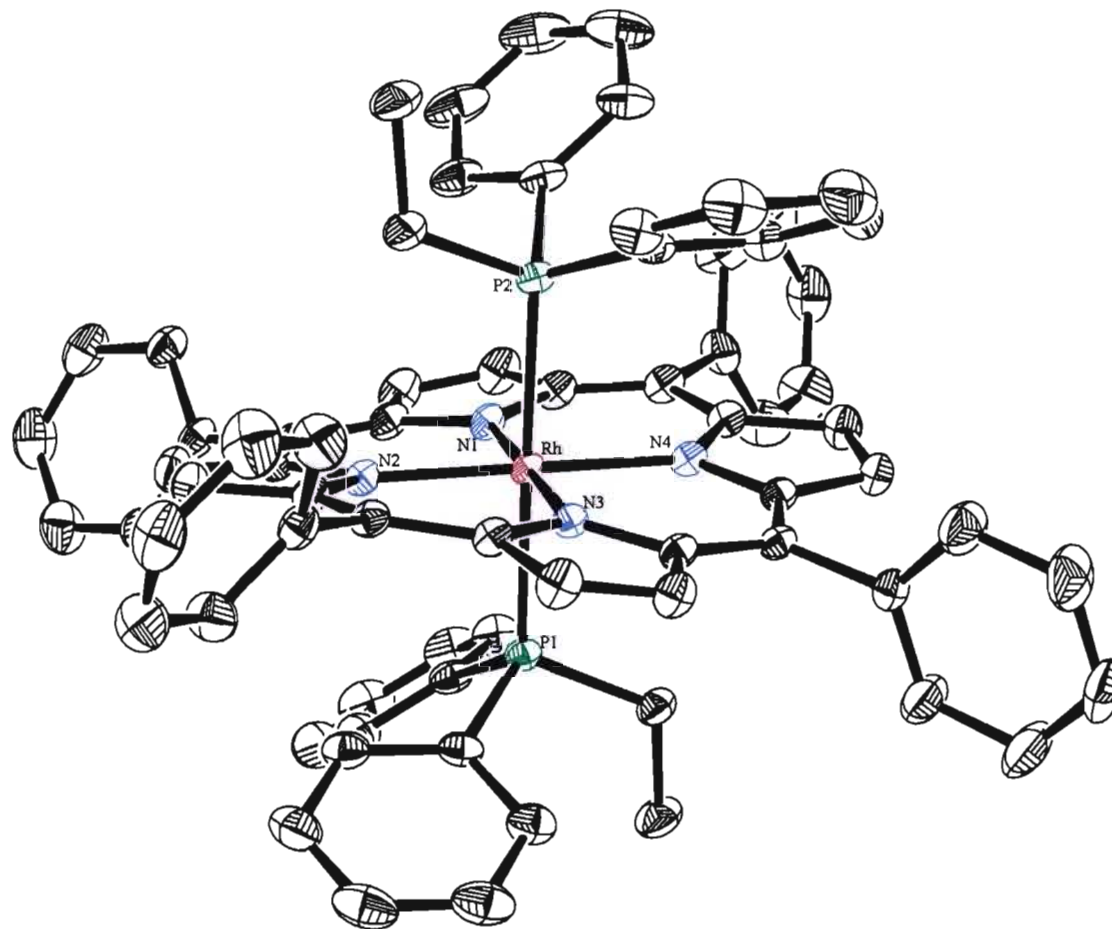
Figure 4.7: Selectively labeled ORTEP diagram of the X-ray crystal structure of [Rh(TPP)(edpp)$_2$](SbF$_6$). Thermal ellipsoids have been drawn at the 30% probability level. H atoms and the counter ion are omitted for clarity.
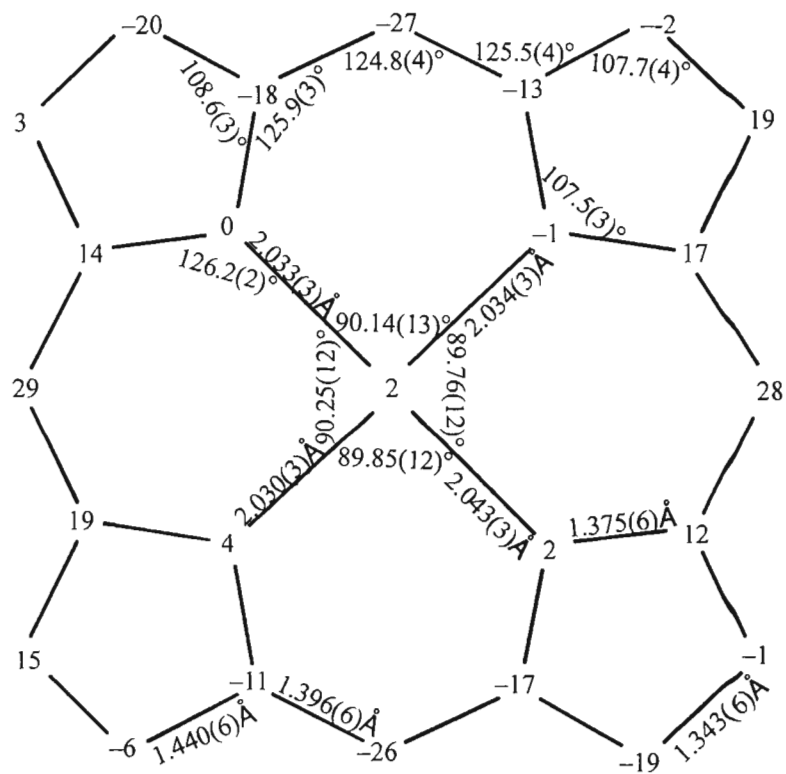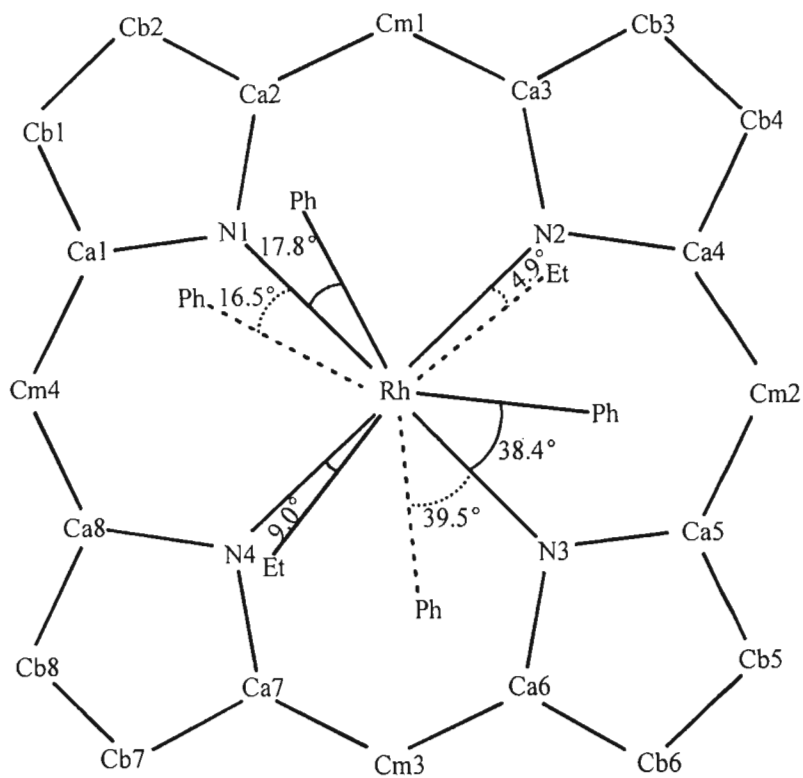
Figure 4.8: Crystallographic information and axial ligand orientations for [Rh(TPP)(edpp)₂](SbF₆). Atomic displacements from the 24-atom mean plane are given in pm.
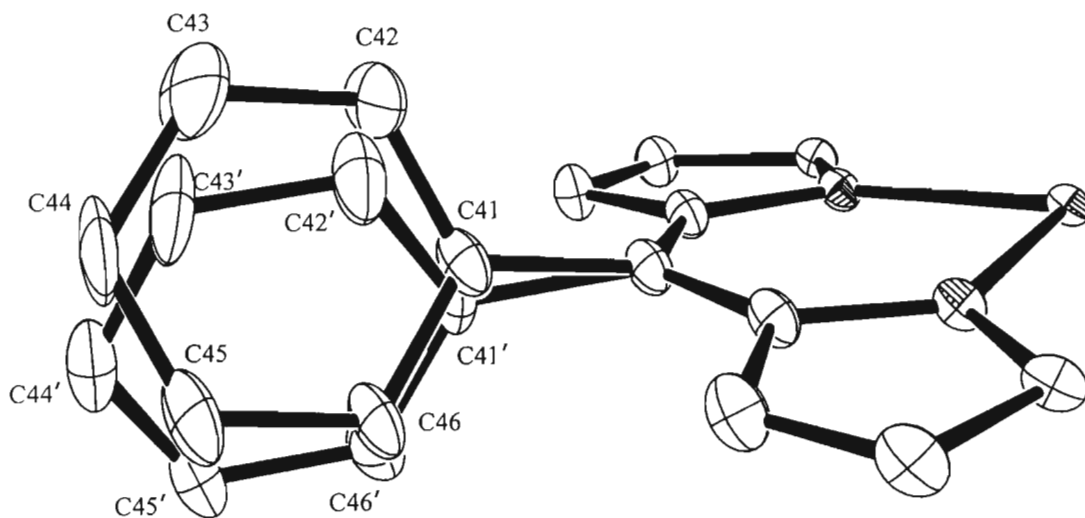
Figure 4.9: Disordered phenyl substituent of [Rh(TPP)(edpp)₂](SbF₆).
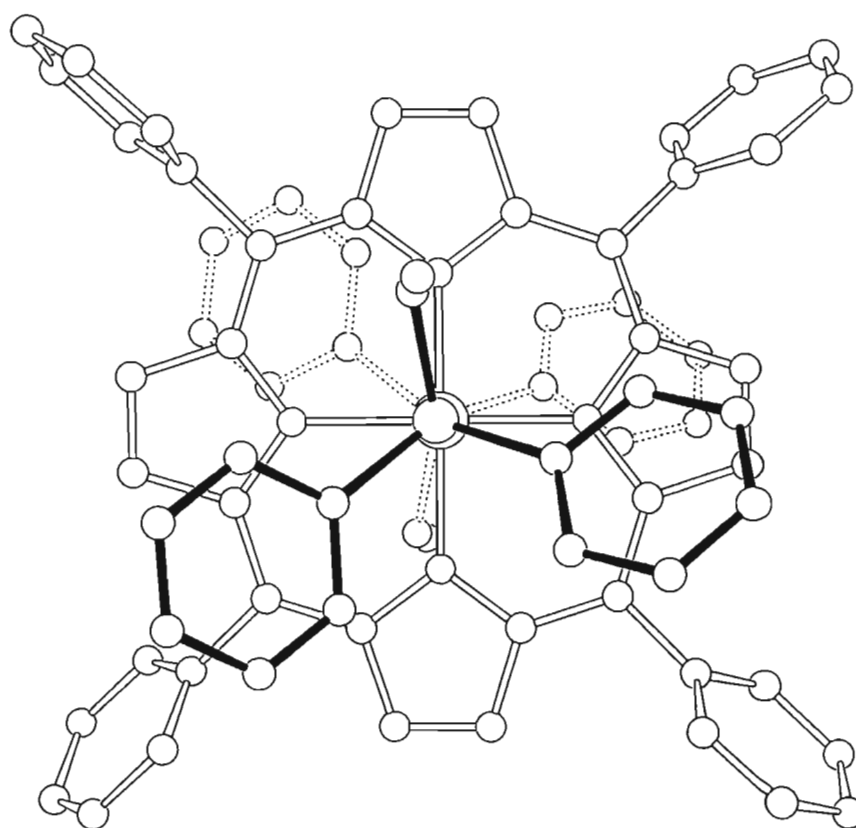
Figure 4.10: ORTEP diagram of the [Rh(TPP)(edpp)₂]⁺ cation (view perpendicular to porphyrin plane along P–Rh–P axis).

Figure 4.11 shows a diagram, generated with Mercury 1.1, displaying the close contacts within the X-ray crystal structure of [Rh(TPP)(edpp)₂](SbF₆). The close contacts within this complex exist only between the dichloromethane solvate and a phenyl substituent of the porphyrin. Here

169

one of the protons of the dichloromethane comes within 2.8 Å of C13 of the porphrin. Interestingly, Mercury 1.1 shows there are no unduly close contacts beween the axial phosphines and the porphyrin core.
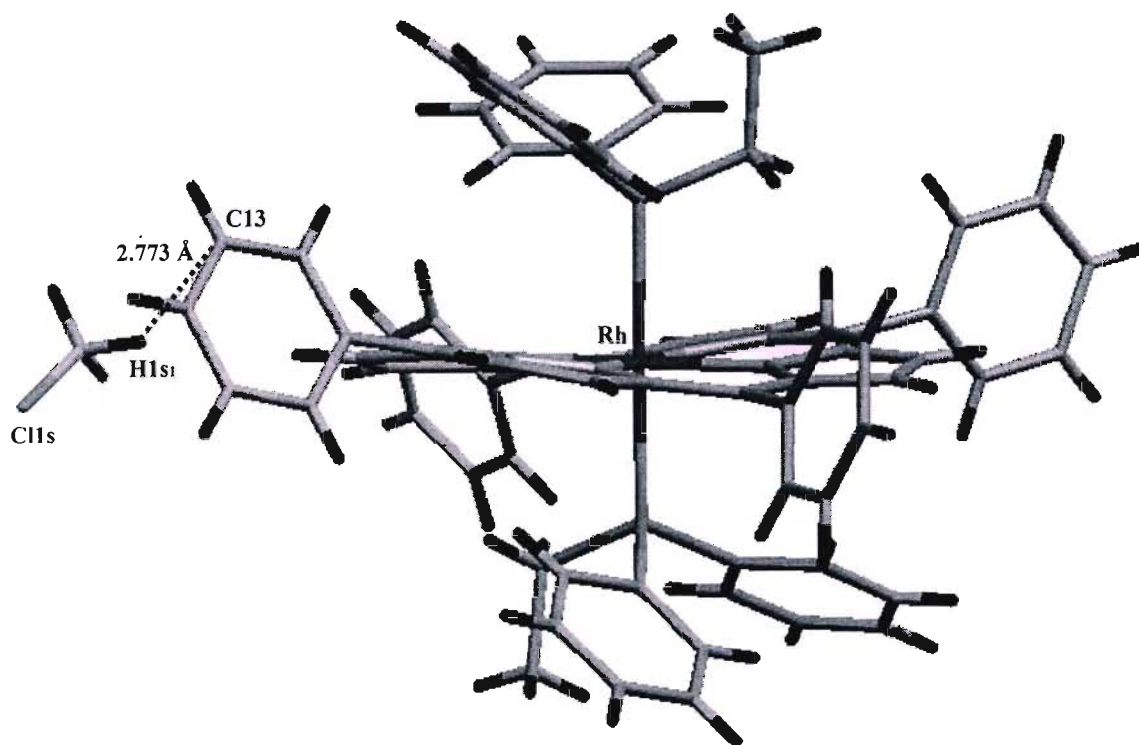
Figure 4.11: Diagram (Mercury 1.1) of close non-bonded contacts within the X-ray crystal structure of [Rh(TPP)(edpp)$_2$](SbF$_6$).

Figure 4.12 displays a packing diagram of the unit cell of [Rh(TPP)(edpp)$_2$](SbF$_6$). The view is down the *b*-axis and shows an ordered arrangement of the complexes with distinct 'holes' into which the SbF$_6^-$ counterions fit.
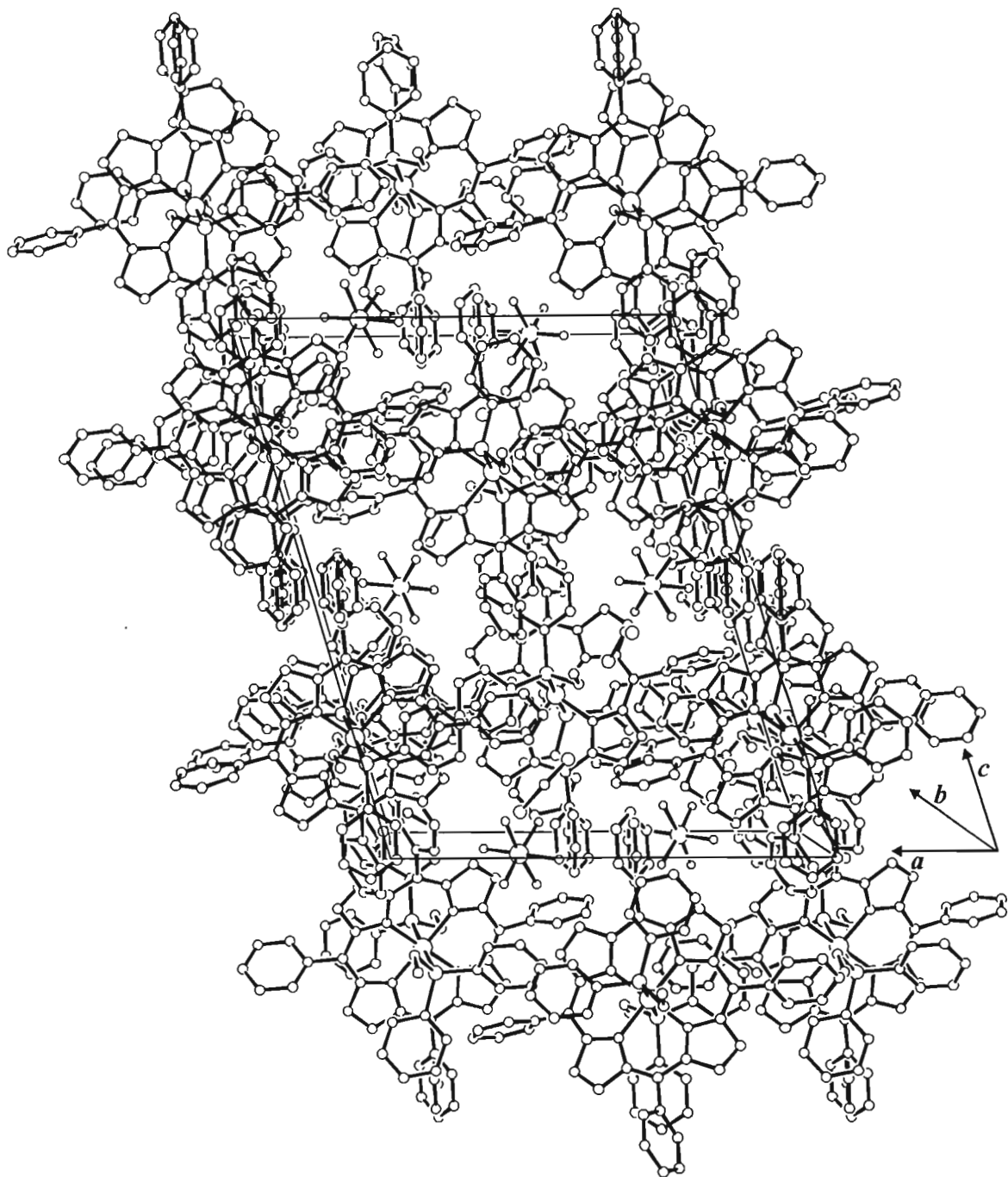
Figure 4.12: ORTEP diagram of the unit cell contents of the monoclinic structure of [Rh(TPP)(edpp)₂](SbF₆) (view along *b* axis).

4.3 Reactions of Phosphonites with Rhodium(III) Porphyrin Precursors

4.3.1 Synthesis and Characterisation of [Rh(TPP)(edppt)$_2$](SbF$_6$)

The phosphonite used in this reaction was ethyldiphenylphosphonite as shown in Figure 4.13 below.
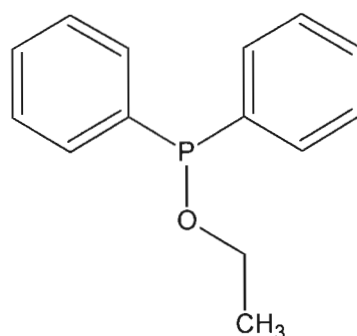
Figure 4.13: Structure of ethyldiphenylphosphonite.

This phosphonite was chosen as it is closely related to the phosphine edpp used in Section 4.2. The only structural difference is the ethoxy substituent, yet since the oxygen is electron withdrawing, there should be a reasonable decrease in the Lewis basicity of the phosphorus donor atom. Balancing this factor out is the fact that the oxygen atom provides a 'pivot' point around which the ethyl chain may rotate and reduce the overall steric size of this substituent, this process is displayed by means of the diagram in Figure 4.14. The final Rh–P bond length will thus be a contribution of both factors.
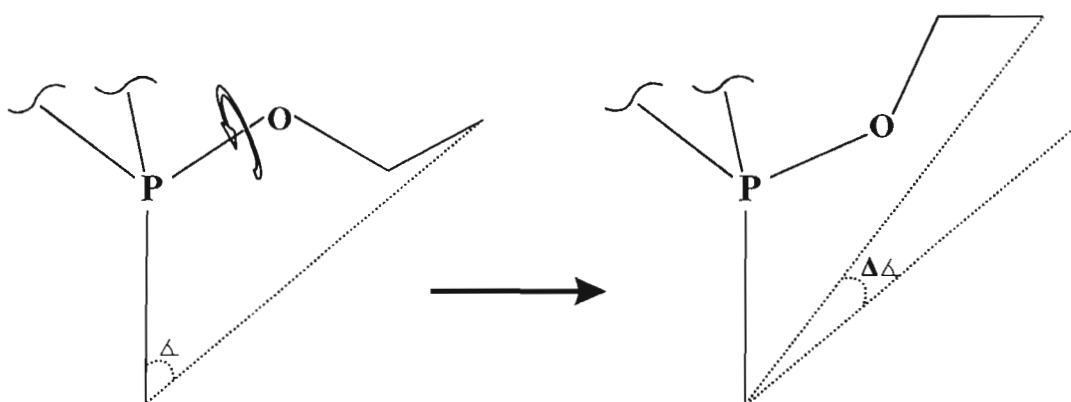
Figure 4.14: Diagram displaying the steric reduction *via* rotation around the P–O bond in a phosphonite.

All solvents were thoroughly dried and degassed before use. A 20 molar excess of the phosphonite was added to the Rh precursor to ensure the crystallization of a 6-coordinate complex.

The reaction procedures are shown in equations 1 and 2 below.

$$[Rh(TPP)Cl] + AgSbF_6 \xrightarrow{\text{THF}} [Rh(TPP)FSbF_5] + AgCl(s) \dots\dots\dots\dots\dots\dots\dots\dots\dots\dots\dots\dots(1)$$

$$[Rh(TPP)FSbF_5] + \text{excess edppt} \xrightarrow{\text{CH}_2\text{Cl}_2} [Rh(TPP)(edppt)_2](SbF_6) \dots\dots\dots\dots\dots\dots\dots\dots\dots(2)$$
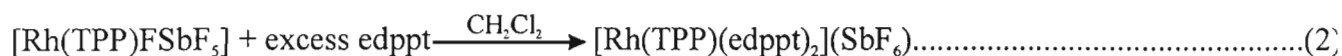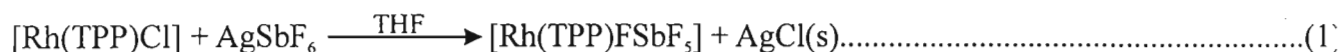
The colour of the complex in solution is a dark maroon. The spectroscopic data for the product complex in equation 2 are summarised in Table 4.2. The ^{13}C NMR spectrum is shown in Appendix IV in Figure AIV.4.

The ^1H NMR spectrum is shown in Figure 4.15, below. The ^1H NMR sample was made up of the same batch of crystals from which the X-ray crystal structure was obtained. No excess of edppt was used and thus the ^1H NMR spectrum shows no signals from the free ligand.

The strong singlet at 8.76 ppm (signal y) has been assigned to the pyrrole protons of the porphyrin ring and has been set as the reference integral to 8 H's. The singlet at 9.0 ppm (signal x) indicates that a second complex exists in the sample. The signal x is of a significantly lower intensity, with a $x:y$ ratio of 1:46. This indicates an insignificant proportion of the second complex. The ^{31}P NMR spectrum shows that this species has the same coupling constant as the 6-coordinate 'major' product. Thus, the notion that the signal x corresponds to a 5-coordinate phosphonite porphyrin complex may be ruled out.

The signals corresponding to the *para-*, *meta-* and *ortho-*protons of the porphyrin ring are positioned in the large broad multiplet at 7.75 ppm. This peak accurately integrates to 20 H's.

173
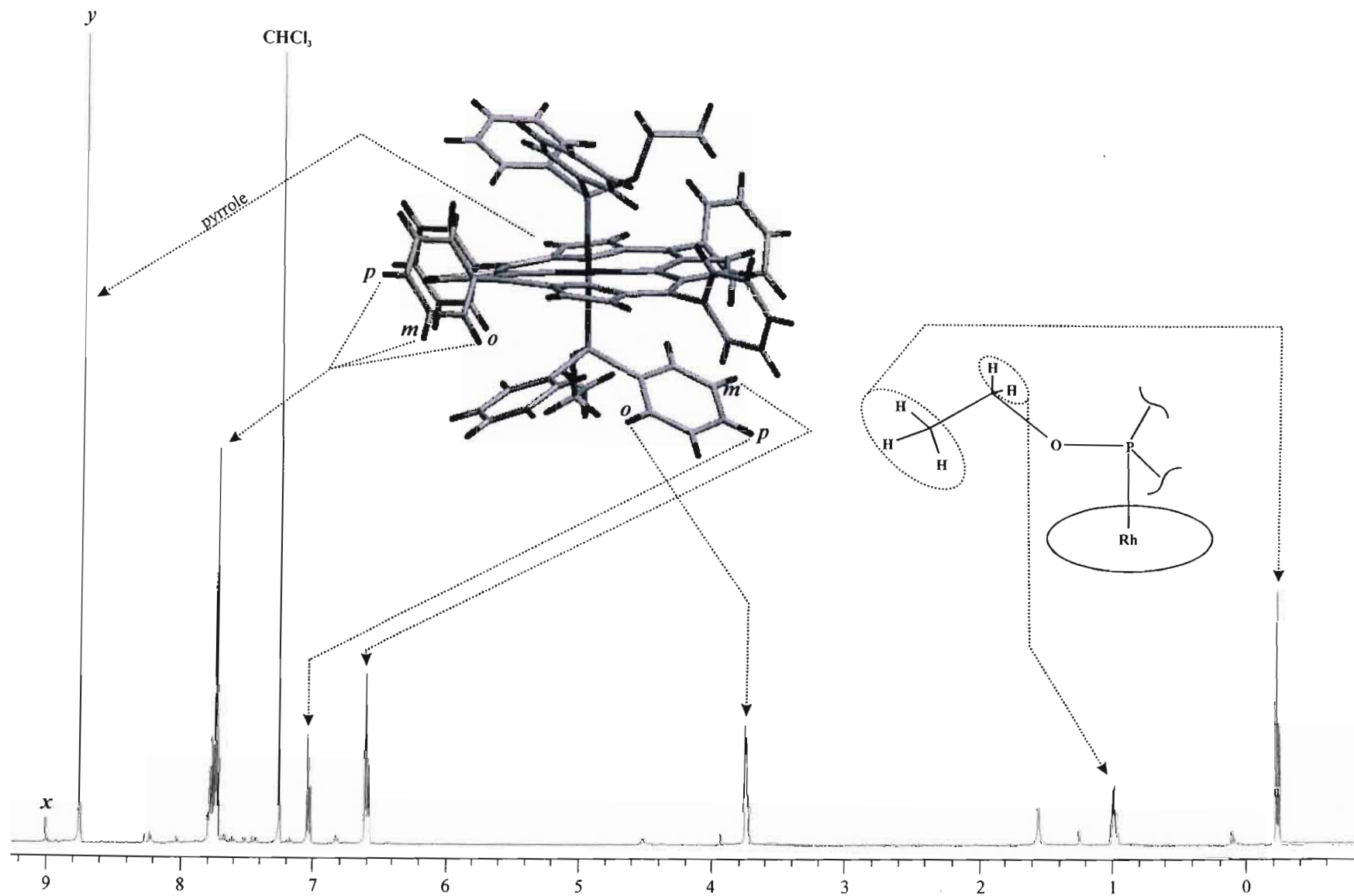
Figure 4.15: ¹H NMR spectrum of [Rh(TPP)(edppt)₂](SbF₆).

The triplet at 7.04 ppm corresponds to the *para*-protons of the phenyls of the coordinated edppt, and integrates accurately to 4 H's. The triplet at 6.60 ppm corresponds to the *meta*-protons and the slightly irregular quintet at 3.75 ppm corresponds to the *para*-protons of the same phenyls and each accurately integrates to 8 H's.

The splitting of the phenyl protons of the porphyrin macrocycle and the co-ordinated phosphonite ligand, discussed above, follows the same generic patterns as discussed in Chapter 1.8 as well as those of the cobalt complexes discussed in Chapter 2.

The multiplet at 0.99 ppm has been assigned to the $-CH_2-$ of the edppt and integrates to 4 protons (J = 3.66 Hz). These protons show equivalence and thus produce one signal; the opposite is found for these protons in $[Rh(TPP)(deppt)_2](SbF_6)$. The clear triplet at -0.23 ppm has been assigned to the terminal $-CH_3$ group of the axial ligand and integrates to 6 H's (J = 6.862 Hz). These protons are further upfield than the $-CH_2-$ protons and, as with $[Co(TPP)(deppt)_2](SbF_6)$, rotation of this alkyl group around the O–P bond most likely results in the terminal methyl group protruding into a less shielding region of the shielding cone

From Table 4.2 it may be noted that the coupling constants for the phenyl proton signals of the coordinated axial phosphine are 7.3 and 7.7 Hz for the *para*- and *meta*-protons, respectively. However, the signal assigned to the *ortho*-protons displays a significantly smaller coupling constant of 3.6 Hz.
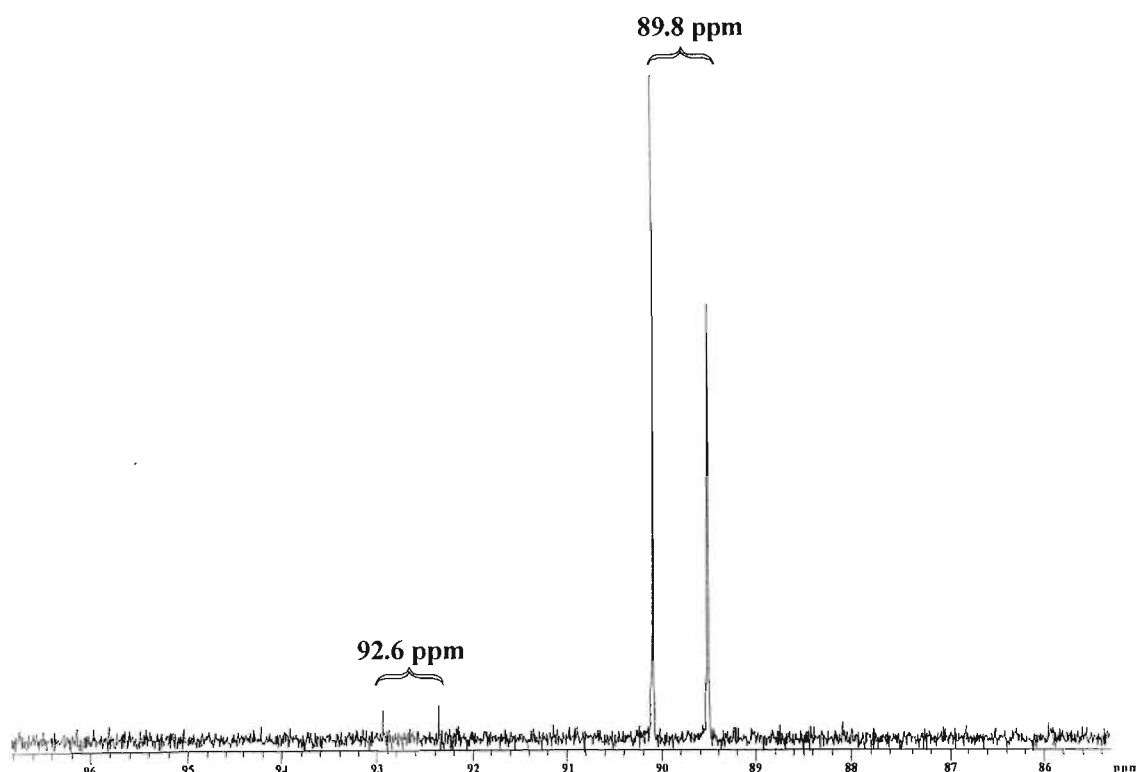
Figure 4.16: ^{31}P NMR spectrum of [Rh(TPP)(edppt)$_2$](SbF$_6$) (300 K).

The ^{31}P NMR, as shown in Figure 4.16 above, exhibits two doublets: an intense doublet at 89.8 ppm, referred to as the 'major' product, corresponding to the coordinated edppt and a less intense doublet at 92.6 ppm, referred to as the 'minor' product. The latter signal has been assigned to an unknown conformational isomer. The ratio of 'major' to 'minor' product is 44:1. There is no temperature dependent relationship evident for the relative intensities of the two isomers in the temperature range 213 to 333 K. The Rh–P coupling constant for both these doublets is 94.96 (41) Hz over the three temperatures (213, 300 and 333 K). Since the 'minor' product displays the same coupling constant as the 'major' product it may be concluded that the 'minor' product has a 6-coordinate conformation and is not a 5-coordinate dissociation product.

The temperature dependence of these chemical shifts has been plotted in Figure 4.17. The ^{31}P NMR shifts of the major product appears to have a greater temperature dependent character than the minor product, though the variation is slight.

176
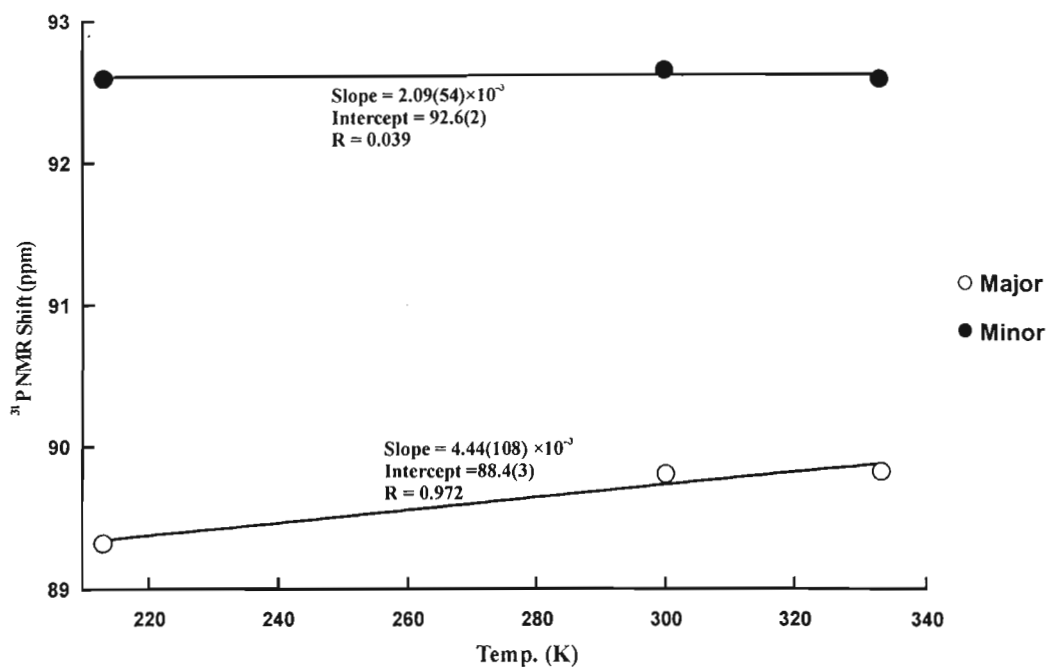
Figure 4.17: Graph showing the temperature dependence of the ^{31}P NMR signals for [Rh(TPP)(edppt)$_2$](SbF$_6$).

Figure 4.18 shows the ^{31}P–^{103}Rh COSY NMR spectrum at 300 K. The ^{103}Rh NMR signal consists of a singlet at 2413 ppm.
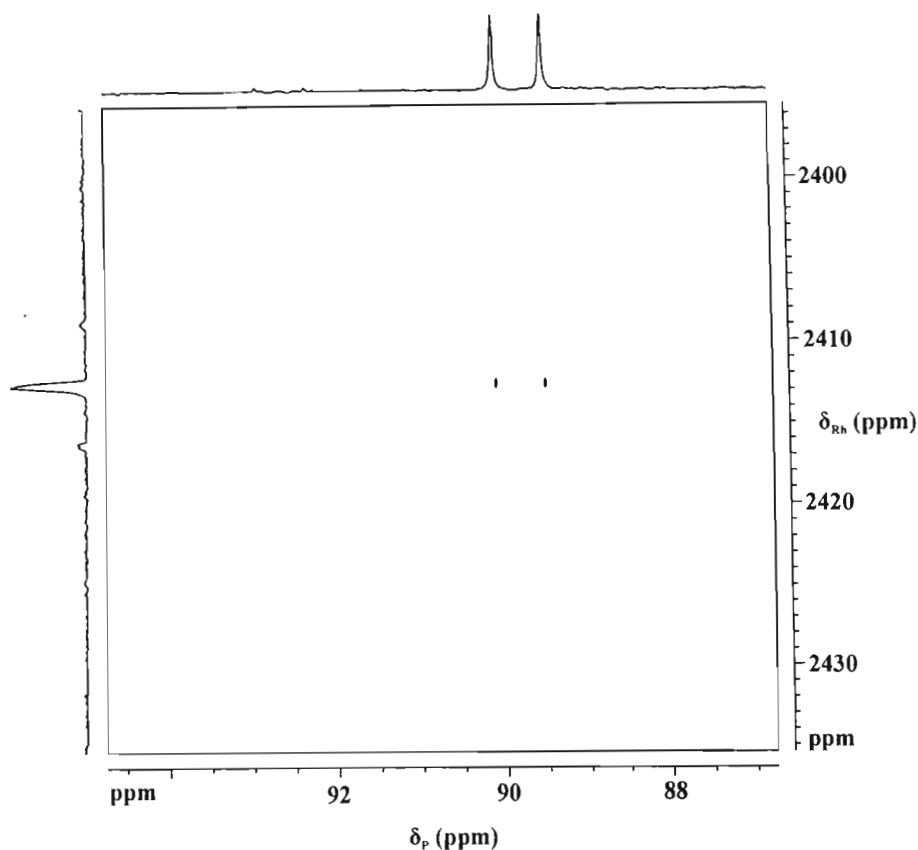
Figure 4.18: 2D ^{31}P–^{103}Rh COSY NMR of Rh(TPP)(edppt)$_2$](SbF$_6$) at 300 K.

The electronic spectrum of [Rh(TPP)(edppt)$_2$](SbF$_6$) is shown in Figure 4.19, and displays the general pattern expected for the typical rhodium(III) porphyrin.[160,179] As with [Rh(TPP)(edpp)$_2$](SbF$_6$), the B(0, 0) and B(1, 0) bands are overlapped to form a single broad band at 421 nm. The Q-bands Q(0, 0), Q(1, 0) and Q(2, 0) are found at 562, 529 and 477 nm, respectively. As with [Rh(TPP)(edpp)$_2$](SbF$_6$), the Q(1, 0) band is irregular and broad and may be concealing another band. The N band is visibly absent, but is presumed to be present in the baseline, as this band is weakly absorbing in rhodium(III) porphyrins.

Table 4.2 Spectroscopic Data for [Rh(TPP)(edppt)₂](SbF₆)

¹H NMR[a]	**TPP:** 8.76 (8 H, sh s, pyrrole H's), 7.75 (20 H, br m, p / m /o –H's) **Edppt:** 7.04 (4 H, t, ^3J = 7.3 Hz, p –H's), 6.60 (8 H, t, ^3J = 7.7 Hz, m –H's), 3.75 (8 H, p, ^3J = 3.6 Hz, o –H's), 0.99 (4 H, m, –CH₂–), –0.23 (6 H, tr, ^3J = 6.6 Hz, –CH₃)			

³¹P NMR	Temp. (K)	213	300	333
	Major (ppm)	89.32	89.80	89.82
	Minor (ppm)	92.59	92.64	92.58

¹³C NMR[a]	140.41 (s, w+br), 132.50 (d, w), 132.00 (d, w), 131.51 (d, w), 130.59 (d, str), 130.49 (d, str), 129.49 (s, str), 128.81 (d, w), 128.27 (d, str), 76,99 (t, str), 67.85 (s, w+br), 65.3 (d, w+br), 25.51 (s, w+br), 18.31 (s, w+br), 16.91 (d, str)
Infrared[b]	1096.1 (w, v(P–O$_{Et}$)), 1439.0 (w, v(P–C$_{Ph}$)), 948.5 (w, v(P–C$_{Ph}$))
Uv-vis[c]	562 (2.3 × 10³), 529 (1.0 × 10⁴), 445 (Beer's Law violation), 477 (1.3 × 10³), 421 (1.1 × 10⁵)
¹⁰³Rh NMR[d]	2413 (95)

[a] Chemical shifts measured in ppm. Measured at 294 K in CDCl₃, s = singlet, d = doublet, t = triplet, m = multiplet, str = strong, w = weak, sh = sharp, br = broad. [b] v̄ (cm⁻¹). KBr disk. [c] λ$_{max}$/nm (ε/dm³ mol⁻¹ cm⁻¹), measured at 298 K in dried and degassed dichloroethane. [d] ppm (J{¹⁰³Rh–³¹P}/Hz)

Figure 4.19: Electronic Spectrum of [Rh(TPP)(edppt)₂](SbF₆) in dichloroethane at 25 °C.

4.3.2 Crystal Structure Determination of [Rh(TPP)(edppt)$_2$](SbF$_6$)

The compound was crystallized via slow diffusion of hexane into CH$_2$Cl$_2$. The compound forms a deep red colour in solution; crystals of the compound are very deep red such that they appear black. Cube-shaped crystals of the compound were isolated and immersed in Paratone$^®$ oil immediately to prevent possible decomposition of the crystals if solvated. They were then mounted on glass microfibres for X-ray analysis. The X-ray data were collected at 219(2) K in order to, in part, prevent decay of the crystal if solvated and to improve the quality of the data collection. The compound crystallized in the monoclinic crystal system in the space group $P2_1/c$. The asymmetric unit is the full complex, full counter-ion, as well as two dichloromethane molecules. There is no inversion symmetry.

The final R_1 = 0.0492 for the structure solution. An ORTEP diagram of the crystal structure is shown in Figure 4.20. From the X-ray crystal structure the mean Rh–P$_{ax}$ bond length is 2.361(9) Å and the Rh–N$_{porph}$ bond lengths average to 2.033(3) Å. The atomic displacements from the porphyrin mean plane indicate a moderately ruffled conformation. The central rhodium ion is largely in the plane of the 24-atom core and deviates from this plane by a relatively small 0.006 Å. The atomic mean plane deviations, bond lengths and angles as well as axial ligand orientations are shown in Figure 4.21.

The dihedral angles of the phenyl substituents relative to the mean plane of the porphyrin macrocycle are: C11–C16 = 63.41°; C21–C26 = 72.67°; C31–C36 = 66.17° and C41–C46 = 79.49°.

The Rh···Sb distance is 12.130 Å, which is a substantial distance of the counter-ion from the center of the complex.

A view along the P–Rh–P axis is shown in Figure 4.22. Here the relative axial ligand orientations are shown more clearly. Figure 4.23 shows the close contacts within the X-ray crystal structure of [Rh(TPP)(edppt)$_2$](SbF$_6$). These close interactions are limited to the SbF$_6^-$ counter-ion and the dichloromethane solvate molecule. Here there is obvious hydrogen bonding between the hydrogen atom of the dichloromethane and one of the fluorine atoms of the SbF$_6^-$ counter-ion. This bond distance is 2.236 Å.
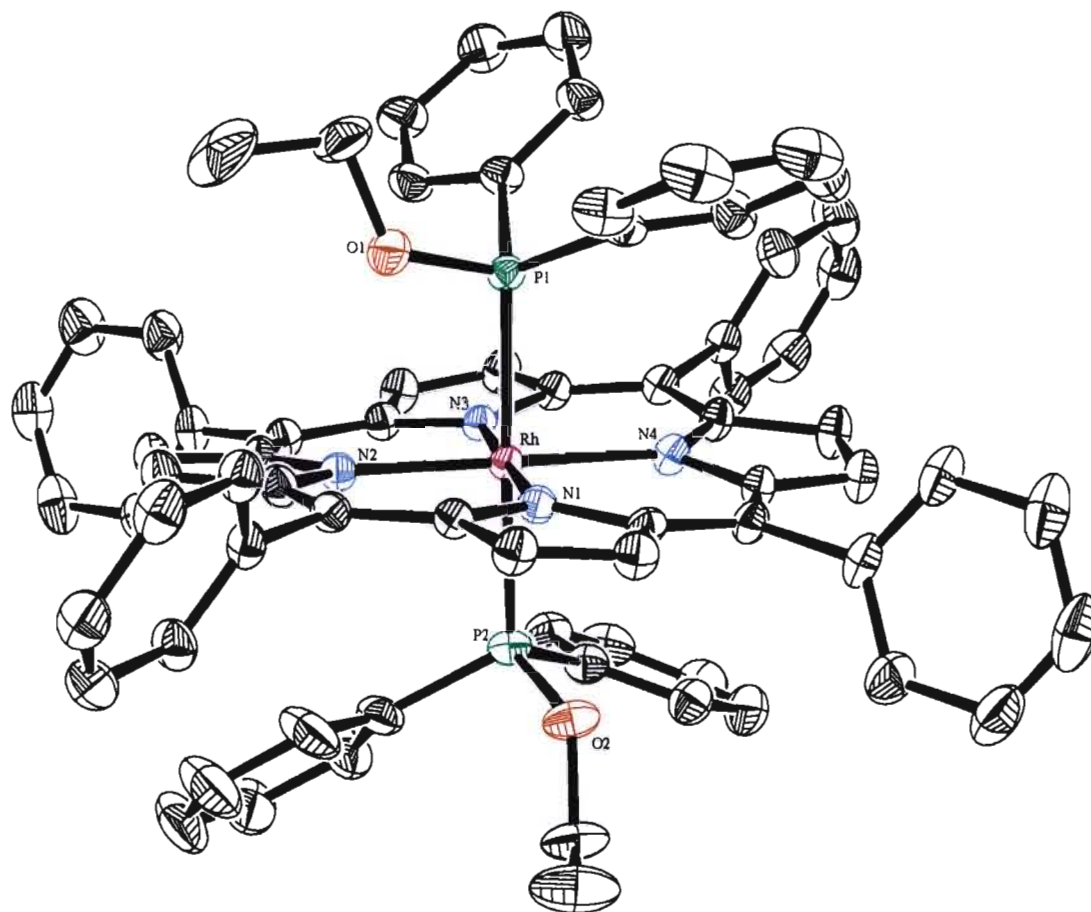
Figure 4.20: Selectively labeled ORTEP diagram of the X-ray crystal structure of [Rh(TPP)(edppt)$_2$](SbF$_6$). Thermal ellipsoids have been drawn at the 30% probability level. Hydrogen atoms and the SbF$_6^-$ counter-ion have been omitted for clarity.
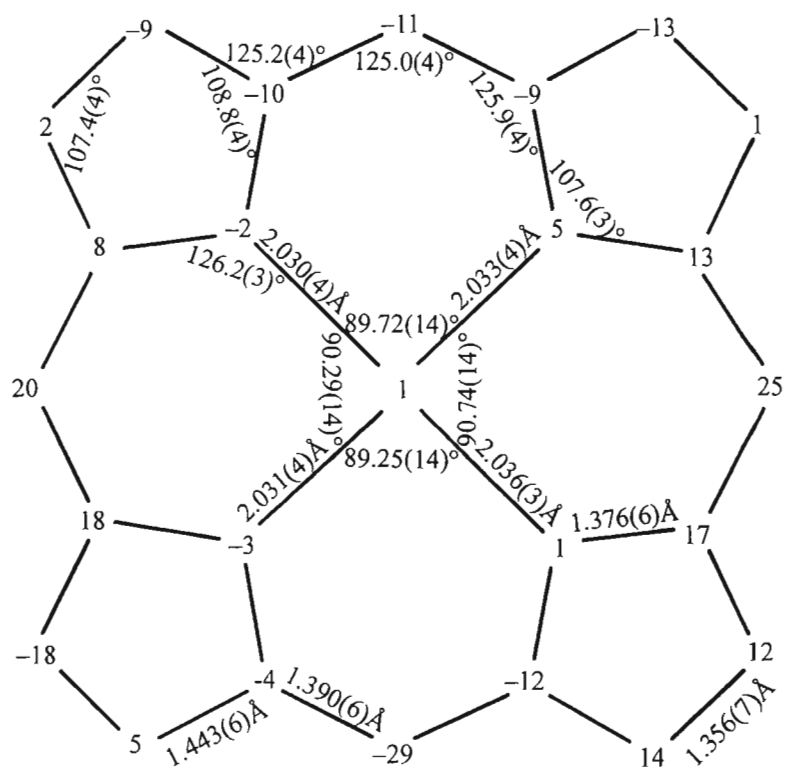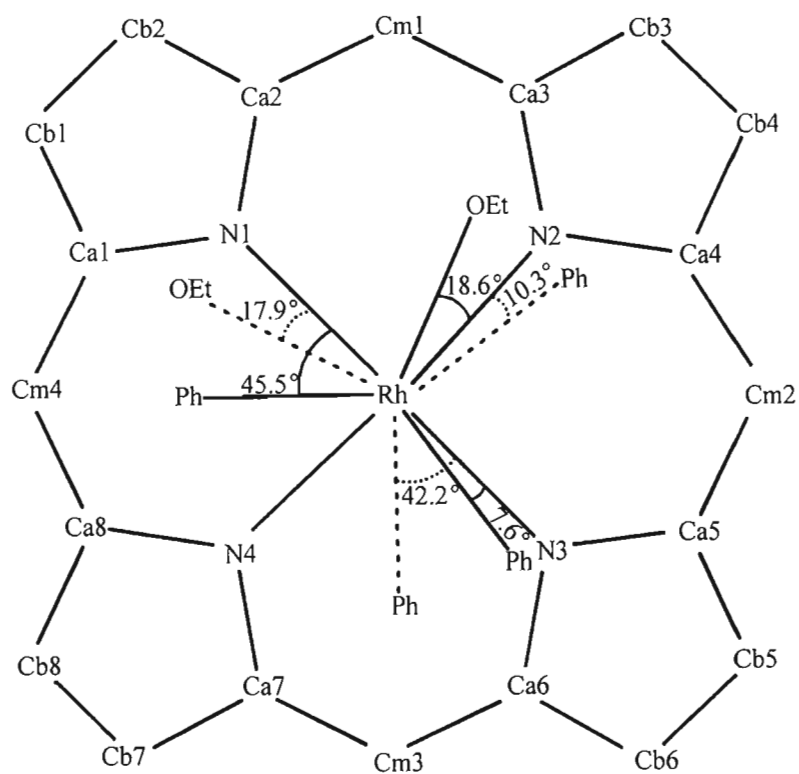
Figure 4.21: Crystallographic information and axial ligand orientations for [Rh(TPP)(edppt)$_2$](SbF$_6$). Displacements from the 24-atom mean plane are given in pm.
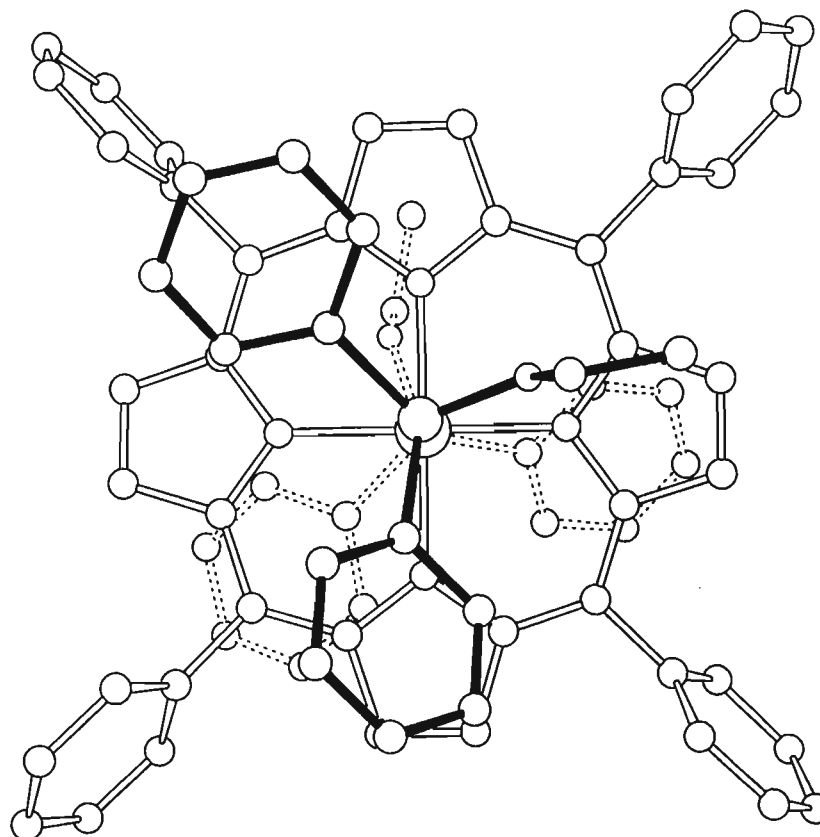
Figure 4.22: ORTEP diagram of the [Rh(TPP)(edppt)₂] cation (view perpendicular to porphyrin plane along P–Rh–P axis).
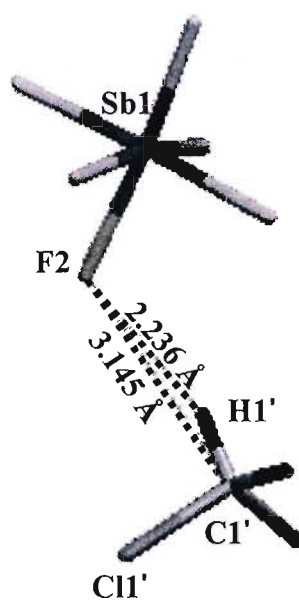
Figure 4.23: Mercury diagram of the close contacts within the X-ray crystal structure of [Rh(TPP)(edppt)₂](SbF₆). All contacts are restricted to SbF₆⁻ and solvate dichloromethane.
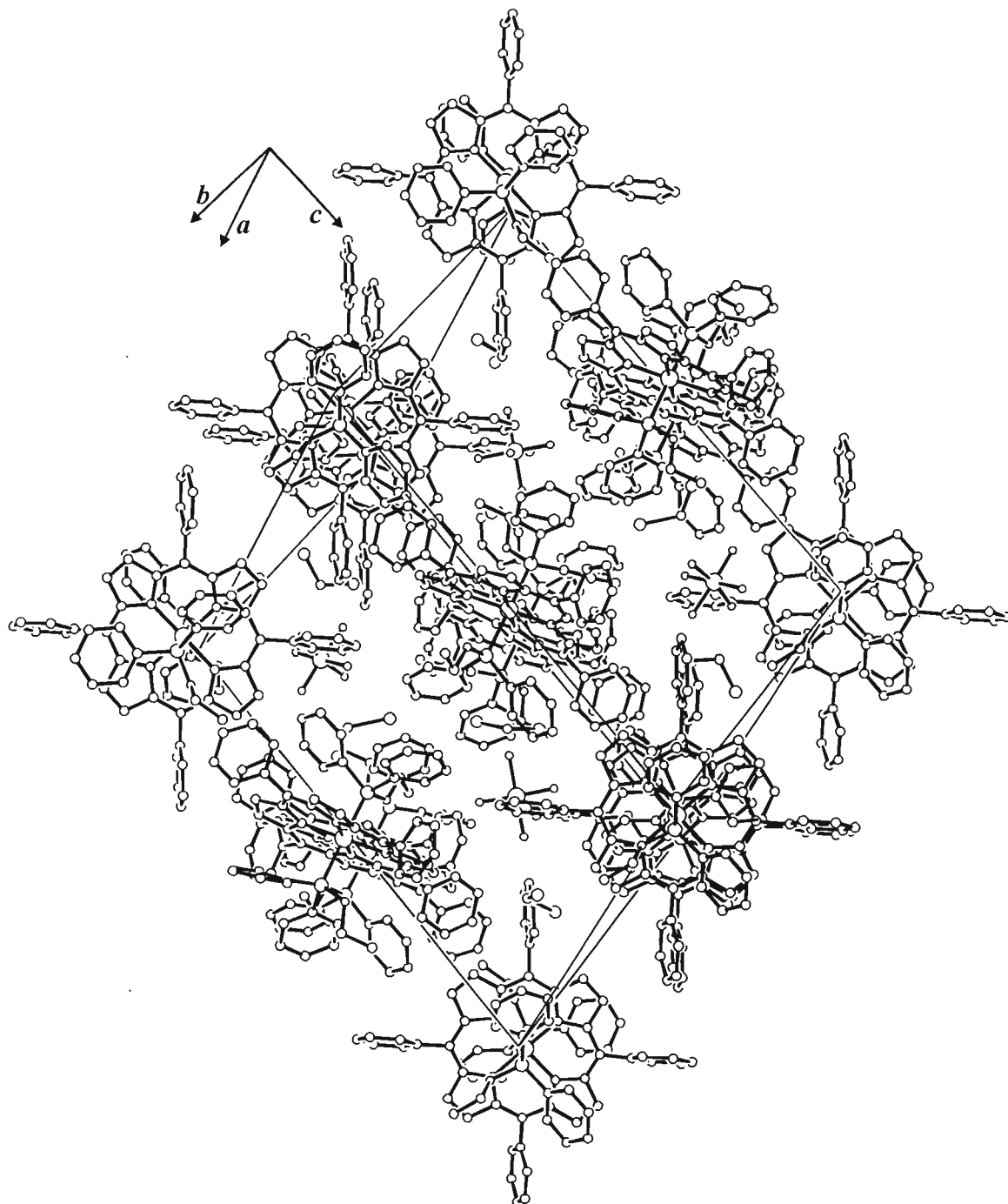
Figure 4.24: ORTEP diagram of the unit cell contents of the monoclinic structure of [Rh(TPP)(edppt)₂](SbF₆).

Figure 4.24 displays the unit cell packing diagram of $[Rh(TPP)(edppt)_2](SbF_6)$. From this diagram it is evident that the SbF_6^- counter-ions and the porphyrin cations form distinctly separate channels.

4.3.3 Synthesis and Characterisation of [Rh(TPP)(deppt)₂](SbF₆)

The phosphonite used in this reaction was diethylphenylphosphonite as shown in Figure 4.25 below.
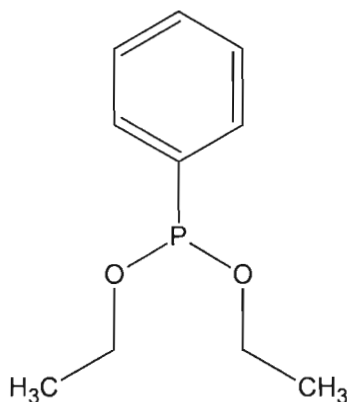
Figure 4.25: Structure of diethylphenylphosphonite.

All solvents were thoroughly dried and degassed before use. A 20 molar excess of the phosphonite was added to the rhodium precursor to ensure the crystallization of a a 6-coordinate complex.

The reaction procedures are shown in equations 1 and 2 below.

$$[Rh(TPP)Cl] + AgSbF_6 \xrightarrow{\quad THF \quad} [Rh(TPP)FSbF_5] + AgCl(s) \dots\dots\dots\dots\dots\dots\dots(1)$$

$$[Rh(TPP)FSbF_5] + excess\ deppt \xrightarrow{\quad CH_2Cl_2 \quad} [Rh(TPP)(deppt)_2](SbF_6) \dots\dots\dots\dots\dots(2)$$
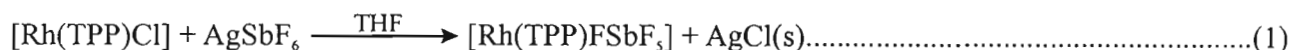
The colour of the complex in solution is a dark maroon. The spectroscopic data for [Rh(TPP)(deppt)₂](SbF₆) have been summarised in Table 4.3. The ^{13}C NMR spectrum is shown in Appendix IV in Figure AIV.5.

The ^{1}H NMR spectrum of [Rh(TPP)(deppt)₂](SbF₆) is shown in Figure 4.26. The ^{1}H NMR sample of this compound was made up of the same batch of crystals from which the X-ray crystal structure was obtained. No excess of the deppt ligand was added to the sample and thus there are no signals in the ^{1}H NMR spectrum corresponding to the free ligand. Assignments were simplified with this procedure.

The sharp singlet at 8.84 ppm (signal y) was set as the reference integral at 8 H's and has been assigned to the pyrrole protons of the macrocycle. The singlet at 9.0 ppm (signal x) indicates, as with [Rh(TPP)(edpp)$_2$](SbF$_6$) and [Rh(TPP)(edppt)$_2$](SbF$_6$), that a second complex exists in the sample. The signal x is of a significantly higher intensity than observed with [Rh(TPP)(edpp)$_2$](SbF$_6$) and [Rh(TPP)(edppt)$_2$](SbF$_6$), with a x:y ratio of 1:4. This indicates a significant quantity of the second isomer. The ^{31}P NMR spectrum shows that this species has the same coupling constant as the 6-coordinate 'major' product. Thus, as noted previously, the notion that the signal x corresponds to a 5-coordinate phosphonite porphyrin complex may be ruled out.

The relatively broad multiplet at 7.97 ppm was assigned to the *ortho*-protons of the TPP phenyls and integrates accurately to 8 H's. The *meta*- and *para*-protons were assigned to the relatively broad multiplet at 7.81 ppm. This multiplet integrates to 12 H's.

The triplet at 7.03 ppm corresponds to the *para*-protons of the phenyls of the coordinated axial deppt and has been set to an integral value of 2 H's. The triplet at 6.57 ppm corresponds to the *meta*-protons and integrates to 4 H's. The *para*-protons produce an irregular quintet at 3.81 ppm that also accurately integrates to 4 H's.

The splitting of the phenyl protons of the porphyrin macrocycle and the co-ordinated phosphonite ligand, discussed above, follows the same generic patterns as discussed in Chapter 1.8 as well as those of the cobalt complexes discussed in Chapter 2.

The $-CH_2-$ protons show a separation from equivalence and produce two multiplets at 0.92 ppm and 0.62 ppm. These signals each integrate accurately to 4 H's. The existence of two multiplets for these protons for this complex, and a single signal for the same protons in [Rh(TPP)(edppt)$_2$](SbF$_6$), may be explained by considering the orientation that the two alkyl groups adopt to avoid steric interactions with each other. It is quite obvious from the inserted crystal structure diagram of the complex in Figure 4.26, that the protons of the $-CH_2-$ groups are in different shielding environments within the shielding cone, and thus would be inequivalent.

The triplet at -0.12 ppm corresponds to the terminal methyl group and integrates accurately to 12 H's.

From Table 4.3 it is evident that the coupling constants for the signals of the coordinated axial phosphine protons are in the range 7.0 to 7.7 Hz, except for the signal assigned to the *ortho*-protons, which displays a coupling constant of 3.5 Hz.
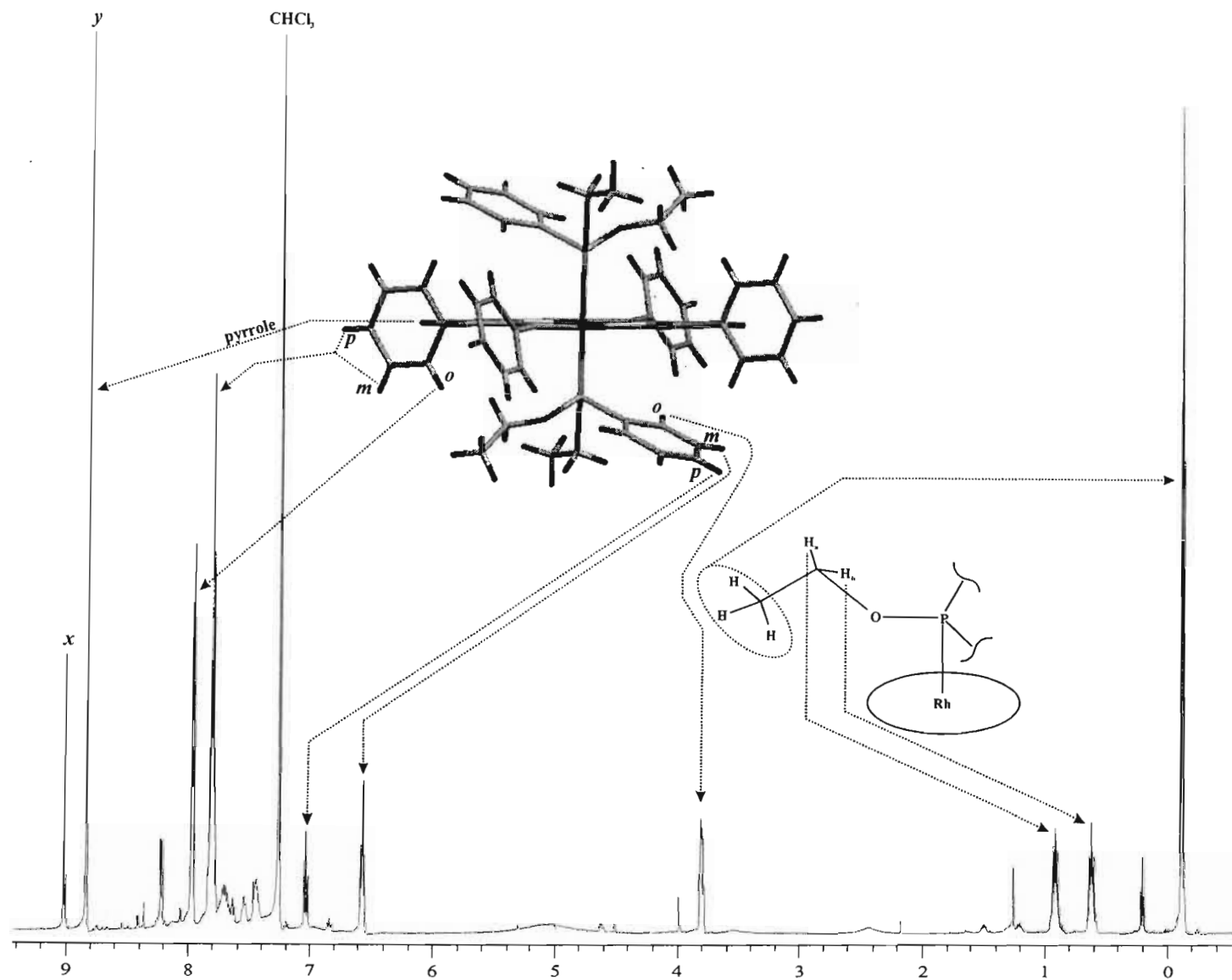
Figure 4.26: ^{1}H NMR of [Rh(TPP)(deppt)$_2$](SbF$_6$).

The ^{31}P NMR spectrum of [Rh(TPP)(deppt)$_2$](SbF$_6$), as shown in Figure 4.27 below, consists of two doublets. The first is at 108.49 ppm and corresponds to the coordinated deppt. This signal has been referred to as the 'major' product. The second and less intense doublet is found at 110.71 ppm, and is referred to as the 'minor' product. This second minor product presumably corresponds to an unknown conformational isomer as is the case with the other two compounds, namely [Rh(TPP)(edpp)$_2$](SbF$_6$) and [Rh(TPP)(edppt)$_2$](SbF$_6$). The ratio of 'major' to 'minor' product is 10:1. There is no temperature dependent relationship evident for the relative intensities of the two isomers in the temperature range 213 to 333 K. Rh–P coupling is thus observed and the coupling constant is 107.67 (51) Hz for both the major and minor doublets over the three temperatures (213, 300 and 333 K).
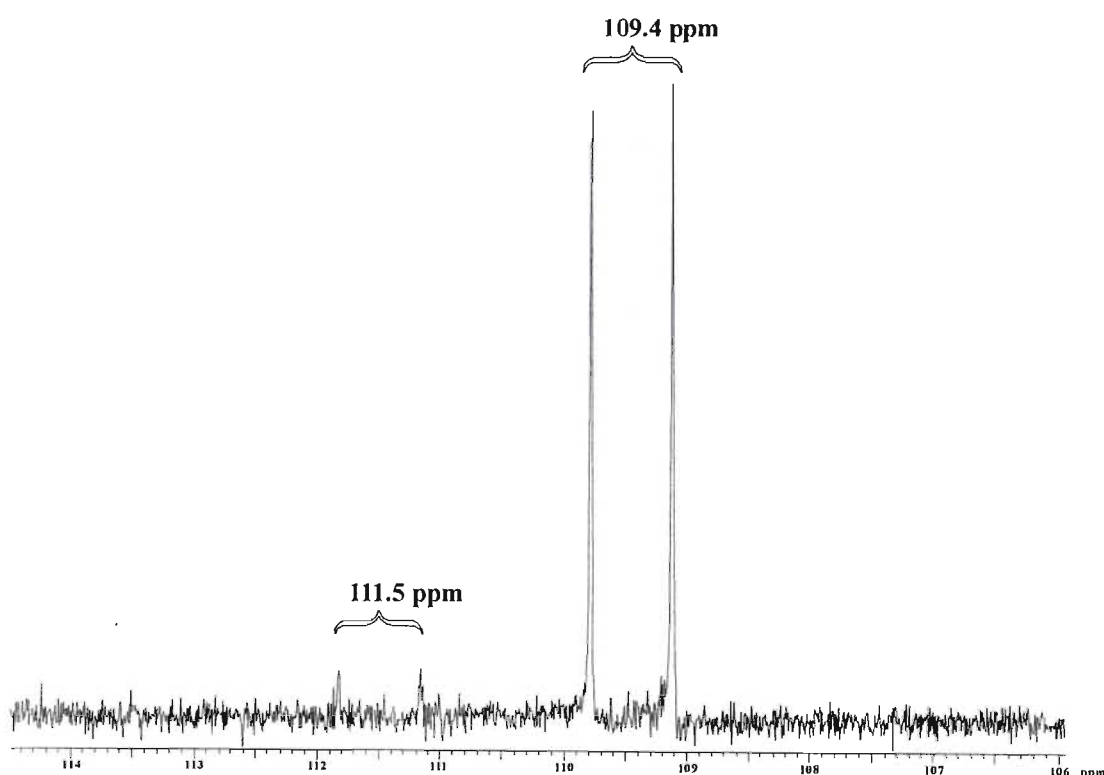
Figure 4.27: ^{31}**P NMR spectrum of [Rh(TPP)(deppt)$_2$](SbF$_6$) (213 K).**

The graph shown in Figure 4.28 is of the temperature-dependence of the ^{31}P NMR shifts of [Rh(TPP)(deppt)$_2$](SbF$_6$). This graph shows that the shifts move up field with an increase in temperature for both the major and minor products.
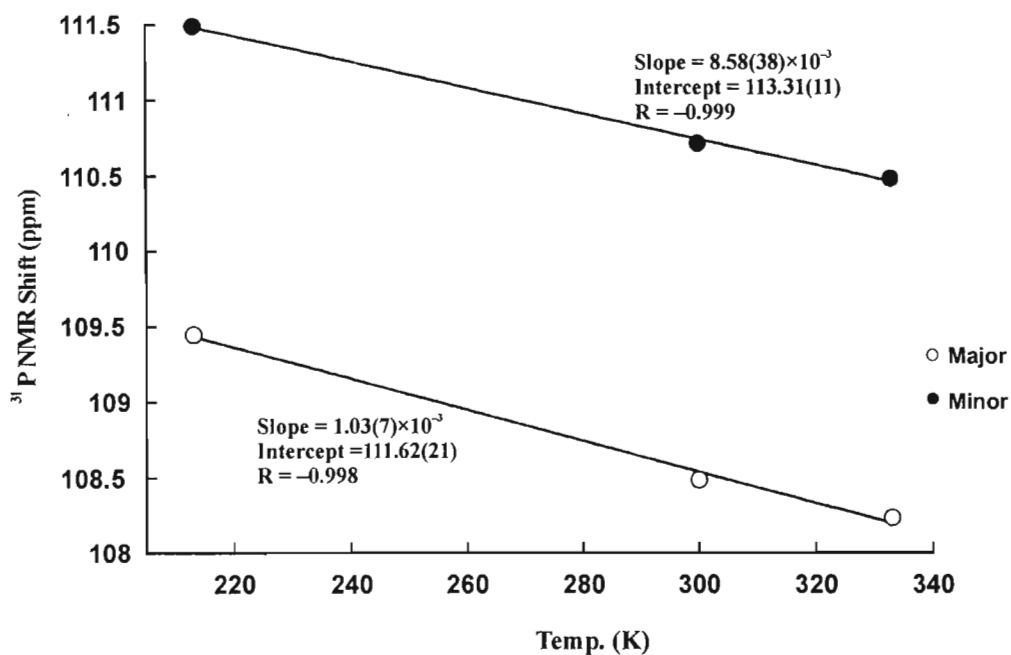
Figure 4.28: Graph showing the temperature dependence of the ^{31}P NMR signals for [Rh(TPP)(deppt)$_2$](SbF$_6$).

Figure 4.29 shows the ^{31}P–^{103}Rh COSY NMR spectrum at 300 K. The ^{103}Rh NMR signal consists of a singlet at 2365 ppm.
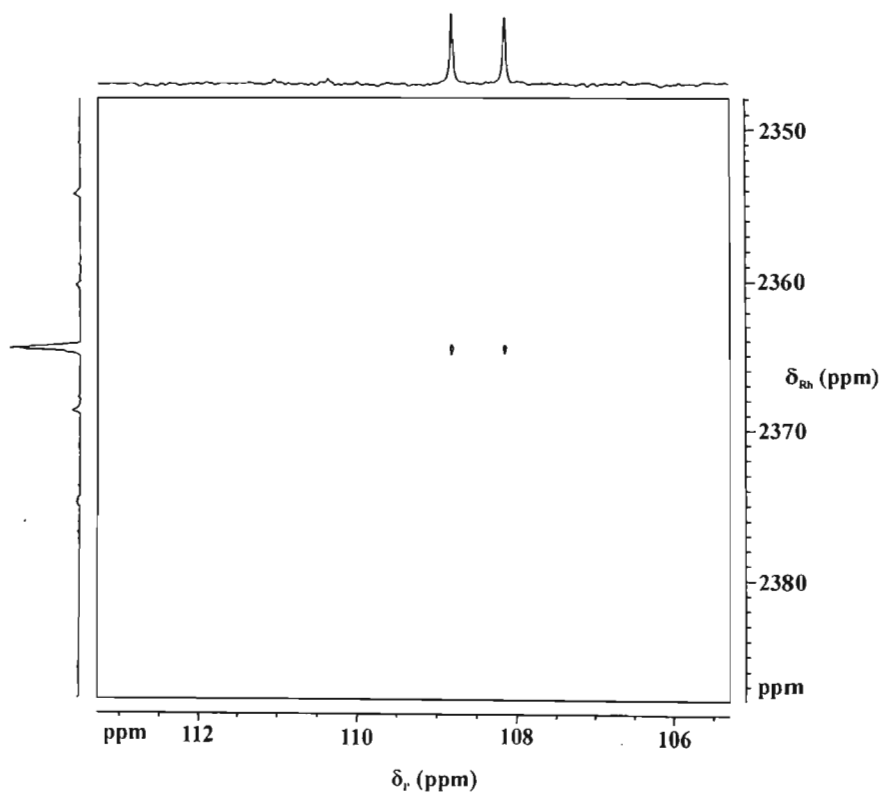
Figure 4.29: 2D ^{31}P–^{103}Rh COSY NMR spectrum of Rh(TPP)(deppt)$_2$](SbF$_6$) at 300 K.

191

The electronic spectrum of [Rh(TPP)(deppt)$_2$](SbF$_6$) is shown in Figure 4.30 and, once again, conforms to the general pattern expected for rhodium(III) porphyrins.[160,179] It is evident from the electronic spectra of all three Rh(III) bis(phosphine/phosphonite) complexes studied thus far that the B(0, 0) and B(1, 0) bands are overlapped as a general rule. For [Rh(TPP)(deppt)$_2$](SbF$_6$), the B(0, 0) band is found at 420 nm and three Q-bands are found at 563, 530 and 478 nm for the Q(0, 0), Q(1, 0) and Q(2, 0) bands, respectively. The suspected N-band is a weak, broad band at 346 nm. As with the other three complexes of Rh in this work, the Q(1, 0) band is broad and appears to be concealing another band.

Table 4.3 Spectroscopic Data for [Rh(TPP)(deppt)$_2$](SbF$_6$)

^{1}H NMR^a	**TPP:** 8.84 (8 H's, sh s, pyrrole H's), 7.97 (8 H's, m, o–H's), 7.81 (12 H's, m, p / m–H's) **Deppt:** 7.03 (2 H's, t, ^3J = 7.7 Hz, p–H's), 6.57 (4 H's, t, ^3J = 7.7 Hz, m–H's), 3.81 (4 H's, p, ^3J = 3.5 Hz, o–H's), 0.92 (4 H's, m, –CH$_a$–), 0.62 (4 H's, m, –CH$_b$–), –0.12 (12 H's, t, ^3J = 7.0 Hz, –CH$_3$)			
^{31}P NMR	**Temp. (K)**	**213**	**300**	**333**
	Major (ppm)	109.45	108.49	108.23
	Minor (ppm)	111.49	110.71	110.47
^{13}C NMR^a	140.57 (s, w + br), 134.22 (t, w), 133.20 (s, w), 132.97 (d, w), 130.78 (d, str), 129.68 (t, str), 128.65 (d, w), 126.92 (s, w), 77.00 (t, str), 62.45 (d, str), 61.92 (d, w), 18.28 (s, w), 16.91 (d, str), 16.25 (t, w)			
Infrared^b	1029.8 (med, ν(P–OEt)), 1440.9 (med, ν(P–Ph)), 949.5 (med, ν(P–Ph))			
Uv-vis^c	563 (4.5 × 10^3), 530 (2.2 × 10^4), 478 (2.2 × 10^3), 420 (2.4 × 10^5), 346 (5.5 × 10^3)			
^{103}Rh NMR^d	2365 (108)			

^{a} Chemical shifts measured in ppm. Measured at 294 K in CDCl$_3$, s = singlet, d = doublet, t = triplet, m = multiplet, str = strong, med = medium, w = weak, sh = sharp, br = broad. ^{b} ṽ (cm^{-1}). KBr disk. ^{c} λ$_{max}$/nm (ε/dm^3 mol^{-1} cm^{-1}), measured at 298 K in dried and degassed dichloroethane. ^{d} ppm (J{^{103}Rh–^{31}P}/Hz)

Figure 4.30: Electronic Spectrum of $[Rh(TPP)(deppt)_2](SbF_6)$ in dichloroethane at 25 °C.

4.3.4 Crystal Structure Determination of [Rh(TPP)(deppt)₂](SbF₆)

The compound was crystallized via slow diffusion of hexane into CH_2Cl_2. The compound forms a deep red colour in solution; crystals of the compound are very deep red such that they appear black. Cube-shaped crystals of the compound were isolated and immersed in Paratone® oil immediately to prevent possible decomposition of the crystals if solvated. They were then mounted on glass microfibres for X-ray analysis. The X-ray data were collected at 219(2) K in order to, in part, prevent decay of the crystal if solvated and to improve the quality of the data collection. The compound crystallized in the monoclinic crystal system in the space group $P2_1/c$. The asymmetric unit, as shown in Figure 4.33, consists of two half porphyrins and each has a centre of inversion at the Rh and thus the central Rh ion is half occupied and lies in the plane of the porphyrin. The two porphyrin complexes have been distinguished from each other with the use of the (') symbol. The antimony hexafluoride counter-ion is fully occupied. The other half of each independent complex is symmetry-derived.

The final R_1 = 0.0492 for the structure solution. An ORTEP diagram of the crystal structure is shown in Figure 4.31. From the X-ray crystal structure the Rh–P_{ax} bond length is 2.332(2) Å and the Rh–N_{porph} bond lengths average to 2.044(3) Å in the first porphyrin complex in the asymmetric unit. The Rh'–P'$_{ax}$ bond length is 2.332(2) Å, and the Rh'–N'$_{porph}$ bond lengths average to 2.039(4) Å in the second porphyrin complex in the asymmetric unit. The distances are therefore experimentally equivalent for the two independent molecules.

The atomic deviations from planarity within the 24-atom mean plane are mostly minimal and no recognizable conformational pattern is observed. The pyrrole nitrogens of the macrocycle appear to deviate most from the plane of the porphyrin. These deviations are 0.09 Å for the first complex and 0.06 Å for the other. A schematic diagram showing the porphyrin core atomic mean plane deviations, axial ligand orientations, as well as bond lengths and angles is shown in Figure 4.32a and 4.32b, for the first and second complex in the asymmetric unit, respectively. From Figure 4.32a it is noteworthy that there is a correlation between the atom that deviates most from the 24-atom mean plane (0.09 Å) and the location of a deppt oxygen atom. The deviation of this nitrogen reflects a steric contact with the oxygen, the spacing between these two atoms is 2.961 Å.

The dihedral angles of the phenyl substituents relative to the mean plane of the porphyrin

macrocycle are: C11–C16 = 68.15°; C21–C26 = 63.53°; C11′–C16′ = 88.51° and C21′–C26′ = 69.67° and the Rh···Sb and Rh′···Sb′ distances are 8.252 Å and 8.536 Å, respectively.
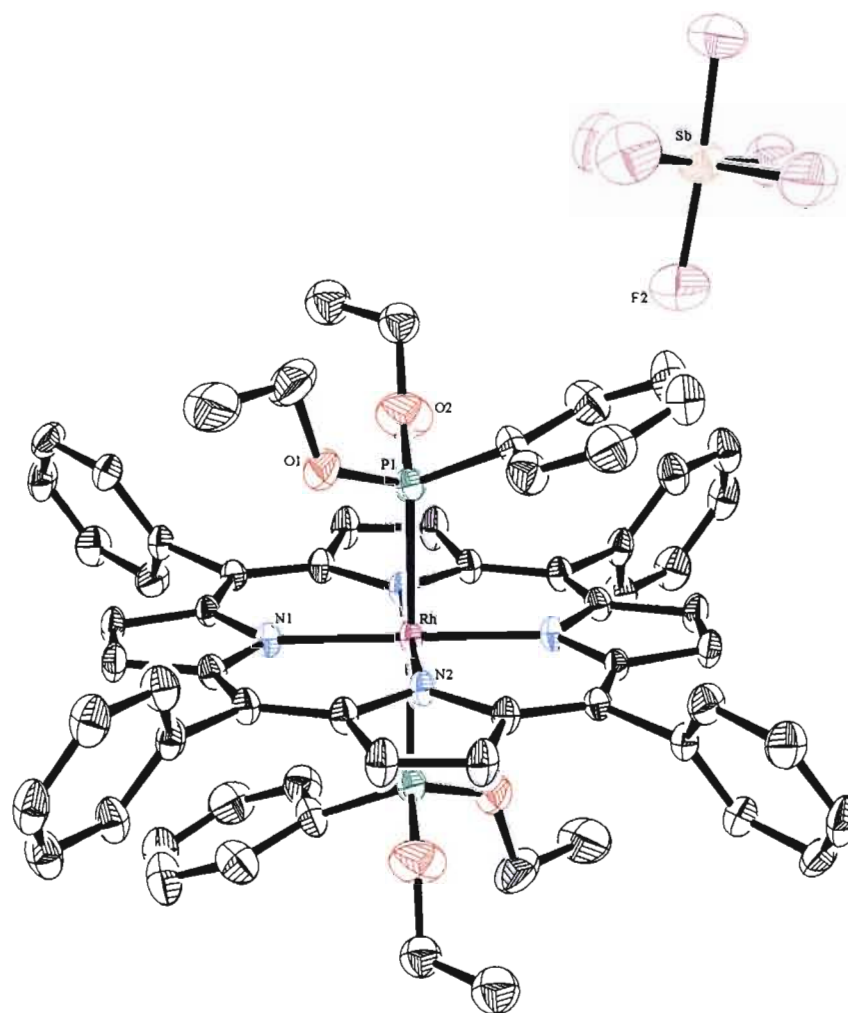
Figure 4.31: Selectively labelled ORTEP diagram of the X-ray crystal structure of [Rh(TPP)(deppt)$_2$](SbF$_6$). Thermal ellipsoids have been drawn at the 30 % probability level. Hydrogen atoms are omitted for clarity.
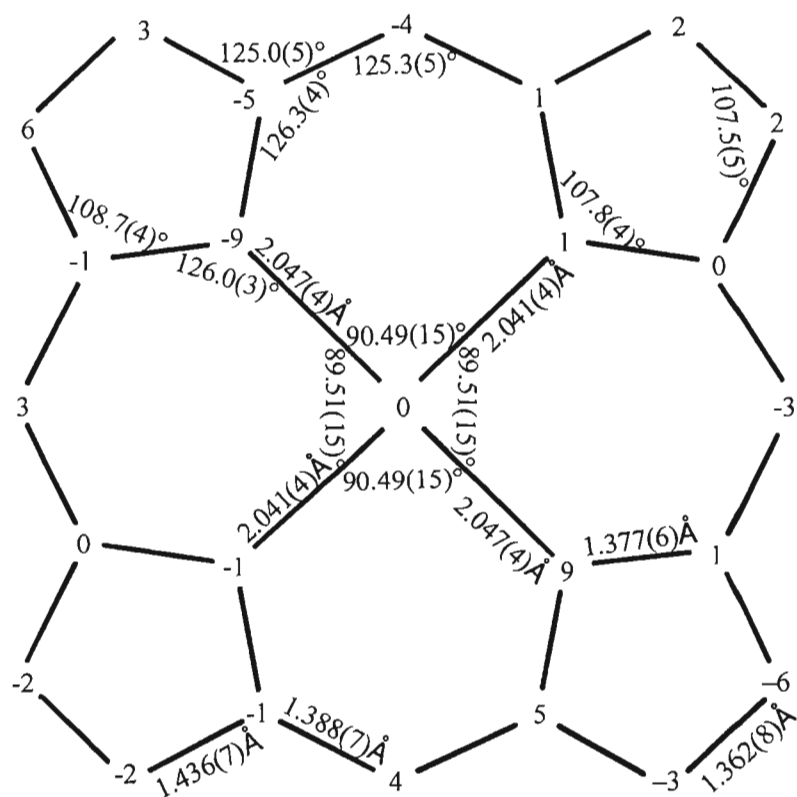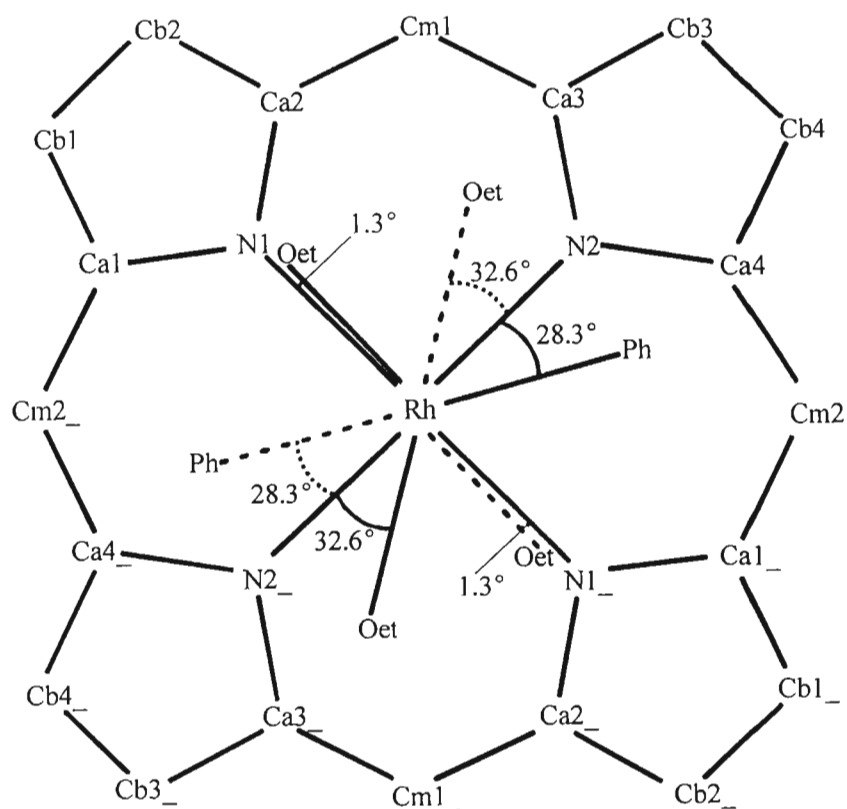
Figure 4.32a: Crystallographic information and axial ligand orientation for [Rh(TPP)(deppt)₂](SbF₆). Underscores designate the symmetry-equivalent atoms. Displacements from the 24-atom mean plane are given in pm.
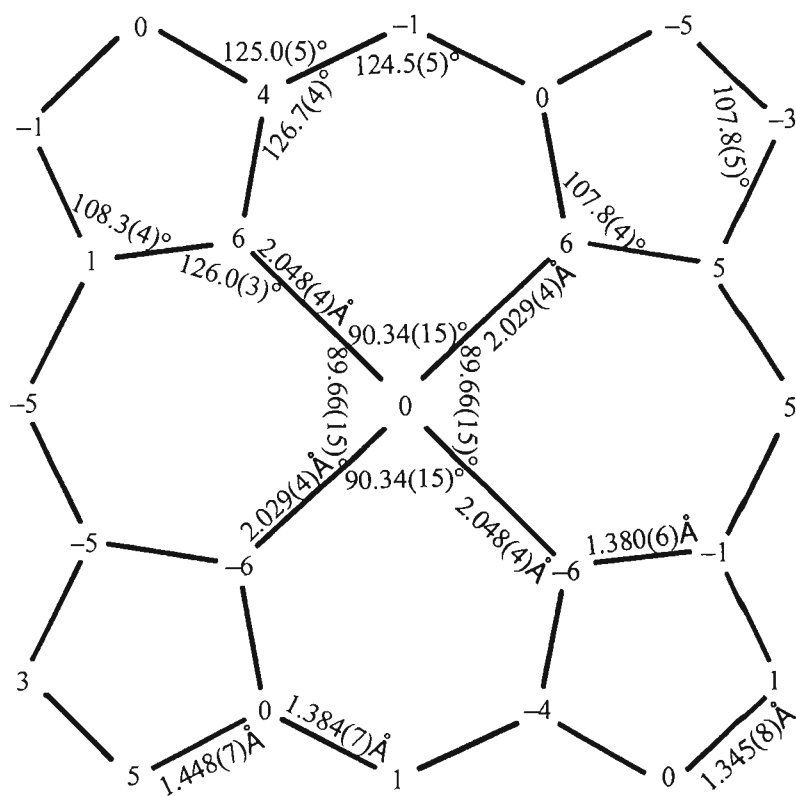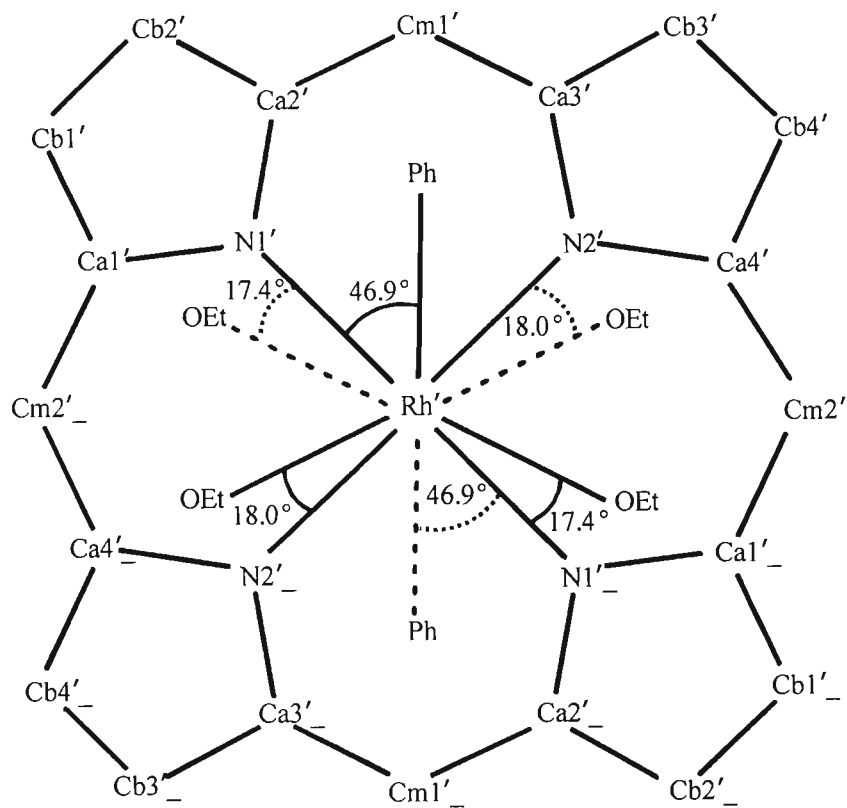
Figure 4.32b: Crystallographic information and axial ligand orientation for [Rh′(TPP)(deppt)₂](SbF₆). Underscores designate the symmetry-equivalent atoms. Displacements from the 24-atom mean plane are given in pm.
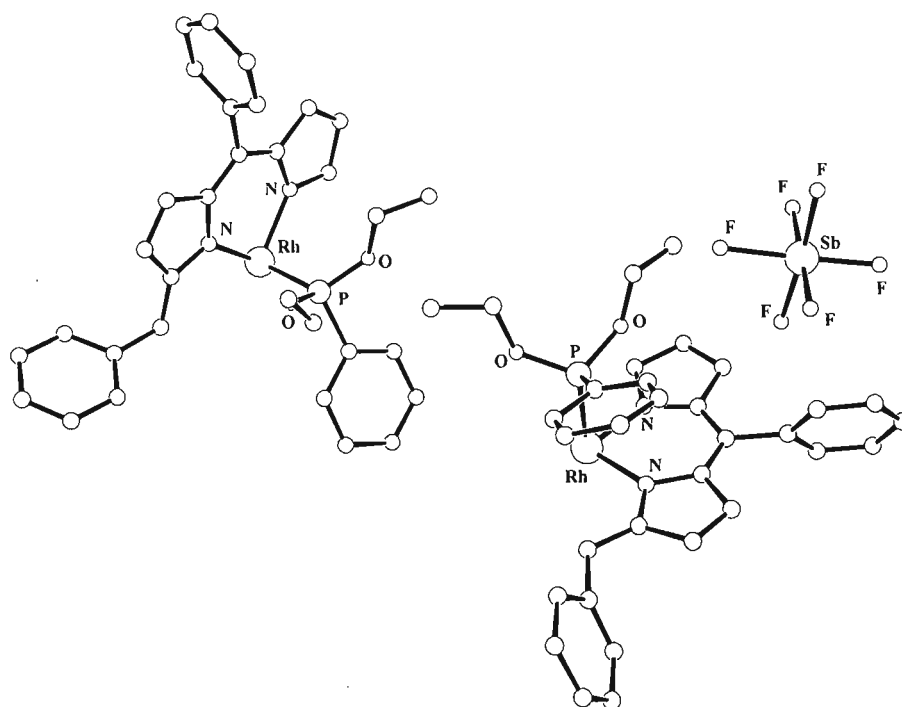
Figure 4.33: ORTEP diagram of the asymmetric unit of the X-ray crystal structure of [Rh(TPP)(deppt)₂](SbF₆).
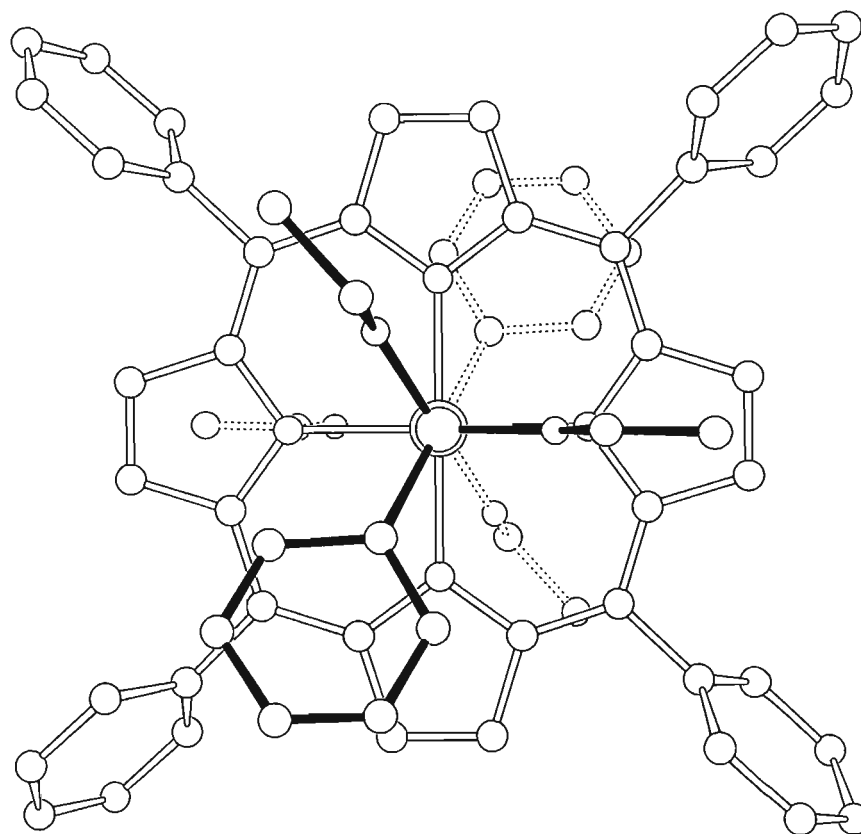
Figure 4.34: ORTEP diagram of the [Rh(TPP)(deppt)₂]⁺ cation (view perpendicular to porphyrin plane along P–Rh–P axis).
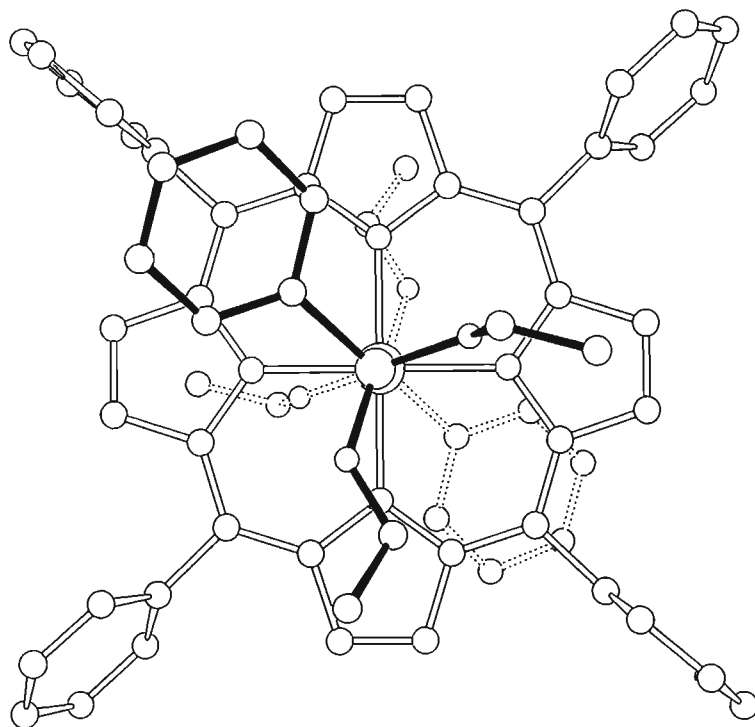
Figure 4.35: ORTEP diagram of the second independent [Rh′(TPP)(deppt)₂]⁺ cation in the asymmetric unit (view perpendicular to porphyrin plane along P′–Rh′–P′ axis).

Figures 4.34 and 4.35 show views of the two complexes down the P–Rh–P and P′–Rh′–P′ axes, respectively. In these figures the relative axial ligand orientations may be observed.

A diagram displaying the close contacts within the X-ray crystal structure of [Rh(TPP)(deppt)₂](SbF₆) is shown in Figure 4.36 below. The close contacts are between the proton on C12 of the porphyrin phenyl closest to the SbF₆⁻ counter-ion and a fluorine atom on the counter-ion. This is obvious hydrogen bonding and the hydrogen bond distance is 2.527 Å. Interestingly, there are no close contacts that are less than the sum of the van der Waals radii of the interacting atoms between the axial phosphonite and the porphyrin core.

The arrangement of the complexes making up the unit cell is shown in Figure 4.37. As is the case with most of the complexes observed thus far, the complexes arrange in such a manner that 'channels' containing the anions and cations result.
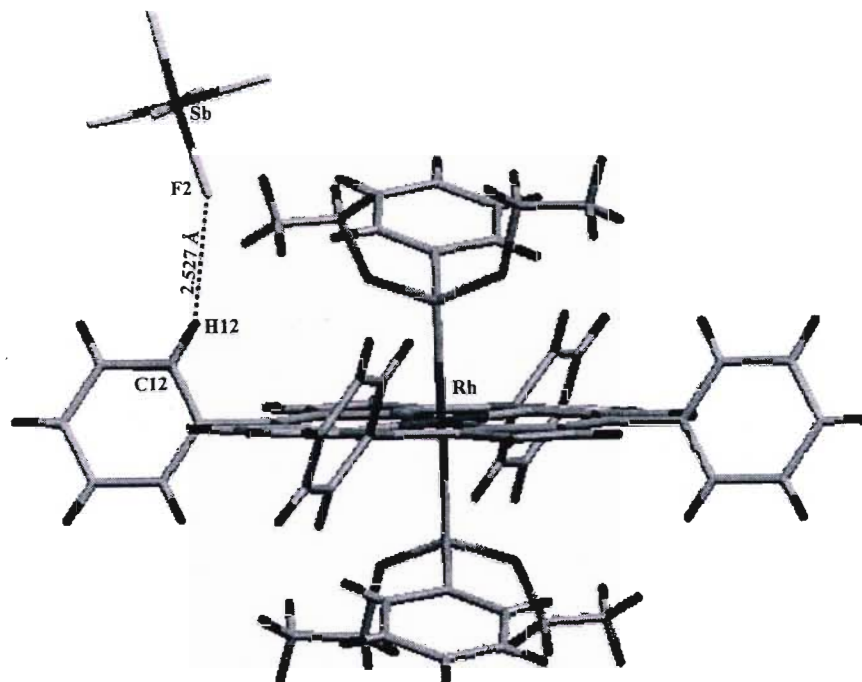
Figure 4.36: Diagram of the close contacts within the X-ray crystal structure of [Rh(TPP)(deppt)₂](SbF₆).
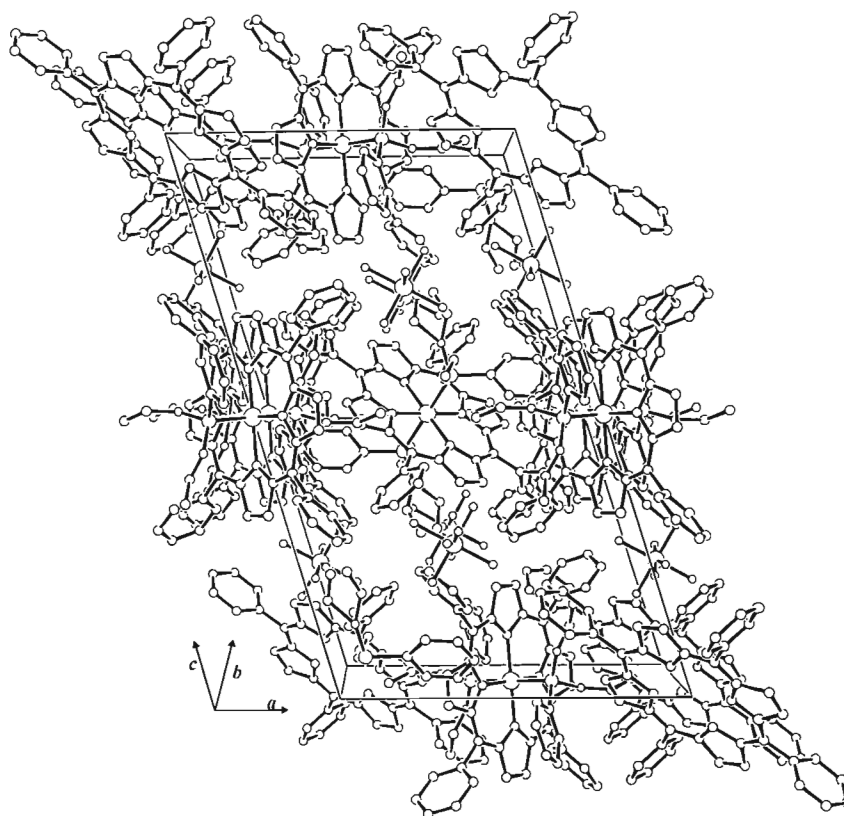
Figure 4.37: ORTEP diagram of the unit cell contents of the monoclinic structure of [Rh(TPP)(deppt)₂](SbF₆) (view along *b* axis). Selected axial ligands and metal ions have been removed for clarity.

4.4 Summary of the Crystallographic and Spectroscopic Data for Bis(Phosphine) and Bis(Phosphonite) Complexes of Rh(III) Porphyrins.

Crystallography. All three of the Rh(III) complexes studied are 6-coordinate and crystallize in the monoclinic crystal system. The single bis(phosphine) complex, [Rh(TPP)(edpp)$_2$](SbF$_6$), displays an axial Rh–P$_{ax}$ bond length of 2.401(2) Å. The two bis(phosphonite) complexes of [Rh(TPP)(edppt)$_2$](SbF$_6$) and [Rh(TPP)(deppt)$_2$](SbF$_6$) exhibit Rh–P$_{ax}$ bond lengths of 2.361(9) Å and 2.332(2) Å, respectively. The trend here is that the bis(phosphonite) complexes display significantly shorter axial bond lengths than the bis(phosphine) complex. This is mostly due to the increased 'flexibility' of the ethoxy substituent of the phosphonites relative to a more rigid ethyl substituent of the phosphine. As mentioned previously in Chapter 1, the oxygen in the ethoxy substituent creates a 'pivot' point around which the ethyl group may rotate away from the porphyrin's steric bulk. There appears to be a weaker dependence of axial bond length on σ-donor strength of the phosphine/phosphonite, as the Soret band λ_{max} in the electronic spectra of each compound was plotted against the Rh–P$_{ax}$ and no relationship is evident. However, this is inconclusive as only three data points exist. In the cobalt complexes discussed in Chapter 3, such a relationship was indeed observed.

Table 4.4: Summary of Important Crystallographic Data for Bis(Phosphine) and Bis(Phosphonite) Compexes of Rh(III) Porphyrins

	[Rh(TPP)(edpp)$_2$](SbF$_6$)	[Rh(TPP)(edppt)$_2$](SbF$_6$)	[Rh(TPP)(deppt)$_2$](SbF$_6$)
Crystal System	Monoclinic	Monoclinic	Monoclinic
Spacegroup	$P2_1/n$	$P2_1/c$	$P2_1/c$
T (K)	259(2)	219(2)	219(2)
Rh–P$_{ax}$ (Å)	2.401(2)	2.361(9)	2.332(2)
Rh–N$_{porph}$ (Å)	2.035(3)	2.033(3)	2.044(3)/2.039(4)
Conformation	Ruffled	Ruffled	Planar
Δ_{Rh} (pm)^a	2	1	0

^{a} Δ_{Rh} = displacement of Rh(III) ion from 24-atom mean plane.

The conformations adopted by the porphyrin cores of [Rh(TPP)(edpp)$_2$](SbF$_6$) and [Rh(TPP)(edppt)$_2$](SbF$_6$) are moderately ruffled, yet for [Rh(TPP)(deppt)$_2$](SbF$_6$), a planar conformation is observed. The ruffled conformations for [Rh(TPP)(edpp)$_2$](SbF$_6$) and [Rh(TPP)(edppt)$_2$](SbF$_6$) are indicative of the steric contacts of the axial ligand with the *meso-*

carbons of the porphyrin core in these complexes. In [Rh(TPP)(edpp)$_2$](SbF$_6$), the *meso*-carbons Cm2 and Cm3 are on opposing sides of the porphyrin mean plane and both are in relatively close proximity to the phenyls of the axial phosphine ligand. In [Rh(TPP)(edppt)$_2$](SbF$_6$), the *meso*-carbons Cm3 and Cm4 are also on opposing sides of the porphyrin mean plane. These carbons are both in relatively close proximity to a phenyl of the axial phosphonite ligand. These two ruffled complexes display *meso*-carbons with the furthest deviations from the 24-atom mean plane, relative to the other atoms of the porphyrin core. It thus follows that [Rh(TPP)(deppt)$_2$](SbF$_6$) will not show a noticeable distortion of the porphyrin core, as the phenyls of the axial ligands are not in such close proximity to any of the *meso*-carbons.

The central rhodium(III) ion is positioned out of the plane of the porphyrin 24-atom core in [Rh(TPP)(edpp)$_2$](SbF$_6$) and [Rh(TPP)(edppt)$_2$](SbF$_6$) by 2 and 1 pm, respectively, while the central Rh(III) ion in [Rh(TPP)(deppt)$_2$](SbF$_6$) lies in the plane of the 24-atom porphyrin core.
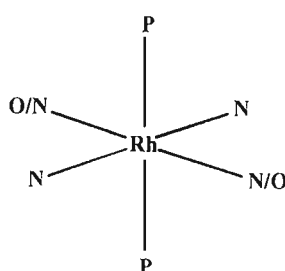
Figure 4.38: Search outline for related complexes.

In a search of the CSD for phosphine and phosphonite complexes of Rh(III) of the type as shown in Figure 4.38 above, only three complexes were found. These complexes are: tris(acetonitrile) nitrosyl-bis(triphenylphosphine) rhodium(III) hexafluorophosphate as is shown in Figure 4.39, cis-bis(diacetyl monoximato)-cis-bis(triphenylphosphine)-rhodium(III) perchlorate chloroform solvate (Figure 4.40), and (2, 3-butanedione 2-imine 3-oximato-N, N')-(dimethylglyoximato-N, N')-bis(triethylphosphine)-rhodium(III) (Figure 4.41). The first two complexes contain triphenylphosphine as the P-donor and exhibit Rh–P bond lengths of 2.405(4) and 2.404(4) Å, respectively. The second complex, interestingly, displays a *cis* arrangement of the two triphenylphosphine ligands despite the large steric size of the triphenylphosphine. The single triethylphosphine complex displays a Rh–P bond length of 2.382(1) Å. The effect that the phosphine's steric size has on Rh–P bond lengths is clearly evident here with the triethylphosphine complex displaying a considerably shorter Rh–P bond length than the

equivalent bond in the triphenylphosphine complexes. These Rh–P distances are all consistent with the equivalent bond measured in the bis(phosphine) porphyrin complex [Rh(TPP)(edpp)$_2$](SbF$_6$), from this work, at 2.401(2) Å.
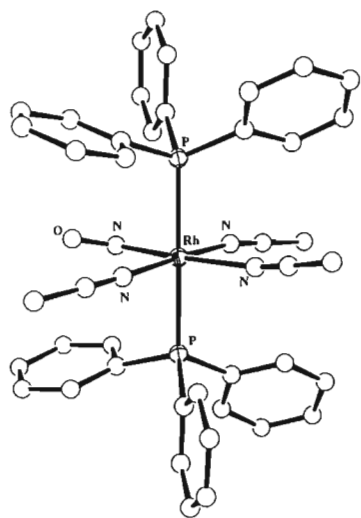
Figure 4.39: ACNPRH.[227]
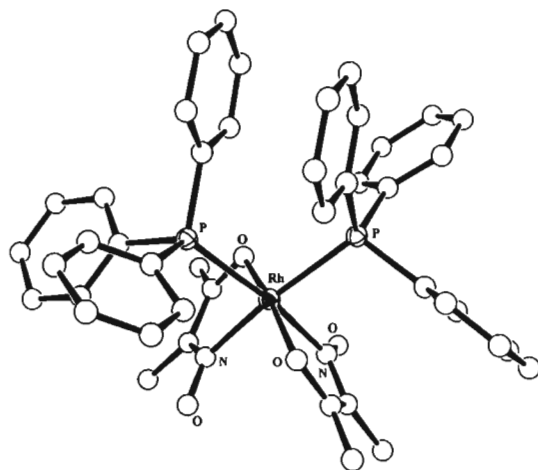
Figure 4.40: REXKOU.[228]
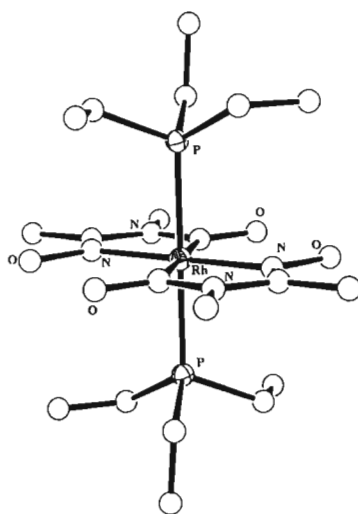
Figure 4.41: YENCEZ.[229]

Spectroscopic/Structural Relationships. In the ^{1}H NMR of the current set of Rh(III) porphyrins, the loss of equivalence of the –CH$_2$– protons of the ethyl or ethoxy substituents of the phosphine or phosphonite ligands is only evident in the complex [Rh(TPP)(deppt)$_2$](SbF$_6$). In this spectrum, the expected single signal for these protons has split and two broader signals result. This complex also displays the shortest axial bond lengths which may explain this splitting in terms of distance from the apex of the shielding cone. There is, however, not enough

data available to substantiate such statements at present. The ^{1}H NMR coupling constants for the signals corresponding to the coordinated axial ligands displayed values in the range 7.0 ~ 7.7 Hz, as is expected for aromatic systems, but for the *ortho*-protons which displayed a substantially weaker coupling constant of 3.6(2) Hz. It thus appears that on coordination to the metal, the phenyl *ortho*-proton of the axial ligand exhibits a weaker coupling to the *para*-proton as well as moving substantially further up field.

The ^{31}P NMR shifts were plotted against the Rh–P bond lengths and the resulting graph is shown in Figure 4.42. A roughly linear trend results and an inverse relationship between the bond distance and ^{31}P NMR shift is evident. In all three of the ^{31}P NMR spectra of the complexes synthesized in this work, two products are evident. An intense doublet, corresponding to the 'major' product and a less intense doublet, termed the 'minor' product, occur in all three spectra at all of the three temperatures (213, 300 and 333 K). The structure of the 'minor' product is unknown and attempts have been made to understand the relationship between this complex and the 'major' product.

The temperature dependence of the ^{31}P shifts of both the 'major' and 'minor' products for [Rh(TPP)(edpp)$_2$](SbF$_6$), [Rh(TPP)(edppt)$_2$](SbF$_6$) and [Rh(TPP)(deppt)$_2$](SbF$_6$) have been shown in Figures 4.4, 4.17 and 4.28, respectively, and discussed in the relevant sections.
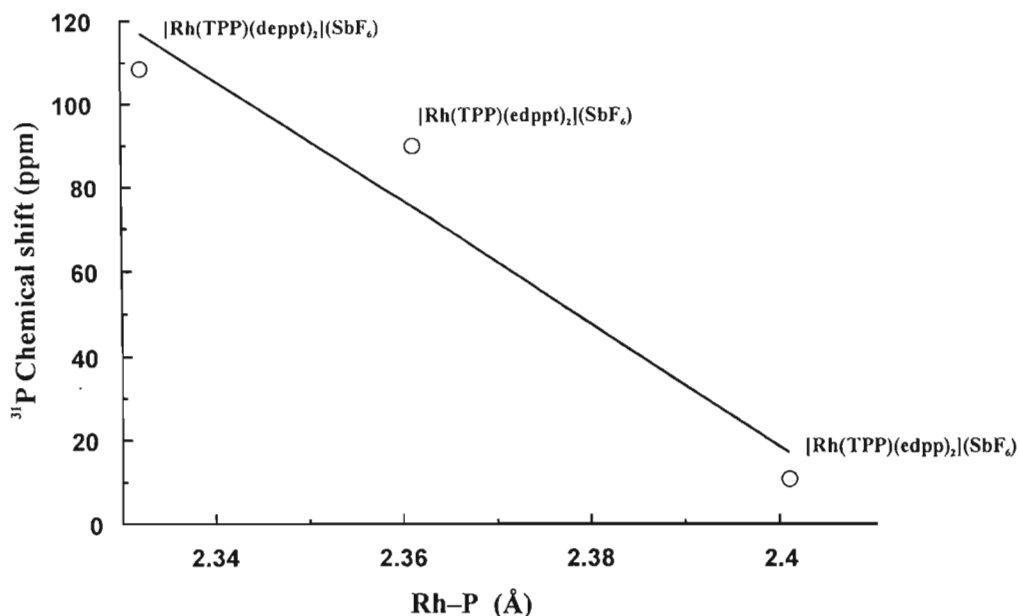
Figure 4.42: Graph of ^{31}P chemical shifts versus Rh–P$_{ax}$ bond lengths for [Rh(TPP)(edpp)$_2$](SbF$_6$), [Rh(TPP)(edppt)$_2$](SbF$_6$) and [Rh(TPP)(deppt)$_2$](SbF$_6$).

In an attempt to determine whether the relationship between the 'major ' and 'minor' products is temperature-dependent, the ratio of major/minor product was plotted *versus* temperature. No possibility for such a relationship was observed for [Rh(TPP)(edpp)$_2$](SbF$_6$), yet for [Rh(TPP)(edppt)$_2$](SbF$_6$) and [Rh(TPP)(deppt)$_2$](SbF$_6$) a relationship is evident.
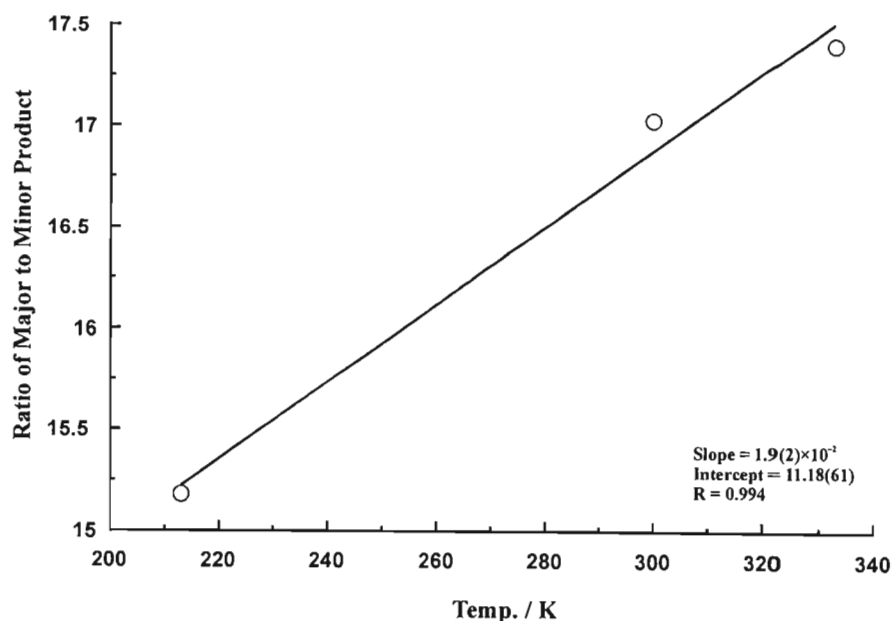
Figure 4.43: Temperature dependence of 'major/minor' product relationship for [Rh(TPP)(edppt)$_2$](SbF$_6$).

Figure 4.43 shows the temperature dependent relationsip between between the 'major' and 'minor' products. The correlation is quite significant, and suggests that the 'major' product ratio increases at a higher temperature in the range shown.

Figure 4.44: **Temperature dependence of 'major/minor' product relationship for [Rh(TPP)(deppt)$_2$](SbF$_6$).**

Figure 4.44 shows the possibility for the opposite relationship to exist between the 'major' and 'minor' products in [Rh(TPP)(deppt)$_2$](SbF$_6$), with an increase in temperature. Even though the correlation is quite poor, an increase in samples may resolve this problem.

4.5 ^{103}Rh NMR Shifts and Rh–P Bond Lengths: The Effects of 3s-Orbital Electron Density and Tolman's Cone Angle.

In order to quantify the effect of alternating substituents on the electron densities and thus Lewis basicity of the phosphorus centers of the phosphine and phosphonite ligands used in this research, use was made of theoretical single-point calculations. Using Hyperchem 6.0 (PM3 model), both a geometry optimization and single-point energy calculation was performed on each ligand.

The s-orbital electron density of the phosphorus center was the orbital under scrutiny since the s-orbital electron density governs the shielding of the nucleus as a result of a node-less

207

wavefunction at the nucleus. The resulting data were compared with the [103]Rh NMR data for the complexes as well as the existing data for the Rh–P bond lengths derived from the structural/crystallographic data obtained in this work, and inserted into Table 4.1. It must be noted, however, that a complete list of both [103]Rh NMR and X-ray structural data for these compounds has not yet been established. The resulting conclusions and graphical representation of trends associated with these two classes of compounds will thus be based on the existing data and will be added to as the research continues and is intended as a mere indication of possible relationships.

From the s-orbital electron density data, the phosphines and phosphonites may be arranged in order of decreasing electron occupation: PPh₃t > Tept > Deppt > Tep > Depp > Edppt > PPh₃ > Edpp. Here it is seen that the rough trend is that the tri-ethoxy/phenoxy phosphonites have higher $3s$ elecron populations followed by the phosphines. However, aside from this, the results follow no further logical pattern.

To investigate whether the s-electron density of the phosphines/phosphonites has any affect on the [103]Rh NMR shifts and thus the Rh nucleus, the s-electron density was plotted against the existing [103]Rh NMR shifts in Figure 4.45. It is noticeable that the possibility may exist for an inverse relationship between s-electron density and Rh shifts, however the plot consisting of five points only is inconclusive. The basic trend in Figure 4.45 illustrates that the results do reflect the expected effects of increased electron density on the central metal ion. This trend is that a low electron density phosphorus center, i.e., a weaker Lewis base, induces a higher-frequency shift of the rhodium nucleus. This probably reflects removal (i.e., deshielding) of electron density from the Rh(III) ion by better π–backbonding to electron deficient phosphonites.

Table 4.1. Summarised 3*s*-Orbital Electron Density, ^{103}Rh NMR Data, Rh–P Bond Lengths as well as Tolman's Cone Angles and Electronic Parameter[230].

Phosphine / Phosphonite	3*s*-Orbital Electron Density[a]	Rh NMR Chemical Shifts[b]	Rh–P Bond Lengths[c]	Tolman's Cone Angle θ[d]	Tolman's Electronic Parameter ν[e]
PPh₃	1.7710	No data	No data	145	2068.9
PPh₃t	1.8277	No data	No data	128	2085.3
Edpp	1.7610	2558	2.4010	140	2066.7
Edppt	1.7734	2413	2.3610	133	2071.6
Depp	1.7757	2456	No data	136	2063.7
Deppt	1.7945	2365	2.3320	116	2074.2
Tep	1.7907	2505	No data	132	2061.7
Tept	1.8057	No data	No data	109	2076.3

[a] Phosphine/Phosphonite geometry optimisation and single point calculations performed with PM3 parameters using Hyperchem 6.0. [b] (ppm); measured at 300 K in CDCl₃. [c] Extracted from X-ray crystallographic data. [d] (°). [e] (cm⁻¹).
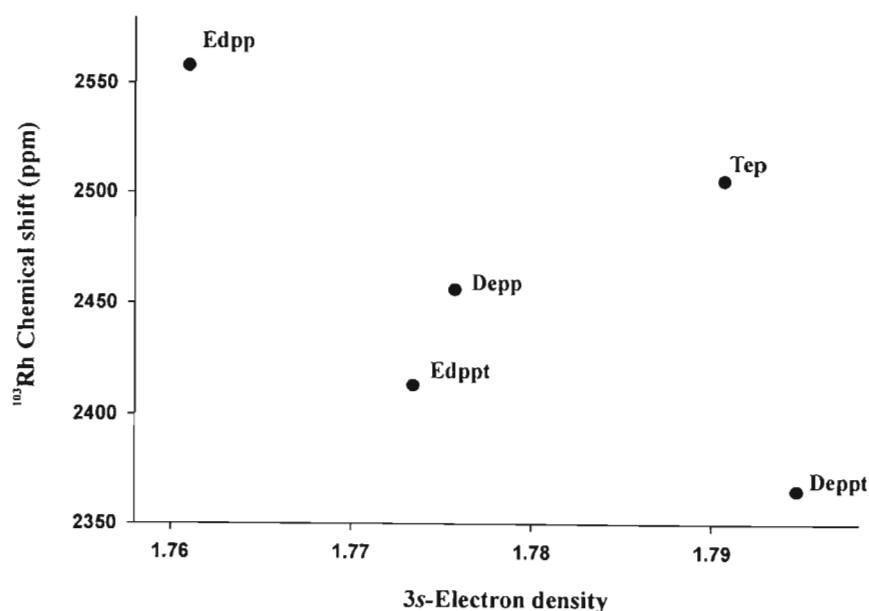
Figure 4.45: Plot of ^{103}Rh chemical shifts *versus* 3*s*-electron density.

Evidence of an interesting relationship may be seen in Figure 4.46, where the *s*-electron density of the phosphine is plotted *versus* the Rh–P bond lengths. Here an inverse relationship is observed where no true relationship was expected. This indicates the significance of the Lewis basicity of the phosphine/phosphonite on the solid-state Rh–P bond lengths. It has been stated

that steric hindrance of the axial phosphines/phosphonites plays a greater role in determining the bond length in phosphorus-based transition metal complexes.[184] Although we require further X-ray structures to establish a definative trend, it appears that σ-donor strength operates in parallel with steric hinderance in determining Rh–P distances in porphyrins; the least hindered ligands are also the better σ-donors.
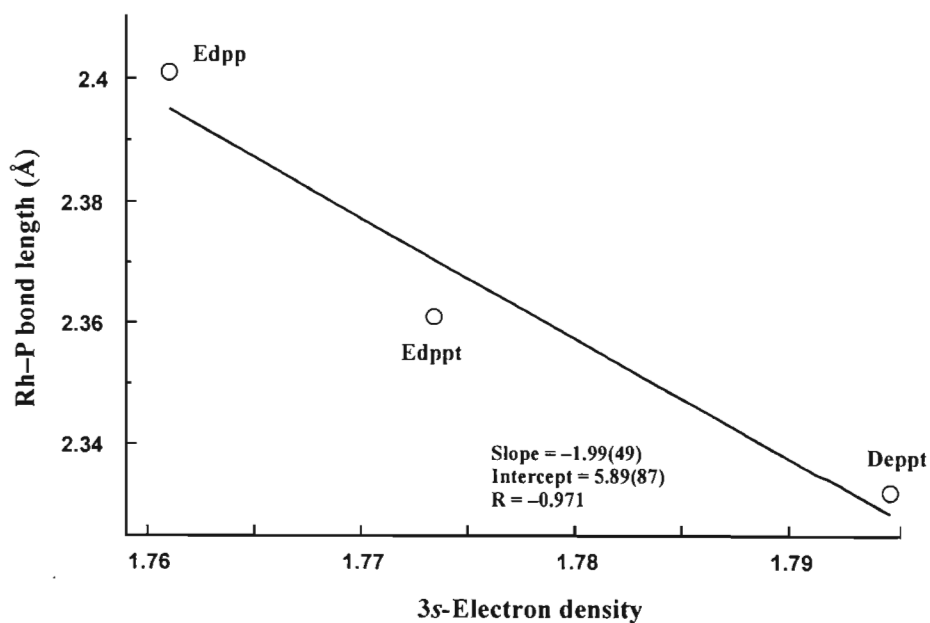
Figure 4.46: Plot of Rh–P bond lengths *versus* 3s-electron density.
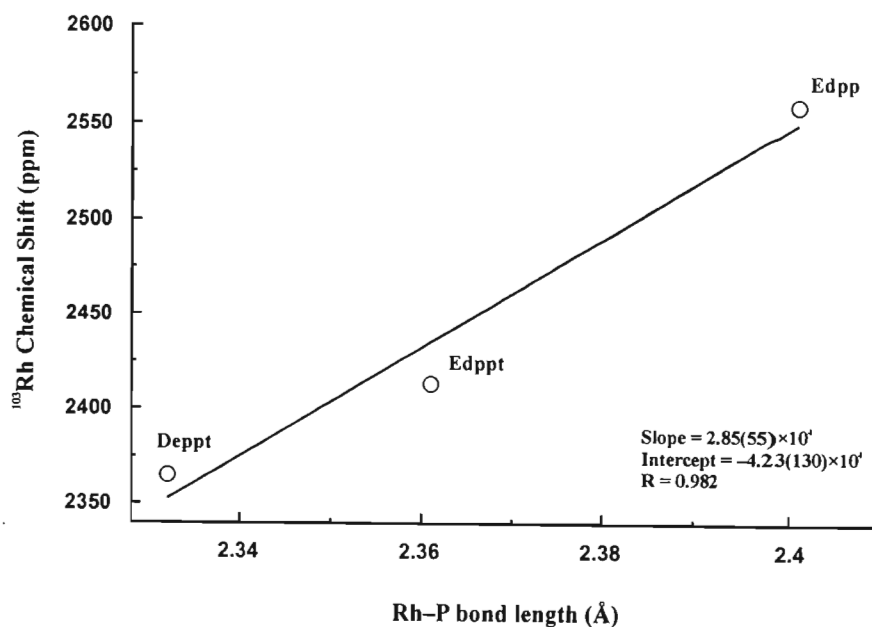
Figure 4.47: Plot of ^{103}Rh chemical shifts *versus* Rh–P bond lengths.

210

A plot of the [103]Rh chemical shifts *versus* the Rh–P bond lengths is shown in Figure 4.47. This plot graphically emphasizes the close relationship between the solid-state bond lengths and the Rh chemical shifts in solution. More importantly, this trend indicates that a stronger σ-donor (shorter Rh–P distance) more effectively shields the Rh nucleus than a weak σ-donor, as might be expected.

In 1977, Chadwick Tolman published a classic review in which he introduced the concept of the "cone angle" to phosphine coordination chemistry.[230] In simplified terms, the cone angle is a measurement of the steric size of a phosphine, in degrees. From his calculations, the phosphines used in this thesis may be arranged in the following order of dereasing steric bulk: PPh$_3$ > Edpp > Depp > Edppt > Tep > PPh$_3$t > Deppt > Tept. This trend is consistent with our earlier assumptions of increased steric contributions from phenyl and alkyl substituents and decreased steric contributions from ethoxy and phenoxy substituents. The effect of the phosphine's cone angle on the [103]Rh chemical shift is inconsistent, as may be observed from the graph in Figure 4.48, and no reliable data can be extracted from it. The rough trend is that the cone angle increase may result in a shift of the [103]Rh resonances to higher frequencies.
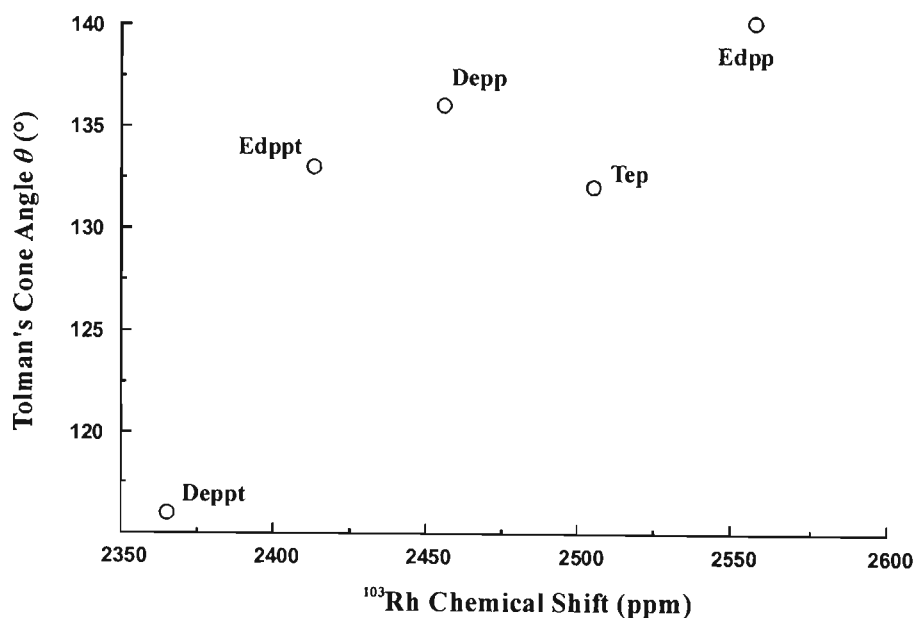
Figure 4.48: Plot of Tolman's cone angle θ *versus* [103]Rh NMR shift.

In his review, Tolman also formally introduced an electronic parameter, ν, as a measure of the σ-donating strength of the phosphine. This value is derived from the stretching frequencies of the carbonyl ligands in the nickel carbonyl complex Ni(CO)$_3$L, where L = phosphine, when the

different phosphines are coordinated to the nickel center. From Tolman's results, the phosphines used in this thesis may be arranged in a decreasing order of σ-donating strength: Tep > Depp > Edpp > PPh$_3$ > Edppt > Deppt > Tept > PPh$_3$t. Immediately noticeable is the distinct difference in the order of the phosphines in this sequence, to those arranged in order of σ-donating strength based on the 3s-orbital electron density theoretical calculations.

However, as is shown in the graph in Figure 4.49 below, there is still no definite trend in the influence of σ-donor strength on the [103]Rh chemical shift. Apart from the Edpp outlier, there does appear to be a trend towards a downfield shift for stronger σ-donor phosphine complexes.
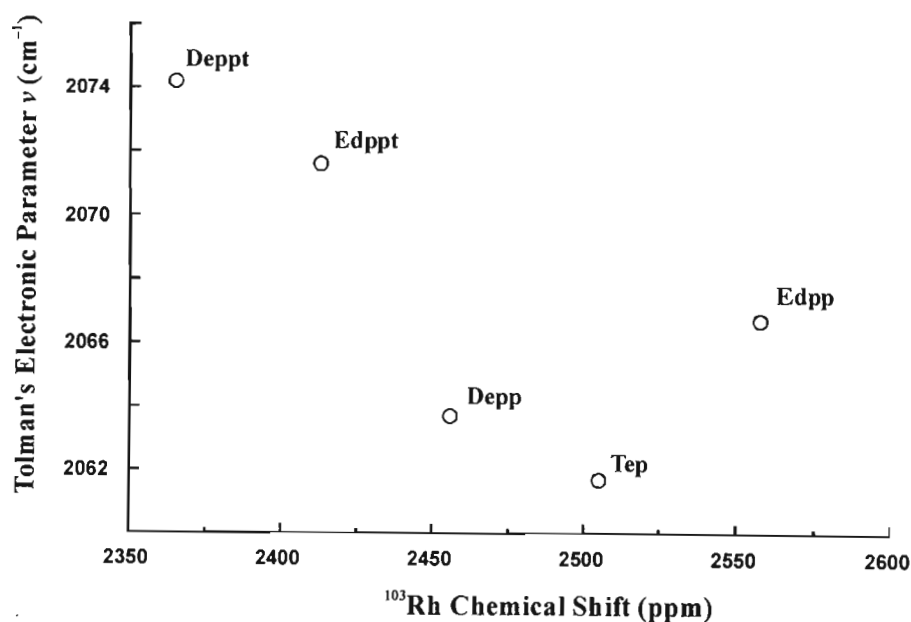
Figure 4.49: Plot of Tolman's electronic parameter v versus [103]Rh NMR shift.

In an attempt to determine which of Tolman's two parameters, i.e., θ or v, plays a more distinct role in governing the rhodium–phosphine bond length, θ and v were plotted against the Rh–P bond length in Figure 4.50 and 4.51, respectively.

Once again, the effect of a lack of data is manifested in these plots and only tentative conclusions on the dependence of the Rh–P bond length on θ and v are possible. The Rh–P bond length does appear to be more rigidly dependant on v than θ, i.e., the Rh–P bond length in bis(phosphine/phosphonite) complexes appears to be more dependant on electronic factors than steric factors. This is more or less expected in these complexes due to the large radius of the rhodium center. Interestingly, as the σ-donor strength of the phosphine increases, the Rh–P bond

212

length increases. The relationship in Figure 4.51 is more linear, and thus appears relatively more conclusive. Specifically, good π-acceptor ligands lead to shorter Rh–P bond distances, consistent with stronger π-backbonding in such complexes.
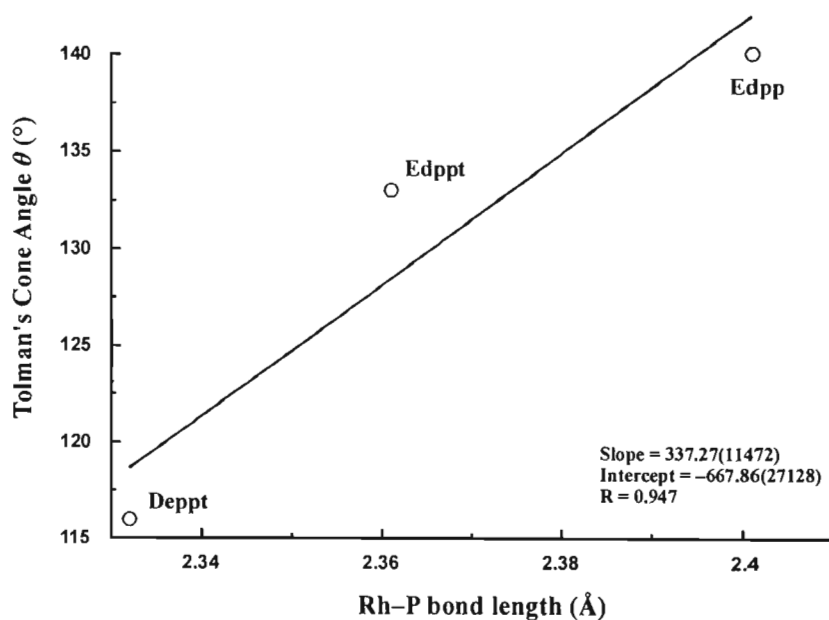
Figure 4.50: Plot of Tolman's cone angle θ *versus* Rh–P bond lengths.
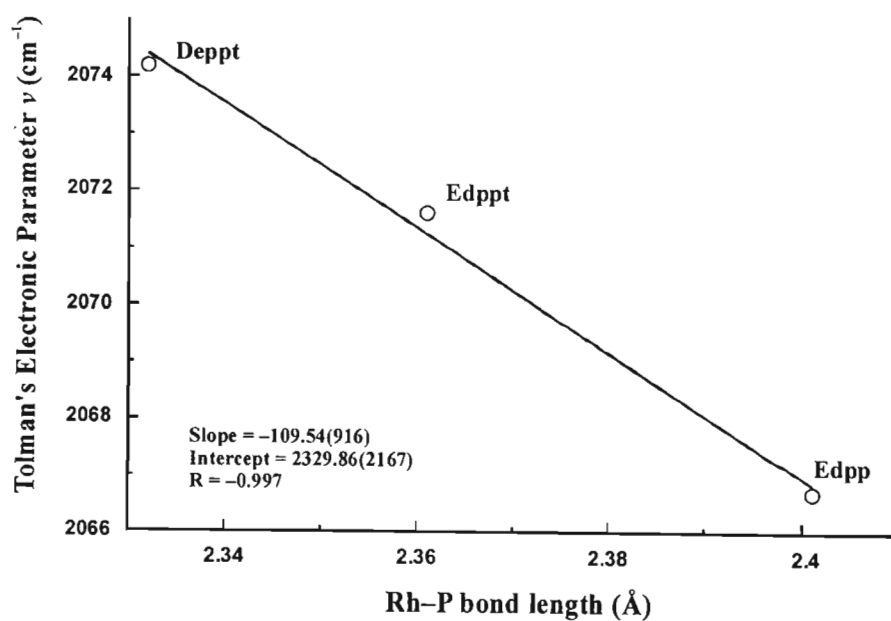
Figure 4.51: Plot of Tolman's electronic parameter v *versus* Rh–P bond lengths.

213

4.6 Experimental

General Information. See Appendix AIII.2.

4.6.1 Synthesis of [Rh(TPP)(edpp)₂](SbF₆)

To [Rh(TPP)Cl] (150 mg, 0.20 mmol) and AgSbF₆ (82 mg, 0.24 mmol) in a 250 ml Schlenk tube under nitrogen was added 50 ml of freshly distilled THF. The solution was allowed to stir for ~12 hr at room temperature. The THF was then removed *in vacuo* and the green-brown solid redissolved in dichloromethane (50 ml). The solution was then filtered, to remove precipitated silver chloride, into a 250 ml Schlenk tube into which edpp (0.82 ml, 4.0 mmol) had been added. The solution was left to stir at room temperature for ~10 min. The purple-red solution was then transferred into 12 Schlenk tubes in ~4 ml portions, and layered with hexane. X-ray-quality crystals were observed after 4 days. Yield: 0.2532 g (92 %).

4.6.2 Single Crystal X-Ray Diffraction Study of [Rh(TPP)(edpp)₂](SbF₆)

As mentioned above, X-ray quality crystals of [Rh(TPP)(edpp)₂](SbF₆) were obtained by slow diffusion of hexane into a CH₂Cl₂ solution of the compound. The crystallographic data and structure refinement details are provided in Table 4.4. The most relevant inter-atomic angles and distances have been averaged and are shown in Figure 4.8. The original bond length and bond angle data have been tabulated in Table AI.6 in Appendix I. The atomic coordinates have been tabulated in Table AII.6 in Appendix II.

Table 4.4. Crystal data and structure refinement for [Rh(TPP)(edpp)$_2$](SbF$_6$)

Identification code	Rhedpp
Empirical formula	C$_{74}$H$_{62}$N$_4$P$_2$RhSbF$_6$Cl$_2$
Formula weight	1478.78
Temperature	259(2) K
Wavelength	0.71073 Å
Crystal system	Monoclinic
Space group	P2$_1$/n
Unit cell dimensions	a = 17.678(5) Å, α = 90°
	b = 17.747(7) Å, β = 106.52(2)°
	c = 22.173(6) Å, γ = 90°
Volume	6669(4) Å^3
Z	4
Density (calculated)	1.473 Mg/m^3
Absorption coefficient	0.843 mm^{-1}
F(000)	2992
Crystal size	0.5 × 0.4 × 0.2 mm
Theta range for data collection	2.08 to 25.00°
Index ranges	$-6 \leq h \leq 20; -1 \leq k \leq 21; -26 \leq l \leq 25$
Reflections collected	14059
Independent reflections	11689 [R(int) = 0.0175]
Reflections observed (>2σ)	9813
Refinement method	Full-matrix least-squares on F^2
Data / restraints / parameters	11689 / 33 / 862
Goodness-of-fit on F^2	0.975
Final R indices [$I > 2\sigma(I)$]	R_1 = 0.0492 wR_2 = 0.1377
R indices (all data)	R_1 = 0.0582 wR_2 = 0.1433
Largest diff. peak and hole	1.096 and -1.230 e Å^{-3}

4.6.3 Synthesis of [Rh(TPP)(edppt)₂](SbF₆)

To [Rh(TPP)Cl] (150 mg, 0.20 mmol) and AgSbF₆ (82 mg, 0.24 mmol) in a 250 ml Schlenk tube under nitrogen was added 50 ml of freshly distilled THF. The solution was allowed to stir for ~12 hr at room temperature. The THF was then removed *in vacuo* and the green-brown solid redissolved in dichloromethane (50 ml). The solution was then filtered, to remove precipitated silver chloride, into a 250 ml Schlenk tube into which edppt (0.86 ml, 4.0 mmol) had been added. The solution was left to stir at room temperature for ~10 min. The purple-red solution was then transferred into 12 Schlenk tubes in ~4 ml portions, and layered with hexane. X-ray-quality crystals were observed after 4 days. Yield: 0.2472 g (88 %).

4.6.4 Single Crystal X-Ray Diffraction Study of [Rh(TPP)(edppt)₂](SbF₆)

As mentioned above, X-ray quality crystals of [Rh(TPP)(edppt)₂](SbF₆) were obtained by slow diffusion of hexane into a CH_2Cl_2 solution of the compound. The crystallographic data and structure refinement details are provided in Table 4.5. The most relevant interatomic angles and distances have been averaged and are shown in Figure 4.21. The original bond length and bond angle data have been tabulated in Table AI.7 in Appendix I. The atomic coordinates have been tabulated in Table AII.7 in Appendix II.

Table 4.5. Crystal data and structure refinement for [Rh(TPP)(edppt)₂](SbF₆)

Identification code	Rhedppt2
Empirical formula	$C_{72}H_{58}N_4O_2P_2RhSbF_6Cl_4$
Formula weight	1553.62
Temperature	219(2) K
Wavelength	0.70930 Å
Crystal system	Monoclinic
Space group	$P2_1/c$
Unit cell dimensions	$a = 17.537(5)$ Å, $\alpha = 90°$
	$b = 17.556(5)$ Å, $\beta = 110.32(2)°$
	$c = 24.285(7)$ Å, $\gamma = 90°$
Volume	7012(3) Å³
Z	4
Density (calculated)	1.472 Mg/m³
Absorption coefficient	0.882 mm⁻¹
$F(000)$	3128
Crystal size	$0.5 \times 0.4 \times 0.2$ mm
Theta range for data collection	2.10 to 24.92°
Index ranges	$-10 \leq h \leq 20; -8 \leq k \leq 20; -28 \leq l \leq 27$
Reflections collected	13676
Independent reflections	11637 [R(int) = 0.0158]
Reflections observed (>2σ)	9037
Refinement method	Full-matrix least-squares on F^2
Data / restraints / parameters	11637 / 0 / 847
Goodness-of-fit on F^2	1.302
Final R indices [$I > 2\sigma(I)$]	$R_1 = 0.0555$ $wR_2 = 0.1779$
R indices (all data)	$R_1 = 0.0706$ $wR_2 = 0.1884$
Largest diff. peak and hole	1.528 and -0.894 e Å⁻³

4.6.5 Synthesis of [Rh(TPP)(deppt)₂](SbF₆)

To [Rh(TPP)Cl] (150 mg, 0.20 mmol) and AgSbF₆ (82 mg, 0.24 mmol) in a 250 ml Schlenk tube under nitrogen was added 50 ml of freshly distilled THF. The solution was allowed to stir for ~12 hr at room temperature. The THF was then removed *in vacuo* and the red-brown solid redissolved in dichloromethane (50 ml). The solution was then filtered, to remove precipitated silver chloride, into a 250 ml Schlenk tube into which deppt (0.77 ml, 4.0 mmol) had been added. The solution was left to stir at room temperature for ~10 min. The purple-red solution was then transferred into 12 Schlenk tubes in ~4 ml portions, and layered with hexane. X-ray-quality crystals were observed after 4 days. Yield: 0.2459 g (91 %).

4.6.6 Single Crystal X-Ray Diffraction Study of [Rh(TPP)(deppt)₂](SbF₆)

As mentioned above, X-ray quality crystals of [Rh(TPP)(deppt)₂](SbF₆) were obtained by slow diffusion of hexane into a CH_2Cl_2 solution of the compound. The crystallographic data and structure refinement details are provided in Table 4.6. The most relevant inter-atomic angles and distances have been averaged and are shown in Figures 4.32a and 4.32b. The original bond length and bond angle data have been tabulated in Table AI.8 in Appendix I. The atomic coordinates have been tabulated in Table AII.8 in Appendix II.

Table 4.6. Crystal data and structure refinement for [Rh(TPP)(deppt)₂](SbF₆).

Identification code	Rhdeppt
Empirical formula	$C_{64}H_{58}N_4O_4P_2RhSbF_6$
Formula weight	1347.74
Temperature	219(2) K
Wavelength	0.70930 Å
Crystal system	Monoclinic
Space group	$P2_1/c$
Unit cell dimensions	$a = 14.772(5)$ Å, $\alpha = 90°$
	$b = 16.729(5)$ Å, $\beta = 106.73(3)°$
	$c = 25.082(8)$ Å, $\gamma = 90°$
Volume	5936(3) Å³
Z	4
Density (calculated)	1.508 Mg/m³
Absorption coefficient	0.857 mm⁻¹
$F(000)$	2728
Crystal size	$0.5 \times 0.4 \times 0.2$ mm
Theta range for data collection	2.08 to 24.94°
Index ranges	$-6 \leq h \leq 17; -8 \leq k \leq 19; -29 \leq l \leq 28$
Reflections collected	12685
Independent reflections	10394 [R(int) = 0.0254]
Reflections observed (>2σ)	7524
Refinement method	Full-matrix least-squares on F^2
Data / restraints / parameters	10394 / 0 / 741
Goodness-of-fit on F^2	1.338
Final R indices [$I > 2\sigma(I)$]	$R_1 = 0.0572$ $wR_2 = 0.1752$
R indices (all data)	$R_1 = 0.0795$ $wR_2 = 0.1870$
Largest diff. peak and hole	1.848 and -1.112 e Å⁻

CHAPTER FIVE

CONCLUSIONS AND FUTURE WORK

The topic of phosphine complexes of the transition metals has been exhaustively studied to date. However, phosphine and phosphonite complexes of metalloporpyrins have largely been ignored and, as such, this thesis has attempted to initiate research into such systems and has not intended to cover the whole field.

Manganese Phosphine and Phosphonite Metalloporphyrins. The bis(phosphine) complex of Mn(III), $[Mn(TPP)(PPh_3)_2](SbF_6)$, was successfully synthesized and its X-ray crystal structure determined. In an attempt to synthesize $[Mn(TPP)(PPh_3t)_2](SbF_6)$, for the sake of comparison, an O-donor complex of $[Mn(TPP)\{(O)PH(OPh)_2\}](SbF_6)$ was instead isolated, and its X-ray crystal structure determined. The latter complex highlighted the relative difficulties in the synthesis of manganese bis(phosphine) and bis(phosphonite) metalloporphyrins. Since time did not permit distillation of the range of phosphines used, and the resulting crystallization attempts were unsuccessful, this research area was left to a later date. This would be an interesting research area for future expansion as it is still largely unexplored, although the paramagnetic manganese(III) centre does make the study of these systems difficult (e.g., by NMR spectroscopy).

Cobalt Phosphine and Phosphonite Metalloporphyrins. Two bis(phosphine) complexes of Co(III), namely $[Co(TPP)(depp)_2](SbF_6)$ and $[Co(TPP)(edpp)_2](SbF_6)$, were synthesized and their X-ray crystal structures determined. One bis(phosphonite) complex, $[Co(TPP)(deppt)_2](SbF_6)$, was successfully synthesized and its X-ray crystal structure determined.

With the limited X-ray structural data available, a possible dependence of the Co–P bond length on the phosphine/phosphonite cone angle, rather than on electronic factors, has been determined. However, the range of bis(phosphine) and bis(phosphonite) complexes of $[Co(TPP)]^+$ needs to be expanded, with more X-ray crystal structures of such systems. This would clearly aid in furthering our understanding of the coordination chemistry of cobalt porphyrins with P-donor ligands and indeed allow verification of the novel trend uncovered in this work.

Rhodium Phosphine and Phosphonite Metalloporphyrins. One rhodium(III) bis(phosphine) complex was successfully synthesized and its X-ray crystal structure determined. Two bis(phosphonite) complexes of [Rh(TPP)(edppt)$_2$](SbF$_6$) and [Rh(TPP)(deppt)$_2$](SbF$_6$) were successfully synthesized and their X-ray crystal structures determined.

The majority of the work in this thesis was centered around the rhodium(III) porphyrins. These complexes produce unprecedented indirect ^{103}Rh NMR spectral collection, made possible by the presence of the coordinated ^{31}P center. Despite numerous attempts to increase the number of X-ray crystal structures of Rh(III) porphyrins in this chapter, our efforts were thwarted by the constant contaminant [Rh(TPP)(NHMe$_2$)](SbF$_6$), which preferentially crystallized. This appears to have originated from the metallation of the H$_2$TPP in DMF. Furthermore, the substitution of the NHMe$_2$ ligands proved to be near-impossible from subsequent cleaning attempts. The major weakness in this chapter is the shortage of Rh–P bond length data due to the shortage of X-ray crystal structures, and this should, without a doubt, be improved on in future work. There does appear, however, to be a more rigid dependence of the Rh–P bond length on the electronic properties of the phosphorous center of the phosphine/phosphonite as opposed to its steric properties or size.

Generally, the ligand substitution thermodynamics of a range of phosphine/phosphonite complexes needs to be studied for all three metals in order to determine the relative binding affinities of each phosphine/phosphonite ligand. It would be interesting to compare these binding constants with the phosphine and phosphonite affinity constant data that Tolman[230] and Wayland[212] have published.

Another interesting area of research suggested for future work on these systems is a study of the electrochemistry of the metal centers of these porphyrins. In particular, it would be interesting to establish if a relationship exists between the reduction potential of the metal and the electronic or donor character of the P-donor ligand.

Also of interest are the distorted conformations of the porphyrin cores in several of the complexes that were crystallized. Molecular modeling of these systems could be employed to understand the experimentally observed conformations in these metalloporphyrins and why they result. A force field for rhodium(III) porphyrins would, however, need to be developed.

APPENDIX I: TABLES OF INTERATOMIC DISTANCES AND ANGLES

Table AI.1: Bond lengths [Å] and angles [°] for [Mn(TPP)(PPh$_3$)$_2$](SbF$_6$)

Bond	Length / Å	Bond	Length / Å
Mn–N(2)	1.995(5)	Mn–N(4)	1.996(5)
Mn–N(1)	1.998(6)	Mn–N(3)	2.004(6)
Mn–P(1)	3.094(2)	Mn–P(2)	3.082(2)
N(1)–CA1	1.378(10)	N(1)–CA2	1.405(8)
N(2)–CA3	1.379(8)	N(2)–CA4	1.400(10)
N(3)–CA5	1.355(9)	N(3)–CA6	1.407(8)
N(4)–CA8	1.359(10)	N(4)–CA7	1.394(8)
CA1–CM4	1.403(9)	CA1–CB1	1.426(11)
CA2–CM1	1.362(11)	CA2–CB2	1.384(13)
CA3–CM1	1.390(12)	CA3–CB3	1.436(11)
CA4–CM2	1.385(10)	CA4–CB4	1.442(9)
CA5–CM2	1.387(9)	CA5–CB5	1.457(10)
CA6–CM3	1.396(10)	CA6–CB6	1.408(11)
CA7–CM3	1.377(11)	CA7–CB7	1.447(10)
CA8–CM4	1.387(10)	CA8–CB8	1.425(8)
CB1–CB2	1.367(11)	CB3–CB4	1.334(11)
CB5–CB6	1.347(10)	CB7–CB8	1.296(11)
CM1–C(11)	1.502(9)	CM2–C(21)	1.519(10)
CM3–C(31)	1.526(9)	CM4–C(41)	1.490(10)
C(11)–C(12)	1.364(11)	C(11)–C(16)	1.394(10)
C(12)–C(13)	1.398(10)	C(13)–C(14)	1.359(13)
C(14)–C(15)	1.320(13)	C(15)–C(16)	1.369(11)
C(21)–C(26)	1.332(14)	C(21)–C(22)	1.363(13)
C(22)–C(23)	1.43(2)	C(23)–C(24)	1.24(3)
C(24)–C(25)	1.36(3)	C(25)–C(26)	1.342(17)
C(31)–C(32)	1.351(10)	C(31)–C(36)	1.389(11)
C(32)–C(33)	1.394(11)	C(33)–C(34)	1.374(15)

Bond	Length / Å	Bond	Length / Å
C(34)–C(35)	1.343(16)	C(35)–C(36)	1.384(12)
C(41)–C(46)	1.357(12)	C(41)–C(42)	1.385(12)
C(42)–C(43) ·	1.395(14)	C(43)–C(44)	1.385(16)
C(44)–C(45)	1.308(14)	C(45)–C(46)	1.417(15)
P(1)–C(61)	1.823(7)	P(1)–C(51)	1.834(9)
P(1)–C(71)	1.846(8)	C(51)–C(56)	1.375(11)
C(51)–C(52)	1.382(13)	C(52)–C(53)	1.405(16)
C(53)–C(54)	1.361(14)	C(54)–C(55)	1.402(17)
C(55)–C(56)	1.387(16)	C(61)–C(62)	1.339(10)
C(61)–C(66)	1.357(13)	C(62)–C(63)	1.397(14)
C(63)–C(64)	1.314(16)	C(64)–C(65)	1.359(16)
C(65)–C(66)	1.345(13)	C(71)–C(76)	1.362(14)
C(71)–C(72)	1.368(13)	C(72)–C(73)	1.446(15)
C(73)–C(74)	1.33(2)	C(74)–C(75)	1.371(18)
C(75)–C(76)	1.401(14)	P(2)–C(91)	1.804(12)
P(2)–C(101) ·	1.807(13)	P(2)–C(81)	1.843(8)
P(2)–C(201)	1.866(10)	C(81)–C(86)	1.379(12)
C(81)–C(82)	1.392(12)	C(82)–C(83)	1.377(12)
C(83)–C(84)	1.355(15)	C(84)–C(85)	1.340(16)
C(85)–C(86)	1.369(11)	C(91)–C(92)	1.366(15)
C(91)–C(96)	1.401(15)	C(92)–C(93)	1.384(19)
C(93)–C(94)	1.30(2)	C(94)–C(95)	1.38(2)
C(95)–C(96)	1.48(2)	C(101)–C(102)	1.3900
C(101)–C(106)	1.3900	C(102)–C(103)	1.3900
C(103)–C(104)	1.3900	C(104)–C(105)	1.3900
C(105)–C(106)	1.3900	C(201)–C(202)	1.3900
C(201)–C(206)	1.3900	C(202)–C(203)	1.3900
C(203)–C(204)	1.3900	C(204)–C(205)	1.3900
C(205)–C(206)	1.3900	Sb–F(3)	1.780(10)
Sb–F(5)	1.807(8)	Sb–F(1)	1.814(10)
Sb–F(4)	1.826(9)	Sb–F(2)	1.834(9)
Sb–F(6)	1.838(11)		

Angle	Degree / °	Angle	Degree / °
N(2)–Mn–N(4)	177.7(2)	N(2)–Mn–N(1)	88.9(2)
N(4)–Mn–N(1)	89.6(2)	N(2)–Mn–N(3)	90.9(2)
N(4)–Mn–N(3)	90.7(2)	N(1)–Mn–N(3)	179.6(3)
CA1–N(1)–CA2	105.0(6)	CA1–N(1)–Mn	127.3(4)
CA2–N(1)–Mn	127.3(6)	CA3–N(2)–CA4	106.5(5)
CA3–N(2)–Mn	128.3(5)	CA4–N(2)–Mn	125.1(4)
CA5–N(3)–CA6	106.8(6)	CA5–N(3)–Mn	126.7(4)
CA6–N(3)–Mn	126.5(5)	CA8–N(4)–CA7	105.2(5)
CA8–N(4)–Mn	127.8(4)	CA7–N(4)–Mn	126.8(5)
N(1)–CA1–CM4	125.7(7)	N(1)–CA1–CB1	109.8(5)
CM4–CA1–CB1	124.3(8)	CM1–CA2–CB2	124.2(7)
CM1–CA2–N(1)	125.4(8)	CB2–CA2–N(1)	110.3(7)
N(2)–CA3–CM1	125.3(7)	N(2)–CA3–CB3	108.8(7)
CM1–CA3–CB3	126.0(6)	CM2–CA4–N(2)	126.8(6)
CM2–CA4–CB4	124.5(7)	N(2)–CA4–CB4	108.6(6)
N(3)–CA5–CM2	126.9(6)	N(3)–CA5–CB5	108.9(5)
CM2–CA5–CB5	124.2(7)	CM3–CA6–N(3)	124.6(7)
CM3–CA6–CB6	126.1(6)	N(3)–CA6–CB6	109.0(6)
CM3–CA7–N(4)	125.6(6)	CM3–CA7–CB7	124.9(6)
N(4)–CA7–CB7	109.5(7)	N(4)–CA8–CM4	126.5(6)
N(4)–CA8–CB8	109.1(6)	CM4–CA8–CB8	124.4(7)
CB2–CB1–CA1	106.9(8)	CB1–CB2–CA2	108.0(7)
CB4–CB3–CA3	108.7(6)	CB3–CB4–CA4	107.4(7)
CB6–CB5–CA5	107.1(7)	CB5–CB6–CA6	108.2(6)
CB8–CB7–CA7	106.0(6)	CB7–CB8–CA8	110.2(7)
CA2–CM1–CA3	124.1(6)	CA2–CM1–C(11)	120.5(8)
CA3–CM1–C(11)	115.4(7)	CA4–CM2–CA5	123.2(7)
CA4–CM2–C(21)	116.5(6)	CA5–CM2–C(21)	120.2(6)
CA7–CM3–CA6	125.2(6)	CA7–CM3–C(31)	119.3(6)
CA6–CM3–C(31)	115.5(7)	CA8–CM4–CA1	123.0(7)
CA8–CM4–C(41)	119.7(6)	CA1–CM4–C(41)	117.3(7)
C(12)–C(11)–C(16)	117.0(7)	C(12)–C(11)–CM1	122.3(7)

Angle	Degree / °	Angle	Degree / °
C(16)–C(11)–CM1	120.6(7)	C(11)–C(12)–C(13)	120.5(8)
C(14)–C(13)–C(12)	120.2(9)	C(15)–C(14)–C(13)	119.8(7)
C(14)–C(15)–C(16)	121.2(8)	C(15)–C(16)–C(11)	121.1(9)
C(26)–C(21)–C(22)	120.5(10)	C(26)–C(21)–CM2	120.7(8)
C(22)–C(21)–CM2	118.5(9)	C(21)–C(22)–C(23)	114.5(15)
C(24)–C(23)–C(22)	125.3(18)	C(23)–C(24)–C(25)	117.6(16)
C(26)–C(25)–C(24)	121.9(16)	C(21)–C(26)–C(25)	119.9(13)
C(32)–C(31)–C(36)	119.6(7)	C(32)–C(31)–CM3	121.5(7)
C(36)–C(31)–CM3	118.5(7)	C(31)–C(32)–C(33)	121.0(9)
C(34)–C(33)–C(32)	119.1(10)	C(35)–C(34)–C(33)	119.8(8)
C(34)–C(35)–C(36)	121.7(9)	C(35)–C(36)–C(31)	118.5(9)
C(46)–C(41)–C(42)	118.2(9)	C(46)–C(41)–CM4	121.4(8)
C(42)–C(41)–CM4	120.3(8)	C(41)–C(42)–C(43)	119.4(10)
C(44)–C(43)–C(42)	120.8(9)	C(45)–C(44)–C(43)	119.6(10)
C(44)–C(45)–C(46)	120.5(10)	C(41)–C(46)–C(45)	121.3(9)
C(61)–P(1)–C(51)	104.8(4)	C(61)–P(1)–C(71)	102.5(4)
C(51)–P(1)–C(71)	104.3(4)	C(56)–C(51)–C(52)	118.3(9)
C(56)–C(51)–P(1)	118.5(7)	C(52)–C(51)–P(1)	123.0(7)
C(51)–C(52)–C(53)	121.8(9)	C(54)–C(53)–C(52)	118.9(11)
C(53)–C(54)–C(55)	120.3(11)	C(56)–C(55)–C(54)	119.6(9)
C(51)–C(56)–C(55)	121.1(10)	C(62)–C(61)–C(66)	117.1(8)
C(62)–C(61)–P(1)	120.3(7)	C(66)–C(61)–P(1)	122.6(6)
C(61)–C(62)–C(63)	120.5(10)	C(64)–C(63)–C(62)	120.1(11)
C(63)–C(64)–C(65)	120.5(10)	C(66)–C(65)–C(64)	118.4(11)
C(65)–C(66)–C(61)	123.3(10)	C(76)–C(71)–C(72)	120.5(9)
C(76)–C(71)–P(1)	115.7(7)	C(72)–C(71)–P(1)	123.8(8)
C(71)–C(72)–C(73)	116.7(13)	C(74)–C(73)–C(72)	122.0(12)
C(73)–C(74)–C(75)	120.7(10)	C(74)–C(75)–C(76)	118.1(14)
C(71)–C(76)–C(75)	121.9(11)	C(91)–P(2)–C(101)	107.3(8)
C(91)–P(2)–C(81)	103.7(4)	C(101)–P(2)–C(81)	105.3(7)
C(91)–P(2)–C(201)	100.3(9)	C(101)–P(2)–C(201)	8.2(12)
C(81)–P(2)–C(201)	103.4(7)	C(86)–C(81)–C(82)	119.3(7)

225

Angle	Degree / °	Angle	Degree / °
C(86)–C(81)–P(2)	118.0(7)	C(82)–C(81)–P(2)	122.7(7)
C(83)–C(82)–C(81)	117.6(9)	C(84)–C(83)–C(82)	123.0(10)
C(85)–C(84)–C(83)	118.4(9)	C(84)–C(85)–C(86)	121.6(11)
C(85)–C(86)–C(81)	119.9(9)	C(96)–C(91)–P(2)	123.4(10)
C(91)–C(92)–C(93)	124.0(14)	C(94)–C(93)–C(92)	119.2(17)
C(93)–C(94)–C(95)	122.7(17)	C(94)–C(95)–C(96)	118.5(14)
C(91)–C(96)–C(95)	117.4(14)	C(102)–C(101)–C(106)	120.0
C(102)–C(101)–P(2)	112.8(11)	C(106)–C(101)–P(2)	127.2(11)
C(103)–C(102)–C(101)	120.0	C(102)–C(103)–C(104)	120.0
C(103)–C(104)–C(105)	120.0	C(104)–C(105)–C(106)	120.0
C(105)–C(106)–C(101)	120.0	C(202)–C(201)–C(206)	120.0
C(202)–C(201)–P(2)	118.9(9)	C(206)–C(201)–P(2)	121.0(9)
C(201)–C(202)–C(203)	120.0	C(204)–C(203)–C(202)	120.0
C(203)–C(204)–C(205)	120.0	C(206)–C(205)–C(204)	120.0
C(205)–C(206)–C(201)	120.0	F(3)–Sb–F(5)	86.0(5)
F(3)–Sb–F(1)	84.9(6)	F(5)–Sb–F(1)	91.7(5)
F(3)–Sb–F(4)	96.4(6)	F(5)–Sb–F(4)	90.7(4)
F(1)–Sb–F(4)	177.3(4)	F(3)–Sb–F(2)	86.3(6)
F(5)–Sb–F(2)	171.4(7)	F(1)–Sb–F(2)	91.6(6)
F(4)–Sb–F(2)	86.2(5)	F(3)–Sb–F(6)	175.4(5)
F(5)–Sb–F(6)	90.3(7)	F(1)–Sb–F(6)	92.4(6)
F(4)–Sb–F(6)	86.4(6)	F(2)–Sb–F(6)	97.5(7)

Table AI.2: Bond lengths [Å] and angles [°] for [Mn(TPP){(O)PH(OPh)₂}](SbF₆)

Bond	Length / Å	Bond	Length / Å
Mn–N(1)	1.998(3)	Mn–N(3)	2.000(3)
Mn–N(4)	2.002(4)	Mn–N(2)	2.006(3)
Mn–O(1)	2.122(3)	P(1)–O(1)	1.440(4)
P(1)–O(3)	1.566(4)	P(1)–O(2)	1.568(5)
N(1)–CA2	1.371(5)	N(1)–CA1	1.374(5)
N(2)–CA3	1.379(5)	N(2)–CA4	1.384(5)
N(3)–CA5	1.381(6)	N(3)–CA6	1.382(6)
N(4)–CA8	1.383(6)	N(4)–CA7	1.394(5)
CA1–CM4	1.392(6)	CA1–CB1	1.433(6)
CA2–CM1	1.408(6)	CA2–CB2	1.413(6)
CA3–CM1	1.364(6)	CA3–CB3	1.438(6)
CA4–CM2	1.387(6)	CA4–CB4	1.426(6)
CA5–CM2	1.394(6)	CA5–CB5	1.422(6)
CA6–CM3	1.390(7)	CA6–CB6	1.429(7)
CA7–CM3	1.376(7)	CA7–CB7	1.400(7)
CA8–CM4	1.375(6)	CA8–CB8	1.433(6)
CB1–CB2	1.318(7)	CB3–CB4	1.327(6)
CB5–CB6	1.331(7)	CB7–CB8	1.326(8)
CM1–C(11)	1.520(6)	CM2–C(21)	1.493(6)
CM3–C(31)	1.500(7)	CM4–C(41)	1.523(6)
O(2)–C(51)	1.396(7)	O(3)–C(61)	1.421(8)
C(11)–C(16)	1.362(7)	C(11)–C(12)	1.377(7)
C(12)–C(13)	1.380(7)	C(13)–C(14)	1.385(10)
C(14)–C(15)	1.329(10)	C(15)–C(16)	1.383(7)
C(21)–C(26)	1.379(7)	C(21)–C(22)	1.382(7)
C(22)–C(23)	1.383(8)	C(23)–C(24)	1.358(9)
C(24)–C(25)	1.371(8)	C(25)–C(26)	1.369(8)
C(31)–C(32)	1.342(11)	C(31)–C(36)	1.375(11)
C(32)–C(33)	1.334(10)	C(33)–C(34)	1.337(19)
C(34)–C(35)	1.417(18)	C(35)–C(36)	1.440(12)

Bond	Length / Å	Bond	Length / Å
C(42)–C(43)	1.401(8)	C(43)–C(44)	1.361(9)
C(44)–C(45)	1.373(9)	C(45)–C(46)	1.419(7)
C(51)–C(52)	1.289(12)	C(51)–C(56)	1.390(11)
C(52)–C(53)	1.310(17)	C(53)–C(54)	1.33(2)
C(54)–C(55)	1.219(19)	C(55)–C(56)	1.367(13)
C(61)–C(66)	1.370(10)	C(61)–C(62)	1.393(10)
C(62)–C(63)	1.403(11)	C(63)–C(64)	1.294(13)
C(64)–C(65)	1.330(14)	C(65)–C(66)	1.411(11)
Sb(1)–F(6)	1.776(8)	Sb(1)–F(3)	1.783(6)
Sb(1)–F(2)	1.801(7)	Sb(1)–F(1)	1.801(6)
Sb(1)–F(4)	1.818(6)	Sb(1)–F(5)	1.863(6)

Angle	Degree / °	Angle	Degree / °
N(1)–Mn–N(3)	171.77(16)	N(1)–Mn–N(4)	89.79(14)
N(3)–Mn–N(4)	89.79(15)	N(1)–Mn–N(2)	89.52(14)
N(3)–Mn–N(2)	89.24(14)	N(4)–Mn–N(2)	168.40(15)
N(1)–Mn–O(1)	92.69(15)	N(3)–Mn–O(1)	95.50(15)
N(4)–Mn–O(1)	98.16(15)	N(2)–Mn–O(1)	93.44(15)
O(1)–P(1)–O(3)	115.3(3)	O(1)–P(1)–O(2)	107.7(3)
O(3)–P(1)–O(2)	107.9(3)	CA2–N(1)–CA1	105.3(3)
CA2–N(1)–Mn	126.5(3)	CA1–N(1)–Mn	126.2(3)
CA3–N(2)–CA4	106.6(3)	CA3–N(2)–Mn	126.2(3)
CA4–N(2)–Mn	127.1(3)	CA5–N(3)–CA6	105.8(3)
CA5–N(3)–Mn	126.9(3)	CA6–N(3)–Mn	125.3(3)
CA8–N(4)–CA7	105.2(4)	CA8–N(4)–Mn	127.2(3)
CA7–N(4)–Mn	127.6(3)	N(1)–CA1–CM4	125.9(4)
N(1)–CA1–CB1	109.3(4)	CM4–CA1–CB1	124.8(4)
N(1)–CA2–CM1	124.0(4)	N(1)–CA2–CB2	109.9(4)
CM1–CA2–CB2	126.0(4)	CM1–CA3–N(2)	125.8(4)
CM1–CA3–CB3	125.5(4)	N(2)–CA3–CB3	108.6(4)
N(2)–CA4–CM2	125.8(4)	N(2)–CA4–CB4	108.4(4)

Angle	Degree / °	Angle	Degree / °
CM2–CA4–CB4	125.6(4)	N(3)–CA5–CM2	125.3(4)
N(3)–CA5–CB5	109.3(4)	CM2–CA5–CB5	125.3(4)
N(3)–CA6–CM3	126.2(4)	N(3)–CA6–CB6	109.1(4)
CM3–CA6–CB6	124.6(4)	CM3–CA7–N(4)	124.4(4)
CM3–CA7–CB7	125.4(4)	CM4–CA8–CB8	125.8(4)
N(4)–CA8–CB8	108.8(4)	CB2–CB1–CA1	107.3(4)
CB1–CB2–CA2	108.1(4)	CB4–CB3–CA3	107.5(4)
CB3–CB4–CA4	108.6(4)	CB6–CB5–CA5	108.0(4)
CB5–CB6–CA6	107.7(4)	CB8–CB7–CA7	108.5(4)
CB7–CB8–CA8	107.8(5)	CA3–CM1–CA2	124.3(4)
CA3–CM1–C(11)	118.5(4)	CA2–CM1–C(11)	117.2(4)
CA4–CM2–CA5	123.3(4)	CA4–CM2–C(21)	118.5(4)
CA5–CM2–C(21)	118.0(4)	CA7–CM3–CA6	124.3(4)
CA7–CM3–C(31)	118.4(4)	CA6–CM3–C(31)	117.2(4)
CA8–CM4–CA1	124.0(4)	CA8–CM4–C(41)	118.5(4)
CA1–CM4–C(41)	117.4(4)	P(1)–O(1)–Mn	146.9(2)
C(51)–O(2)–P(1)	124.8(5)	C(61)–O(3)–P(1)	123.6(4)
C(16)–C(11)–C(12)	119.0(4)	C(16)–C(11)–CM1	122.0(4)
C(12)–C(11)–CM1	119.0(4)	C(11)–C(12)–C(13)	120.6(5)
C(12)–C(13)–C(14)	118.6(6)	C(15)–C(14)–C(13)	121.0(5)
C(14)–C(15)–C(16)	120.3(6)	C(11)–C(16)–C(15)	120.5(6)
C(26)–C(21)–C(22)	117.8(5)	C(26)–C(21)–CM2	122.8(4)
C(22)–C(21)–CM2	119.3(4)	C(21)–C(22)–C(23)	121.3(6)
C(24)–C(23)–C(22)	119.4(6)	C(23)–C(24)–C(25)	120.4(5)
C(26)–C(25)–C(24)	120.1(5)	C(25)–C(26)–C(21)	121.0(5)
C(32)–C(31)–C(36)	118.6(7)	C(32)–C(31)–CM3	121.9(7)
C(36)–C(31)–CM3	119.5(7)	C(33)–C(32)–C(31)	125.4(11)
C(32)–C(33)–C(34)	118.6(13)	C(33)–C(34)–C(35)	121.4(9)
C(34)–C(35)–C(36)	117.1(11)	C(31)–C(36)–C(35)	118.9(10)
C(42)–C(41)–C(46)	122.2(5)	C(42)–C(41)–CM4	119.7(5)
C(46)–C(41)–CM4	118.1(5)	C(41)–C(42)–C(43)	118.3(6)

Angle	Degree / °	Angle	Degree / °
C(44)–C(43)–C(42)	120.7(6)	C(43)–C(44)–C(45)	121.4(5)
C(44)–C(45)–C(46)	118.5(5)	C(41)–C(46)–C(45)	119.0(6)
C(52)–C(51)–C(56)	117.7(8)	C(52)–C(51)–O(2)	125.8(9)
C(56)–C(51)–O(2)	116.5(7)	C(51)–C(52)–C(53)	121.1(13)
C(52)–C(53)–C(54)	121.0(13)	C(55)–C(54)–C(53)	119.9(12)
C(54)–C(55)–C(56)	121.8(12)	C(55)–C(56)–C(51)	117.5(10)
C(66)–C(61)–C(62)	122.6(7)	C(66)–C(61)–O(3)	115.8(8)
C(64)–C(63)–C(62)	121.3(9)	C(63)–C(64)–C(65)	123.4(9)
C(64)–C(65)–C(66)	119.6(8)	C(61)–C(66)–C(65)	116.8(8)
F(6)–Sb(1)–F(3)	92.4(7)	F(6)–Sb(1)–F(2)	171.9(6)
F(3)–Sb(1)–F(2)	95.6(6)	F(6)–Sb(1)–F(1)	92.8(6)
F(3)–Sb(1)–F(1)	91.4(3)	F(2)–Sb(1)–F(1)	86.5(4)
F(6)–Sb(1)–F(4)	89.0(6)	F(3)–Sb(1)–F(4)	89.9(3)
F(2)–Sb(1)–F(4)	91.5(5)	F(1)–Sb(1)–F(4)	177.8(4)
F(6)–Sb(1)–F(5)	88.0(6)	F(3)–Sb(1)–F(5)	179.3(5)
F(2)–Sb(1)–F(5)	84.0(4)	F(1)–Sb(1)–F(5)	89.1(3)
F(4)–Sb(1)–F(5)	89.6(3)		

Table AI.3: Bond lengths [Å] and angles [°] for [Co(TPP)(depp)₂](SbF₆)

Bond	Length / Å	Bond	Length / Å
F(1)–Sb(3)	1.290(8)	F(1)–Sb(1)	1.859(5)
F(1)–Sb(2)	2.051(5)	F(2)–Sb(3)	1.709(9)
F(2)–Sb(2)	1.852(6)	F(2)–Sb(1)	1.867(4)
F(3)–Sb(3)	1.592(9)	F(3)–Sb(1)	1.869(4)
F(3)–Sb(2)	1.998(7)	Sb(1)–F(1)#1	1.859(5)
Sb(1)–F(2)#1	1.867(4)	Sb(1)–F(3)#1	1.869(4)
Sb(3)–Sb(3)#1	2.42(2)	Co–N(1)	1.971(3)
Co–N(1)#2	1.971(3)	Co–N(2)	1.988(3)
Co–N(2)#2	1.988(3)	Co–P(1)#2	2.3117(9)
Co–P(1)	2.3117(9)	P(1)–C(51)	1.814(4)
P(1)–C(3)	1.825(4)	P(1)–C(1)	1.843(4)
N(1)–CA2	1.367(5)	N(1)–CA1	1.392(4)
N(2)–CA3	1.363(5)	N(2)–CA4	1.390(4)
CA1–CM2#2	1.388(5)	CA1–CB1	1.417(5)
CA2–CM1	1.399(4)	CA2–CB2	1.446(5)
CA3–CM1	1.386(5)	CA3–CB3	1.447(4)
CA4–CM2	1.364(5)	CA4–CB4	1.442(5)
CB1–CB2	1.352(5)	CB3–CB4	1.332(6)
CM1–C(11)	1.493(5)	CM2–CA1#2	1.388(5)
CM2–C(21)	1.401(5)	C(12)–C(13)	1.388(6)
C(13)–C(14)	1.394(6)	C(14)–C(15)	1.366(7)
C(15)–C(16)	1.377(6)	C(21)–C(22)	1.377(5)
C(21)–C(26)	1.385(5)	C(22)–C(23)	1.386(5)
C(24)–C(25)	1.353(7)	C(24)–C(23)	1.370(7)
C(25)–C(26)	1.398(5)	C(51)–C(52)	1.379(6)
C(51)–C(56)	1.394(6)	C(52)–C(53)	1.407(7)
C(53)–C(54)	1.332(9)	C(54)–C(55)	1.395(10)
C(55)–C(56)	1.421(8)	C(1)–C(2)	1.478(8)
C(3)–C(4)	1.533(6)		

Angle	Degree / °	Angle	Degree / °
Sb(3)–F(1)–Sb(1)	40.4(5)	Sb(3)–F(1)–Sb(2)	33.6(5)
Sb(1)–F(1)–Sb(2)	73.28(18)	Sb(3)–F(2)–Sb(2)	39.5(4)
Sb(3)–F(2)–Sb(1)	39.2(4)	Sb(2)–F(2)–Sb(1)	77.90(19)
Sb(3)–F(3)–Sb(1)	39.9(4)	Sb(3)–F(3)–Sb(2)	179.9(3)
F(1)–Sb(1)–F(2)	89.7(2)	F(1)#1–Sb(1)–F(2)	90.3(2)
F(1)–Sb(1)–F(2)#1	90.3(2)	F(1)#1–Sb(1)–F(2)#1	89.7(2)
F(2)–Sb(1)–F(2)#1	90.0(2)	F(1)–Sb(1)–F(3)#1	89.9(2)
F(1)#1–Sb(1)–F(3)#1	90.0(2)	F(2)–Sb(1)–F(3)#1	178.75(18)
F(2)#1–Sb(1)–F(3)#1	88.8(2)	F(1)–Sb(1)–F(3)	90.0(2)
F(1)#1–Sb(1)–F(3)	89.9(2)	F(2)–Sb(1)–F(3)	88.8(2)
F(2)#1–Sb(1)–F(3)	178.75(18)	F(3)#1–Sb(1)–F(3)	92.4(3)
F(2)–Sb(2)–F(3)	85.5(3)	F(2)–Sb(2)–F(1)	84.5(2)
F(3)–Sb(2)–F(1)	81.2(2)	F(1)–Sb(3)–F(3)	132.0(7)
F(1)–Sb(3)–F(2)	121.9(6)	F(3)–Sb(3)–F(2)	104.7(5)
F(1)–Sb(3)–Sb(3)#1	96.2(6)	F(3)–Sb(3)–Sb(3)#1	79.9(5)
F(2)–Sb(3)–Sb(3)#1	80.2(5)	N(1)–Co–N(1)#2	180.00(16)
N(1)–Co–N(2)	89.88(11)	N(1)#2–Co–N(2)	90.12(11)
N(1)–Co–N(2)#2	90.12(11)	N(1)#2–Co–N(2)#2	89.88(11)
N(2)–Co–N(2)#2	180.00(14)	N(1)–Co–P(1)#2	90.40(8)
N(1)#2–Co–P(1)#2	89.60(8)	N(2)–Co–P(1)#2	91.42(8)
N(2)#2–Co–P(1)#2	88.58(8)	N(1)–Co–P(1)	89.60(8)
N(1)#2–Co–P(1)	90.40(8)	N(2)–Co–P(1)	88.58(8)
N(2)#2–Co–P(1)	91.42(8)	P(1)#2–Co–P(1)	180.000(1)
C(51)–P(1)–C(3)	105.7(2)	C(51)–P(1)–C(1)	101.51(18)
C(3)–P(1)–C(1)	104.7(2)	C(51)–P(1)–Co	114.12(14)
C(3)–P(1)–Co	113.08(12)	C(1)–P(1)–Co	116.45(13)
CA2–N(1)–CA1	105.1(3)	CA2–N(1)–Co	127.5(2)
CA1–N(1)–Co	127.4(2)	CA3–N(2)–CA4	106.1(3)
CA3–N(2)–Co	127.2(2)	CA4–N(2)–Co	126.7(2)
CM2#2–CA1–N(1)	110.0(3)	N(1)–CA2–CM1	126.6(3)
N(1)–CA2–CB2	110.8(3)	CM1–CA2–CB2	122.5(3)
N(2)–CA3–CM1	127.0(3)	N(2)–CA3–CB3	110.1(3)

Angle	Degree / °	Angle	Degree / °
CM1–CA3–CB3	122.8(3)	CM2–CA4–N(2)	126.6(3)
CM2–CA4–CB4	124.4(3)	N(2)–CA4–CB4	108.8(3)
CB2–CB1–CA1	108.3(3)	CB1–CB2–CA2	105.8(3)
CB4–CB3–CA3	106.9(3)	CB3–CB4–CA4	108.1(3)
CA3–CM1–CA2	121.7(3)	CA4–CM2–CA1#2	123.3(3)
CA4–CM2–C(21)	118.9(3)	CA1#2–CM2–C(21)	117.8(3)
C(12)–C(11)–C(16)	118.9(4)	C(12)–C(11)–CM1	120.2(3)
C(16)–C(11)–CM1	120.8(4)	C(11)–C(12)–C(13)	121.0(4)
C(12)–C(13)–C(14)	119.5(4)	C(15)–C(14)–C(13)	119.6(4)
C(14)–C(15)–C(16)	121.0(4)	C(15)–C(16)–C(11)	120.0(4)
C(22)–C(21)–C(26)	118.5(3)	C(22)–C(21)–CM2	120.3(3)
C(26)–C(21)–CM2	121.2(3)	C(21)–C(22)–C(23)	120.6(4)
C(25)–C(24)–C(23)	119.9(3)	C(24)–C(25)–C(26)	120.4(4)
C(21)–C(26)–C(25)	120.2(4)	C(52)–C(51)–C(56)	119.2(4)
C(52)–C(51)–P(1)	120.2(3)	C(56)–C(51)–P(1)	120.6(3)
C(51)–C(52)–C(53)	120.8(5)	C(54)–C(53)–C(52)	120.2(5)
C(53)–C(54)–C(55)	121.1(5)	C(54)–C(55)–C(56)	119.3(5)
C(51)–C(56)–C(55)	119.2(5)	C(24)–C(23)–C(22)	120.4(4)
C(2)–C(1)–P(1)	118.3(4)	C(4)–C(3)–P(1)	116.0(3)

Symmetry transformations used to generate equivalent atoms: #1 –x, y, –z+1/2; #2 –x+1/2, –y+1/2, –z.

Table AI.4: Bond lengths [Å] and angles [°] for [Co(TPP)(edpp)₂](SbF₆)

Bond	Length / Å	Bond	Length / Å
Cl(1S)–C(1S)	1.750(3)	Cl(2S)–C(1S)	1.769(4)
Sb(1)–F(4)	1.8554(18)	Sb(1)–F(6)	1.8654(17)
Sb(1)–F(3)	1.8673(16)	Sb(1)–F(1)	1.8758(16)
Sb(1)–F(5)	1.8762(16)	Sb(1)–F(2)	1.8815(18)
Co(1)–N(1)	1.9586(15)	Co(1)–N(3)	1.9744(15)
Co(1)–N(2)	1.9755(18)	Co(1)–N(4)	1.9789(17)
Co(1)–P(2)	2.3161(11)	Co(1)–P(1)	2.3301(11)
P(2)–C(81)	1.8150(17)	P(2)–C(91)	1.821(2)
P(2)–C(73)	1.8331(18)	P(1)–C(51)	1.816(2)
P(1)–C(61)	1.8237(18)	P(1)–C(71)	1.8343(18)
N(3)–CA5	1.3788(19)	N(3)–CA6	1.378(2)
N(1)–CA2	1.377(2)	N(1)–CA1	1.3824(19)
N(2)–CA3	1.379(2)	N(2)–CA4	1.3808(19)
CA5–CM2	1.399(2)	CA5–CB5	1.442(2)
N(4)–CA7	1.371(2)	N(4)–CA8	1.3770(19)
CA2–CM1	1.394(2)	CA2–CB2	1.437(2)
CA8–CM4	1.388(2)	CA8–CB8	1.441(2)
CA7–CM3	1.392(2)	CA7–CB7	1.440(2)
C(81)–C(86)	1.400(2)	C(81)–C(82)	1.400(2)
C(51)–C(52)	1.400(2)	C(51)–C(56)	1.403(2)
CA6–CM3	1.393(2)	CA6–CB6	1.433(2)
CB2–CB1	1.356(2)	CM2–CA4	1.391(2)
CM2–C(21)	1.495(2)	CM3–C(31)	1.491(2)
C(21)–C(26)	1.394(2)	C(21)–C(22)	1.401(2)
C(91)–C(92)	1.392(2)	C(91)–C(96)	1.405(2)
CA1–CM4	1.391(2)	CA1–CB1	1.431(2)
C(73)–C(74)	1.535(2)	CA4–CB4	1.437(2)
C(31)–C(32)	1.397(2)	C(31)–C(36)	1.397(2)
C(52)–C(53)	1.384(3)	C(41)–C(46)	1.390(2)
C(41)–C(42)	1.397(2)	C(41)–CM4	1.490(2)
C(92)–C(93)	1.396(3)	C(61)–C(62)	1.395(2)

Bond	Length / Å	Bond	Length / Å
C(61)–C(66)	1.400(3)	C(82)–C(83)	1.386(2)
CB5–CB6	1.356(2)	C(71)–C(72)	1.529(2)
C(86)–C(85)	1.386(2)	CM1–CA3	1.398(2)
CM1–C(11)	1.493(2)	C(22)–C(23)	1.394(2)
C(56)–C(55)	1.388(3)	CA3–CB3	1.439(2)
C(26)–C(25)	1.393(2)	C(96)–C(95)	1.388(3)
CB4–CB3	1.356(2)	C(83)–C(84)	1.388(3)
C(53)–C(54)	1.393(3)	C(11)–C(12)	1.396(2)
C(11)–C(16)	1.397(2)	CB7–CB8	1.346(2)
C(36)–C(35)	1.394(3)	C(62)–C(63)	1.395(2)
C(35)–C(34) .	1.382(3)	C(12)–C(13)	1.391(3)
C(95)–C(94)	1.389(3)	C(24)–C(23)	1.385(3)
C(24)–C(25)	1.387(3)	C(16)–C(15)	1.397(3)
C(54)–C(55)	1.385(3)	C(85)–C(84)	1.384(3)
C(42)–C(43)	1.387(2)	C(44)–C(43)	1.383(3)
C(44)–C(45)	1.386(3)	C(45)–C(46)	1.387(2)
C(66)–C(65)	1.387(3)	C(34)–C(33)	1.383(3)
C(33)–C(32)	1.385(3)	C(63)–C(64)	1.380(3)
C(64)–C(65)	1.391(3)	C(13)–C(14)	1.383(3)
C(94)–C(93)	1.380(3)	C(15)–C(14)	1.378(3)

Angle	Degree / °	Angle	Degree / °
Cl(1S)–C(1S)–Cl(2S)	110.28(17)	F(4)–Sb(1)–F(6)	92.00(9)
F(4)–Sb(1)–F(3)	90.69(9)	F(6)–Sb(1)–F(3)	90.00(8)
F(4)–Sb(1)–F(1)	91.00(9)	F(6)–Sb(1)–F(1)	91.23(8)
F(3)–Sb(1)–F(1)	177.88(8)	F(4)–Sb(1)–F(5)	90.02(9)
F(6)–Sb(1)–F(5)	177.94(8)	F(3)–Sb(1)–F(5)	90.34(8)
F(1)–Sb(1)–F(5)	88.37(7)	F(4)–Sb(1)–F(2)	178.92(8)
F(6)–Sb(1)–F(2)	88.72(9)	F(3)–Sb(1)–F(2)	90.11(9)
F(1)–Sb(1)–F(2)	88.18(8)	F(5)–Sb(1)–F(2)	89.26(9)
N(1)–Co(1)–N(3)	179.20(5)	N(1)–Co(1)–N(2)	89.96(7)
N(3)–Co(1)–N(2)	90.81(7)	N(1)–Co(1)–N(4)	89.91(7)

Angle	Degree / °	Angle	Degree / °
N(3)–Co(1)–N(4)	89.32(7)	N(2)–Co(1)–N(4)	179.85(6)
N(1)–Co(1)–P(2)	88.96(5)	N(3)–Co(1)–P(2)	91.24(5)
N(2)–Co(1)–P(2)	91.14(6)	N(4)–Co(1)–P(2)	88.80(6)
N(1)–Co(1)–P(1)	90.19(5)	N(3)–Co(1)–P(1)	89.57(5)
N(2)–Co(1)–P(1)	90.88(6)	N(4)–Co(1)–P(1)	89.19(6)
P(2)–Co(1)–P(1)	177.816(17)	C(81)–P(2)–C(91)	108.28(8)
C(81)–P(2)–C(73)	105.51(8)	C(91)–P(2)–C(73)	100.80(9)
C(81)–P(2)–Co(1)	111.15(6)	C(91)–P(2)–Co(1)	116.84(6)
C(73)–P(2)–Co(1)	113.25(6)	C(51)–P(1)–C(61)	108.38(8)
C(51)–P(1)–C(71)	105.17(9)	C(61)–P(1)–C(71)	100.88(8)
C(51)–P(1)–Co(1)	111.70(7)	C(61)–P(1)–Co(1)	116.08(7)
C(71)–P(1)–Co(1)	113.60(6)	CA5–N(3)–CA6	105.93(13)
CA5–N(3)–Co(1)	126.47(11)	CA6–N(3)–Co(1)	127.41(10)
CA2–N(1)–CA1	105.85(13)	CA2–N(1)–Co(1)	127.43(10)
CA1–N(1)–Co(1)	126.68(11)	CA3–N(2)–CA4	105.56(13)
CA3–N(2)–Co(1)	127.43(10)	CA4–N(2)–Co(1)	127.00(11)
N(3)–CA5–CM2	126.21(14)	N(3)–CA5–CB5	109.76(14)
CM2–CA5–CB5	123.73(13)	CA7–N(4)–CA8	105.36(13)
CA7–N(4)–Co(1)	127.30(10)	CA8–N(4)–Co(1)	127.29(11)
N(1)–CA2–CM1	126.32(14)	N(1)–CA2–CB2	109.84(13)
CM1–CA2–CB2	123.61(15)	N(4)–CA8–CM4	125.42(14)
N(4)–CA8–CB8	110.30(14)	CM4–CA8–CB8	124.20(14)
N(4)–CA7–CM3	126.41(14)	N(4)–CA7–CB7	110.44(13)
CM3–CA7–CB7	122.97(15)	C(86)–C(81)–C(82)	118.69(14)
C(86)–C(81)–P(2)	120.16(13)	C(82)–C(81)–P(2)	121.02(13)
C(52)–C(51)–C(56)	118.39(16)	C(52)–C(51)–P(1)	121.22(12)
C(56)–C(51)–P(1)	120.30(13)	N(3)–CA6–CM3	125.90(14)
N(3)–CA6–CB6	110.10(13)	CM3–CA6–CB6	123.97(15)
CB1–CB2–CA2	107.16(14)	CA4–CM2–CA5	123.05(14)
CA4–CM2–C(21)	120.18(14)	CA5–CM2–C(21)	116.64(14)
CA7–CM3–CA6	121.68(15)	CA7–CM3–C(31)	117.03(14)
CA6–CM3–C(31)	121.29(14)	C(26)–C(21)–C(22)	119.04(14)

Angle	Degree / °	Angle	Degree / °
C(26)–C(21)–CM2	119.56(15)	C(22)–C(21)–CM2	121.24(15)
C(92)–C(91)–C(96)	118.44(15)	C(92)–C(91)–P(2)	124.61(12)
C(96)–C(91)–P(2)	116.80(13)	N(1)–CA1–CM4	126.50(14)
N(1)–CA1–CB1	110.00(14)	CM4–CA1–CB1	123.41(13)
C(74)–C(73)–P(2)	115.56(12)	N(2)–CA4–CM2	125.57(14)
N(2)–CA4–CB4	109.97(14)	CM2–CA4–CB4	124.34(14)
C(32)–C(31)–C(36)	118.33(16)	C(32)–C(31)–CM3	118.79(15)
C(36)–C(31)–CM3	122.83(15)	C(53)–C(52)–C(51)	120.86(15)
CB2–CB1–CA1	107.13(14)	C(46)–C(41)–C(42)	118.98(14)
C(46)–C(41)–CM4	119.04(14)	C(42)–C(41)–CM4	121.98(15)
C(91)–C(92)–C(93)	120.52(16)	C(62)–C(61)–C(66)	118.89(15)
C(62)–C(61)–P(1)	124.07(13)	C(66)–C(61)–P(1)	117.02(13)
C(83)–C(82)–C(81)	120.26(17)	CB6–CB5–CA5	106.99(14)
C(72)–C(71)–P(1)	115.47(12)	C(85)–C(86)–C(81)	120.57(17)
CA2–CM1–CA3	121.93(15)	CA2–CM1–C(11)	116.64(14)
CA3–CM1–C(11)	121.34(14)	CA8–CM4–CA1	122.36(14)
CA8–CM4–C(41)	119.22(14)	CA1–CM4–C(41)	118.42(14)
C(23)–C(22)–C(21)	120.14(16)	C(55)–C(56)–C(51)	120.65(16)
N(2)–CA3–CM1	125.53(14)	N(2)–CA3–CB3	110.36(13)
CM1–CA3–CB3	124.00(15)	CB5–CB6–CA6	107.18(15)
C(21)–C(26)–C(25)	120.48(16)	C(95)–C(96)–C(91)	120.68(16)
CB3–CB4–CA4	107.32(14)	C(82)–C(83)–C(84)	120.41(17)
C(52)–C(53)–C(54)	119.97(16)	C(12)–C(11)–C(16)	118.16(16)
C(12)–C(11)–CM1	119.21(15)	C(16)–C(11)–CM1	122.35(15)
CB8–CB7–CA7	107.02(15)	CB4–CB3–CA3	106.64(15)
CB7–CB8–CA8	106.83(14)	C(35)–C(36)–C(31)	120.35(17)
C(61)–C(62)–C(63)	119.99(17)	C(34)–C(35)–C(36)	120.35(17)
C(13)–C(12)–C(11)	120.96(17)	C(96)–C(95)–C(94)	120.19(16)
C(23)–C(24)–C(25)	119.98(15)	C(11)–C(16)–C(15)	120.58(18)
C(24)–C(25)–C(26)	120.08(17)	C(55)–C(54)–C(53)	119.99(17)
C(84)–C(85)–C(86)	120.24(18)	C(43)–C(42)–C(41)	120.03(17)
C(43)–C(44)–C(45)	119.54(15)	C(56)–C(55)–C(54)	120.10(16)

Angle	Degree / °	Angle	Degree / °
C(24)–C(23)–C(22)	120.26(17)	C(44)–C(45)–C(46)	120.12(17)
C(65)–C(66)–C(61)	120.87(17)	C(35)–C(34)–C(33)	119.87(17)
C(34)–C(33)–C(32)	119.99(17)	C(64)–C(63)–C(62)	120.54(17)
C(63)–C(64)–C(65)	120.06(17)	C(85)–C(84)–C(83)	119.79(16)
C(33)–C(32)–C(31)	121.10(17)	C(14)–C(13)–C(12)	120.11(18)
C(93)–C(94)–C(95)	119.68(17)	C(45)–C(46)–C(41)	120.66(16)
C(44)–C(43)–C(42)	120.67(17)	C(66)–C(65)–C(64)	119.64(19)
C(94)–C(93)–C(92)	120.46(17)	C(14)–C(15)–C(16)	120.28(19)
C(15)–C(14)–C(13)	119.85(18)		

Table AI.5: Bond lengths [Å] and angles [°] for [Co(TPP)(deppt)₂](SbF₆)

Bond	Length / Å	Bond	Length / Å
Co(1)–N(1)#1	1.969(3)	Co(1)–N(1)	1.969(3)
Co(1)–N(2)	1.990(4)	Co(1)–N(2)#1	1.990(4)
Co(1)–P(1)	2.2575(14)	Co(1)–P(1)#1	2.2575(14)
Co(1')–N(1')#2	1.984(4)	Co(1')–N(1')	1.984(4)
Co(1')–N(2')	1.983(3)	Co(1')–N(2')#2	1.983(3)
Co(1')–P(1')#2	2.2576(19)	Co(1')–P(1')	2.2576(19)
P(1)–O(2)	1.557(5)	P(1)–O(1)	1.562(4)
P(1)–C(31)	1.804(6)	P(1')–O(1')	1.593(5)
P(1')–O(2')	1.598(4)	P(1')–C(31')	1.728(6)
O(1)–C(41)	1.390(8)	O(1')–C(41')	1.286(12)
O(2)–C(51)	1.272(10)	O(2')–C(51')	1.414(9)
N(2)–CA2	1.374(6)	N(2)–CA4	1.370(6)
N(2')–CA4'	1.370(6)	N(2')–CA2'	1.381(6)
N(1)–CA1	1.366(6)	N(1)–CA3	1.382(6)
N(1')–CA1'	1.377(6)	N(1')–CA3'	1.378(6)
CA1–CM2#1	1.392(7)	CA1–CB1	1.424(7)
CA1'–CM2'#2	1.366(6)	CA1'–CB1'	1.429(7)
CA2–CM1	1.386(7)	CA2'–CB3'	1.426(6)
CA2'–CM1'	1.380(6)	CA2–CB3	1.427(7)
CA3–CM1	1.376(7)	CA3–CB2	1.423(7)
CA3'–CM1'	1.382(7)	CA3'–CB2'	1.426(7)
CA4–CM2	1.391(7)	CA4–CB4	1.423(7)
CA4'–CM2'	1.383(6)	CA4'–CB4'	1.438(6)
CB1–CB2	1.343(8)	CB1'–CB2'	1.334(7)
CB3–CB4	1.326(7)	CB3'–CB4'	1.340(7)
CM1–C(11)	1.509(7)	CM1'–C(11')	1.500(7)
CM2–CA1#1	1.392(7)	CM2–C(21)	1.497(6)
CM2'–CA1'#2	1.366(6)	CM2'–C(21')	1.510(6)
C(11)–C(12)	1.366(8)	C(11)–C(16)	1.385(8)
C(12)–C(13)	1.404(8)	C(13)–C(14)	1.340(9)
C(14)–C(15)	1.367(10)	C(15)–C(16)	1.374(8)

Bond	Length / Å	Bond	Length / Å
C(11')–C(16')	1.371(8)	C(11')–C(12')	1.379(8)
C(12')–C(13')	1.407(9)	C(13')–C(14')	1.334(11)
C(14')–C(15')	1.368(11)	C(15')–C(16')	1.396(8)
C(21)–C(22)	1.365(8)	C(21)–C(26)	1.379(8)
C(22)–C(23)	1.386(10)	C(23)–C(24)	1.355(12)
C(24)–C(25)	1.322(11)	C(25)–C(26)	1.382(8)
C(21')–C(26')	1.375(8)	C(21')–C(22')	1.378(8)
C(22')–C(23')	1.383(8)	C(23')–C(24')	1.344(10)
C(24')–C(25')	1.356(11)	C(25')–C(26')	1.376(8)
C(31)–C(32)	1.367(9)	C(31)–C(36)	1.401(9)
C(32)–C(33)	1.412(11)	C(33)–C(34)	1.344(14)
C(34)–C(35)	1.377(13)	C(35)–C(36)	1.397(10)
C(31')–C(36')	1.391(9)	C(31')–C(32')	1.405(10)
C(32')–C(33')	1.360(12)	C(33')–C(34')	1.301(14)
C(34')–C(35')	1.364(13)	C(35')–C(36')	1.381(11)
C(41)–C(42)	1.429(11)	C(41')–C(42')	1.350(16)
C(51)–C(52)	1.326(12)	C(51')–C(52')	1.501(12)
Sb(1)–F(6)	1.715(8)	Sb(1)–F(4)	1.782(6)
Sb(1)–F(1)	1.806(6)	Sb(1)–F(2)	1.837(6)
Sb(1)–F(3)	1.848(7)	Sb(1)–F(5)	1.887(7)

Angle	Degree / °	Angle	Degree / °
N(1)#1–Co(1)–N(1)	180.0(2)	N(1)#1–Co(1)–N(2)	90.14(15)
N(1)–Co(1)–N(2)	89.85(15)	N(1)#1–Co(1)–N(2)#1	89.86(15)
N(1)–Co(1)–N(2)#1	90.14(15)	N(2)–Co(1)–N(2)#1	180.0
N(1)#1–Co(1)–P(1)	89.31(12)	N(1)–Co(1)–P(1)	90.69(12)
N(2)–Co(1)–P(1)	90.52(12)	N(2)#1–Co(1)–P(1)	89.48(12)
N(1)#1–Co(1)–P(1)#1	90.69(12)	N(1)–Co(1)–P(1)#1	89.31(12)
N(2)–Co(1)–P(1)#1	89.48(12)	N(2)#1–Co(1)–P(1)#1	90.52(12)
P(1)–Co(1)–P(1)#1	180.0	N(1')#2–Co(1')–N(1')	180.00(13)
N(1')#2–Co(1')–N(2')	89.85(15)	N(1')–Co(1')–N(2')	90.15(15)
N(1')#2–Co(1')–N(2')#2	90.15(15)	N(1')–Co(1')–N(2')#2	89.85(15)

Angle	Degree / °	Angle	Degree / °
N(2')–Co(1')–N(2')#2	180.000(1)	N(1')#2–Co(1')–P(1')#2	91.25(12)
N(1')–Co(1')–P(1')#2	88.75(12)	N(2')–Co(1')–P(1')#2	89.41(12)
N(2')#2–Co(1')–P(1')#2	⁻90.59(12)	N(1')#2–Co(1')–P(1')	88.75(12)
N(1')–Co(1')–P(1')	91.25(12)	N(2')–Co(1')–P(1')	90.59(12)
N(2')#2–Co(1')–P(1')	89.41(12)	P(1')#2–Co(1')–P(1')	180.00(6)
O(2)–P(1)–O(1)	110.1(3)	O(2)–P(1)–C(31)	101.6(3)
O(1)–P(1)–C(31)	104.7(3)	O(2)–P(1)–Co(1)	113.9(2)
O(1)–P(1)–Co(1)	110.82(18)	C(31)–P(1)–Co(1)	115.06(19)
O(1')–P(1')–O(2')	110.3(3)	O(1')–P(1')–C(31')	105.0(3)
O(2')–P(1')–C(31')	104.4(3)	O(1')–P(1')–Co(1')	111.0(2)
O(2')–P(1')–Co(1')	110.79(17)	C(31')–P(1')–Co(1')	115.0(2)
C(41)–O(1)–P(1)	131.8(5)	C(41')–O(1')–P(1')	135.8(8)
C(51)–O(2)–P(1)	141.9(7)	C(51')–O(2')–P(1')	128.4(5)
CA2–N(2)–CA4	105.2(4)	CA2–N(2)–Co(1)	127.1(3)
CA4–N(2)–Co(1)	127.6(3)	CA4'–N(2')–CA2'	105.8(4)
CA4'–N(2')–Co(1')	126.9(3)	CA2'–N(2')–Co(1')	127.2(3)
CA1–N(1)–CA3	105.4(4)	CA1–N(1)–Co(1)	127.1(3)
CA3–N(1)–Co(1)	127.3(3)	CA1'–N(1')–CA3'	105.9(4)
CA1'–N(1')–Co(1')	126.8(3)	CA3'–N(1')–Co(1')	126.9(3)
N(1)–CA1–CM2#1	126.9(4)	N(1)–CA1–CB1	110.7(4)
CM2#1–CA1–CB1	122.4(4)	CM2'#2–CA1'–N(1')	126.7(4)
CM2'#2–CA1'–CB1'	124.0(4)	N(1')–CA1'–CB1'	109.3(4)
N(2)–CA2–CM1	126.3(4)	N(2)–CA2–CB3	109.8(4)
CM1–CA2–CB3	123.9(4)	CM1'–CA2'–N(2')	125.8(4)
CM1'–CA2'–CB3'	124.1(4)	N(2')–CA2'–CB3'	110.0(4)
CM1–CA3–N(1)	126.5(4)	CM1–CA3–CB2	124.1(4)
N(1)–CA3–CB2	109.4(4)	N(1')–CA3'–CM1'	126.3(4)
N(1')–CA3'–CB2'	109.6(4)	CM1'–CA3'–CB2'	124.0(4)
N(2)–CA4–CM2	125.6(4)	N(2)–CA4–CB4	110.1(4)
CM2–CA4–CB4	124.2(4)	N(2')–CA4'–CM2'	126.6(4)
N(2')–CA4'–CB4'	109.3(4)	CM2'–CA4'–CB4'	124.0(4)
CB2–CB1–CA1	106.6(5)	CB2'–CB1'–CA1'	107.8(4)

Angle	Degree / °	Angle	Degree / °
CB1–CB2–CA3	107.9(4)	CB1'–CB2'–CA3'	107.4(5)
CB4–CB3–CA2	107.4(4)	CB4'–CB3'–CA2'	107.0(4)
CB3–CB4–CA4	107.4(5)	CB3'–CB4'–CA4'	107.7(4)
CA3–CM1–CA2	122.7(4)	CA3–CM1–C(11)	117.5(4)
CA2–CM1–C(11)	119.8(4)	CA2'–CM1'–CA3'	123.5(4)
CA2'–CM1'–C(11')	118.8(4)	CA3'–CM1'–C(11')	117.6(4)
CA4–CM2–CA1#1	122.6(4)	CA4–CM2–C(21)	119.6(4)
CA1#1–CM2–C(21)	117.8(4)	CA1'#2–CM2'–CA4'	122.9(4)
CA1'#2–CM2'–C(21')	118.1(4)	CA4'–CM2'–C(21')	119.0(4)
C(12)–C(11)–C(16)	119.2(5)	C(12)–C(11)–CM1	120.4(5)
C(16)–C(11)–CM1	120.2(5)	C(11)–C(12)–C(13)	119.0(6)
C(14)–C(13)–C(12)	121.3(6)	C(13)–C(14)–C(15)	119.8(6)
C(16)–C(15)–C(14)	120.2(6)	C(15)–C(16)–C(11)	120.5(6)
C(16')–C(11')–C(12')	118.9(5)	C(16')–C(11')–CM1'	120.6(5)
C(12')–C(11')–CM1'	120.3(5)	C(11')–C(12')–C(13')	119.4(6)
C(14')–C(13')–C(12')	121.3(7)	C(13')–C(14')–C(15')	119.9(6)
C(14')–C(15')–C(16')	120.1(7)	C(11')–C(16')–C(15')	120.4(7)
C(22)–C(21)–C(26)	117.5(5)	C(22)–C(21)–CM2	123.1(5)
C(26)–C(21)–CM2	119.4(5)	C(21)–C(22)–C(23)	120.8(8)
C(24)–C(23)–C(22)	119.7(8)	C(25)–C(24)–C(23)	120.8(7)
C(24)–C(25)–C(26)	120.2(8)	C(21)–C(26)–C(25)	120.9(7)
C(26')–C(21')–C(22')	117.8(5)	C(26')–C(21')–CM2'	121.2(5)
C(22')–C(21')–CM2'	120.9(5)	C(23')–C(22')–C(21')	119.9(6)
C(24')–C(23')–C(22')	121.1(7)	C(23')–C(24')–C(25')	120.1(7)
C(24')–C(25')–C(26')	119.6(7)	C(21')–C(26')–C(25')	121.5(7)
C(32)–C(31)–C(36)	120.0(7)	C(32)–C(31)–P(1)	121.3(6)
C(36)–C(31)–P(1)	118.5(5)	C(31)–C(32)–C(33)	119.8(9)
C(34)–C(33)–C(32)	118.7(9)	C(33)–C(34)–C(35)	123.7(9)
C(34)–C(35)–C(36)	117.6(9)	C(35)–C(36)–C(31)	120.1(8)
C(36')–C(31')–C(32')	111.4(6)	C(36')–C(31')–P(1')	123.0(5)
C(32')–C(31')–P(1')	125.5(6)	C(33')–C(32')–C(31')	122.9(9)
C(34')–C(33')–C(32')	122.6(11)	C(33')–C(34')–C(35')	119.6(11)

Angle	Degree / °	Angle	Degree / °
C(34')–C(35')–C(36')	117.9(10)	C(35')–C(36')–C(31')	125.2(8)
O(1)–C(41)–C(42)	114.2(8)	O(1')–C(41')–C(42')	122.4(14)
O(2)–C(51)–C(52)	127.7(11)	O(2')–C(51')–C(52')	108.4(8)
F(6)–Sb(1)–F(4)	94.1(6)	F(6)–Sb(1)–F(1)	89.8(4)
F(4)–Sb(1)–F(1)	91.1(4)	F(6)–Sb(1)–F(2)	90.1(3)
F(4)–Sb(1)–F(2)	86.9(4)	F(1)–Sb(1)–F(2)	177.9(3)
F(6)–Sb(1)–F(3)	91.5(5)	F(4)–Sb(1)–F(3)	173.9(4)
F(1)–Sb(1)–F(3)	91.4(4	F(2)–Sb(1)–F(3)	90.6(4)
F(6)–Sb(1)–F(5)	178.6(5)	F(4)–Sb(1)–F(5)	86.8(5)
F(1)–Sb(1)–F(5)	91.3(4)	F(2)–Sb(1)–F(5)	88.9(4)
F(3)–Sb(1)–F(5)	87.6(4)		

Symmetry transformations used to generate equivalent atoms: #1 –x–1, –y+1, –z; #2 –x–1, –y+1, –z+1.

Table AI.6: Bond lengths [Å] and angles [°] for [Rh(TPP)(edpp)₂](SbF₆)

Bond	Length / Å	Bond	Length / Å
Rh–N(4)	2.030(3)	Rh–N(1)	2.033(3)
Rh–N(2)	2.034(3)	Rh–N(3)	2.043(3)
Rh–P(1)	2.3987(13)	Rh–P(2)	2.4030(13)
N(1)–CA2	1.370(5)	N(1)–CA1	1.382(5)
N(2)–CA3	1.375(5)	N(2)–CA4	1.379(5)
N(3)–CA5	1.368(5)	N(3)–CA6	1.370(5)
N(4)–CA8	1.375(5)	N(4)–CA7	1.377(5)
CA1–CM4	1.387(6)	CA1–CB1	1.439(6)
CA2–CM1	1.395(6)	CA2–CB2	1.437(6)
CA3–CM1	1.400(6)	CA3–CB3	1.439(6)
CA4–CM2	1.390(5)	CA4–CB4	1.440(6)
CA5–CM2	1.401(5)	CA5–CB5	1.446(5)
CA6–CM3	1.392(5)	CA6–CB6	1.442(5)
CA7–CM3	1.399(5)	CA7–CB7	1.434(5)
CA8–CM4	1.401(6)	CA8–CB8	1.441(6)
CB1–CB2	1.341(7)	CB3–CB4	1.344(6)
CB5–CB6	1.339(6)	CB7–CB8	1.346(6)
CM1–C(11)	1.500(5)	CM2–C(21)	1.500(5)
CM3–C(31)	1.498(5)	CM4–C(41')	1.471(7)
CM4–C(41)	1.526(6)	C(11)–C(12)	1.386(7)
C(11)–C(16)	1.401(6)	C(12)–C(13)	1.370(7)
C(13)–C(14)	1.371(9)	C(14)–C(15)	1.366(9)
C(15)–C(16)	1.385(7)	C(21)–C(26)	1.383(6)
C(21)–C(22)	1.386(6)	C(22)–C(23)	1.389(7)
C(23)–C(24)	1.355(8)	C(24)–C(25)	1.374(8)
C(25)–C(26)	1.387(7)	C(31)–C(32)	1.373(6)
C(31)–C(36)	1.376(6)	C(32)–C(33)	1.382(7)
C(33)–C(34)	1.351(9)	C(34)–C(35)	1.375(9)
C(35)–C(36)	1.381(7)	C(41)–C(42)	1.3900
C(41)–C(46)	1.3900	C(42)–C(43)	1.3900
C(43)–C(44)	1.3900	C(44)–C(45)	1.3900

Bond	Length / Å	Bond	Length / Å
C(45)–C(46)	1.3900	C(41')–C(42')	1.3900
C(41')–C(46')	1.3900	C(42')–C(43')	1.3900
C(43')–C(44')	1.3900	C(44')–C(45')	1.3900
C(45')–C(46')	1.3900	P(1)–C(51)	1.822(4)
P(1)–C(71)	1.827(4)	P(1)–C(61)	1.830(4)
C(51)–C(52)	1.375(6)	C(51)–C(56)	1.404(6)
C(52)–C(53)	1.383(7)	C(53)–C(54)	1.378(8)
C(54)–C(55)	1.355(8)	C(55)–C(56)	1.384(7)
C(61)–C(62)	1.379(6)	C(61)–C(66)	1.393(6)
C(62)–C(63)	1.391(7)	C(63)–C(64)	1.371(9)
C(64)–C(65)	1.351(9)	C(65)–C(66)	1.380(7)
C(71)–C(72)	1.535(6)	P(2)–C(81)	1.822(4)
P(2)–C(100)	1.829(4)	P(2)–C(91)	1.837(4)
C(81)–C(82)	1.378(6)	C(81)–C(86)	1.394(6)
C(82)–C(83)	1.394(7)	C(83)–C(84)	1.370(9)
C(84)–C(85)	1.369(9)	C(85)–C(86)	1.386(7)
C(91)–C(92)	1.380(7)	C(91)–C(96)	1.395(6)
C(92)–C(93)	1.385(7)	C(93)–C(94)	1.363(9)
C(94)–C(95)	1.369(10)	C(95)–C(96)	1.390(7)
C(100)–C(101)	1.538(6)	Sb–F(1)	1.723(7)
Sb–F(4)	1.780(7)	Sb–F(3)	1.786(6)
Sb–F(5)	1.822(7)	Sb–F(6)	1.864(6)
Sb–F(2)	1.868(7)	Cl(1)–C(1S)	1.559(13)
Cl(2)–C(1S)	1.706(12)	Cl(3)–C(2S)	1.566(9)
Cl(4)–C(2S)	1.591(9)		

Angle	Degree / °	Angle	Degree / °
N(4)–Rh–N(1)	90.25(12)	N(4)–Rh–N(2)	179.60(12)
N(1)–Rh–N(2)	90.14(13)	N(4)–Rh–N(3)	89.85(12)
N(1)–Rh–N(3)	179.52(13)	N(2)–Rh–N(3)	89.76(12)
N(4)–Rh–P(1)	90.72(9)	N(1)–Rh–P(1)	90.45(10)

Angle	Degree / °	Angle	Degree / °
N(2)–Rh–P(1)	89.21(9)	N(3)–Rh–P(1)	89.08(9)
N(4)–Rh–P(2)	88.84(9)	N(1)–Rh–P(2)	91.57(10)
N(2)–Rh–P(2)	91.21(9)	N(3)–Rh–P(2)	88.91(9)
P(1)–Rh–P(2)	177.94(3)	CA2–N(1)–CA1	107.4(3)
CA2–N(1)–Rh	126.6(3)	CA1–N(1)–Rh	126.0(3)
CA3–N(2)–CA4	107.5(3)	CA3–N(2)–Rh	126.0(3)
CA4–N(2)–Rh	126.4(2)	CA5–N(3)–CA6	107.9(3)
CA5–N(3)–Rh	126.0(2)	CA6–N(3)–Rh	126.0(2)
CA8–N(4)–CA7	107.3(3)	CA8–N(4)–Rh	126.5(2)
CA7–N(4)–Rh	126.2(2)	N(1)–CA1–CM4	125.7(3)
N(1)–CA1–CB1	108.3(4)	CM4–CA1–CB1	126.0(4)
N(1)–CA2–CM1	125.6(4)	N(1)–CA2–CB2	108.8(4)
CM1–CA2–CB2	125.6(4)	N(2)–CA3–CM1	126.0(4)
N(2)–CA3–CB3	108.7(3)	CM1–CA3–CB3	125.2(4)
N(2)–CA4–CM2	126.0(3)	N(2)–CA4–CB4	108.3(3)
CM2–CA4–CB4	125.7(4)	N(3)–CA5–CM2	126.6(3)
N(3)–CA5–CB5	108.3(3)	CM2–CA5–CB5	125.1(3)
N(3)–CA6–CM3	126.3(3)	N(3)–CA6–CB6	108.5(3)
CM3–CA6–CB6	125.2(3)	N(4)–CA7–CM3	126.1(3)
N(4)–CA7–CB7	108.9(3)	CM3–CA7–CB7	125.0(3)
N(4)–CA8–CM4	125.2(4)	N(4)–CA8–CB8	108.6(3)
CM4–CA8–CB8	126.1(4)	CB2–CB1–CA1	107.8(4)
CB1–CB2–CA2	107.7(4)	CB4–CB3–CA3	107.6(4)
CB3–CB4–CA4	107.8(4)	CB6–CB5–CA5	107.7(3)
CB5–CB6–CA6	107.6(3)	CB8–CB7–CA7	107.5(4)
CB7–CB8–CA8	107.7(4)	CA2–CM1–CA3	125.0(4)
CA2–CM1–C(11)	117.4(4)	CA3–CM1–C(11)	117.6(4)
CA4–CM2–CA5	124.2(3)	CA4–CM2–C(21)	119.0(3)
CA5–CM2–C(21)	116.8(3)	CA6–CM3–CA7	124.5(3)
CA6–CM3–C(31)	117.6(3)	CA7–CM3–C(31)	117.9(3)
CA1–CM4–CA8	125.6(4)	CA1–CM4–C(41')	115.9(5)
CA8–CM4–C(41')	118.3(5)	CA1–CM4–C(41)	116.8(5)

Angle	Degree / °	Angle	Degree / °
CA8–CM4–C(41)	117.1(5)	C(41')–CM4–C(41)	12.1(5)
C(12)–C(11)–C(16)	119.3(4)	C(12)–C(11)–CM1	119.7(4)
C(16)–C(11)–CM1	121.0(4)	C(13)–C(12)–C(11)	120.4(5)
C(12)–C(13)–C(14)	120.2(6)	C(15)–C(14)–C(13)	120.3(5)
C(14)–C(15)–C(16)	120.7(5)	C(15)–C(16)–C(11)	119.0(5)
C(26)–C(21)–C(22)	117.8(4)	C(26)–C(21)–CM2	119.5(4)
C(22)–C(21)–CM2	122.7(4)	C(21)–C(22)–C(23)	120.3(5)
C(24)–C(23)–C(22)	120.9(5)	C(23)–C(24)–C(25)	120.1(5)
C(24)–C(25)–C(26)	119.3(5)	C(21)–C(26)–C(25)	121.6(5)
C(32)–C(31)–C(36)	118.0(4)	C(32)–C(31)–CM3	120.0(4)
C(36)–C(31)–CM3	121.9(4)	C(31)–C(32)–C(33)	121.2(5)
C(34)–C(33)–C(32)	120.8(6)	C(33)–C(34)–C(35)	118.6(5)
C(34)–C(35)–C(36)	121.0(5)	C(31)–C(36)–C(35)	120.4(5)
C(42)–C(41)–C(46)	120.0	C(42)–C(41)–CM4	121.4(5)
C(46)–C(41)–CM4	118.6(5)	C(41)–C(42)–C(43)	120.0
C(42)–C(43)–C(44)	120.0	C(45)–C(44)–C(43)	120.0
C(46)–C(45)–C(44)	120.0	C(45)–C(46)–C(41)	120.0
C(42')–C(41')–C(46')	120.0	C(42')–C(41')–CM4	119.8(6)
C(46')–C(41')–CM4	120.1(6)	C(41')–C(42')–C(43')	120.0
C(42')–C(43')–C(44')	120.0	C(45')–C(44')–C(43')	120.0
C(44')–C(45')–C(46')	106.1(2)	C(51)–P(1)–C(61)	107.06(19)
C(71)–P(1)–C(61)	102.1(2)	C(51)–P(1)–Rh	112.12(13)
C(71)–P(1)–Rh	112.27(14)	C(61)–P(1)–Rh	116.30(13)
C(52)–C(51)–C(56)	118.8(4)	C(52)–C(51)–P(1)	121.5(3)
C(56)–C(51)–P(1)	119.6(3)	C(51)–C(52)–C(53)	120.8(5)
C(54)–C(53)–C(52)	119.9(5)	C(55)–C(54)–C(53)	120.0(5)
C(54)–C(55)–C(56)	121.2(5)	C(55)–C(56)–C(51)	119.3(5)
C(62)–C(61)–C(66)	117.8(4)	C(62)–C(61)–P(1)	124.9(3)
C(66)–C(61)–P(1)	117.3(3)	C(61)–C(62)–C(63)	120.8(5)
C(64)–C(63)–C(62)	119.6(5)	C(65)–C(64)–C(63)	120.7(5)
C(64)–C(65)–C(66)	119.9(5)	C(65)–C(66)–C(61)	121.1(5)
C(72)–C(71)–P(1)	115.9(3)	C(81)–P(2)–C(100)	105.8(2)

Angle	Degree / °	Angle	Degree / °
C(81)–P(2)–C(91)	107.0(2)	C(100)–P(2)–C(91)	101.6(2)
C(81)–P(2)–Rh	112.24(13)	C(100)–P(2)–Rh	112.24(15)
C(91)–P(2)–Rh	116.85(14)	C(82)–C(81)–C(86)	118.8(4)
C(82)–C(81)–P(2)	121.1(3)	C(86)–C(81)–P(2)	120.0(3)
C(81)–C(82)–C(83)	120.4(5)	C(84)–C(83)–C(82)	120.1(5)
C(85)–C(84)–C(83)	120.0(5)	C(84)–C(85)–C(86)	120.4(5)
C(85)–C(86)–C(81)	120.1(5)	C(92)–C(91)–C(96)	119.3(4)
C(92)–C(91)–P(2)	124.7(4)	C(96)–C(91)–P(2)	115.9(4)
C(91)–C(92)–C(93)	120.6(5)	C(94)–C(93)–C(92)	119.9(6)
C(93)–C(94)–C(95)	120.4(5)	C(94)–C(95)–C(96)	120.7(6)
C(95)–C(96)–C(91)	119.0(5)	C(101)–C(100)–P(2)	115.9(3)
F(1)–Sb–F(4)	89.7(6)	F(1)–Sb–F(3)	88.3(7)
F(4)–Sb–F(5)	90.1(5)	F(3)–Sb–F(5)	172.3(6)
F(1)–Sb–F(6)	92.7(5)	F(4)–Sb–F(6)	174.1(5)
F(3)–Sb–F(6)	97.1(4)	F(5)–Sb–F(6)	84.6(4)
F(1)–Sb–F(2)	176.9(5)	F(4)–Sb–F(2)	92.3(5)
F(3)–Sb–F(2)	83.3(4)	F(5)–Sb–F(2)	89.4(6)
F(6)–Sb–F(2)	85.0(4)	Cl(1)–C(1S)–Cl(2)	126.3(9)
Cl(3)–C(2S)–Cl(4)	124.7(8)		

Table AI.7: Bond lengths [Å] and angles [°] for [Rh(TPP)(edppt)₂](SbF₆)

Bond	Length / Å	Bond	Length / Å
Rh(1)–N(1)	2.030(4)	Rh(1)–N(4)	2.031(4)
Rh(1)–N(2)	2.033(4)	Rh(1)–N(3)	2.036(3)
Rh(1)–P(1)	2.3548(12)	Rh(1)–P(2)	2.3676(13)
N(1)–CA2	1.378(5)	N(1)–CA1	1.379(6)
N(2)–CA3	1.372(6)	N(2)–CA4	1.373(6)
N(3)–CA6	1.367(6)	N(3)–CA5	1.376(6)
N(4)–CA8	1.376(6)	N(4)–CA7	1.386(6)
P(1)–O(1)	1.602(3)	P(1)–C(51)	1.801(4)
P(1)–C(61)	1.814(5)	P(2)–O(2)	1.594(4)
P(2)–C(71)	1.801(5)	P(2)–C(81)	1.818(5)
O(1)–C(1)	1.443(6)	O(2)–C(3)	1.452(6)
CA1–CM1	1.386(6)	CA1–CB1	1.441(6)
CA2–CM2	1.397(6)	CA2–CB2	1.434(6)
CA3–CM2	1.401(6)	CA3–CB3	1.433(7)
CA4–CM3	1.392(6)	CA4–CB4	1.442(6)
CA5–CM3	1.379(6)	CA5–CB5	1.454(6)
CA6–CM4	1.390(6)	CA6–CB6	1.443(6)
CA7–CM4	1.385(6)	CA7–CB7	1.458(6)
CA8–CM1	1.387(6)	CA8–CB8	1.436(6)
CB1–CB2	1.351(7)	CB3–CB4	1.350(7)
CB5–CB6	1.370(7)	CB7–CB8	1.354(7)
CM1–C(11)	1.500(6)	CM2–C(21)	1.503(6)
CM3–C(31)	1.509(6)	CM4–C(41)	1.500(6)
Cl(1')–C(1')	1.708(17)	Cl(2')–C(1')	1.635(18)
Cl(1")–C(1")	1.434(16)	Cl(2")–C(1")	1.955(16)
C(1)–C(2)	1.452(11)	C(3)–C(4)	1.460(9)
C(11)–C(12)	1.373(8)	C(11)–C(16)	1.399(8)
C(12)–C(13)	1.403(9)	C(13)–C(14)	1.355(11)
C(14)–C(15)	1.375(11)	C(15)–C(16)	1.382(8)
C(21)–C(26)	1.372(7)	C(21)–C(22)	1.383(7)
C(22)–C(23)	1.389(7)	C(23)–C(24)	1.388(9)

Bond	Length / Å	Bond	Length / Å
C(24)–C(25)	1.342(8)	C(25)–C(26)	1.407(7)
C(31)–C(36)	1.379(7)	C(31)–C(32)	1.378(8)
C(32)–C(33)	1.370(8)	C(33)–C(34)	1.361(10)
C(34)–C(35)	1.351(10)	C(35)–C(36)	1.429(8)
C(41)–C(42)	1.365(8)	C(41)–C(46)	1.410(7)
C(42)–C(43)	1.405(7)	C(43)–C(44)	1.358(10)
C(44)–C(45)	1.368(10)	C(45)–C(46)	1.383(8)
C(51)–C(52)	1.370(7)	C(51)–C(56)	1.395(7)
C(52)–C(53)	1.375(8)	C(53)–C(54)	1.340(9)
C(54)–C(55)	1.388(8)	C(55)–C(56)	1.380(8)
C(61)–C(62)	1.380(7)	C(61)–C(66)	1.394(7)
C(62)–C(63)	1.388(8)	C(63)–C(64)	1.359(10)
C(64)–C(65)	1.348(11)	C(65)–C(66)	1.376(9)
C(71)–C(76)	1.390(7)	C(71)–C(72)	1.388(7)
C(72)–C(73)	1.383(8)	C(73)–C(74)	1.357(9)
C(74)–C(75)	1.374(9)	C(75)–C(76)	1.383(9)
C(81)–C(86)	1.394(8)	C(81)–C(82)	1.405(9)
C(82)–C(83)	1.373(11)	C(83)–C(84)	1.382(13)
C(84)–C(85)	1.370(13)	C(85)–C(86)	1.422(10)
Sb(1)–F(5)	1.697(7)	Sb(1)–F(1)	1.705(9)
Sb(1)–F(6)	1.715(8)	Sb(1)–F(3)	1.802(10)
Sb(1)–F(4)	1.858(5)	Sb(1)–F(2)	1.873(5)

Angle	Degree / °	Angle	Degree / °
N(1)–Rh(1)–N(4)	90.29(14)	N(1)–Rh(1)–N(2)	89.72(14)
N(4)–Rh(1)–N(2)	179.87(15)	N(1)–Rh(1)–N(3)	179.17(14)
N(4)–Rh(1)–N(3)	89.25(14)	N(2)–Rh(1)–N(3)	90.74(14)
N(1)–Rh(1)–P(1)	86.78(11)	N(4)–Rh(1)–P(1)	90.12(11)
N(2)–Rh(1)–P(1)	90.01(11)	N(3)–Rh(1)–P(1)	92.53(11)
N(1)–Rh(1)–P(2)	91.45(11)	N(4)–Rh(1)–P(2)	89.00(11)
N(2)–Rh(1)–P(2)	90.87(11)	N(3)–Rh(1)–P(2)	89.24(11)

250

Angle	Degree / °	Angle	Degree / °
P(1)–Rh(1)–P(2)	178.02(4)	CA2–N(1)–CA1	107.4(3)
CA2–N(1)–Rh(1)	127.0(3)	CA1–N(1)–Rh(1)	125.6(3)
CA3–N(2)–CA4	107.4(4)	CA3–N(2)–Rh(1)	126.9(3)
CA4–N(2)–Rh(1)	125.6(3)	CA6–N(3)–CA5	107.9(3)
CA6–N(3)–Rh(1)	126.9(3)	CA5–N(3)–Rh(1)	125.2(3)
CA8–N(4)–CA7	107.5(3)	CA8–N(4)–Rh(1)	125.9(3)
CA7–N(4)–Rh(1)	126.5(3)	O(1)–P(1)–C(51)	105.3(2)
O(1)–P(1)–C(61)	106.1(2)	C(51)–P(1)–C(61)	107.0(2)
O(1)–P(1)–Rh(1)	105.94(14)	C(51)–P(1)–Rh(1)	116.93(16)
C(61)–P(1)–Rh(1)	114.55(15)	O(2)–P(2)–C(71)	106.8(2)
O(2)–P(2)–C(81)	104.8(2)	C(71)–P(2)–C(81)	106.2(2)
O(2)–P(2)–Rh(1)	107.32(14)	C(71)–P(2)–Rh(1)	112.93(16)
C(81)–P(2)–Rh(1)	117.98(17)	C(1)–O(1)–P(1)	124.6(4)
C(3)–O(2)–P(2)	123.7(4)	CM1–CA1–N(1)	126.2(4)
CM1–CA1–CB1	125.1(4)	N(1)–CA1–CB1	108.7(4)
N(1)–CA2–CM2	125.5(4)	N(1)–CA2–CB2	108.6(4)
CM2–CA2–CB2	125.8(4)	N(2)–CA3–CM2	125.5(4)
N(2)–CA3–CB3	108.9(4)	CM2–CA3–CB3	125.5(4)
N(2)–CA4–CM3	125.9(4)	N(2)–CA4–CB4	108.8(4)
CM3–CA4–CB4	125.2(4)	N(3)–CA5–CM3	126.4(4)
N(3)–CA5–CB5	108.8(4)	CM3–CA5–CB5	124.6(4)
N(3)–CA6–CM4	126.1(4)	N(3)–CA6–CB6	109.2(4)
CM4–CA6–CB6	124.6(4)	N(4)–CA7–CM4	126.0(4)
N(4)–CA7–CB7	108.3(4)	CM4–CA7–CB7	125.7(4)
N(4)–CA8–CM1	125.8(4)	N(4)–CA8–CB8	109.1(4)
CM1–CA8–CB8	125.1(4)	CB2–CB1–CA1	107.3(4)
CB1–CB2–CA2	108.0(4)	CB4–CB3–CA3	107.7(4)
CB3–CB4–CA4	107.1(4)	CB6–CB5–CA5	106.6(4)
CB5–CB6–CA6	107.4(4)	CB8–CB7–CA7	107.1(4)
CB7–CB8–CA8	108.0(4)	CA1–CM1–CA8	125.2(4)
CA1–CM1–C(11)	116.3(4)	CA8–CM1–C(11)	118.4(4)
CA3–CM2–CA2	125.0(4)	CA3–CM2–C(21)	117.1(4)

Angle	Degree / °	Angle	Degree / °
CA2–CM2–C(21)	117.7(4)	CA5–CM3–CA4	125.6(4)
CA5–CM3–C(31)	118.1(4)	CA4–CM3–C(31)	116.1(4)
CA7–CM4–CA6	124.3(4)	CA7–CM4–C(41)	117.0(4)
CA6–CM4–C(41)	118.7(4)	Cl(2')–C(1')–Cl(1')	118.5(9)
Cl(1")–C(1")–Cl(2")	119.8(8)	C(2)–C(1)–O(1)	108.2(6)
C(4)–C(3)–O(2)	109.3(5)	C(12)–C(11)–C(16)	119.1(5)
C(12)–C(11)–CM1	120.8(5)	C(16)–C(11)–CM1	120.1(4)
C(11)–C(12)–C(13)	119.5(7)	C(14)–C(13)–C(12)	120.8(6)
C(13)–C(14)–C(15)	120.4(6)	C(16)–C(15)–C(14)	119.7(7)
C(15)–C(16)–C(11)	120.5(6)	C(26)–C(21)–C(22)	119.2(4)
C(26)–C(21)–CM2	119.5(4)	C(22)–C(21)–CM2	121.3(4)
C(21)–C(22)–C(23)	120.3(5)	C(24)–C(23)–C(22)	119.4(5)
C(25)–C(24)–C(23)	120.8(5)	C(24)–C(25)–C(26)	119.8(5)
C(21)–C(26)–C(25)	120.4(5)	C(36)–C(31)–C(32)	118.7(5)
C(36)–C(31)–CM3	120.4(5)	C(32)–C(31)–CM3	120.9(5)
C(33)–C(32)–C(31)	122.1(6)	C(34)–C(33)–C(32)	119.4(7)
C(35)–C(34)–C(33)	121.0(6)	C(34)–C(35)–C(36)	120.0(6)
C(31)–C(36)–C(35)	118.8(6)	C(42)–C(41)–C(46)	118.4(5)
C(42)–C(41)–CM4	120.7(4)	C(46)–C(41)–CM4	120.8(5)
C(41)–C(42)–C(43)	120.8(6)	C(44)–C(43)–C(42)	120.6(6)
C(43)–C(44)–C(45)	119.1(5)	C(44)–C(45)–C(46)	121.7(6)
C(45)–C(46)–C(41)	119.4(6)	C(52)–C(51)–C(56)	117.9(4)
C(52)–C(51)–P(1)	126.0(4)	C(56)–C(51)–P(1)	116.1(4)
C(51)–C(52)–C(53)	120.9(5)	C(54)–C(53)–C(52)	121.0(6)
C(53)–C(54)–C(55)	120.0(5)	C(56)–C(55)–C(54)	119.1(5)
C(55)–C(56)–C(51)	120.9(5)	C(62)–C(61)–C(66)	119.4(5)
C(62)–C(61)–P(1)	122.6(4)	C(66)–C(61)–P(1)	117.9(4)
C(61)–C(62)–C(63)	119.3(6)	C(64)–C(63)–C(62)	120.4(7)
C(63)–C(64)–C(65)	120.4(6)	C(64)–C(65)–C(66)	121.1(6)
C(65)–C(66)–C(61)	119.2(6)	C(76)–C(71)–C(72)	118.9(5)
C(76)–C(71)–P(2)	118.4(4)	C(72)–C(71)–P(2)	122.5(4)
C(73)–C(72)–C(71)	120.3(5)	C(74)–C(73)–C(72)	120.6(6)

Angle	Degree / °	Angle	Degree / °
C(73)–C(74)–C(75)	119.7(6)	C(74)–C(75)–C(76)	121.0(6)
C(75)–C(76)–C(71)	119.4(5)	C(86)–C(81)–C(82)	118.7(6)
C(86)–C(81)–P(2)	125.5(4)	C(82)–C(81)–P(2)	115.7(5)
C(83)–C(82)–C(81)	120.0(8)	C(84)–C(83)–C(82)	121.6(8)
C(83)–C(84)–C(85)	119.9(7)	C(84)–C(85)–C(86)	119.6(8)
C(81)–C(86)–C(85)	120.2(7)	F(5)–Sb(1)–F(1)	96.1(10)
F(5)–Sb(1)–F(6)	97.2(10)	F(1)–Sb(1)–F(6)	166.6(10)
F(5)–Sb(1)–F(3)	176.2(5)	F(1)–Sb(1)–F(3)	83.9(9)
F(6)–Sb(1)–F(3)	82.8(9)	F(5)–Sb(1)–F(4)	90.3(4)
F(1)–Sb(1)–F(4)	88.1(3)	F(6)–Sb(1)–F(4)	91.6(4)
F(3)–Sb(1)–F(4)	93.5(4)	F(5)–Sb(1)–F(2)	91.1(4)
F(1)–Sb(1)–F(2)	91.4(4)	F(6)–Sb(1)–F(2)	88.5(4)
F(3)–Sb(1)–F(2)	85.1(4)	F(4)–Sb(1)–F(2)	178.5(3)

Table AI.8: Bond lengths [Å] and angles [°] for [Rh(TPP)(deppt)₂](SbF₆)

Bond	Length / Å	Bond	Length / Å
Rh–N(2)	2.041(4)	Rh–N(2)#1	2.041(4)
Rh–N(1)#1	2.047(4)	Rh–N(1)	2.047(4)
Rh–P(1)#1	2.3317(16)	Rh–P(1)	2.3317(16)
N(1)–CA2	1.370(6)	N(1)–CA1	1.378(6)
N(2)–CA4	1.376(6)	N(2)–CA3	1.384(6)
P(1)–O(1)	1.592(4)	P(1)–O(2)	1.592(5)
P(1)–C(71)	1.766(6)	O(1)–C(51)	1.429(8)
O(2)–C(61)	1.358(13)	O(2)–C(61X)	1.76(4)
CA1–CM2#1	1.386(7)	CA1–CB1	1.438(7)
CA2–CM1	1.386(7)	CA2–CB2	1.442(7)
CA3–CM1	1.390(7)	CA3–CB3	1.425(7)
CA4–CM2	1.388(7)	CA4–CB4	1.440(7)
CB1–CB2	1.359(7)	CB3–CB4	1.365(8)
CM1–C(11)	1.504(7)	CM2–CA1#1	1.386(7)
CM2–C(21)	1.504(7)	C(11)–C(12)	1.381(8)
C(11)–C(16)	1.384(8)	C(12)–C(13)	1.394(8)
C(13)–C(14)	1.357(10)	C(14)–C(15)	1.392(10)
C(15)–C(16)	1.385(9)	C(21)–C(22)	1.370(8)
C(21)–C(26)	1.411(8)	C(22)–C(23)	1.392(8)
C(23)–C(24)	1.361(9)	C(24)–C(25)	1.369(10)
C(25)–C(26)	1.394(8)	C(51)–C(52)	1.504(12)
C(61)–C(62)	1.36(2)	C(61X)–C(62X)	1.31(4)
C(71)–C(76)	1.373(9)	C(71)–C(72)	1.424(9)
C(72)–C(73)	1.355(10)	C(73)–C(74)	1.378(12)
C(74)–C(75)	1.313(12)	C(75)–C(76)	1.359(11)
Rh'–N(2')	2.029(4)	Rh'–N(2')#2	2.029(4)
Rh'–N(1')#2	2.048(4)	Rh'–N(1')	2.048(4)
Rh'–P(1')#2	2.3308(14)	Rh'–P(1')	2.3308(14)
P(1')–O(1')	1.560(5)	P(1')–O(2')	1.570(4)
P(1')–C(71')	1.798(6)	N(1')–CA1'	1.368(6)

Bond	Length / Å	Bond	Length / Å
N(1')–CA2'	1.380(6)	N(2')–CA4'	1.374(6)
N(2')–CA3'	1.391(6)	O(1')–C(51')	1.312(9)
O(2')–C(61')	1.418(8)	CA1'–CM2'#2	1.398(7)
CA1'–CB1'	1.445(7)	CA2'–CM1'	1.396(7)
CA2'–CB2'	1.428(7)	CA3'–CM1'	1.377(7)
CA3'–CB3'	1.448(7)	CA4'–CM2'	1.378(7)
CA4'–CB4'	1.447(7)	CM1'–C(11')	1.501(7)
CM2'–CA1'#2	1.398(7)	CM2'–C(21')	1.499(7)
C(11')–C(12')	1.373(8)	C(11')–C(16')	1.376(8)
C(12')–C(13')	1.377(8)	C(13')–C(14')	1.395(9)
C(14')–C(15')	1.330(9)	C(15')–C(16')	1.413(8)
C(21')–C(26')	1.367(8)	C(21')–C(22')	1.394(8)
C(22')–C(23')	1.375(8)	C(23')–C(24')	1.361(11)
C(24')–C(25')	1.358(11)	C(25')–C(26')	1.392(9)
CB1'–CB2'	1.346(8)	CB3'–CB4'	1.344(8)
C(51')–C(52')	1.440(12)	C(61')–C(62')	1.445(11)
C(71')–C(76')	1.366(9)	C(71')–C(72')	1.410(9)
C(72')–C(73')	1.403(10)	C(73')–C(74')	1.389(12)
C(74')–C(75')	1.371(12)	C(75')–C(76')	1.404(10)
Sb–F(6)	1.796(9)	Sb–F(4)	1.846(5)
Sb–F(1)	1.855(5)	Sb–F(2)	1.852(6)
Sb–F(3)	1.855(5)	Sb–F(5)	1.901(6)
Sb–F(6X)	1.91(2)		

Angle	Degree / °	Angle	Degree / °
N(2)–Rh–N(2)#1	180.0	N(2)–Rh–N(1)#1	89.51(15)
N(2)#1–Rh–N(1)#1	90.49(15)	N(2)–Rh–N(1)	90.49(15)
N(2)#1–Rh–N(1)	89.51(15)	N(1)#1–Rh–N(1)	180.00(14)
N(2)–Rh–P(1)#1	89.47(12)	N(2)#1–Rh–P(1)#1	90.53(12)
N(1)#1–Rh–P(1)#1	90.75(12)	N(1)–Rh–P(1)#1	89.25(12)
N(2)–Rh–P(1)	90.53(12)	N(2)#1–Rh–P(1)	89.47(12)

Angle	Degree / °	Angle	Degree / °
N(1)#1–Rh–P(1)	89.25(12)	N(1)–Rh–P(1)	90.75(12)
P(1)#1–Rh–P(1)	180.0	CA2–N(1)–CA1	107.8(4)
CA2–N(1)–Rh	125.4(3)	CA1–N(1)–Rh	126.2(3)
CA4–N(2)–CA3	107.7(4)	CA4–N(2)–Rh	126.6(3)
CA3–N(2)–Rh	125.7(3)	O(1)–P(1)–O(2)	111.6(3)
O(1)–P(1)–C(71)	105.1(3)	O(2)–P(1)–C(71)	103.6(3)
O(1)–P(1)–Rh	109.86(18)	O(2)–P(1)–Rh	110.2(2)
C(71)–P(1)–Rh	116.3(2)	C(51)–O(1)–P(1)	128.0(5)
C(61)–O(2)–P(1)	136.1(7)	C(61)–O(2)–C(61X)	59.4(14)
P(1)–O(2)–C(61X)	119.5(14)	N(1)–CA1–CM2#1	126.2(4)
N(1)–CA1–CB1	108.7(4)	CM2#1–CA1–CB1	125.1(5)
N(1)–CA2–CM1	126.8(4)	N(1)–CA2–CB2	108.7(4)
CM1–CA2–CB2	124.4(5)	N(2)–CA3–CM1	126.0(4)
N(2)–CA3–CB3	108.8(4)	CM1–CA3–CB3	125.2(5)
N(2)–CA4–CM2	126.2(4)	N(2)–CA4–CB4	108.5(4)
CM2–CA4–CB4	125.4(4)	CB2–CB1–CA1	107.5(4)
CB1–CB2–CA2	107.3(5)	CB4–CB3–CA3	107.7(5)
CB3–CB4–CA4	107.4(4)	CA2–CM1–CA3	125.3(5)
CA2–CM1–C(11)	116.3(4)	CA3–CM1–C(11)	118.4(4)
CA1#1–CM2–CA4	125.0(4)	CA1#1–CM2–C(21)	117.4(4)
CA4–CM2–C(21)	117.5(4)	C(12)–C(11)–C(16)	118.7(5)
C(12)–C(11)–CM1	120.8(5)	C(16)–C(11)–CM1	120.4(5)
C(11)–C(12)–C(13)	120.3(6)	C(14)–C(13)–C(12)	121.0(6)
C(13)–C(14)–C(15)	119.2(6)	C(16)–C(15)–C(14)	120.1(6)
C(15)–C(16)–C(11)	120.7(6)	C(22)–C(21)–C(26)	118.1(5)
C(22)–C(21)–CM2	121.9(5)	C(26)–C(21)–CM2	119.8(5)
C(21)–C(22)–C(23)	121.5(6)	C(24)–C(23)–C(22)	119.7(6)
C(23)–C(24)–C(25)	120.8(6)	C(24)–C(25)–C(26)	120.0(6)
C(25)–C(26)–C(21)	119.9(6)	O(1)–C(51)–C(52)	107.6(7)
O(2)–C(61)–C(62)	117.2(14)	C(62X)–C(61X)–O(2)	100(3)
C(76)–C(71)–C(72)	114.4(6)	C(76)–C(71)–P(1)	125.2(5)
C(72)–C(71)–P(1)	119.9(5)	C(73)–C(72)–C(71)	122.5(7)

Angle	Degree / °	Angle	Degree / °
C(72)–C(73)–C(74)	119.2(8)	C(75)–C(74)–C(73)	119.3(8)
C(74)–C(75)–C(76)	122.8(8)	C(75)–C(76)–C(71)	121.7(8)
N(2')–Rh'–N(2')#2	180.0(2)	N(2')–Rh'–N(1')#2	89.66(15)
N(2')#2–Rh'–N(1')#2	90.34(15)	N(2')–Rh'–N(1')	90.34(15)
N(2')#2–Rh'–N(1')	89.66(15)	N(1')#2–Rh'–N(1')	180.000(1)
N(2')–Rh'–P(1')#2	89.32(12)	N(2')#2–Rh'–P(1')#2	90.68(12)
N(1')#2–Rh'–P(1')#2	90.75(12)	N(1')–Rh'–P(1')#2	89.25(12)
N(2')–Rh'–P(1')	90.68(12)	N(2')#2–Rh'–P(1')	89.32(12)
N(1')#2–Rh'–P(1')	89.25(12)	N(1')–Rh'–P(1')	90.75(12)
P(1')#2–Rh'–P(1')	180.0	O(1')–P(1')–O(2')	109.6(3)
O(1')–P(1')–C(71')	99.4(3)	O(2')–P(1')–C(71')	106.8(3)
O(1')–P(1')–Rh'	118.2(2)	O(2')–P(1')–Rh'	108.62(18)
C(71')–P(1')–Rh'	113.39(19)	CA1'–N(1')–CA2'	107.4(4)
CA1'–N(1')–Rh'	126.4(3)	CA2'–N(1')–Rh'	125.9(3)
CA4'–N(2')–CA3'	108.1(4)	CA4'–N(2')–Rh'	126.3(3)
CA3'–N(2')–Rh'	125.4(3)	C(51')–O(1')–P(1')	131.4(6)
C(61')–O(2')–P(1')	127.5(5)	N(1')–CA1'–CM2'#2	126.1(4)
N(1')–CA1'–CB1'	108.5(4)	CM2'#2–CA1'–CB1'	125.4(5)
N(1')–CA2'–CM1'	126.2(5)	N(1')–CA2'–CB2'	108.9(4)
CM1'–CA2'–CB2'	124.9(5)	CM1'–CA3'–N(2')	127.3(4)
CM1'–CA3'–CB3'	125.1(5)	N(2')–CA3'–CB3'	107.7(4)
N(2')–CA4'–CM2'	127.0(4)	N(2')–CA4'–CB4'	108.2(4)
CM2'–CA4'–CB4'	124.7(5)	CA3'–CM1'–CA2'	124.6(5)
CA3'–CM1'–C(11')	116.1(4)	CA2'–CM1'–C(11')	119.3(4)
CA4'–CM2'–CA1'#2	124.4(5)	CA4'–CM2'–C(21')	117.1(4)
CA1'#2–CM2'–C(21')	118.5(4)	C(12')–C(11')–C(16')	119.4(5)
C(12')–C(11')–CM1'	120.6(5)	C(16')–C(11')–CM1'	119.8(5)
C(11')–C(12')–C(13')	120.7(6)	C(12')–C(13')–C(14')	119.5(6)
C(15')–C(14')–C(13')	120.6(6)	C(14')–C(15')–C(16')	120.2(6)
C(11')–C(16')–C(15')	119.6(6)	C(26')–C(21')–C(22')	118.1(5)
C(26')–C(21')–CM2'	122.7(5)	C(22')–C(21')–CM2'	119.2(5)
C(23')–C(22')–C(21')	121.0(6)	C(24')–C(23')–C(22')	119.8(7)

APPENDIX II: TABLES OF ATOMIC COORDINATES AND ISOTROPIC DISPLACEMENT PARAMETERS

Table AII.1: Atomic coordinates (x 10^4) and equivalent isotropic displacement parameters ($Å^2$ x 10^3) for [Mn(TPP)(PPh$_3$)$_2$](SbF$_6$). U(eq) is defined as one third of the trace of the orthogonalized Uij tensor.

Atom	x	y	z	U(eq)
Mn	2391(1)	−2541(1)	−215(1)	41(1)
N(1)	2042(4)	−2962(3)	−922(2)	51(2)
N(2)	3799(4)	−2652(3)	−394(2)	43(1)
N(3)	2748(4)	−2126(3)	496(2)	46(1)
N(4)	974(4)	−2470(3)	−44(2)	45(1)
CA1	1119(6)	−3083(4)	−1127(3)	54(2)
CA2	2678(6)	−3124(4)	−1343(3)	53(2)
CA3	4197(6)	−2918(3)	−855(3)	50(2)
CA4	4582(5)	−2504(4)	−47(3)	50(2)
CA5	3662(5)	−2007(3)	689(3)	45(2)
CA6	2096(5)	−1882(3)	885(3)	45(2)
CA7	571(5)	−2245(3)	436(3)	45(2)
CA8	201(5)	−2677(3)	−350(3)	46(2)
CB1	1182(6)	−3306(5)	−1671(3)	69(2)
CB2	2153(7)	−3332(5)	−1793(4)	76(3)
CB3	5239(5)	−2950(4)	−787(3)	51(2)
CB4	5477(6)	−2701(4)	−304(3)	57(2)
CB5	3593(6)	−1669(4)	1208(3)	55(2)
CB6	2636(6)	−1608(4)	1318(3)	55(2)
CB7	−677(5)	−2571(4)	−58(3)	54(2)
CM1	3671(6)	−3120(4)	−1309(3)	54(2)
CM2	4534(5)	−2191(3)	451(3)	44(2)
CM3	1084(5)	−1964(3)	861(3)	46(2)
CM4	239(5)	−2951(3)	−863(3)	49(2)
C(11)	4274(5)	−3328(4)	−1782(3)	55(2)

Atom	x	y	z	U(eq)
C(12)	4234(6)	−3963(4)	−1994(3)	63(2)
C(13)	4805(8)	−4135(5)	−2436(4)	82(3)
C(14)	5403(6)	−3668(6)	−2661(3)	69(2)
C(15)	5395(7)	−3040(5)	−2484(4)	79(3)
C(16)	4855(6)	−2858(4)	−2047(3)	63(2)
C(21)	5498(6)	−2072(4)	744(3)	60(2)
C(22)	6062(9)	−1541(7)	590(6)	125(5)
C(23)	6990(12)	−1499(13)	862(10)	195(11)
C(24)	7281(10)	−1886(16)	1220(7)	190(13)
C(25)	6700(11)	−2416(9)	1348(5)	125(6)
C(26)	5829(8)	−2515(6)	1107(4)	84(3)
C(31)	533(5)	−1733(4)	1359(3)	55(2)
C(32)	430(6)	−1071(4)	1478(3)	64(2)
C(33)	−140(8)	−863(6)	1909(4)	90(3)
C(34)	−617(7)	−1342(8)	2208(4)	95(4)
C(35)	−497(7)	−2000(7)	2096(4)	85(3)
C(36)	37(6)	−2213(5)	1658(3)	68(2)
C(41)	−685(5)	−3137(4)	−1150(3)	52(2)
C(42)	−917(7)	−3809(4)	−1239(3)	64(2)
C(43)	−1789(9)	−3972(6)	−1503(4)	87(4)
C(44)	−2449(7)	−3473(6)	−1651(4)	76(3)
C(45)	−2228(7)	−2838(6)	−1569(4)	87(3)
C(46)	−1330(7)	−2659(5)	−1318(4)	73(2)
P(1)	2451(2)	−3857(1)	456(1)	61(1)
C(51)	3151(6)	−3829(4)	1090(3)	59(2)
C(52)	3960(8)	−4229(5)	1188(4)	85(3)
C(53)	4511(10)	−4174(6)	1667(5)	107(4)
C(54)	4242(9)	−3709(6)	2040(4)	90(3)
C(55)	3430(10)	−3292(5)	1946(5)	93(4)
C(56)	2912(8)	−3347(4)	1465(4)	72(3)
C(61)	2885(6)	−4613(4)	114(3)	56(2)
C(62)	3353(9)	−4561(5)	−354(4)	95(4)

Atom	x	y	z	U(eq)
C(63)	3690(13)	−5139(7)	−617(5)	134(6)
C(64)	3539(11)	−5740(6)	−409(5)	108(4)
C(65)	3063(9)	−5806(5)	65(6)	109(4)
C(66)	2734(8)	−5245(5)	308(5)	97(4)
C(71)	1209(6)	−4104(4)	660(4)	63(2)
C(72)	953(8)	−4232(6)	1181(5)	107(4)
C(73)	−65(10)	−4380(8)	1275(6)	132(6)
C(74)	−720(8)	−4408(6)	877(7)	106(5)
C(75)	−451(9)	−4292(6)	355(7)	111(4)
C(76)	528(7)	−4132(4)	257(5)	76(3)
P(2)	2494(2)	−1112(1)	−699(1)	66(1)
C(81)	1947(6)	−422(4)	−306(3)	56(2)
C(82)	1271(6)	28(4)	−524(4)	63(2)
C(83)	904(7)	520(5)	−190(4)	76(3)
C(84)	1202(8)	596(5)	328(5)	83(3)
C(85)	1834(8)	147(4)	535(4)	76(3)
C(86)	2221(7)	−359(4)	228(3)	64(2)
C(91)	1918(8)	−1033(5)	−1353(4)	79(3)
C(92)	1053(10)	−1360(5)	−1444(5)	99(3)
C(93)	549(14)	−1345(7)	−1930(7)	129(5)
C(94)	924(11)	−1023(11)	−2337(7)	137(6)
C(95)	1765(17)	−645(10)	−2293(6)	160(8)
C(96)	2310(11)	−652(9)	−1773(5)	136(6)
C(101)	3763(10)	−880(9)	−773(9)	74(8)
C(102)	4220(14)	−1237(10)	−1181(9)	64(6)
C(103)	5207(14)	−1136(9)	−1278(7)	119(12)
C(104)	5737(10)	−678(12)	−966(9)	97(9)
C(105)	5280(12)	−322(14)	−558(11)	139(15)
C(106)	4292(12)	−423(11)	−461(9)	94(9)
C(201)	3741(9)	−788(9)	−852(11)	64(7)
C(202)	4459(13)	−1245(8)	−1003(11)	82(9)
C(203)	5377(12)	−1013(10)	−1148(11)	119(13)

Atom	x	y	z	U(eq)
C(204)	5578(10)	−325(12)	−1142(7)	85(7)
C(205)	4860(17)	132(10)	−992(13)	154(18)
C(206)	3941(15)	−100(10)	−847(15)	170(20)
Sb	2385(1)	763(1)	2437(1)	89(1)
F(1)	2815(9)	512(7)	3101(4)	185(4)
F(2)	2923(11)	9(6)	2130(5)	250(7)
F(3)	1357(10)	245(5)	2579(5)	202(6)
F(4)	2003(10)	997(5)	1756(3)	182(5)
F(5)	1680(8)	1449(4)	2714(3)	160(4)
F(6)	3426(10)	1334(9)	2341(5)	259(7)

Table AII.2: Atomic coordinates (x 10^4) and equivalent isotropic displacement parameters (Å^2 x 10^3) for [Mn(TPP){(O)PH(OPh)$_2$}](SbF$_6$). U(eq) is defined as one third of the trace of the orthogonalized Uij tensor.

Atom	x	y	z	U(eq)
Mn	3221(1)	5029(1)	4341(1)	39(1)
P(1)	1213(1)	4082(1)	4517(1)	69(1)
N(1)	3199(3)	5660(2)	5204(2)	42(1)
N(2)	3981(3)	4419(2)	5047(2)	40(1)
N(3)	3436(3)	4444(2)	3456(2)	44(1)
N(4)	2729(3)	5709(2)	3598(2)	46(1)
CA1	2770(3)	6257(2)	5168(2)	42(1)
CA2	3367(3)	5530(2)	5975(2)	43(1)
CA3	4203(3)	4502(2)	5827(2)	42(1)
CA4	4370(3)	3832(2)	4855(2)	42(1)
CA5	3755(3)	3814(2)	3499(2)	45(1)
CA6	3049(4)	4530(2)	2707(2)	51(1)
CA7	2576(4)	5659(3)	2799(3)	56(1)
CA8	2490(4)	6336(2)	3768(2)	48(1)
CB1	2657(4)	6484(2)	5935(3)	55(1)
CB2	3008(4)	6038(2)	6415(3)	59(1)
CB3	4810(3)	3976(2)	6106(2)	47(1)
CB4	4896(3)	3575(2)	5522(3)	47(1)
CB5	3558(4)	3513(2)	2770(3)	55(1)
CB6	3152(4)	3948(3)	2286(3)	63(1)
CB7	2270(5)	6252(3)	2489(3)	74(2)
CB8	2232(5)	6670(3)	3062(3)	67(2)
CM1	3852(3)	4977(2)	6270(2)	43(1)
CM2	4221(3)	3525(2)	4148(2)	43(1)
CM3	2672(4)	5099(2)	2391(3)	57(1)
CM4	2476(3)	6590(2)	4497(3)	45(1)
O(1)	1853(3)	4630(2)	4582(2)	63(1)
O(2)	1593(4)	3626(3)	3886(3)	103(2)
O(3)	115(3)	4237(2)	4286(3)	85(1)

Atom	x	y	z	U(eq)
C(11)	3971(4)	4906(2)	7142(2)	46(1)
C(12)	3556(4)	4386(3)	7481(3)	61(1)
C(13)	3632(5)	4313(3)	8272(3)	78(2)
C(14)	4163(6)	4763(4)	8715(3)	91(2)
C(15)	4562(5)	5268(3)	8390(3)	79(2)
C(16)	4474(4)	5344(3)	7598(3)	62(1)
C(21)	4493(3)	2833(2)	4096(2)	45(1)
C(22)	4052(4)	2389(2)	4549(3)	62(1)
C(23)	4265(5)	1741(3)	4507(4)	80(2)
C(24)	4918(5)	1537(3)	4009(3)	72(2)
C(25)	5368(4)	1969(3)	3556(3)	64(1)
C(26)	5155(4)	2609(2)	3599(3)	55(1)
C(31)	2346(5)	5094(3)	1549(3)	73(2)
C(32)	1497(7)	4828(4)	1283(4)	110(3)
C(33)	1153(10)	4814(5)	546(5)	147(5)
C(34)	1683(12)	5085(5)	17(6)	152(6)
C(35)	2576(12)	5403(5)	229(5)	156(6)
C(36)	2914(7)	5390(4)	1032(3)	110(3)
C(41)	2123(4)	7278(2)	4584(3)	50(1)
C(42)	1179(5)	7432(3)	4361(4)	70(2)
C(43)	881(5)	8072(3)	4438(4)	81(2)
C(44)	1527(6)	8528(3)	4711(3)	75(2)
C(45)	2479(5)	8376(3)	4937(3)	72(2)
C(46)	2788(4)	7730(2)	4866(3)	63(1)
C(51)	1089(5)	3092(3)	3577(4)	84(2)
C(52)	852(14)	2591(5)	3957(7)	189(7)
C(53)	360(18)	2118(7)	3616(9)	276(13)
C(54)	81(12)	2144(8)	2866(10)	210(9)
C(55)	379(9)	2574(7)	2469(7)	160(6)
C(56)	855(7)	3098(5)	2786(5)	121(3)
C(61)	−202(4)	4626(3)	3645(4)	81(2)
C(62)	24(6)	5278(4)	3647(6)	106(3)

Atom	x	y	z	U(eq)
C(63)	−347(7)	5627(5)	3000(6)	121(3)
C(64)	−941(7)	5367(5)	2479(6)	125(4)
C(65)	−1154(6)	4744(6)	2462(5)	121(3)
C(66)	−763(5)	4340(4)	3058(5)	96(2)
Sb(1)	2134(1)	2378(1)	6581(1)	79(1)
F(1) .	1891(6)	1973(5)	5672(3)	193(3)
F(2)	1162(6)	2919(4)	6265(6)	219(4)
F(3)	3087(8)	2839(6)	6206(5)	292(7)
F(4)	2329(6)	2796(5)	7497(4)	213(4)
F(5)	1133(5)	1904(4)	6979(3)	182(3)
F(6)	2961(8)	1774(5)	6939(10)	351(9)

Table AII.3: Atomic coordinates (x 10^4) and equivalent isotropic displacement parameters (Å^2 x 10^3) for [Co(TPP)(depp)$_2$](SbF$_6$). U(eq) is defined as one third of the trace of the orthogonalized Uij tensor.

Atom	x	y	z	U(eq)
F(1)	−434(3)	3636(3)	3270(2)	110(2)
F(2)	−478(3)	2774(2)	1808(2)	120(2)
F(3)	−486(2)	4479(2)	1788(2)	105(2)
Sb(1)	0	3635(1)	2500	73(1)
Sb(2)	−1002(2)	3555(2)	1992(2)	44(1)
Sb(3)	−504(5)	3680(5)	2424(5)	97(2)
Co	2500	2500	0	15(1)
P(1)	2751(1)	1234(1)	−576(1)	22(1)
N(1)	1683(1)	2213(2)	−580(2)	18(1)
N(2)	2501(1)	1828(2)	1079(2)	20(1)
CA1	1337(2)	2435(2)	−1441(2)	22(1)
CA2	1332(2)	1762(2)	−219(2)	22(1)
CA3	2047(2)	1409(2)	1214(2)	25(1)
CA4	2960(2)	1722(2)	1865(2)	23(1)
CB1	776(2)	2102(2)	−1606(2)	29(1)
CB2	757(2)	1701(2)	−852(2)	27(1)
CB3	2219(2)	1027(3)	2101(2)	36(1)
CB4	2771(2)	1220(2)	2491(2)	33(1)
CM1	1488(2)	1381(2)	633(2)	24(1)
CM2	3496(1)	2067(2)	2050(2)	20(1)
C(11)	1034(2)	948(2)	923(2)	26(1)
C(12)	634(2)	1439(2)	1143(2)	33(1)
C(13)	212(2)	1047(3)	1420(3)	41(1)
C(14)	189(2)	140(3)	1461(3)	42(1)
C(15)	595(2)	−349(3)	1262(3)	44(1)
C(16)	1014(2)	38(2)	986(3)	36(1)
C(21)	3941(2)	1878(2)	2948(2)	24(1)
C(22)	4362(2)	1266(2)	3019(3)	38(1)
C(24)	4773(2)	1543(3)	4591(2)	43(1)

Atom	x	y	z	U(eq)
C(25)	4358(2)	2138(3)	4537(2)	49(1)
C(26)	3936(2)	2312(3)	3716(2)	40(1)
C(51)	2322(2)	292(2)	−505(2)	35(1)
C(52)	1807(2)	136(3)	−1169(3)	43(1)
C(53)	1494(3)	−632(4)	−1166(4)	68(2)
C(54)	1688(3)	−1212(4)	−508(5)	78(2)
C(55)	2192(4)	−1062(4)	203(5)	83(2)
C(56)	2516(3)	−296(3)	203(3)	59(2)
C(23)	4784(2)	1113(3)	3835(3)	47(1)
C(1)	2671(2)	1243(2)	−1780(2)	37(1)
C(2)	3131(4)	1645(4)	−2060(4)	81(2)
C(3)	3496(2)	913(3)	−18(3)	43(1)
C(4)	3695(2)	84(3)	−374(4)	66(2)

Table AII.4: Atomic coordinates (x 10^4) and equivalent isotropic displacement parameters ($Å^2$ x 10^3) for [Co(TPP)(edpp)$_2$](SbF$_6$). U(eq) is defined as one third of the trace of the orthogonalized Uij tensor.

Atom	x	y	z	U(eq)
Cl(1S)	7317(1)	5729(1)	182(1)	73(1)
Cl(2S)	8557(1)	6214(1)	1319(1)	93(1)
C(1S)	7816(2)	6518(2)	613(2)	51(1)
Sb(1)	7208(1)	8646(1)	11(1)	23(1)
F(5)	6999(1)	7744(1)	−488(1)	45(1)
F(1)	6755(1)	8188(1)	637(1)	42(1)
F(6)	7448(1)	9526(1)	528(1)	46(1)
F(2)	8195(1)	8238(1)	480(1)	48(1)
F(3)	7684(1)	9071(1)	−609(1)	48(1)
F(4)	6227(1)	9032(1)	−449(1)	58(1)
Co(1)	8(1)	2143(1)	2267(1)	8(1)
P(2)	−124(1)	3359(1)	2659(1)	9(1)
P(1)	90(1)	920(1)	1850(1)	10(1)
N(3)	712(1)	2525(1)	1736(1)	10(1)
N(1)	−703(1)	1763(1)	2782(1)	9(1)
N(2)	935(1)	1937(1)	3025(1)	10(1)
CA5	1532(1)	2494(1)	1908(1)	11(1)
N(4)	−923(1)	2349(1)	1509(1)	10(1)
CA2	−509(1)	1588(1)	3447(1)	11(1)
CA8	−1691(1)	2097(1)	1428(1)	11(1)
CA7	−933(1)	2748(1)	943(1)	11(1)
C(81)	−1164(1)	3622(1)	2512(1)	12(1)
C(51)	−166(1)	915(1)	950(1)	12(1)
CA6	496(1)	2928(1)	1150(1)	11(1)
CB2	−1198(1)	1299(1)	3625(1)	13(1)
CM2	2019(1)	2205(1)	2501(1)	11(1)
CM3	−280(1)	3074(1)	781(1)	11(1)
C(21)	2895(1)	2214(1)	2570(1)	12(1)

Atom	x	y	z	U(eq)
C(91)	370(1)	3545(1)	3527(1)	12(1)
CA1	−1501(1)	1587(1)	2542(1)	10(1)
C(73)	322(1)	4102(1)	2253(1)	14(1)
CA4	1727(1)	1966(1)	3027(1)	11(1)
C(31)	−446(1)	3587(1)	191(1)	12(1)
C(52)	342(1)	1235(1)	602(1)	13(1)
CB1	−1804(1)	1290(1)	3065(1)	13(1)
C(41)	−2807(1)	1431(1)	1725(1)	12(1)
C(92)	−20(1)	3726(1)	4009(1)	14(1)
C(61)	1039(1)	431(1)	2156(1)	13(1)
C(82)	−1639(1)	3306(1)	2891(1)	14(1)
CB5	1830(1)	2881(1)	1414(1)	13(1)
C(71)	−590(1)	233(1)	2074(1)	15(1)
C(86)	−1519(1)	4109(1)	1987(1)	16(1)
CM1	248(1)	1616(1)	3884(1)	12(1)
CM4	−1971(1)	1712(1)	1901(1)	11(1)
C(22)	3406(1)	2682(1)	3037(1)	16(1)
C(56)	−903(1)	626(1)	586(1)	15(1)
CA3	929(1)	1748(1)	3664(1)	12(1)
CB6	1190(1)	3162(1)	956(1)	13(1)
C(26)	3205(1)	1789(1)	2132(1)	16(1)
C(96)	1206(1)	3553(1)	3704(1)	17(1)
CB4	2218(1)	1762(1)	3670(1)	15(1)
C(83)	−2438(1)	3493(1)	2758(1)	19(1)
C(53)	134(1)	1244(1)	−84(1)	17(1)
C(11)	304(1)	1453(1)	4596(1)	13(1)
CB7	−1717(1)	2735(1)	494(1)	15(1)
CB3	1728(1)	1657(1)	4072(1)	15(1)
CB8	−2182(1)	2325(1)	788(1)	14(1)
C(36)	−218(1)	3411(1)	−385(1)	17(1)
C(62)	1562(1)	271(1)	1770(1)	15(1)
C(35)	−420(1)	3896(1)	−932(1)	21(1)

Atom	x	y	z	$U(eq)$
C(74)	335(1)	4907(1)	2545(1)	19(1)
C(12)	−136(1)	1895(1)	4927(1)	17(1)
C(95)	1631(1)	3750(1)	4342(1)	21(1)
C(24)	4510(1)	2308(1)	2612(1)	20(1)
C(16)	724(1)	827(1)	4928(1)	18(1)
C(25)	4009(1)	1840(1)	2150(1)	19(1)
C(54)	−593(1)	940(1)	−438(1)	19(1)
C(85)	−2322(1)	4280(1)	1849(1)	22(1)
C(42)	−3456(1)	1929(1)	1592(1)	17(1)
C(44)	−4359(1)	863(1)	1379(1)	21(1)
C(55)	−1110(1)	635(1)	−103(1)	18(1)
C(72)	−489(1)	−597(1)	1882(1)	21(1)
C(23)	4212(1)	2723(1)	3058(1)	20(1)
C(45)	−3718(1)	366(1)	1514(1)	21(1)
C(66)	1236(1)	187(1)	2817(1)	19(1)
C(34)	−842(1)	4560(1)	−909(1)	21(1)
C(33)	−1074(1)	4739(1)	−343(1)	21(1)
C(63)	2262(1)	−134(1)	2041(1)	21(1)
C(64)	2441(1)	−383(1)	2689(1)	24(1)
C(84)	−2782(1)	3978(1)	2236(1)	23(1)
C(32)	−877(1)	4257(1)	201(1)	18(1)
C(13)	−176(1)	1705(1)	5564(1)	23(1)
C(94)	1233(1)	3950(1)	4812(1)	23(1)
C(46)	−2947(1)	649(1)	1688(1)	17(1)
C(43)	−4225(1)	1642(1)	1421(1)	21(1)
C(65)	1928(1)	−223(1)	3082(1)	24(1)
C(93)	412(1)	3932(1)	4647(1)	21(1)
C(15)	702(1)	654(1)	5576(1)	25(1)
C(14)	245(1)	1086(1)	5887(1)	27(1)

Table AII.5: Atomic coordinates (x 10^4) and equivalent isotropic displacement parameters ($Å^2$ x 10^3) for [Co(TPP)(deppt)$_2$](SbF$_6$). U(eq) is defined as one third of the trace of the orthogonalized Uij tensor.

Atom	x	y	z	U(eq)
Co(1)	−5000	5000	0	34(1)
Co(1')	−5000	5000	5000	35(1)
P(1)	−3811(1)	4131(1)	64(1)	46(1)
P(1')	−3980(1)	4281(1)	5663(1)	47(1)
O(1)	−2996(3)	4539(3)	−114(2)	76(1)
O(1')	−3981(4)	4574(4)	6265(2)	103(2)
O(2)	−3429(3)	3743(4)	647(2)	109(2)
O(2')	−4217(3)	3346(2)	5592(2)	81(1)
N(2)	−4709(3)	5037(2)	822(1)	40(1)
N(2')	−4003(2)	5785(2)	4991(2)	40(1)
N(1)	−4152(3)	5913(2)	22(1)	39(1)
N(1')	−5363(2)	5650(2)	5567(2)	38(1)
CA1	−3956(3)	6277(3)	−420(2)	46(1)
CA1'	−6019(3)	5454(3)	5838(2)	43(1)
CA2	−4071(4)	5525(3)	1177(2)	49(1)
CA2'	−3763(3)	6464(3)	5314(2)	44(1)
CA3	−3574(3)	6278(3)	486(2)	47(1)
CA3'	−4934(3)	6339(3)	5818(2)	48(1)
CA4	−5040(3)	4538(3)	1157(2)	44(1)
CA4'	−3425(3)	5774(3)	4653(2)	40(1)
CB1	−3252(4)	6874(4)	−236(2)	70(2)
CB1'	−5988(4)	6032(3)	6262(2)	64(2)
CB2	−3018(4)	6870(4)	320(2)	67(2)
CB2'	−5338(4)	6575(3)	6245(3)	64(2)
CB3	−4023(4)	5328(4)	1737(2)	65(2)
CB3'	−3005(4)	6867(3)	5185(2)	59(1)
CB4	−4618(4)	4731(4)	1723(2)	63(2)
CB4'	−2792(4)	6444(3)	4784(2)	56(1)
CM1	−3519(3)	6105(3)	1029(2)	46(1)

271

Atom	x	y	z	U(eq)
CM1'	–4189(3)	6728(3)	5703(2)	47(1)
CM2	–5653(3)	3900(3)	978(2)	45(1)
CM2'	–3417(3)	5208(3)	4252(2)	43(1)
C(11)	–2801(4)	6554(3)	1472(2)	54(1)
C(12)	–3030(5)	7263(4)	1674(2)	67(2)
C(13)	–2330(5)	7694(4)	2058(2)	78(2)
C(14)	–1444(5)	7429(5)	2224(2)	76(2)
C(15)	–1213(4)	6721(4)	2023(3)	73(2)
C(16)	–1884(4)	6285(4)	1647(2)	65(2)
C(11')	–3841(4)	7483(3)	6017(2)	53(1)
C(12')	–4403(5)	8155(4)	5944(3)	73(2)
C(13')	–4075(6)	8848(4)	6258(3)	85(2)
C(14')	–3227(6)	8869(5)	6623(3)	87(2)
C(15')	–2668(5)	8203(5)	6703(3)	85(2)
C(16')	–2979(4)	7505(4)	6401(3)	68(2)
C(21)	–5909(3)	3374(3)	1395(2)	51(1)
C(22)	–6471(5)	3622(5)	1709(3)	82(2)
C(23)	–6711(6)	3103(7)	2077(3)	105(3)
C(24)	–6377(6)	2343(6)	2131(3)	97(3)
C(25)	–5841(5)	2084(5)	1828(3)	90(2)
C(26)	–5587(4)	2595(4)	1463(2)	69(2)
C(21')	–2767(3)	5325(3)	3893(2)	49(1)
C(22')	–2894(4)	5951(4)	3522(2)	66(2)
C(23')	–2324(5)	6020(4)	3175(3)	80(2)
C(24')	–1639(6)	5485(6)	3193(3)	95(2)
C(25')	–1504(5)	4861(6)	3552(3)	95(2)
C(26')	–2065(4)	4784(4)	3901(3)	77(2)
C(31)	–4108(4)	3257(4)	–374(3)	67(2)
C(32)	–4404(4)	2564(4)	–187(4)	90(2)
C(33)	–4656(5)	1900(5)	–545(5)	105(3)
C(34)	–4602(6)	1968(6)	–1068(6)	124(4)
C(35)	–4336(5)	2660(6)	–1281(4)	111(3)

Atom	x	y	z	U(eq)
C(36)	−4090(4)	3318(5)	−926(3)	83(2)
C(31')	−2824(4)	4344(3)	5655(2)	59(1)
C(32')	−2139(6)	4839(5)	6000(4)	108(3)
C(33')	−1239(7)	4869(7)	5972(6)	130(4)
C(34')	−930(7)	4407(7)	5645(5)	128(3)
C(35')	−1536(6)	3909(6)	5286(4)	112(3)
C(36')	−2444(5)	3861(5)	5322(3)	91(2)
C(41)	−2137(6)	4248(6)	−149(5)	121(3)
C(41')	−3681(16)	4295(11)	6760(5)	300(13)
C(42)	−1377(6)	4798(6)	40(5)	140(4)
C(42')	−4037(16)	4531(14)	7173(5)	371(19)
C(51)	−2685(9)	3673(11)	1045(5)	234(9)
C(51')	−3789(8)	2706(5)	5941(5)	132(4)
C(52)	−2562(7)	3245(7)	1504(4)	152(4)
C(52')	−4191(9)	1933(5)	5671(5)	182(6)
Sb(1)	416(1)	4101(1)	2278(1)	102(1)
F(1)	−476(5)	3974(5)	2631(3)	191(3)
F(2)	1291(5)	4238(4)	1895(3)	162(2)
F(3)	1350(5)	3848(5)	2914(3)	203(3)
F(4)	−432(5)	4448(6)	1671(3)	212(4)
F(5)	586(8)	5184(4)	2499(4)	206(3)
F(6)	293(8)	3114(5)	2080(5)	251(5)

Table AII.6: Atomic coordinates (x 10^4) and equivalent isotropic displacement parameters (Å^2 x 10^3) for [Rh(TPP)(edpp)$_2$](SbF$_6$). U(eq) is defined as one third of the trace of the orthogonalized Uij tensor.

Atom	x	y	z	U(eq)
Rh	−17(1)	2176(1)	2170(1)	25(1)
N(1)	966(2)	1958(2)	2888(2)	33(1)
N(2)	663(2)	2611(2)	1654(1)	30(1)
N(3)	−1003(2)	2386(2)	1444(1)	28(1)
N(4)	−703(2)	1741(2)	2680(1)	29(1)
CA1	982(2)	1702(2)	3480(2)	38(1)
CA2	1733(2)	2023(2)	2873(2)	39(1)
CA3	1474(2)	2615(2)	1821(2)	35(1)
CA4	399(2)	2994(2)	1092(2)	33(1)
CA5	−1026(2)	2766(2)	903(2)	32(1)
CA6	−1750(2)	2136(2)	1398(2)	31(1)
CA7	−1500(2)	1598(2)	2465(2)	30(1)
CA8	−457(2)	1527(2)	3301(2)	35(1)
CB1	1792(3)	1599(3)	3838(2)	53(1)
CB2	2245(2)	1774(3)	3465(2)	49(1)
CB3	1725(3)	3016(3)	1348(2)	45(1)
CB4	1075(2)	3263(2)	915(2)	42(1)
CB5	−1829(2)	2756(2)	500(2)	41(1)
CB6	−2263(2)	2361(2)	795(2)	39(1)
CB7	−1759(2)	1282(2)	2967(2)	38(1)
CB8	−1129(3)	1250(3)	3479(2)	43(1)
CM1	1977(2)	2315(2)	2374(2)	38(1)
CM2	−385(2)	3093(2)	747(2)	33(1)
CM3	−1989(2)	1752(2)	1860(2)	30(1)
CM4	326(2)	1533(2)	3681(2)	39(1)
C(11)	2846(2)	2318(2)	2442(2)	42(1)
C(12)	3143(3)	1867(3)	2052(3)	56(1)
C(13)	3938(3)	1838(4)	2126(3)	69(2)
C(14)	4447(3)	2264(4)	2580(3)	76(2)

Atom	x	y	z	U(eq)
C(15)	4167(3)	2717(3)	2965(3)	67(2)
C(16)	3366(3)	2753(3)	2906(2)	51(1)
C(21)	−571(2)	3577(2)	169(2)	38(1)
C(22)	−344(3)	3388(3)	−361(2)	53(1)
C(23)	−526(4)	3861(3)	−882(2)	63(1)
C(24)	−928(3)	4511(3)	−883(3)	65(2)
C(25)	−1178(4)	4703(3)	−371(3)	70(2)
C(26)	−995(3)	4235(3)	152(2)	56(1)
C(31)	−2826(2)	1482(2)	1697(2)	33(1)
C(32)	−3007(3)	758(3)	1488(3)	62(1)
C(33)	−3779(3)	507(4)	1304(3)	78(2)
C(34)	−4378(3)	967(4)	1331(2)	63(2)
C(35)	−4204(3)	1693(4)	1542(3)	75(2)
C(36)	−3436(3)	1952(3)	1719(3)	64(1)
C(41)	483(6)	1228(4)	4348(3)	47(3)
C(42)	470(6)	459(4)	4465(3)	73(3)
C(43)	647(6)	196(4)	5080(4)	78(3)
C(44)	836(6)	702(5)	5578(3)	75(4)
C(45)	849(7)	1471(5)	5462(3)	94(6)
C(46)	672(7)	1734(4)	4847(4)	83(5)
C(41')	477(6)	1407(5)	4360(3)	50(4)
C(42')	944(5)	804(5)	4647(3)	61(3)
C(43')	1130(6)	710(6)	5295(4)	95(5)
C(44')	849(8)	1219(7)	5657(3)	110(7)
C(45')	383(7)	1822(7)	5370(4)	137(9)
C(46')	196(7)	1916(5)	4722(4)	81(5)
P(1)	79(1)	961(1)	1723(1)	31(1)
C(51)	−181(2)	992(2)	867(2)	38(1)
C(52)	312(3)	1313(2)	559(2)	45(1)
C(53)	113(4)	1319(3)	−91(2)	58(1)
C(54)	−601(4)	1027(3)	−436(2)	65(2)
C(55)	−1102(3)	727(3)	−139(2)	63(1)

275

Atom	x	y	z	U(eq)
C(56)	−911(3)	704(3)	511(2)	47(1)
C(61)	1036(2)	488(2)	1996(2)	39(1)
C(62)	1529(3)	338(3)	1627(2)	49(1)
C(63)	2243(3)	−33(3)	1875(3)	65(1)
C(64)	2455(3)	−263(3)	2491(3)	71(2)
C(65)	1980(3)	−128(3)	2861(3)	67(2)
C(66)	1274(3)	247(3)	2619(2)	52(1)
C(71)	−583(2)	271(2)	1917(2)	41(1)
C(72)	−508(3)	−540(3)	1701(3)	56(1)
P(2)	−160(1)	3397(1)	2592(1)	32(1)
C(81)	−1188(2)	3628(2)	2513(2)	36(1)
C(82)	−1582(3)	3314(3)	2906(2)	46(1)
C(83)	−2365(3)	3505(3)	2844(3)	63(1)
C(84)	−2753(3)	3999(4)	2386(3)	71(2)
C(85)	−2375(3)	4300(3)	1982(3)	65(1)
C(86)	−1593(3)	4124(3)	2043(2)	49(1)
C(91)	393(3)	3568(2)	3416(2)	42(1)
C(92)	57(3)	3781(3)	3881(2)	54(1)
C(93)	527(4)	3943(3)	4482(3)	75(2)
C(94)	1327(4)	3893(3)	4618(3)	80(2)
C(95)	1670(4)	3674(3)	4165(3)	75(2)
C(96)	1212(3)	3519(3)	3556(2)	55(1)
C(100)	209(3)	4151(2)	2189(2)	46(1)
C(101)	231(4)	4942(3)	2477(3)	61(1)
Sb	2066(1)	6263(1)	4989(1)	82(1)
F(1)	2836(7)	6816(7)	4917(8)	361(9)
F(2)	1200(4)	5710(4)	5068(5)	204(3)
F(3)	2615(4)	5564(6)	5514(4)	226(4)
F(4)	2165(9)	5691(5)	4356(4)	309(7)
F(5)	1395(8)	6885(6)	4432(4)	295(7)
F(6)	1862(4)	6891(4)	5598(3)	162(2)
Cl(1)	4757(2)	3840(2)	1672(1)	108(1)

Atom	x	y	z	U(eq)
Cl(2)	3280(2)	3931(2)	669(2)	125(1)
C(1S)	4021(8)	3471(8)	1205(9)	196(9)
Cl(3)	8002(4)	5752(3)	864(3)	296(4)
Cl(4)	8684(3)	7099(6)	1413(3)	429(8)
C(2S)	8110(5)	6627(5)	859(4)	99(3)

Table AII.7: Atomic coordinates (x 10^4) and equivalent isotropic displacement parameters ($\mathring{A}^2$ x 10^3) for [Rh(TPP)(edppt)$_2$](SbF$_6$). U(eq) is defined as one third of the trace of the orthogonalized Uij tensor.

Atom	x	y	z	U(eq)
Rh(1)	2470(1)	2536(1)	26(1)	28(1)
N(1)	1985(2)	2167(2)	−816(2)	34(1)
N(2)	1765(2)	3486(2)	−193(2)	34(1)
N(3)	2950(2)	2893(2)	875(2)	33(1)
N(4)	3175(2)	1589(2)	245(2)	34(1)
P(1)	1404(1)	1880(1)	200(1)	32(1)
P(2)	3538(1)	3166(1)	−175(1)	39(1)
O(1)	595(2)	2357(2)	−131(2)	51(1)
O(2)	3580(2)	2818(2)	−770(1)	53(1)
CA1	2237(3)	1536(3)	−1045(2)	34(1)
CA2	1369(3)	2505(2)	−1267(2)	33(1)
CA3	1164(3)	3634(3)	−720(2)	39(1)
CA4	1775(3)	4079(3)	178(2)	38(1)
CA5	2812(3)	3592(3)	1080(2)	37(1)
CA6	3450(3)	2487(3)	1342(2)	36(1)
CA7	3673(3)	1377(3)	804(2)	39(1)
CA8	3285(3)	1066(3)	−143(2)	37(1)
CB1	1741(3)	1466(3)	−1656(2)	43(1)
CB2	1216(3)	2057(3)	−1788(2)	43(1)
CB3	766(3)	4332(3)	−672(2)	49(1)
CB4	1139(3)	4609(3)	−125(2)	49(1)
CB5	3263(3)	3633(3)	1707(2)	45(1)
CB6	3638(3)	2942(3)	1867(2)	45(1)
CB7	4107(3)	686(3)	756(2)	49(1)
CB8	3884(3)	519(3)	177(2)	48(1)
CM1	2855(3)	1039(3)	−741(2)	37(1)
CM2	990(3)	3193(3)	−1229(2)	36(1)
CM3	2286(3)	4145(3)	761(2)	39(1)
CM4	3762(2)	1765(3)	1319(2)	36(1)

Atom	x	y	z	U(eq)
Cl(1')	4626(3)	8488(4)	1615(4)	289(4)
Cl(2')	3439(4)	8032(5)	514(2)	290(4)
Cl(1")	370(3)	8777(2)	3680(3)	201(2)
Cl(2")	1623(2)	7587(2)	4087(2)	143(1)
C(1')	3658(10)	8529(11)	1119(7)	200(7)
C(1")	665(11)	8076(7)	3527(6)	196(8)
C(1)	−178(3)	2237(4)	−57(3)	71(2)
C(2)	−702(5)	2877(8)	−318(5)	142(5)
C(3)	4072(4)	3137(4)	−1086(2)	72(2)
C(4)	3657(5)	3024(6)	−1716(3)	101(3)
C(11)	3060(3)	426(3)	−1097(2)	44(1)
C(12)	3548(4)	578(4)	−1420(3)	68(2)
C(13)	3701(4)	2(5)	−1769(3)	78(2)
C(14)	3372(4)	−701(4)	−1790(3)	74(2)
C(15)	2885(4)	−862(4)	−1468(3)	74(2)
C(16)	2739(3)	−306(3)	−1114(3)	58(2)
C(21)	387(3)	3513(3)	−1785(2)	40(1)
C(22)	−327(3)	3133(3)	−2085(2)	46(1)
C(23)	−860(3)	3424(4)	−2609(2)	58(1)
C(24)	−675(3)	4104(4)	−2826(2)	59(1)
C(25)	13(3)	4482(4)	−2535(2)	58(1)
C(26)	555(3)	4187(3)	−2005(2)	49(1)
C(31)	2198(3)	4864(3)	1074(2)	44(1)
C(32)	1811(4)	4854(3)	1480(3)	63(2)
C(33)	1712(5)	5500(4)	1765(3)	78(2)
C(34)	2027(4)	6171(3)	1660(3)	63(2)
C(35)	2422(4)	6210(3)	1272(3)	68(2)
C(36)	2511(3)	5544(3)	962(2)	51(1)
C(41)	4242(3)	1378(3)	1884(2)	40(1)
C(42)	3965(4)	722(3)	2051(2)	57(1)
C(43)	4425(4)	345(4)	2571(3)	74(2)
C(44)	5162(4)	620(4)	2912(3)	77(2)

Atom	x	y	z	U(eq)
C(45)	5447(4)	1275(4)	2747(2)	66(2)
C(46)	5008(3)	1659(3)	2239(2)	52(1)
C(51)	1452(3)	1813(3)	952(2)	40(1)
C(52)	1498(4)	1153(3)	1263(2)	54(1)
C(53)	1552(4)	1171(4)	1841(3)	69(2)
C(54)	1564(4)	1834(4)	2118(3)	67(2)
C(55)	1485(4)	2515(3)	1814(3)	62(2)
C(56)	1437(4)	2501(3)	1234(2)	51(1)
C(61)	1223(3)	927(3)	−105(2)	40(1)
C(62)	1719(4)	318(3)	148(2)	53(1)
C(63)	1526(5)	−401(3)	−101(3)	76(2)
C(64)	871(5)	−501(4)	−598(3)	80(2)
C(65)	405(5)	98(4)	−860(3)	77(2)
C(66)	568(3)	819(4)	−625(2)	56(1)
C(71)	4517(3)	3009(3)	382(2)	44(1)
C(72)	4749(3)	3360(3)	928(2)	53(1)
C(73)	5504(3)	3212(4)	1344(3)	65(2)
C(74)	6012(4)	2698(4)	1235(3)	66(2)
C(75)	5772(4)	2318(4)	708(3)	68(2)
C(76)	5029(4)	2467(3)	278(3)	55(1)
C(81)	3450(3)	4188(3)	−300(2)	52(1)
C(82)	2804(4)	4427(4)	−799(3)	87(2)
C(83)	2700(5)	5187(5)	−939(5)	119(4)
C(84)	3218(5)	5733(5)	−597(5)	115(4)
C(85)	3863(5)	5519(4)	−113(5)	106(3)
C(86)	3988(4)	4734(3)	37(3)	71(2)
Sb(1)	2111(1)	8732(1)	2134(1)	68(1)
F(1)	2870(10)	9226(8)	2643(4)	361(12)
F(2)	2049(3)	8041(4)	2705(3)	139(2)
F(3)	2932(11)	8139(8)	2099(8)	335(10)
F(4)	2199(4)	9406(3)	1569(2)	117(2)
F(5)	1334(9)	9251(7)	2204(8)	364(11)

Atom	*x*	*y*	*z*	U(eq)
F(6)	1533(11)	8116(6)	1606(4)	348(11)

Table AII.8: Atomic coordinates (x 10^4) and equivalent isotropic displacement parameters (Å^2 x 10^3) for [Rh(TPP)(depp)$_2$](SbF$_6$). U(eq) is defined as one third of the trace of the orthogonalized Uij tensor.

Atom	x	y	z	U(eq)
Rh	5000	5000	5000	27(1)
N(1)	4626(3)	5673(2)	5585(2)	30(1)
N(2)	6039(3)	5798(2)	4989(2)	30(1)
P(1)	6059(1)	4267(1)	5697(1)	37(1)
O(1)	5795(3)	3342(3)	5629(2)	63(1)
O(2)	6063(4)	4592(4)	6294(2)	91(2)
CA1	3973(3)	5468(3)	5858(2)	33(1)
CA2	5079(3)	6352(3)	5829(2)	35(1)
CA3	6271(3)	6474(3)	5319(2)	34(1)
CA4	6620(3)	5775(3)	4648(2)	30(1)
CB1	4013(4)	6047(3)	6287(2)	45(1)
CB2	4684(4)	6593(3)	6268(3)	48(1)
CB3	7027(4)	6877(3)	5185(2)	44(1)
CB4	7254(4)	6447(3)	4779(2)	40(1)
CM1	5821(4)	6738(3)	5703(2)	36(1)
CM2	6609(3)	5199(3)	4248(2)	31(1)
C(11)	6166(4)	7497(3)	6018(2)	40(1)
C(12)	7051(4)	7535(4)	6399(3)	51(2)
C(13)	7350(5)	8234(4)	6700(3)	61(2)
C(14)	6786(5)	8889(4)	6625(3)	62(2)
C(15)	5897(5)	8860(4)	6238(3)	62(2)
C(16)	5589(4)	8164(3)	5942(3)	49(1)
C(21)	7258(3)	5319(3)	3889(2)	36(1)
C(22)	7156(4)	5952(3)	3531(2)	45(1)
C(23)	7723(5)	6033(4)	3176(3)	54(2)
C(24)	8391(5)	5470(4)	3181(3)	59(2)
C(25)	8501(5)	4818(4)	3523(3)	59(2)
C(26)	7942(4)	4734(4)	3883(3)	49(1)
C(51)	6250(6)	2693(5)	5973(4)	82(2)

Atom	x	y	z	U(eq)
C(52)	5848(8)	1929(5)	5683(4)	116(4)
C(61)	6508(9)	4398(8)	6832(5)	61(4)
C(62)	6309(18)	4852(15)	7236(10)	131(8)
C(61X)	5470(30)	4050(20)	6693(17)	178(17)
C(62X)	5792(14)	4410(13)	7175(8)	76(6)
C(71)	7260(4)	4316(3)	5710(3)	48(1)
C(72)	7589(5)	3853(4)	5327(3)	60(2)
C(73)	8489(5)	3898(5)	5298(3)	76(2)
C(74)	9107(6)	4428(6)	5638(4)	84(2)
C(75)	8811(6)	4876(5)	5984(4)	81(2)
C(76)	7910(5)	4848(5)	6019(3)	70(2)
Rh'	0	0	5000	25(1)
P(1')	1216(1)	912(1)	5053(1)	35(1)
N(1')	314(3)	−24(2)	5850(2)	31(1)
N(2')	897(3)	−926(2)	5022(2)	29(1)
O(1')	1627(3)	1377(4)	5610(2)	80(2)
O(2')	2037(3)	472(3)	4890(2)	58(1)
CA1'	−24(3)	486(3)	6174(2)	33(1)
CA2'	975(4)	−512(3)	6203(2)	35(1)
CA3'	1490(3)	−1266(3)	5503(2)	35(1)
CA4'	1083(3)	−1282(3)	4571(2)	33(1)
CM1'	1533(4)	−1086(3)	6045(2)	35(1)
CM2'	676(4)	−1102(3)	4018(2)	35(1)
C(11')	2264(4)	−1530(3)	6486(2)	39(1)
C(12')	3178(4)	−1258(4)	6667(2)	45(1)
C(13')	3863(4)	−1693(4)	7044(2)	51(2)
C(14')	3620(5)	−2411(4)	7249(2)	52(2)
C(15')	2735(5)	−2679(4)	7082(2)	54(2)
C(16')	2032(4)	−2242(4)	6689(2)	51(2)
C(21')	924(4)	−1631(3)	3598(2)	38(1)
C(22')	646(4)	−2430(4)	3560(2)	47(1)
C(23')	890(5)	−2944(4)	3196(3)	62(2)

Atom	x	y	z	U(eq)
C(24')	1401(5)	−2669(5)	2861(3)	66(2)
C(25')	1672(5)	−1891(6)	2886(3)	72(2)
C(26')	1439(5)	−1370(4)	3258(3)	56(2)
CB1'	423(4)	294(4)	6752(2)	44(1)
CB2'	1032(4)	−310(4)	6765(2)	46(1)
CB3'	2067(4)	−1858(4)	5334(2)	48(2)
CB4'	1826(4)	−1864(3)	4775(2)	45(1)
C(51')	2254(8)	1172(7)	6077(4)	116(4)
C(52')	2546(9)	1774(6)	6502(4)	134(5)
C(61')	2913(5)	799(5)	4870(4)	82(2)
C(62')	3673(5)	227(5)	5042(5)	93(3)
C(71')	866(4)	1743(4)	4585(3)	48(1)
C(72')	887(4)	1658(4)	4029(3)	58(2)
C(73')	618(5)	2289(5)	3648(4)	76(2)
C(74')	345(5)	3001(5)	3841(5)	87(3)
C(75')	316(5)	3095(4)	4379(4)	67(2)
C(76')	562(4)	2448(4)	4749(3)	63(2)
Sb	9551(1)	5891(1)	7742(1)	68(1)
F(1)	8636(4)	5757(3)	8108(3)	109(2)
F(2)	8636(4)	6172(4)	7092(3)	129(2)
F(3)	10482(4)	6001(4)	7384(2)	124(2)
F(4)	10437(4)	5539(5)	8379(2)	126(2)
F(5)	9380(5)	4809(3)	7503(3)	126(2)
F(6)	9799(12)	6896(6)	7994(6)	106(4)
F(6X)	9380(20)	7019(12)	7787(11)	85(9)

Atom	x	y	z	U(eq)
C(24')	1401(5)	−2669(5)	2861(3)	66(2)
C(25')	1672(5)	−1891(6)	2886(3)	72(2)
C(26')	1439(5)	−1370(4)	3258(3)	56(2)
CB1'	423(4)	294(4)	6752(2)	44(1)
CB2'	1032(4)	−310(4)	6765(2)	46(1)
CB3'	2067(4)	−1858(4)	5334(2)	48(2)
CB4'	1826(4)	−1864(3)	4775(2)	45(1)
C(51')	2254(8)	1172(7)	6077(4)	116(4)
C(52')	2546(9)	1774(6)	6502(4)	134(5)
C(61')	2913(5)	799(5)	4870(4)	82(2)
C(62')	3673(5)	227(5)	5042(5)	93(3)
C(71')	866(4)	1743(4)	4585(3)	48(1)
C(72')	887(4)	1658(4)	4029(3)	58(2)
C(73')	618(5)	2289(5)	3648(4)	76(2)
C(74')	345(5)	3001(5)	3841(5)	87(3)
C(75')	316(5)	3095(4)	4379(4)	67(2)
C(76')	562(4)	2448(4)	4749(3)	63(2)
Sb	9551(1)	5891(1)	7742(1)	68(1)
F(1)	8636(4)	5757(3)	8108(3)	109(2)
F(2)	8636(4)	6172(4)	7092(3)	129(2)
F(3)	10482(4)	6001(4)	7384(2)	124(2)
F(4)	10437(4)	5539(5)	8379(2)	126(2)
F(5)	9380(5)	4809(3)	7503(3)	126(2)
F(6)	9799(12)	6896(6)	7994(6)	106(4)
F(6X)	9380(20)	7019(12)	7787(11)	85(9)

APPENDIX III: GENERAL EXPERIMENTAL DETAILS

AIII.1 Instrumentation

NMR. ^{31}P NMR and ^{1}H NMR spectra were recorded on a Varian 500 MHz spectrometer. The ^{31}P spectra were calibrated with a standard 85% H_3PO_4 as an external reference and were measured at 25 °C. ^{103}Rh NMR spectra were recorded on a Bruker AMX400 spectrometer by Prof. Laurence Carlton (University of the Witwatersrand).

IR Spectroscopy. All IR spectra were recorded as KBr disks on a Perkin Elmer Spectrum One FTIR spectrometer.

Electronic Spectra. Uv-vis spectra were recorded using a Perkin Elmer Lambda 45 double-beam scanning spectrometer using dry, degassed dichloroethane solutions in 1.0 cm pathlength quartz cuvettes.

AIII.2 Experimental Techniques

Technical. All reactions unless otherwise stated were performed under an inert, dried nitrogen atmosphere using Schlenk apparatus and techniques. All glassware was flame dried before use.

Solvents. All solvents used were thoroughly dried and stored under nitrogen. All solvents were freshly distilled before use. THF was dried over Na/K alloy. Dichloromethane and dichloroethane were dried over CaH_2. Hexane was dried over freshly pressed Na wire. Immediately after distillation and prior to use the fresh solvents were placed over molecular sieves and degassed using the freeze-pump-thaw method.

Reagents. Silver antimony hexafluoride was stored in an inert atmosphere glovebox and used as received. Phosphines and phosphonites were stored under nitrogen and refrigerated as a precautionary measure.

Synthesis of Common Reagents. H₂TPP was synthesized using published procedures.[231] [Mn(TPP)Cl], [Co(TPP)Cl] and [Rh(TPP)Cl] were prepared by metallation of H₂TPP with anhydrous manganous chloride, cobaltous chloride, and rhodium trichloride, respectively, in refluxing DMF following the method reported by Adler *et al.*[232]

AIII.3 Crystal Structure Determination

Data Collection. In general, translucent and pale crystals were avoided as higher levels of solvation for these crystals was presumed possible. Reflections were measured with an Enraf-Nonius CAD4 diffractometer using graphite monochromated Mo-K_α radiation. Initial unit cell dimensions and orientation matrix data were examined to eliminate poorer quality crystals and optimize data collection. Where the unit cell volumes were consistent with reasonable levels of solvation, the temperature of the data collections were lowered to avoid crystal decay. As such, no deliberate attempts were made for data collection at a standard temperature.

The data for the X-ray crystal structure of [Co(TPP)(edpp)₂](SbF₆) were collected on an Oxford Xcalibur 2 CCD diffractometer at an X-ray power of 2.0 kW (Mo $K\alpha$ radiation). Lorentz, scan speed scaling, and overlap corrections were applied during data reduction with the program CrysAlis RED.

Structure Solution and Refinement.

Structure solutions were performed using Oscail Version 8.[233] Direct methods were employed for all initial structure solutions and difference Fourier synthesis employed subsequently for the remaining atomic placements. Least-squares refinement cycles were performed on isotropic and subsequent anisotropic temperature factors for all heavy atoms. Hydrogen atom positions were calculated and not located unless otherwise stated.
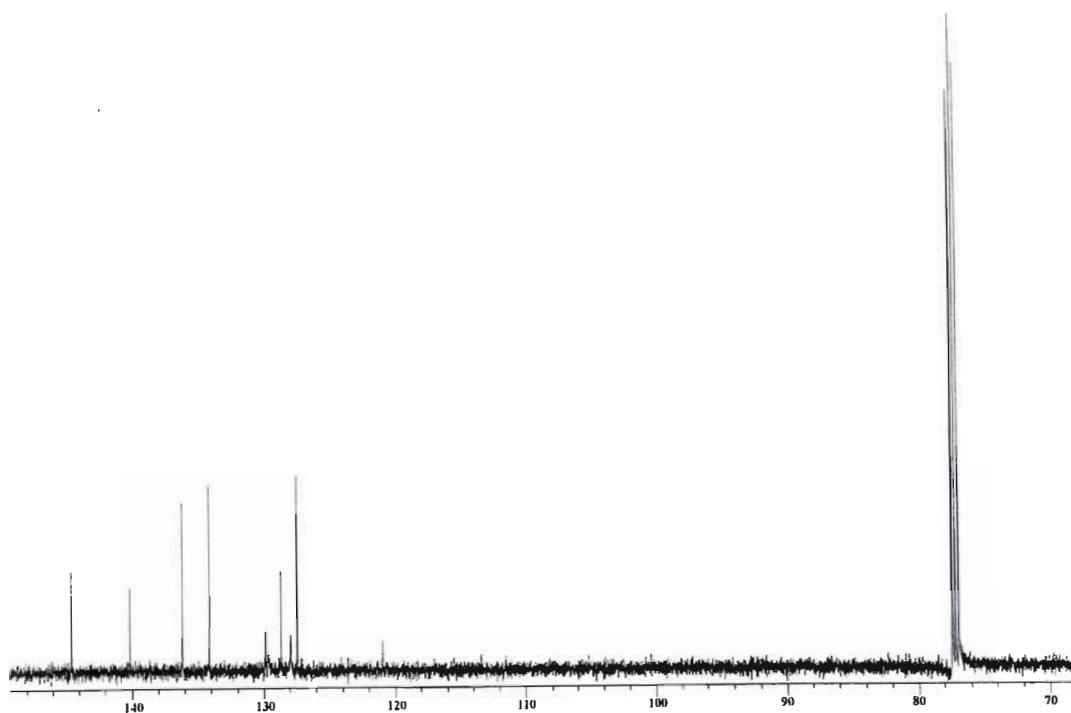
APPENDIX IV: ^{13}C NMR SPECTRA

Figure AIV.1: ^{13}C NMR spectrum of [Co(TPP)(edpp)$_2$](SbF$_6$).
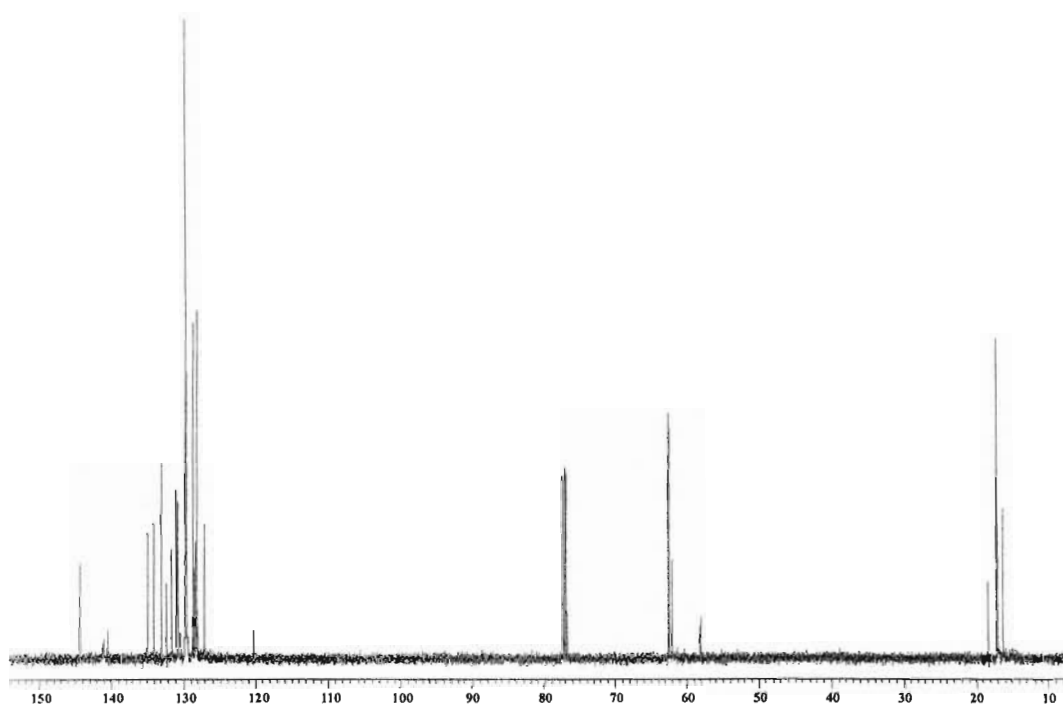
Figure AIV.2: ^{13}C NMR spectrum of [Co(TPP)(deppt)$_2$](SbF$_6$).
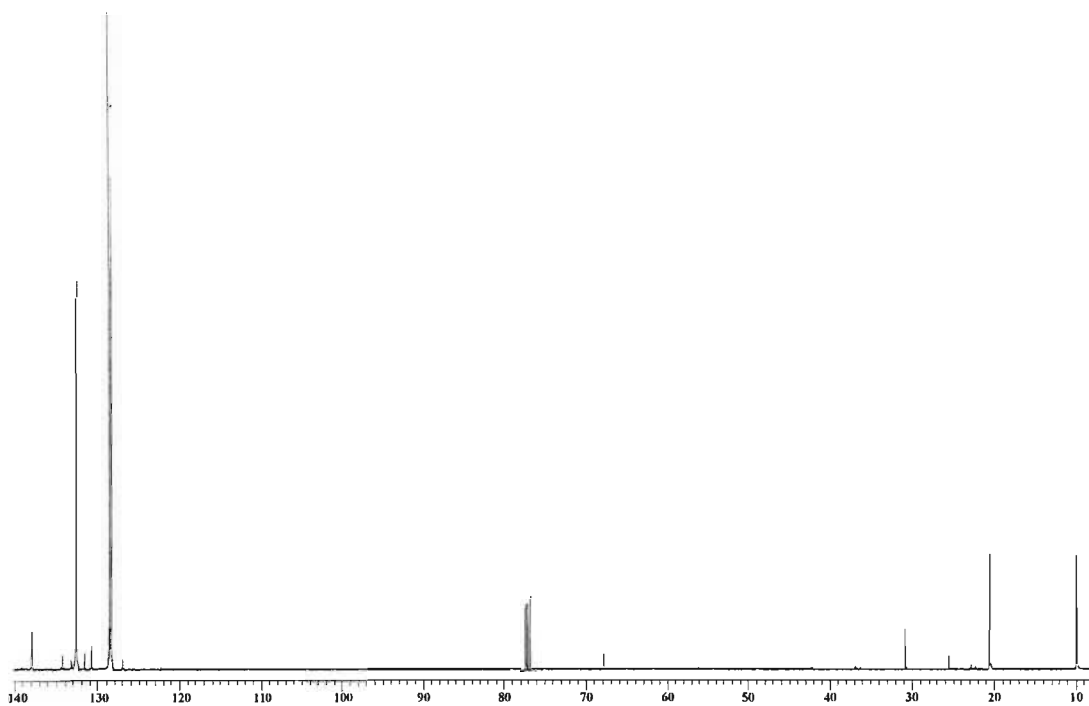
Figure AIV.3: ^{13}C NMR spectrum of [Rh(TPP)(edpp)$_2$](SbF$_6$).
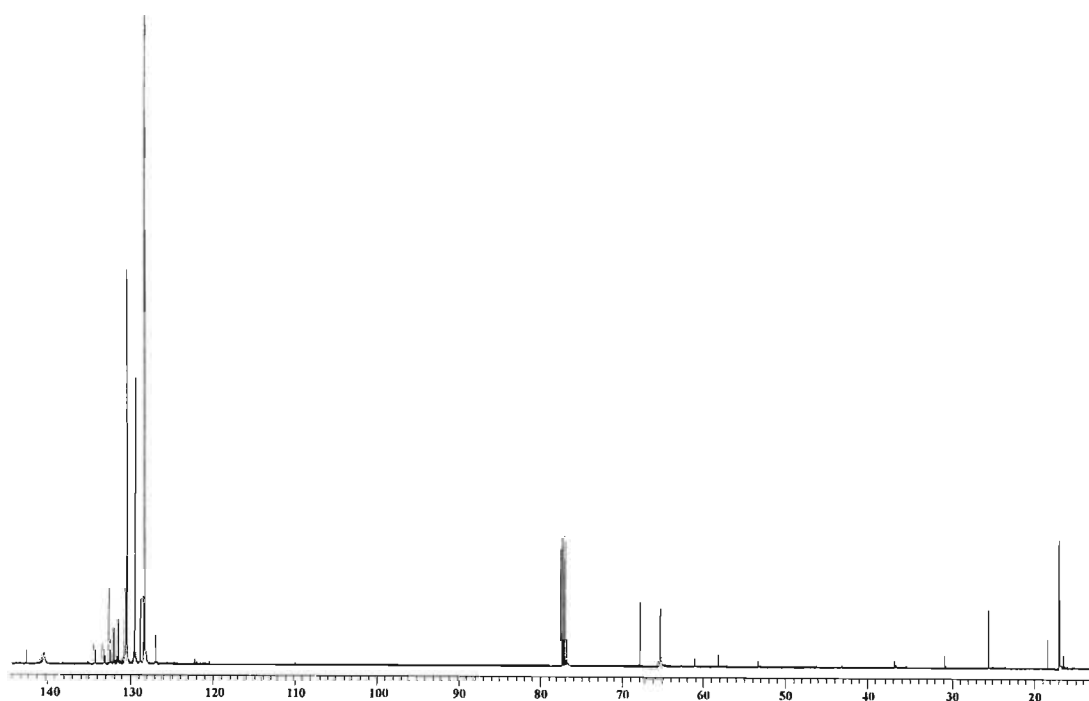
Figure AIV.4: ^{13}C NMR spectrum of [Rh(TPP)(edppt)$_2$](SbF$_6$).
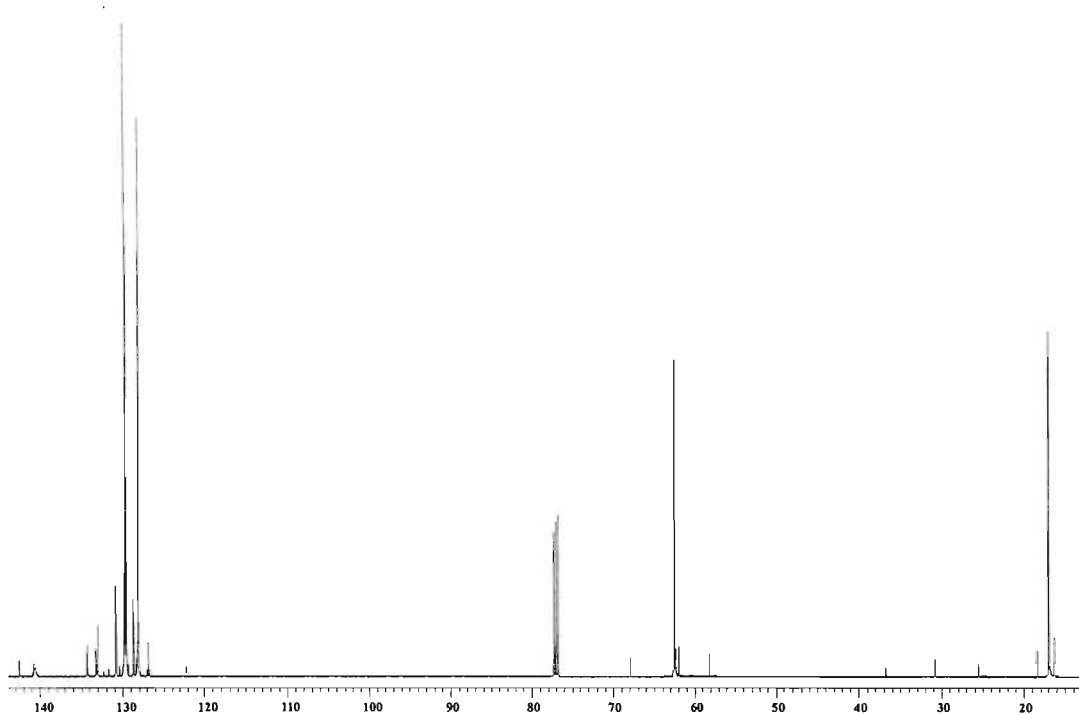
Figure AIV.5: ^{13}C NMR spectrum of [Rh(TPP)(deppt)$_2$](SbF$_6$).

REFERENCE LIST

[1] Scheidt, W. R.; Kadish, K. M.; Smith, K. M.; Guilard, R. Eds.; *Porphyrins and Metalloporphyrins, Vol. 3/Inorganic, Organometallic and Coordination Cemistry,* Academic Press, **2000**, *16*, 49.

[2] Navaza, A.; De Rango, C.; Charpin, P. *Acta Crystallogr. Sect. C* **1983**, *39*, 1625.

[3] Sharma, C. V. K.; Broker, G. A.; Huddlestone, J. G.; Baldwin, J. W.; Metzger, R. M.; Rogers, R. D. *J. Am. Chem. Soc.* **1999**, *121*, 1137.

[4] Wijesekera, T. P.; Paine, J. B.; Dolphin, D.; Einstein, F. W. B.; Jones, T. *J. Am. Chem. Soc.* **1983**, *105*, 6747.

[5] Traylor, T. G.; Koga, N.; Deardurff, L. A.; Swepston, P. N.; Ibers, J. A. *J. Am. Chem. Soc.* **1984**, *106*, 5132.

[6] Gold, K. W.; Hodgson, D. J.; Gold, A.; Savrin, J. E.; Toney, G. E. *Chem. Commun.* **1985**, 563.

[7] Balch, A. L.; Yee Wai Chan; Olmstead, M.; Renner, M. W. *J. Am. Chem. Soc.* **1985**, *107*, 2393.

[8] Latos-Grazynski, L.; Cheng, Ru-Jen; La Mar, G. N.; Balch, A. L. *J. Am. Chem. Soc.* **1981**, *103*, 4270.

[9] Chevrier, B.; Weiss, R. *J. Am. Chem. Soc.* **1981**, *103*, 2899.

[10] Olmstead, M. M.; Cheng, Ru-Jen; Balch, A. L. *Inorg. Chem.* **1982**, *21*, 4143.

[11] Arnold, D. P.; Sakata, Y.; Sugiura, K.; Worthington, E. I. *Chem. Commun.* **1998**, 2331.

[12] Staab, H. A.; Nikolic, S.; Krieger, C. *Eur. J. Org. Chem.* **1999**, 1459.

[13] Kimoon Kim.; Collman, J. P.; Ibers, J. A. *J. Am. Chem. Soc.* **1988**, *110*, 4242.

[14] Collman, J. P.; Brauman, J. I.; Fitzgerald, J. P.; Hampton, P. D.; Naruta, Y.; Sparapany. J. W.; Ibers, J. A. *J. Am. Chem. Soc.* **1988**, *110*, 3477.

[15] Anderson, O. P.; Lavallee, D. K. *Inorg. Chem.* **1977**, *16*, 1634,.

[16] Arasasingham, R. D.; Balch, A. L.; Olmstead, M. M.; Renner, M. W. *Inorg. Chem.* **1987**, *26*, 3562.

[17] Clement, T. E.; Nurco, D. J.; Smith, K. M. *Inorg. Chem.* **1998**, *37*, 1150.

[18] Guilard, R.; Brandes, S.; Tabard, A.; Bouhmaida, N.; Lecomte, C.; Richard, P.; Latour, J., -M. *J. Am. Chem. Soc.* **1994,** *116*, 10202.

[19] Bartczak, T. J. *Acta Crystallogr., Sect. A* **1978**, *34*, S127.

[20] Olmstead, M.; Maitra, K.; Fisher, A. J.; Balch, A. L.; Dorn, H. C. *Nature (London)* **1999**, *401*, 55.

[21] Olmstead, M. M.; Costa, D. A.; Maitra, K.; Noll, B. C.; Phillips, S. L.; Van Calcar, P. M.; Balch, A. L. *J. Am. Chem. Soc.* **1999**, *121*, 7090.

[22] Anderson, O. P.; Lavallee, D. K. *J. Am. Chem. Soc.* **1977**, *99*, 1404.

[23] Elliott, C. M.; Arnette, J. K.; Krebs, R. R. *J. Am. Chem. Soc.* **1985**, *107*, 4904.

[24] Arasasingham, R. D.; Balch, A. L.; Olmstead, M. M.; Renner, M. W. *Inorg. Chem.* **1987**, *26*, 3562.

[25] Sparapany, J. W.; Crossley, M. J.; Baldwin, J. E.; Ibers, J. A. *J. Am. Chem. Soc.* **1988**, *110*, 4559.

[26] Guilard, R.; Lopez, M. A.; Tabard, A.; Richard, P.; Lecomte, C.; Brandes, S.; Hutchison, J. E.; Collman, J. P. *J. Am. Chem. Soc.* **1992**, *114*, 9877.

[27] Collman, J. P.; Hutchison, J. E.; Lopez, M. A.; Tabard, A.; Guilard, R.; Seok, Won K.; Ibers, J. A.; L'Her, M. *J. Am. Chem. Soc.* **1992**, *114*, 9869.

[28] Medforth, C. J.; Senge, M. O.; Smith, K. M.; Sparks, L. D.; Shelnutt, J. A. *J. Am. Chem. Soc.* **1992**, *114*, 9859.

[29] Chang, C. J.; Deng, Yonqi; Shi, Chunnian; Chang, C. K.; Anson, F. C.; Nocera, D. G. *Chem. Commun.* **2000**, 1355.

[30] Clement, T. E.; Nurco, D. J.; Smith, K. M. *Inorg. Chem.* **1998**, *37*, 1150.

[31] Riche, C.; Chiaroni, A.; Gouedard, M.; Gaudemer, A. *J. Chem. Res.* **1978**, *32*, 534.

[32] Setsune, J.; Takeda, H.; Ito, S.; Saito, Y.; Ishimaru, Y.; Fukuhara, K.; Kitao, T.; Adachi, T. *Inorg. Chem.* **1998**, *37*, 2235.

[33] Olmstead, M. M.; de Bettencourt-Dias, A.; Duchamp, J. C.; Stevenson, S.; Marciu, D.; Dorn, H. C.; Balch, A. L. *Angew. Chem., Int. Ed. Engl.* **2001**, *40*, 1223.

[34] Gridnev, A. A.; Ittel, S. D.; Wayland, B. B.; Fryd, M. *Organometallics* **1996**, *15*, 5116.

[35] Goldberg, I.; Krupitsky, H.; Stein, Z.; Hsiou, Yu; Strouse, C. E. *Supramolecular Chemistry* **1994**, *4*, 203.

[36] Hazen, R. M.; Hoering, T. C.; Hofmeister, A. M. *J. Phys. Chem.* **1987**, *91*, 5042.

[37] Yakushi, K.; Yamakado, H.; Ida, T.; Ugawa, A. *Solid State Commun.* **1991**, *78*, 919.

[38] Jene, P. G.; Ibers, J. A. *Inorg. Chem.* **2000**, *39*, 5796.

[39] Jones, N. L.; Carroll, P. J.; Wayland, B. B. *Organometallics* **1986**, *5*, 33.

[40] Turner, P.; Gunter, M. J.; Skelton, B. W.; White, A. H.; Hambley, T. W. *J. Chem. Res.* **1996**, *18*, 220.

[41] Beisong Cheng; Cukiernik, F.; Fries, P. H.; Marchon, J. –C.; Scheidt, W. R. *Inorg. Chem.* **1995**, *34*, 4627.

[42] Williamson, M. M.; Hill, C. L. *Inorg. Chem.* **1987**, *26*, 4155.

[43] Williamson, M. M.; Hill, C. L. *Inorg. Chem.* **1986**, *25*, 4668.

[44] Byrn, M. P.; Curtis, C. J.; Hsiou, Yu.; Khan, S. I.; Sawin, P. A.; Tendick. S. K.; Terzis, A.; Strouse, C. E. *J. Am. Chem. Soc.* **1993**, *115*, 9480.

[45] Camenzind, M. J.; Hollander, F. J.; Hill, C. L. *Inorg. Chem.* **1982**, *21*, 4301.

[46] Prince, S.; Korber, F.; Cooke, P. R.; Smith, J. R. L.; Mazid, M. A. *Acta Crystallogr., Sect. C (Cr. Str. Comm.)* **1993**, *49*, 1158.

[47] Hatano, K.; Anzai, K.; [Iitaka], Y. *Bull. Chem. Soc. Jpn.* **1983**, *56*, 422.

[48] Scheidt, W. R.; Pearson, W. B. Gosal, N. *Acta Crystallogr., Sect. C (Cr. Str. Comm.)* **1988**, *44*, 927.

[49] Cheng, Beisong; Scheidt, W. R. *Acta Crystallogr., Sect. C (Cr. Str. Comm.)* **1996**, *52*, 585.

[50] Van Atta, R. B.; Strouse, C. E.; Hanson, L. K.; Valentine, J. S. *J. Am. Chem. Soc.* **1987**, *109*, 1425.

[51] Hill, C. L.; Williamson, M. M. *Inorg. Chem.* **1985**, *24*, 2836.

[52] Bhyrappa, P.; Wilson, S. R.; Suslick, K. S. *J. Am. Chem. Soc.* **1997**, *119*, 8492.

[53] Turner, P.; Gunter, M. J.; Skelton, B. W.; White, A. H. *Aust. J. Chem.* **1998**, *51*, 835.

[54] Hill, C. L.; Williamson, M. M. *Inorg. Chem.* **1985**, *24*, 3024.

[55] Williamson, M. M.; Hill, C. L. *Inorg. Chim. Acta* **1987**, *133*, 107.

[56] Brandon, E. J.; Rogers, R. D.; Burkhart, B. M.; Miller, J. S. *Chemistry-A European Journal* **1998**, *4*, 1938.

[57] Fox, S. J.; Chen, Li; Khan, M. A.; Richter-Addo, G. B. *Inorg. Chem.* **1997**, *36*, 6465.

[58] Suslick, K. S.; Watson, R. A. *Inorg. Chem.* **1991**, *30*, 912.

[59] Cheng, Beisong; Scheidt, W. R. *Acta Crystallogr., Sect. C (Cr. Str. Comm.)* **1995**, *51*, 825.

[60] Suslick, K. S.; Watson, R. A.; Wilson, S. R. *Inorg. Chem.* **1991**, *30*, 2311.

[61] Hill, C. L.; Hollander, F. J. *J. Am. Chem. Soc.* **1982**, *104*, 7318.

[62] Camenzind, M. J.; Hollander, F. J.; Hill, C. L. *Inorg. Chem.* **1983**, *22*, 3776.

[63] Rittenberg, D. K.; Sugiura, K. -i.; Sakata, Y.; Guzei, I. A.; Rheingold, A. L.; Miller, J. S. *Chemistry-A European Journal* **1999**, *5*, 1874.

[64] Rittenberg, D. K.; Miller, J. S. *Inorg. Chem.* **1999**, *38*, 4838.

[65] Brandon, E. J.; Arif, A. M.; Burkhart, B. M.; Miller, J. S. *Inorg. Chem.* **1998**, *37*, 2792.

[66] Rittenberg, D. K.; Sugiura, K.; Arif, A. M.; Sakata, Y.; Incarvito, C. D.; Rheingold, A. L.; Miller, J. S. *Chemistry-A European Journal* **2000**, *6*, 1811.

[67] Day, V. W.; Stults, B. R.; Tasset, E. L.; Marianelli, R. S.; Boucher, L. J. *Inorg. Nuclear Chem. Lett.* **1975**, *11*, 505.

[68] Scheidt, W. R.; Hatano, K.; Rupprecht, G. A.; Piciulo, P. L. *Inorg. Chem.* **1979**, *18*, 292.

[69] Kirner, J. F.; Reed, C. A.; Scheidt, W. R. *J. Am. Chem. Soc.* **1977**, *99*, 2557.

[70] Scheidt, W. R.; Lee, Y. J.; Luangdilok, W.; Haller, K. J.; Anzai, K.; Hatano, K. *Inorg. Chem.* **1983**, *22*, 1516.

[71] Galich, L.; Huckstadt, H.; Homborg, H. *J. Porphyrins and Phthalocyanines* **1998**, *2*, 79.

[72] Guilard, R.; Perie, K.; Barbe, J. -M.; Nurco, D. J.; Smith, K. M.; Van Caemelbecke, E.; Kadish, K. M. *Inorg. Chem.* **1998**, *37*, 973.

[73] Cheng, Beisong; Scheidt, W. R. *Acta Crystallogr., Sect. C (Cr. Str. Comm.)* **1996**, *52*, 361.

[74] Tulinsky, A.; Chen, B. M. L. *J. Am. Chem. Soc.* **1977**, *99*, 3647.

[75] Armstrong, R. S.; Foran, G. J.; Hambley, T. W. *Acta Crystallogr., Sect. C (Cr. Str. Comm.)* **1993**, *49*, 236.

[76] Behere, D. V.; Mitra, S. *Inorg. Chem.* **1980**, *19*, 992.

[77] Spreer, L. O.; Maliyackel, A. C.; Holbrook, S.; Otvos, J. W.; Calvin, M. *J. Am. Chem. Soc.* **1986**, *108*, 1949.

[78] Simonato, J. -P.; Pecaut, J.; Scheidt, W. R.; Marchon, J. -C. *Chem. Commun.* **1999**, 989.

[79] Mikami, S.; Sugiura, K. -i.; Miller, J. S.; Sakata, Y. *Chem. Lett.* **1999**, 413.

[80] Sugiura, K.; Mikami, S.; Johnson, M. T.; Miller, J. S.; Iwasaki, K.; Umishita, K.; Hino, S.; Sakata, Y. *Chem. Lett.* **1999**, 925.

[81] Johnson, M. T.; Arif, A. M.; Miller, J. S. *Eur. J. Inorg. Chem.* **2000**, 1781.

[82] Sugiura, K.; Mikami, S.; Johnson, M. T.; Miller, J. S.; Iwasaki, K.; Umishita K.; Hino, S.; Sakata, Y. *J. Mater. Chem.* **2000**, *10*, 959.

[83] Sugiura, K. -i.; Mikami, S.; Tanaka, T.; Sawada, M.; Manson, J. L.; Miller, J. S.; Sakata, Y. *Chem. Lett.* **1997**, 1071.

[84] Rittenberg, D. K.; Arif, A. M.; Miller, J. S. *J. Chem. Soc., Dalton Trans.* **2000**, 3939.

[85] Bohm, A.; Vazquez, C.; McLean, R. S.; Calabrese, J. C.; Kalm, S. E.; Manson, J. L.; Epstein, A. J.; Miller, J. S. *Inorg. Chem.* **1996**, *35*, 3083.

[86] Miller, J. S.; Calabrese, J. C.; McLean, R. S.; Epstein, A. J. *Advanced Materials* **1992**, *4*, 498.

[87] Brandon, E. J.; Rittenberg, D. K.; Arif, A. M.; Miller, J. S. *Inorg. Chem.* **1998**, *37*, 3376.

[88] Miller, J. S.; Vazquez, C.; Jones, N. L.; McLean, R. S.; Epstein, A. J. *J. Mater. Chem.* **1995**, *5*, 707.

[89] Sugiura, K. -i.; Mikami, S.; Tanaka, T.; Sawada, M.; Sakata, Y. *Chem. Lett.* **1998**, 103.

[90] Sugiura, Ken-ichi; Arif, A. M.; Rittenberg, D. K.; Schweizer, J.; Ohrstrom, L.; Epstein, A. J.; Miller, J. S. *Chemistry-A European Journal* **1997**, *3*, 138.

[91] Yates, M. L.; Arif, A. M.; Manson, J. L.; Kalm, B. A.; Burkhart, B. M.; Miller, J. S. *Inorg. Chem.* **1998**, *37*, 840.

[92] Kumar, R. K.; Balasubramanian, S.; Goldberg, I. *Chem. Commun.* **1998**, 1435.

[93] Landrum, J. T.; Reed, C. A.; Hatano, K.; Scheidt, W. R. *J. Am. Chem. Soc.* **1978**, *100*, 3232.

[94] Landrum, J. T.; Hatano, K.; Scheidt, W. R., Reed, C.A. *J. Am. Chem. Soc.* **1980**, *102*, 6729.

[95] Kumar, R. K.; Goldberg, I. *Angew. Chem., Int. Ed. Engl.* **1998**, *37*, 3027.

[96] Schardt, B. C.; Hollander, F. J.; Hill, C. L. *Chem. Commun.* **1981**, 765.

[97] Schardt, B. C.; Hollander, F. J.; Hill, C. L. *J.Am. Chem. Soc.*, **1982**, *104*, 3964.

[98] Turner, P.; Gunter, M. J.; Hambley, T. W.; White, A. H.; Skelton, B. W. *Inorg. Chem.* **1992**, *31*, 2295.

[99] Cheng, Beisong; Fries, P. H.; Marchon, J. -C.; Scheidt, W. R. *Inorg. Chem.* **1996**, *35*, 1024.

[100] Brandon, E. J.; Yap, G. P. A.; Rheingold, A. L.; Arif, A.; Miller, J. S. *Inorg. Chim. Acta* **1995**, *240*, 515.

[101] Day, V. W.; Stults, B. R.; Tasset, E. L.; Day, R. O.; Marianelli, R. S. *J. Am. Chem. Soc.* **1974**, *96*, 2650.

[102] Kirner, J. F.; Scheidt, W. R. *Inorg. Chem.* **1975**, *14*, 2081.

[103] Lai, Tat-Shing; Kwong, Hoi-Lun; Che, Chi-Ming; Peng, Shie-Ming. *Chem. Commun.* **1997**, 2373.

[104] Zheng, Guo-dong; An, Qing-da; Wang, Tao; Wang, Feng-shan; Cao, Xi-zhang. *Gaodeng Xuexiao Huaxue Xuebao(Chem. J. Chin. Uni.)* **1992**, *13*, 727.

[105] Kirner, J. F.; Reed, C. A.; Scheidt, W. R. *J. Am. Chem. Soc.* **1977**, *99*, 1093.

[106] Lin, Kuan-Jiuh. *Angew. Chem.,Int. Ed. Engl.* **1999**, *38*, 2730.

[107] Kastner, M. E.; Scheidt, W. R. *J. Organomet. Chem.* **1978**, *157*, 109.

[108] Masuda, H.; Taga, T.; Sugimoto; H.; Mori; M. *J. Organomet. Chem.* **1984**, *273*, 385.

[109] Summers, J. S.; Petersen, J. L.; Stolzenberg, A. M. *J. Am. Chem. Soc.* **1994**, *116*, 7189.

[110] Cao, Yang; Petersen, J. L.; Stolzenberg, A. M. *Inorg. Chim. Acta* **1997**, *263*, 139.

[111] Hoshino, M.; Sonoki, H.; Miyazaki, Y.; Iimura, Y.; Yamamoto, K. *Inorg. Chem.* **2000**, *39*, 4850.

[112] Runge, S.; Senge, M. O.; Ruhlandt-Senge, K. *Z. Naturforsch.,Teil B* **1999**, *54*, 662.

[113] Smirnov, V. V.; Woller, E. K.; DiMagno, S. G. *Inorg. Chem.* **1998**, *37*, 4971.

[114] Padmanabhan, M.; Poojari, M. D.; Krishnan, V. *Proc. Indian Acad. Sci., Chem. Sci.* **1993**, *105*, 161.

[115] Masuda, H.; Taga, T.; Osaki, K.; Sugimoto, H.; Mori, M. *Bull. Chem. Soc. Jpn.* **1982**, *55*, 4.

[116] Simonato, J. -P.; Pecaut, J.; Marchon, J. -C. *Inorg. Chim. Acta* **2000**, *304*, 288.

[117] Scheidt, W. R. *J. Am. Chem. Soc.* **1974**, *96*, 90.

[118] Jene, P. G.; Ibers, J. A. *Inorg. Chem.* **2000**, *39*, 5796.

[119] Little, R. G.; Ibers, J. A. *J. Am. Chem. Soc.* **1974**, *96*, 4452.

[120] Byrn, M. P.; Curtis, C. J.; Hsiou, Yu.; Khan, S. I.; Sawin, P. A., Tendick, S. K.; Terzis, A.; Strouse, C. E. *J. Am. Chem. Soc.* **1993**, *115*, 9480.

[121] Summers, J. S.; Petersen, J. L.; Stolzenberg, A. M. *J. Am. Chem. Soc.* **1994**, *116*, 7189.

[122] Little, R. G.; Ibers, J. A. *J. Am. Chem. Soc.* **1974**, *96*, 4440.

[123] Balch, A. L.; Mazzanti, M.; Olmstead, M. M. *Inorg. Chem.* **1993**, *32*, 4737.

[124] Scheidt, W. R.; Hoard, J. L. *J. Am. Chem. Soc.* **1973**, *95*, 8281.

[125] Kadish, K. M.; Ou, Zhongping; Tan, Xiaoyu; Boschi, T.; Monti, D.; Fares, V.; Tagliatesta, P. *J. Chem. Soc., Dalton Trans.* **1999**, 1595.

[126] Godbout, N.; Sanders, L. K.; Salzmann, R.; Havlin, R. H.; Wojdelski, M.; Oldfield, E. *J. Am. Chem. Soc.* **1999**, *121*, 3829.

[127] Ellison, M. K.; Scheidt, W. R. *Inorg. Chem.* **1998**, *37*, 382.

[128] Richter-Addo, G. B.; Hodge, S. J.; Yi, Geun-Bae; Khan, M. A.; Ma, Tianshu; Van Caemelbecke, E.; Guo, Ning; Kadish, K. M. *Inorg. Chem.* **1996**, *35*, 6530.

[129] Kaduk, J. A.; Scheidt, W. R. *Inorg. Chem.* **1974**, *13*, 1875.

[130] Bang, H.; Edwards, J. O.; Kim, J.; Lawler, R. G.; Reynolds, K.; Ryan, W. J.; Sweigart, D. A. *J. Am. Chem. Soc.* **1992**, *114*, 2843.

[131] Simonato, J. -P.; Pecaut, J.; Marchon, J. -C. *J. Am. Chem. Soc.* **1998**, *120*, 7363.

[132] Scheidt, W. R. *J. Am. Chem. Soc.* **1974**, *96*, 84.

[133] Toronto, D.; Sarrazin, F.; Pecaut, J.; Marchon, J. -C.; Shang, M.; Scheidt, W. R. *Inorg. Chem.* **1998**, *37*, 526.

[134] Munro, O. Q.; Shabalala, S. C.; Brown, N. J. *Inorg. Chem.* **2001**, *40*, 3303.

[135] Guangdi, Yang; Xizhang, Cao; Fengshan, Wang; Guodong, Zheng. *Jilin Daxue Ziran Kex. Xue.* **1988**, 118-3.

[136] Doppelt, P.; Fischer, J.; Ricard, L.; Weiss, R. *New J. Chem. (Nouv. J. Chim.)* **1987**, *11*, 357.

[137] Doppelt, P.; Fischer, J.; Weiss, R. *J. Am. Chem. Soc.* **1984**, *106*, 5188.

[138] Lin, Kuan-Jiuh. *Angew. Chem., Int. Ed. Engl.* **1999**, *38*, 2730.

[139] Senge, M. O. *J. Porphyrins and Phthalocyanines* **1998**, *2*, 107.

[140] Sakurai, T.; Yamamoto, K.; Naito, H.; Nakamoto. N. *Bull. Chem. Soc. Jpn.* **1976**, *49*, 3042.

[141] Cao, Yang; Petersen, J. L.; Stolzenberg, A. M. *Inorg. Chem.* **1998**, *37*, 5173.

[142] Tse, A. K. -S.; Wang, Ru-ji; Mak, T. C. W.; Chan, Kin Shing. *Chem. Commun.* **1996**, 173.

[143] Jene, P. G.; Ibers, J. A. *Inorg. Chem.* **2000**, *39*, 3823.

[144] Yamamoto, K.; Iitaka, Y. *Chem. Lett.* **1989**, 697.

[145] Mikolaiski, W.; Baum, G.; Massa, W.; Hoffmann, R. W. *J. Organomet. Chem.* **1989**, *376*, 397.

[146] Toronto, D.; Sarrazin, F.; Pecaut, J.; Marchon, J. -C.; Shang, M.; Scheidt, W. R. *Inorg. Chem.* **1998**, *37*, 526.

[147] Iimura, Y.; Sakurai, T.; Yamamoto, K. *Bull. Chem. Soc. Jpn.* **1988**, *61*, 821.

[148] Ohba, S.; Eishima, M.; Seki, H. *Acta Crystallogr.,Sect. C (Cr. Str. Comm.)* **2000**, *56*, e555.

[149] Ciurli, S.; Gambarotta, S.; Floriani, C.; Chiesi-Villa, A.; Guastini, C. *Angew. Chem., Int. Ed. Engl.* **1986**, *25*, 553.

[150] Doppelt, P.; Fischer, J.; Weiss, R. *Inorg. Chem.* **1984**, *23*, 2958.

[151] Madura, P.; Scheidt, W. R. *Inorg. Chem.* **1976**, *15*, 3182.

[152] Stevens, E. D. *J. Am. Chem. Soc.* **1981**, *103*, 5087.

[153] Park, S.; Chamberlain, J. R.; Ondrias, M. R.; Senge, M. O.; Smith, K. M.; Shelnutt, J. A. *J. Am. Chem. Soc.* **1993**, *115*, 581.

[154] DiMagno, S. G.; Wertsching, A. K.; Ross, C. R. II. *J. Am. Chem. Soc.* **1995**, *117*, 8279.

[155] Goldberg, I.; Krupitsky, H.; Stein, Z.; Hsiou, Yu; Strouse, C. E. *Supramolecular Chemistry* **1994**, *4*, 203.

[156] Scheidt, W. R.; Turowska-Tyrk, I. *Inorg. Chem.* **1994**, *33*, 1314.

[157] Liou, K.; Newcomb, T. P.; Heagy, M. D.; Thompson, J. A.; Heuer, W. B.; Musselman, R. L.; Jacobsen, C. S.; Hoffman, B. M.; Ibers, J. A. *Inorg. Chem.* **1992**, *31*, 4517.

[158] Xiangdong, Jiao; Jinwang, Huang; Liangnian, Ji; Xing, Wang. *Wuji Huaxue Xuebao(Chinese J. Inorg. Chem.)* **1997**, *13*, 129-2.

[159] Kadish, K. M.; Araullo-McAdams, C.; Han, B. C.; Franzen, M. M. *J. Am. Chem. Soc.* **1990**, *112*, 8364.

[160] Kim, H. -J.; Redman, J. E.; Nakash, M.; Feeder, N.; Teat, S. J.; Sanders, J. K. M. *Inorg. Chem.* **1999**, *38*, 5178.

[161] Nelson, A. P.; DiMagno, S. G. *J. Am. Chem. Soc.* **2000**, *122*, 8569.

[162] Takenaka, A.; Syal, S. K.; Sasada, Y.; Omura, T.; Ogoshi, H.; Yoshida, Z. -I. *Acta Crystallogr., Sect. B* **1976**, *32*, 62.

[163] Whang, Dongmok; Kim, Kimoon. *Acta Crystallogr., Sect. C (Cr. Str. Comm.)* **1991**, *47*, 2547.

[164] Grigg, R.; Trocha-Grimshaw, J.; Henrick, K. *Acta Crystallogr., Sect. B* **1982**, *38*, 2455.

[165] Zhou, Xiang, Li, Qi, Mak, T. C. W.; Chan, Kin Shing. *Inorg. Chim. Acta* **1998**, *270*, 551.

[166] Boschi, T.; Licoccia, S.; Paolesse, R.; Tagliatesta, P.; Pelizzi, G.; Vitali, F. *Organometallics* **1989**, *8*, 330.

[167] Miller, R. G.; Kyle, J. A.; Coates, G. W.; Anderson; D. J.; Fanwick, P. E. *Organometallics* **1993**, *12*, 1161.

[168] Poszmik, G.; Carroll, P. J.; Wayland, B. B. *Organometallics* **1993**, *12*, 3410.

[169] Mak, Kin Wah; Xue, Feng; Mak, T. C. W.; Chan, Kin Shing. *J. Chem. Soc., Dalton Trans.* **1999**, 3333.

[170] Collman, J. P.; Boulatov, R. *Inorg. Chem.* **2001**, *40*, 560.

[171] Leung, Wa-Hung; Lai, W.; Williams, I. D. *J. Organomet. Chem.* **2000**, *604*, 197.

[172] Wayland, B. B.; Woods, B. A.; Pierce, R. *J. Am. Chem. Soc.* **1982**, *104*, 302.

[173] Hanson, L. K., Gouterman, M.; Hanson, J. C. *J. Am. Chem. Soc.* **1973**, *95*, 4822.

[174] Fleischer, E. B.; Dixon, F. L.; Florian, R. *Inorg. Nuclear Chem. Lett.* **1973**, *9*, 1303.

[175] Zhou, Xiang; Wang, Ru-Ji; Xue, Feng; Mak, T. C. W.; Chan, Kin Shing. *J. Organomet. Chem.* **1999**, *580*, 22.

[176] Mizutani, T.; Uesaka, T.; Ogoshi, H. *Organometallics* **1995**, *14*, 341.

[177] Tse, A. K. -S.; Wu, Bo-Mu ; Mak, T. C. W.; Chan, Kin Shing. *J. Organomet. Chem.* **1998**, *568*, 257.

[178] Licoccia, S.; Paolesse, R.; Boschi, T.; Bandoli, G.; Dolmella, A. *Acta Crystallogr., Sect. C (Cr. Str. Comm.)* **1995**, *51*, 833.

[179] Thackray, D. C.; Ariel, S.; Leung, T. W.; Menon, K.; James, B. R.; Trotter, J. *Can. J. Chem. Vol 64* **1986**, 2440.

[180] Kim, H. -J.; Redman, J. E., Nakash, M.; Feeder, N.; Teat, S. J.; Sanders, J. K. M. *Inorg. Chem.* **1999**, *38*, 5178.

[181] Jameson, G. B.; Collman, J. P.; Boulatov, R. *Acta Crystallogr., Sect. C (Cr. Str. Comm.)* **2001**, *57*, 406.

[182] Zhou, Xiang; Tse, Man Kin; Wu, De-Dong; Mak, T. C. W.; Chan, Kin Shing. *J. Organomet. Chem.* **2000**, *598*, 80.

[183] Fleischer, E. B.; Lavallee, D. *J. Am. Chem. Soc.* **1967**, *89*, 7132.

[184] Cotton, F. A.; Wilkinson, G. *Advanced Inorganic Chemistry;* Fifth Ed., John Wiley and sons: USA, 1988.

[185] Hansen, A. P.; Goff, H. M. *Inorg. Chem.* **1984**, *23*, 4519.

[186] Falk, J. E. (Edited by Smith, K. M.) *Porphyrins and Metalloporphyrins*; Elsevier Scientific Publishing Company: Amsterdam-Oxford-New York, 1975.

[187] Ferrersueta, G.; Batinichaberle, I.; Spasojevic, I.; Fridovich, I.; Radi, R. *Chemical Research in Toxicology* **1999**, *12*, 442.

[188] Bloodsworth, A.; Odonnell, V. B.; Batinichaberle, I.; Chumley, P. H.; Hurt, J. B.; Day, B. J.; Crow, J. P.; Freeman, B. A. *Free Radical Biology and Medicine* **2000**, *28*, 1017.

[189] Chen, F. C.; Cheng, S. H.; Yu, C. H.; Liu, M. H.; Su, Y. O. *Journal of Electroanalytical Chemistry* **1999**, *474*, 52.

[190] Tsuda, Y.; Takahashi, K.; Yanaguchi, T.; Matsui, S.; Komura, T.; Nishiguchi, I. *Journal of Molecular Catalysis A – Chemical* **1999**, *138*, 145.

[191] Neys, P. E. F.; Vankelecom, I. F. J.; Parton, R. F.; Dehaen, W.; Labbe, G.: Jacobs, P. A. *Journal of Molecular Catalysis A – Chemical* **1999**, *144*, 373.

[192] Martinezlorente, M. A. F.; Battioni, P.; Kleemis, W.; Bartoli, J. F.; Mansuy, D. *Journal of Molecular Catalysis A – Chemical* **1996**, *113*, 343.

[193] Nam, H.; Hwang, W.; Ahn, J. M.; Yi, S. Y.; Jhon, G. J. *Bulletin of the Korean Chemical Society* **1996**, *94*, 3393.

[194] Oyaizu, K.; Haryono, A.; Yonemaru, H.; Tsuchida, E. *Journal of the Chemical Society – Faraday Trans.* **1998**, *17*, 414.

[195] Neys, P. E. F.; Severeyns, A.; Vankelecom, I. F. J.; Ceulemans, E.; Dehaen, W.; Jacobs, P. A. *Journal of Molecular Catalysis A – Chemical* **1997**, *126*, L9.

[196] Jakobs, A.; Bernadou, J.; Meunier, B. *Journal of Organic Chemistry* **1997**, *62*, 3505.

[197] Pattou, D.; Labat, G.; Defrance, S.; Seris, J. L.; Meunier, B. *Bulletin De La Societe Chimique De France* **1994**, *131*, 78.

[198] Balakrishnan, T.; Palani, T. *Journal of Applied Polymer Science* **2000**, *77*, 104.

[199] Chen, S. M. *Journal of Molecular Catalysis A – Chemical* **1999**, *138*, 1.

[200] Hu, X. M.; Huang, Z. T.; Gu, G. B.; Wang, L. F.; Chen, B. Y. *Journal of Molecular Catalysis A – Chemical* **1998**, *132*, 171.

[201] Liu, S. Q.; Xu, J. Q.; Sun, H. R.; Li, D. M. *Inorganica Chimica Acta* **2000**, *306*, 87.

[202] Chung, T. D.; Anson, F. C. *Journal of Electroanalytical Chemistry* **2001**, *508*, 115.

[203] Araki, K.; Dovidauskas, S.; Winnischofer, H.; Alexiou, A. D. P.; Toma, H. E. *Journal of Electroanalytical Chemistry* **2001**, *498*, 152.

[204] Elmouahid, O.; Coutanceau, C.; Belgsir, E. M.; Crouigneau, P.; Leger, J. M.; Lamy. C. *Journal of Electroanalytical Chemistry* **1997**, *426*, 117.

[205] Vichezaguado, F.; Gutierrezgranados, S.; Sucarsuccar, S.; Biedcharreton, C.; Bedioui, F. *New Journal of Chemistry* **1997**, *21*, 1009.

[206] Griveau, S.; Bedioui, F. *Electroanalysis* **2001**, *13*, 253.

[207] Castellani, A. M.; Gushikem, Y. *Journal of Colloid and Interface Science* **2000**, *230*, 195.

[208] Aoyama, Y.; Yamagishi, A.; Yasutaka, T.; Tooi, H.; Ogoshi, H. *J. Am. Chem. Soc.* **1987**, *109*, 4735.

[209] Aoyama, Y.; Fujisawa, T.; Watanabe, T.; Tooi, H.; Ogoshi, H. *J. Am. Chem. Soc.* **1986**, *108*, 943.

[210] Coffin, V. L.; Brennen, W.; Wayland, B. B. *J. Am. Chem. Soc.* **1988**, *110*, 6063.

[211] Aoyama, Y.; Asakawa, M.; Yamagishi, A.; Tooi, H.; Ogoshi, H. *J. Am. Chem. Soc.* **1990**, *112*, 3145.

[212] Wayland, B. B.; Abd-Elmageed, M. E. *J. Am. Chem. Soc.* **1974**, *96*, 4809.

[213] Farrugia, L. J. *ORTEP-3 for Windows, v1.05* Dept of Chemistry, University of Glascow see Farrugia, L. J. *J. Appl. Cryst.* **1997**, *30*, 565.

[214] Medforth, C. J.; Kadish, K. M.; Smith, K. M.; Guilard, R Eds.; *The Porphyrin Handbook Vol. 5 / NMR and EPR, Chap. 35;* Academic Press: 2000.

[215] ^{1}H NMR spectra obtained from Sigma-Aldrich Co. and Abraham, R. J.; Medforth, C. J. *J. Chem. Soc., Chem. Commun.* **1987**, 1637.

[216] Walker, F. A.; Kadish, K. M.; Smith, K. M.; Guilard, R Eds.; *The Porphyrin Handbook Vol. 5 / NMR and EPR, Chap. 36;* Academic Press: 2000.

[217] Parish, R. V. *NMR, NQR, EPR, And Mössbauer Spectroscopy In Inorganic Chemistry*; Ellis Horwood Ltd.: West Sussex, England, 1990.

[218] Spiccia, L.; Aramini, J. M.; Crimp, S. J.; Drljaca, A.; Lawrenz, E. T.; Tedesco, V.; Vogel, H. J. *J. Chem. Soc., Dalton Trans.* **1997**, 4603.

[219] Read, M. C.; Glaser, J.; Sandström, M.; Toth, I. *Inorg. Chem.* **1992**, *31*, 4155.

[220] Read, M. C.; Glaser, J.; Persson, I.; Sandström, M. *J. Chem. Soc., Dalton Trans.* **1994**, 3243.

[221] Leitner, W.; Bühl, M.; Fornika, R.; Six, C.; Baumann, W.; Dinjus, E.; Kessler, M.; Krüger, C.; Rufińska, A. *Organometallics* **1999**, *18*, 1196.

[222] Daasch, L. W.; Smith, D. C. *Analytical Chemistry* **1951**, *23*, 853.

[223] Suslick, K. S.; Watson, R. A. *New J. Chem.* **1992**, *16*, 633.

[224] Gouterman, M., *The Porphyrins Vol. III, Pg. 1;* Dolphin D. Academic Press: N. Y., 1978.

[225] Botoshanskii, M. M.; Simonov, Y. A.; Bologa, O, A. *Zh. Strukt. Khim.* **1981**, *22*, 132.

[226] Simonov, Y. A.; Gerbeleu, N, V.; Gdanets, M.; Bourosh, P. N.; Koropchanu, E. B.; Bologa, O. A. *Koord. Khim.* **2001**, *27*, 368.

[227] Kelly, B. A.; Welch, A. J.; Woodward, P. *J. Chem. Soc., Dalton Trans.* **1977**, 2237.

[228] Moszner, M.; Glowiak, T.; Kubiak, M.; Ziolkowski, J. J.; Costa, G.; Tavagnacco, C. *Polyhedron* **1997**, *16*, 307.

[229] Dreos, R.; Tauzher, G.; Geremia, S.; Randaccio, L.; Asaro, F.; Pellizer, G.; Tavagnacco, C.; Costa, G. *Inorg. Chem.* **1994**, *33*, 5404.

[230] Tolman, C. A. *Chemical Reviews* **1977**, *77*, 313.

[231] Barnett, G. H.; Hudson, M. F.; Smith, K. M. *J. Chem. Soc., Perkin Trans. 1* **1975**, 1401.

[232] Adler, A. D.; Longo, F. R.; Kampas, F.; Kim, J. *J. Inorg. Nucl. Chem.* **1970**, *32*, 2443.

[233] McArdle, P. *J. Appl. Cryst.* **1995**, *28*, 65.